AD-A163 899 RSRE (ROYAL SIGNALS AND RADAR ESTABLISHMENT) 1985 1/3
RESEARCH REVIEW(U) ROYAL SIGNALS AND RADAR
ESTABLISHMENT MALVERN (ENGLAND) A J GRANT ET AL. 1985
UNCLASSIFIED DRIC-BR-98221 F/G 17/9 NL

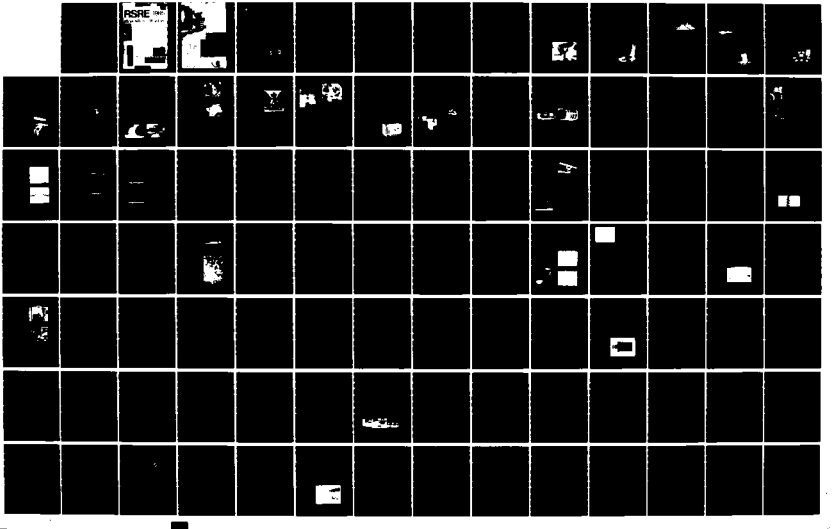

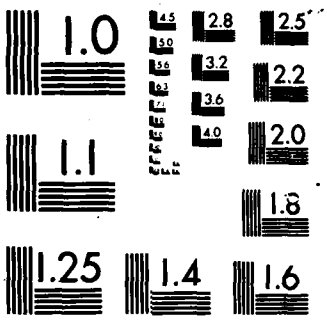

2

RSRE 1985 RESEARCH REVIEW

ROYAL SIGNALS & RADAR ESTABLISHMENT, MALVERN, UK

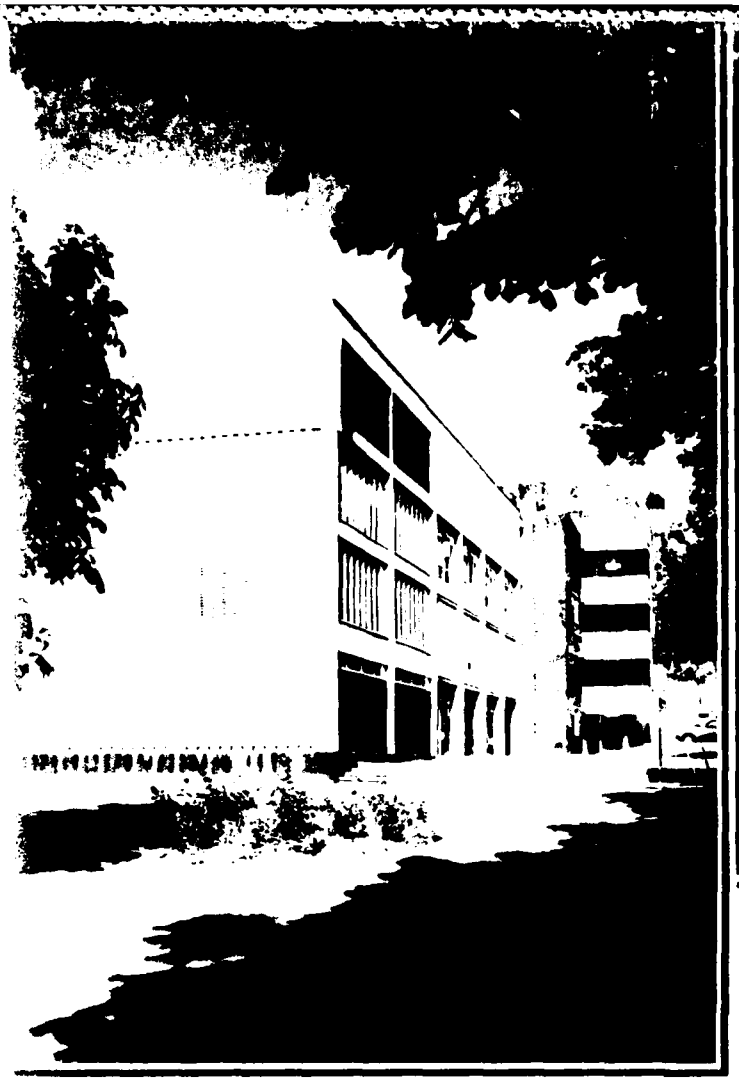

Materials research building

APPLIED PHYSICS DEPARTMENT

- PHYSICS
- MICROWAVE AND ELECTRO-OPTICS
- SIGNAL PROCESSING

INFORMATION SYSTEMS DEPARTMENT

- AIR DEFENCE AND ATC
- COMMUNICATIONS AND COMPUTING
- BATTLEFIELD SYSTEMS

Micrograph of GaAs/GaAlAs semiconductor superlattice

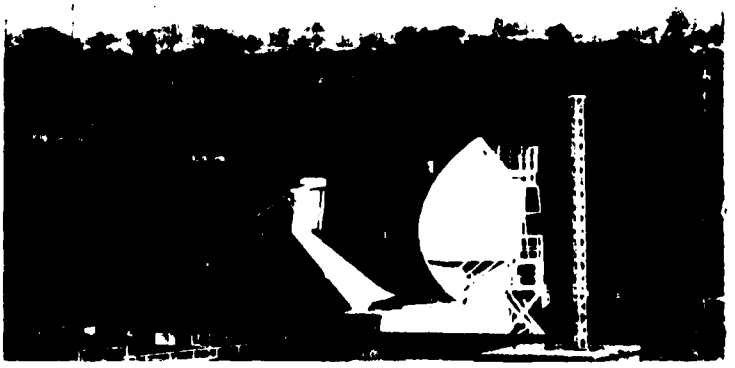

BYSON research radar

UNCLASSIFIED

ROYAL SIGNALS & RADAR ESTABLISHMENT

1985 RESEARCH REVIEW

EDITORIAL BOARD
A J Grant
E Jakeman
J Clarke

UNCLASSIFIED

PREFACE

A selection of our research activities is presented in this 1985 Research Review for the use and benefit of colleagues in University, Industrial and Government communities in the United Kingdom and abroad. The Royal Signals and Radar Establishment carries out research and development in the fields of electronics technology and systems engineering. Beginning with the invention and exploitation of radar the Establishment has been active in electronics research, though under a number of names, for 50 years now. Our present research areas include basic physics and materials technology, infra-red devices and systems, silicon sub-micron VLSI technology, lasers, computing, and communications, as well as radar.

The excellence of the research we carry out on behalf of the Ministry of Defence, the Department of Trade and Industry, and the Civil Aviation Authority is, I believe, beyond question. The Establishment has won a total of five Queen's Awards for Technology – an unequalled achievement – two Rank Prizes for Optoelectronics, and a number of other major awards. A major objective for the Establishment is to ensure the timely exploitation of the products of our research, and I hope that this Review will contribute to this through new and mutually beneficial contacts.

DR A C BAYNHAM
Director, RSRE

Acknowledgements

Designed, printed and published by RSRE MOD(PE), Malvern.

Cover printing and binding: Severn Side Printers Ltd, Upton-upon-Severn.

Layout: Pioneer Design and Technical Services Ltd, Malvern.

CONTENTS

RADAR
AND
MICROWAVES

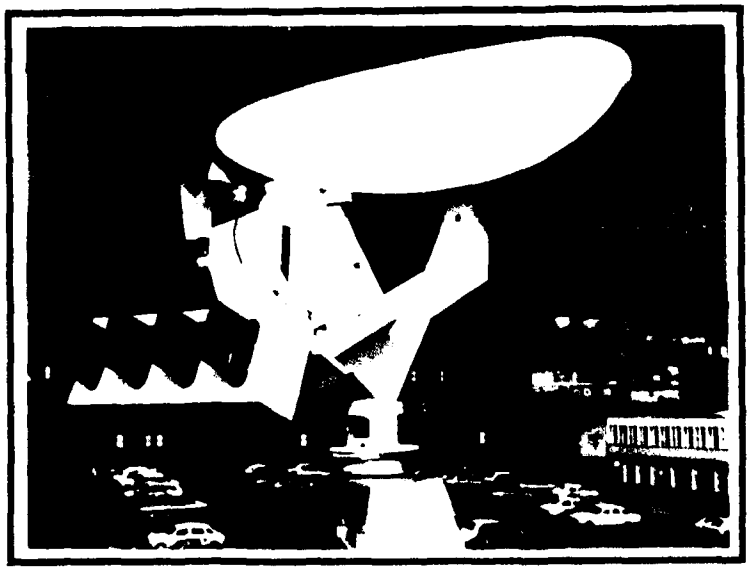

THE UK RADAR SCENE TODAY

J Clarke

Summary

A review of primary radar systems in the United Kingdom that have recently entered service or are at an advanced stage of development is presented. The breadth of activities that endeavours at RSRE support and nurture is thereby illustrated. Naval, airborne and land-based types are discussed covering both civil and military interests, although particular emphasis is given to airborne equipments.

Introduction

The radar community in Britain is large and active. Most of the major electronics companies have divisions devoted to one or more aspects of radar. Many different types of equipment are being supported in service or are in production; the majority of these benefit from work of the Royal Signals and Radar Establishment. It is almost always the new or novel aspects to which the RSRE effort is applied, be it at the system concept level, the antenna, microwave technologies, or signal processing. For military radars, RSRE is often nominated as the sole Technical Agency for the Project Manager to advise on the specification, technical approach, testing methods and performance achievement.

To contain the scope of this article, some constraints have been applied: radars above 100 GHz are not addressed, such that laser radar and laser rangefinder are excluded. Secondary radars, instrumentation radars, HF radar, and a number of radio navigational aids (altimeters, Doppler navigators) have also been omitted as have radar data processors. Component technology is considered to be generally outside the scope of this review. Finally, it is worth recalling that there are a number of University teams active in the radar field though their work is not included here; some of these research programmes are directly sponsored by RSRE.

The review has been partitioned very simply into the subjects of ground radar, naval/marine radar, airborne radar and seekers, and is presented in that order. For a number of reasons, it has not been possible to give a comprehensive treatment throughout the paper, though a serious attempt has been made in this respect in the airborne radar section. The preparation of this review has been inhibited by security restrictions and this is reflected in technical details being unavailable in many areas.

Ground Radar

Starting with the most powerful systems, two major long-range three-dimensional air defence radars have appeared in recent years. European weather and target environments make multiple beam search desirable, and both radars have this capability or its equivalent.

The Marconi MARTELLO L-band transportable radar was first announced in 1978. It has a wideband, coherent, frequency-agile transmitter of over 10 kW mean power and a low sidelobe planar antenna made up of a stack of wideband linear arrays (Fig 1). Nine simultaneous receiving beams are formed at intermediate frequency by a resistive

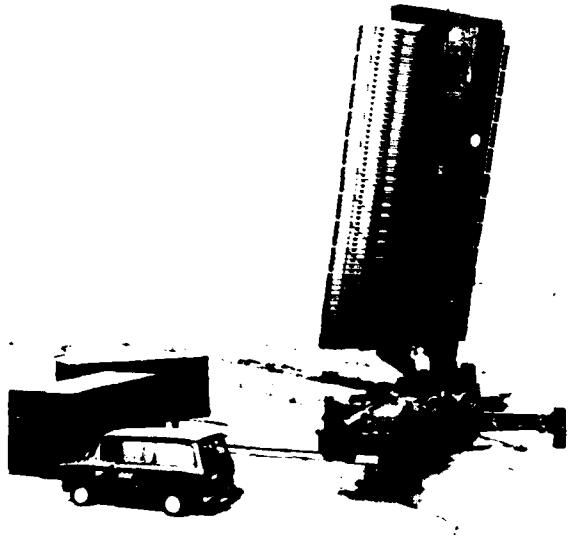

Fig 1 MARTELLO

matrix beam forming network which enables the beams to be individually tailored without any orthogonality constraints. The stack of receiving beams provide three-dimensional data, accurate elevation interpolation being possible since all beams share the same transmission frequency. The antenna is demountable, and the whole radar can be set up on an unprepared site in under 6 hours. A digital signal processor is used with adaptive clutter cancellation, the thresholds being set from a continually updated clutter map. The radar has complete plot extraction, data handling and display facilities, and can operate as a self-contained station or as part of an air defence network.

A solid-state version of MARTELLO has now been developed and is in production for NATO. This uses the same principles as the earlier model described above, but has a distributed transmitter with its inherent fail-soft characteristic. Solid state transmitter modules, each of 3 kW peak output power, are mounted in the spine behind the planar array and connected directly to the individual horizontal linear arrays. The new MARTELLO has a wider horizontal aperture than the earlier version giving it better azimuth resolution and enhanced range performance. The vertical aperture has been reduced, but more efficient use of the aperture and improved signal processing allows adequate height accuracy and performance in clutter to be maintained. Coverage of small aircraft is about 250 nm in range and over 100 kft in altitude.

The second new radar, the S-band Plessey/ITT Gilfillan AR320, is based on the earlier Plessey AR3D and ITT Gilfillan S320 designs. The AR320 uses the elevation within-pulse frequency-scanning principle of the AR3D (Fig 2), the frequency sweep also being used to provide pulse compression. The low sidelobe planar array antenna is developed from that of the S320 and includes phase shifters to permit independent variation of frequency and elevation beam position. This also gives the AR320 a limited look-back potential. The AR320 transmitter uses a crossed field amplifier output stage to provide a mean power of over 24 kW. It can operate over a variety of pulse durations and repetition frequencies and has an adaptive Doppler processor. A fully automatic three-dimensional plot extractor is incorporated. The AR320 can be configured to meet fixed site, transportable, or mobile air defence requirements.

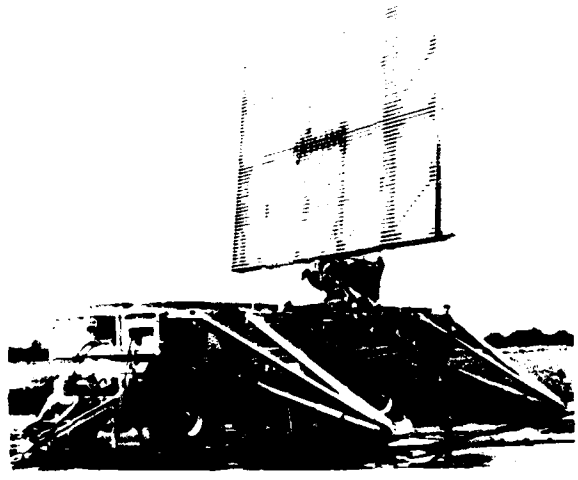

Fig 2 Plessey AR3D

The Marconi ASRS511 is an example of an airfield surveillance radar and gives detection of 10 m^2 targets out to 100 nm. The frequency band is 2.7 to 2.9 GHz and a pulse width of 0.85 μs is used at 650 kW peak. A 6-period staggered PRF is employed together with a 4-pulse canceller having time varied weighting. Temporal threshold integration is used in both the MTI channel and a noncoherent processing channel for clutter adaptive thresholding. Two beams, overlapped in elevation are available from the 33.5 dB gain antenna: the main beam having continuously variable (between circular and linear vertical) polarization and the auxiliary upper beam having fixed circular polarization.

Marconi Radar also offer the 700 series of low level radar systems. These employ similar electronic units and operate in the 10 cm band. The transmitter is 160kW peak, 2 kW mean and provides 16 spot frequencies over a 300 MHz band. The pulse width is 12 μsec compressed by a ratio 20:1 in the receiver. Digital processing follows a 12 bit A/D converter and features 4 pulse MTI, CFAR, jamming strobe detection and sidelobe blanking. A variety of vehicles and antenna sizes is available; one example is the S711 with 1.5° beamwidth $cosec^2$

antenna elevated on a 18 m hydraulic mast. For civilian applications Racal-Decca manufacture and employ S- and X-band radars in vessel traffic management systems (VTMS): these are pulse radars similar to their large marine radars. Antennas are up to 7m aperture (see Fig 3) with transmitters up to 75 kW, though more typically 20 kW. More than 300 of these radars have been installed for harbour and waterway surveillance; for example, in the United Kingdom there is the English Channel system, the Thames Barrier system, Teesport, and Portsmouth. The radars are often supplied under Racal-Decca turnkey contracts covering operations centre, data processor, communications, recorders and so forth.

Fig 3 Decca VTMS

Ferranti continue to develop their high power CW radar technology. The Radar type 86 which is used with the Bloodhound II SAM system has been updated by the incorporation of many improvements including a new advanced digital signal processing system. Extensive modifications to increase reliability and to reduce the costs of maintaining the equipment have also been incorporated. A new experimental CW radar which operates at Ku-band has been produced under RSRE funding. This equipment has a very high power transmitter and a sensitive receiver which incorporates clutter cancellation and full target tracking capabilities.

At a much lower power level, ie 0.5 W, Ferranti market the PACER muzzle velocity measuring equipment. This has a fixed 10° beam at 10.5 GHz and is placed adjacent to an artillery or mortar. It measures exit muzzle velocity in the range 100 to 1400 m/s to an accuracy of 0.1 percent in less than 1 s. Several measurements are made of Doppler along the trajectory and a least squares fit calculation performed to extrapolate back to muzzle velocity: correction for cosine error arising from sightline offset is included.

The well known RAPIER air-defence system employs two radars, a Racal-Decca surveillance radar, and a Marconi guidance radar, although optical guidance is also widely used. RSRE have supported the Rapier development throughout its life. The weapon system has a range of 12 km and covers from ground level to 3000 m. The system is lightweight and mobile, and there are two basic versions, either towed by a small Land Rover or fitted on a tracked vehicle (RCM 748). The surveillance radar is an S-band pulse-Doppler type to combat severe ground clutter. The scanner rotates at 360°/s and this is a key contributor to the average short reaction time of 6s. The radar features automatic detection, a PPI display is not provided: the operator does have a sector display by way of a ring of 32 lamps, though this is not essential to engagement. Once a moving target is detected, it is interrogated by way of an integral IFF and, if considered hostile, a system alarm is generated. The four missiles on their turntable slew to the bearing of the target together with the optical tracker and the guidance radar. The operator is alerted by a tone in his earphones. The guidance radar, known as DN181 BLINDFIRE, operates in the millimetric band and hence has a narrow beamwidth, provided by an aperture of 1.5m. BLINDFIRE, Fig 4, is a monopulse radar and acquires the

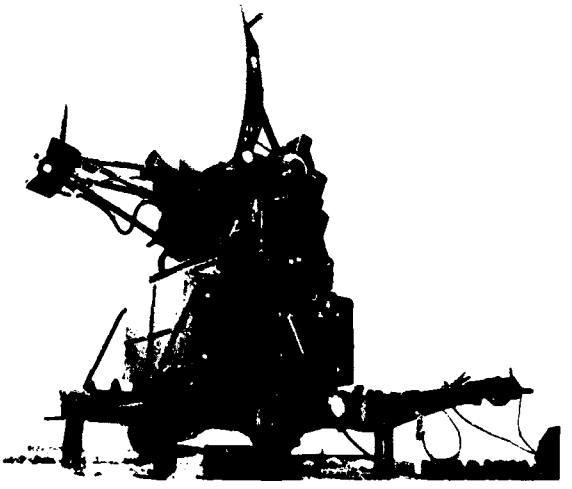

Fig 4 Rapier Blindfire

target by way of a small vertical scan. The antenna is an offset Cassegrain type. The weapon system can be inhibited in designated sectors by way of a ring of switches next to the sector display lamps. It is of interest to note that the surveillance radar transmitted pulse shape and high receiver selectivity have been specially designed to permit dense deployments.

Recently, further work has been undertaken in the field of Airport Surface Surveillance Radar by Racal-Decca: their ASMI-18X uses a low cost, modular approach while still providing good performance by comparison with 35 GHz types. The scanner has an 18 ft slotted waveguide radiator horizontally polarized, producing 36 dB gain and 0.4° azimuth beamwidth: the rotation rate is 60 rev/min. The radar operates at 9410 MHz and transmits 40 ns pulses from a 20 kW magnetron at a PRF of 4 kHz. The receiver noise figure is better than 10 dB and a logarithmic successive detection IF amplifier is employed. The sensitivity is sufficient to detect a crawling person at 2 km on the runways, and resolution is sufficient to clearly show the shape of large aircraft. The display is fed via a high resolution scan converter. The use of X-band allows maintainance of this performance in all weathers, including blowing sand.

The ZB298 radar, manufactured by GEC Avionics, is a radar in use by the British Army for the ground surveillance role. It is an X-band clutter-locked pulse-Doppler type with a range of 5000 m against personnel and 10 000 m against vehicles. It can be either vehicle mounted or used from the ground. In the latter case the radar can be carried by two men and can be put into operation within 3 min.

When operated from the ground the equipment comprises three major units:

(1) radar head (0.5 m x 0.5 m x 0.2 m), which contains all the microwave circuitry including the 2 kW peak power magnetron transmitter

(2) tripod and angulation head

(3) control box and visual display unit, which allows remote operation of the radar head at distances greater than 20 m

In its surveillance role ZB298 can acquire targets to an accuracy of ±20 m in range and ±10 mil in bearing. It can also be used for the adjustment of artillery fire and surveillance of frontiers, rivers and coasts. The system is in use by the infantry, artillery observation units, and armoured units of the British Army. The radar has been exported to several countries, including Holland and Denmark.

A series of hand-held and manpack radars has been produced over the last decade for use by the Army. One of the latest is the surveillance radar SCAMPI conceived by RSRE and partly designed and built by the Marconi Research Laboratories. The equipment employs a tripod mount for mechanical scanning of the radar head which may be used independently or combined with a remote visual display and control unit. The K_u-band radar head employs a planar array antenna, a fully coherent solid-state transmitter, and a microwave integrated circuit duplexer/receiver. The display and control unit controls the scanning mechanism, gives a full sector visual display (using a dc electroluminescent panel), automatic detection, and programmed setting up instructions. Extensive trials of SCAMPI have shown the system to perform very well. The radar is being extended to allow target tracking and artillery fire control modes. A larger antenna and more powerful transmitter are being used together with FFT signal processing and microprocessor controlled data and display processing.

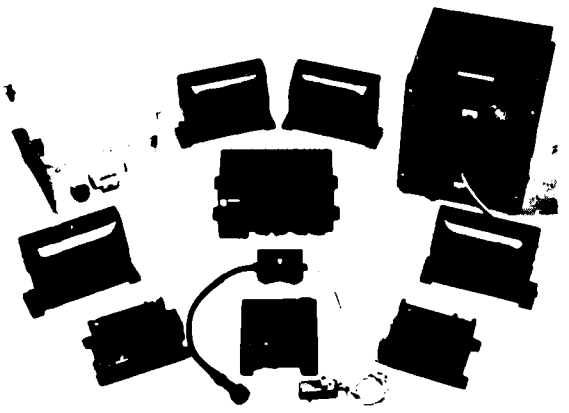

Fig 5 Hostile fire indicator

The Hostile Fire Indicator GS20 was put into

production in 1978 by MESL for the British Army. This is an X-band radar for the detection of all calibers of projectile, including bullets. It provides continuous coverage of 360° azimuth by the use of 4 static heads (Fig 5). Each head contains a CW transmitter and a bonded triplate microwave circuit with 4 balanced mixers. These mixers function as homodyne receivers by utilizing a -13 dB bleed from the transmitter. The Doppler band of interest is 10 to 110 kHz and sensitivity of -100 dBm with an overall noise figure of 10 dB achieved. Signal processing and target declaration are undertaken mainly by digital circuits using custom LSI. The false alarm interval is of the order of months. The display is one of the smallest units and indicates the direction from which a ballistic projectile was fired.

Naval/Marine Radar

Britain continues to develop advanced two-dimensional radars, a recent example being the Marconi type 1830 S-band naval surveillance and target indication radar. This has back-to-back parabolic cylinder reflector antennas with low sidelobe linear array feeds. The 5m equal path "squintless" feeds are machined from solid aluminium by a numerically controlled mill. The antenna operates over the band 2.7 to 3.2GHz. It has a first sidelobe level better than -35 dB and a wide angle sidelobe level better than -60 dB. The high power frequency agile transmitter has nonlinear chirp pulse compression. The receiver features multiple-mode processing and automatic velocity compensation for the clutter cancellation system. The prototype has successfully completed its sea trials.

The newest production radar is the Type 1022 L-band system, which uses a single rotating antenna of the same wideband low sidelobe configuration. This radar is based on the Dutch LW-08 radar (HSA) and is fitted with a Marconi manufactured antenna.

The combination of a high power coherent transmitter and a rotating linear array antenna is again used in the Marconi Type 967 naval search radar. This is an L-band pulse-Doppler radar designed specifically for the detection of small fast approaching targets in severe clutter, for engagement by the Seawolf missile system. A medium PRF gives a wide velocity space enabling sea, land, and weather clutter to be filtered out. The radar is range ambiguous, and an unusually high stability has to be maintained to ensure that distant targets are not masked by near-in clutter breakthrough.

The DOLPHIN radar is an important new addition to the Plessey product line; it was designed specifically to meet target indication requirements of close-in weapon systems and is included within the Contraves Seaguard defence system. It is a lightweight system suited for craft as small as fast patrol boats. The radar is a dual-beam C-band type with high angle coverage, up to 70°, provided by a linear array of dipoles housed in a corner reflector (Fig 6). This array is Taylor weighted by the strip-line feed network to produce -29 dB first azimuthal sidelobe. The cosec^2 low coverage beam is produced by a reflector fed by an array similar to the high beam. The azimuthal beamwidth is 1.5° and providing this beamwidth from a modest 2.5 m masthead aperture was one of the main driving forces for the choice of the RF band. The beam is 2 axis stabilized and rotates at 60 rev/min. The total masthead weight is 500 kg. The 1 kW mean transmitter uses a single TWT and this is connected to the two antenna feeds via a frequency multiplexing diplexer. The agile transmitter operates over a 500 MHz

Fig 6 Dolphin

bandwidth. The use of a TWT transmitter

allows phase weighted pulse compression operation as well as fully coherent processing. The equipment frequency reference is 70 MHz and the IF chirp is coherent with the reference oscillator. Direct frequency synthesis is used for the RF channels, based upon the use of 4 crystal oscillators: change of frequency can be accomplished within 5 μs and the spectral noise of the source is less than -77 dBC/Hz at 1 kHz from carrier. In the receiver, echoes are compressed to a pulse length of 125 ns with time sidelobes below -36 dB (equivalent range cell 19 m). The main signal processing is digital and includes multiple MTI loops, adaptive notch, and CFAR detectors. A parallel non-MTI channel is also provided which includes an adaptive clutter map. The Dolphin design addresses a difficult detection range requirement of 0.1 m^2 RCS at 8 km at a data rate of 1 Hz with accuracies of 50 m in range and 0.5° in azimuth.

The Plessey AWS5 is a high power S-band radar for surface and air target warning which has recently entered service with a NATO navy. A dual beam stabilized antenna combined with a high mean power TWT transmitter provides the long range detection capability required by ships of frigate class. The use of adaptive high speed MTI processing and a small radar resolution cell provides good detection performance in heavy clutter, as demonstrated by comprehensive trials. The system includes a number of advanced features to combat ECM.

It is of interest to note that the use of millimeter-wave radars to overcome multipath errors in low level tracking has been investigated and a 2-plane monopulse system at 80 GHz developed. A maritime version of the DN181 BLINDFIRE RAPIER tracking radar is being purchased by the Royal Navy for incorporation into the Seawolf weapon system.

Racal-Decca have a large range of marine radars in both S- and X-bands. Power levels range from 6 kW to 75 kW and antenna apertures up to 4m. The introduction of solid-state RF ampmlifiers has recently improved the noise figure of X-band sets by 4 dB. A range of displays and display processors is available to suit individual customer requirements. The "Clearscan" processor is now recommended which automatically adjusts the detection threshold on each sweep to suppress sea and rain clutter; all detections are hard-limited and pulse stretched to ensure visibility; pulse-to-pulse correlation is also applied to remove effects like interference from other radars. At the 1983 London Boat Show, the introduction of a new range of digital scan-converter colour displays was announced. This radar technology is exploited in the Racal-Decca 2459F/I intended for the military market (Fig 7): it is a dual frequency radar having both S- and X-band transmitter/receivers working with a common signal processor. The aperture is 4m, giving a beamwidth of 2°, and the rotation rate is 22 rev/min; pulse length is 1 μs at 825 Hz and 0.05 μs at 3.3 kHz. The radar provides both a surface and an air picture with a sensitivity sufficient for 15 nm detection range on medium-sized aircraft and 25 nm on large aircraft.

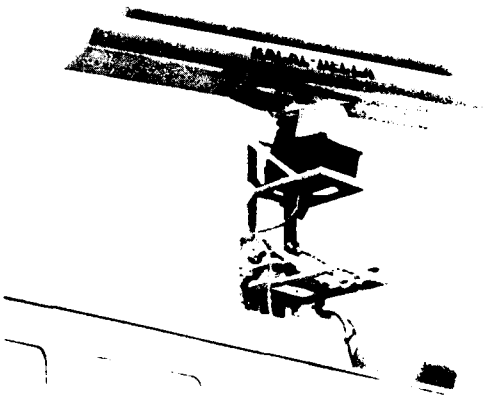

Fig 7 Racal-Decca 2459 F/I

Recent innovations at Racal-Decca have been directed toward signal and data processing improvements to meet automatic radar plotting aids (ARPA) standards set by IMCO and the US Coast Guard. Automatic tracking of 20 targets is now achieved in severe clutter by the provision of automatic threshold control in each tracking window. The tracker uses an α-β algorithm with twin coefficient sets dependent upon the track life.

Airborne Radar

Virtually all types and aspects of airborne

radar are being manufactured or studied in the United Kingdom; several different companies are involved, as well as the Royal Signals and Radar Establishment. It is convenient to review this work in order of the power level of the various equipments, from long range air-surveillance to lightweight helicopter sets.

Airborne Early Warning

Airborne Early Warning (AEW) is considered to be a very important capability. For 30 years the S-band AN/APS-20 has been in service continuously, although several different fixed-wing propeller aircraft have been used as platforms. The radars are currently fitted in a squadron of Shackletons. Some years ago the radars were uprated to APS-20 FI standard by the addition of a digital AMTI signal processor specially developed by the Post Design Service Contractor GEC Avionics. The new processor is contained within a single 1-ATR case and its output is fed to the standard display. The digital clutter canceller has proved to be effective in enabling air target detection in heavy sea clutter.

As a successor to that AEW, a medium-PRF pulse-Doppler radar has been developed by GEC Avionics and is installed in the NIMROD Mk 3 airframe. Good, though undisclosed, performance has been demonstrated in the system development programme. The radar design is unique in that two scanners are used, each having an angular coverage of 180°. This approach has the particular advantage of providing the radar with a field of view clear of any airframe obstructions by locating the antennas at the longitudinal extremities of the vehicle. Conventional electrically driven scanners providing a 10 s data rate are located in large radomes. The twist reflector Cassegrain antennas operate at both the S-band radar frequency and at the SSR/IFF frequency; their elliptical apertures are 2.4m x 1.8m as shown in Fig 8. The two antennas are alternately fed from a single transmitter. Received signals are similarly fed from the fore-and-aft antennas to a common receiver and processing system. The transmitter includes the basic microwave source, a medium power amplifying stage, and the high power output stage.

The radar receiver design complies with stringent requirements for linearity. Pulse compression and phase-locked local oscillators (compensating for aircraft velocity and radar beam pointing angles, hence the removal of self-movement) are applied prior to analog-to-digital conversion. Initial digital signal processing is undertaken in hard-wired fast processors which include the frequency analysis stage. Target detection is automatic using CFAR techniques, and resolution of the range and velocity ambiguities is achieved using the staggered PRF transmission. Azimuth and elevation beam sharpening are applied to give the radar plot report.

Thorn-EMI revealed at Farnborough 84 a small AEW to be known as the AEW Defender. The radar is a radical development of the Searchwater ASW radar (see below). The aircraft employed is a Pilatus Britten-Norman as shown in Fig 9 and the transmitter is housed in the rear fuselage. The scanner is installed in the distinctive nose radome

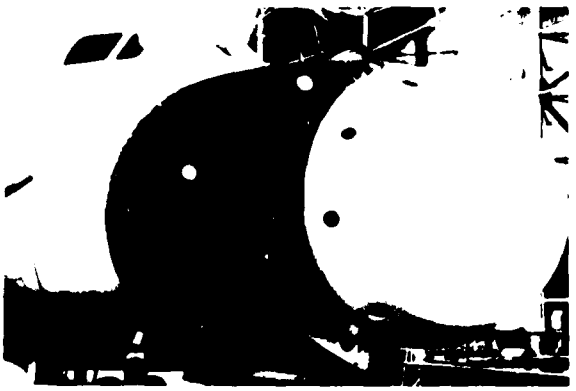

Fig 8 Nimrod AEW Mk 3

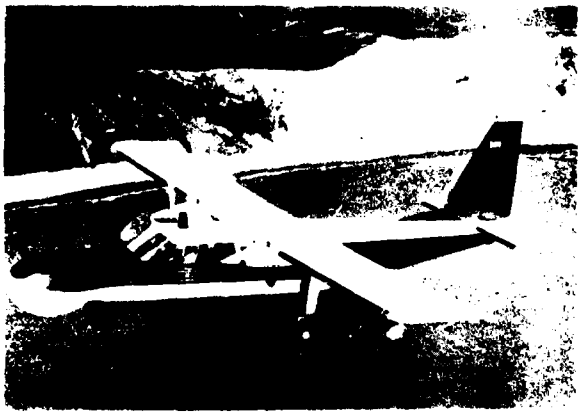

Fig 9 AEW Defender

and provides 360° coverage of low-level targets. Signal processing is mainly digital and the circuitry is housed within the display console. The operator can be given alphanumeric track data on two targets simultaneously together with his own track such that air interception co-ordination can be performed. A touch plasma panel display and roller ball are employed, and the mission computer can store up to 250 tracks. Two consoles are provided.

Airborne Interception

The United Kingdom has a long history of producing airborne interceptor (AI) radars for fighters, dating from operational service in World War II. Still in use is the Ferranti AIRPASS (air interception radar pilot attack sighting system) which was designed and developed for the RAF Lightning aircraft. This was the first high power monopulse airborne radar to enter squadron service anywhere in the world and it is still in service with the RAF and Saudi Arabian Forces. RSRE was the Technical Authority for this development.

The most recent AI radar is the GEC Avionics AI24 FOXHUNTER radar for the Tornado ADV aircraft. Target acquisition range is over 100 nm and TWS allows multiple target tracking. Digital processing, including microprocessors, is used to reduce size and weight while increasing reliability. The Cassegrain antenna has a very clean radiation pattern, which confers good performance, ground-clutter rejection and ECM resistance. The X-band antenna has a front hyperbolic subreflector and a larger rear parabolic reflector, the dual reflectors are separated by glassfiber-honeycomb skirt at the periphery. The four common horns for transmit and receive are in the center of the rear reflector at the focal point of the front reflector. A transmitted wave (horizontally polarized at the horn) reflects from the front reflector back on to the main reflector, which collimates and vertically polarizes the signal. The polarized signal can pass through the subreflector because it is composed of parallel, horizontal conductors. Ferranti is responsible for the development and production of the transmitter and scanner mechanism (Fig 10) for the FOXHUNTER radar. The transmitter uses TWTs and also provides a CW illumination for missile guidance.

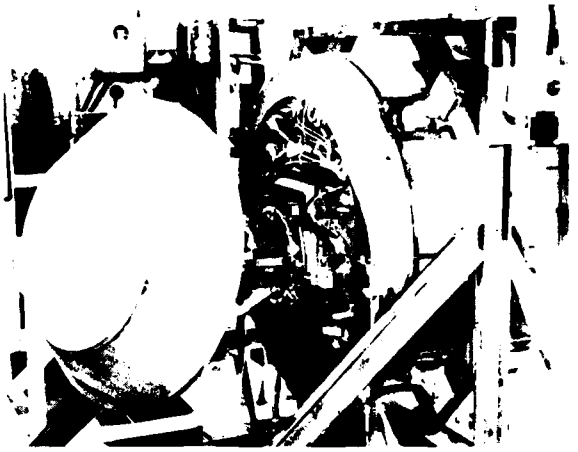

Fig 10 Foxhunter for Tornado ADV

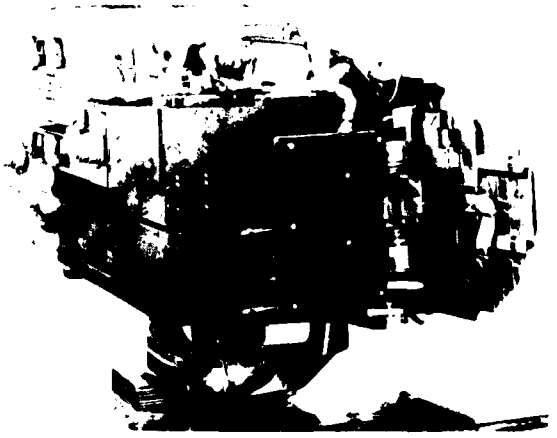

Fig 11 Blue Fox for Sea Harrier

The Sea Harrier is currently fitted with the BLUE FOX radar (Fig 11) for both interception and surface attack. This Ferranti radar was developed from their SEASPRAY experience (see below). The radar operates in X-band with frequency agility and a two-plane monopulse split, using a planar antenna for increased detection range and low sidelobes. A digital scan converter provides a bright TV raster display with picture freeze facility. It is in production and being delivered to both the Royal Navy and Indian Navy. The total radar system weight is 85 kg. Ferranti are continuing to develop this class of radar with BLUE VIXEN, a coherent pulse-Doppler radar selected to replace Blue Fox in the Sea Harrier update programme. Accent is on

flexibility in operation and novel concepts are being employed in the application of medium and high PRF transmissions and in the associated signal processing. A major design goal is to achieve compatibility with the stringent size and weight constraints of the emerging lightweight and VSTOL fighter aircraft.

GEC Avionics also manufacture a lightweight X-band airborne ranging radar consisting of only 3 line replaceable units (LRUs); it is suited to small airframes. The radar provides range and range-rate measurements for gun and missile fire control. The radar exhibits pulse-to-pulse random frequency agility over more than a 5 percent RF range. Range resolution achieved is 150 m. Output is by way of an ARINC 429 highway. The equipment weight is 37 kg and the cooling is by conduction and radiation; power consumed is about 400 W.

Looking toward future AI radars, research is dominated by the needs of a multimission fighter concept employing a multimode radar offering a complete range of air-to-air and air-to-surface modes. This is feasible due to the continual developments in the digital signal processing area and the availability of programmable radar signal processors in which mode changes are accomplished by loading, from bulk store, a variety of program segments. This study is currently being supported by RSRE, GEC Avionics, and Ferranti where efforts are directed toward identifying the algorithms which will be required and the signal processing architectures which are suitable. Airborne trials are being staged using a low duty ratio pulse-Doppler radar, including clutter data gathering.

Maritime Reconnaissance

Another important area in which the United Kingdom has always been active is maritime reconnaissance, for antisubmarine and antiship roles as well as other duties. A long established equipment is ASV21 which is in service use in several countries including the United Kingdom (Nimrod MR1) and Canada (Argus). Transmission is in X-band using a magnetron to generate pulses which vary in width according to displayed range selected. The stablized 360° scanning aerial employs a cosec^2 elevation beamshape. The PPI display uses a long persistence phosphor. Additional facilities include variable width sector scan about any desired heading.

Based upon an RSRE research and flight trials programme, Thorn-EMI developed the SEARCHWATER radar (Fig 12) for the Nimrod MR2, and this equipment is now in service.

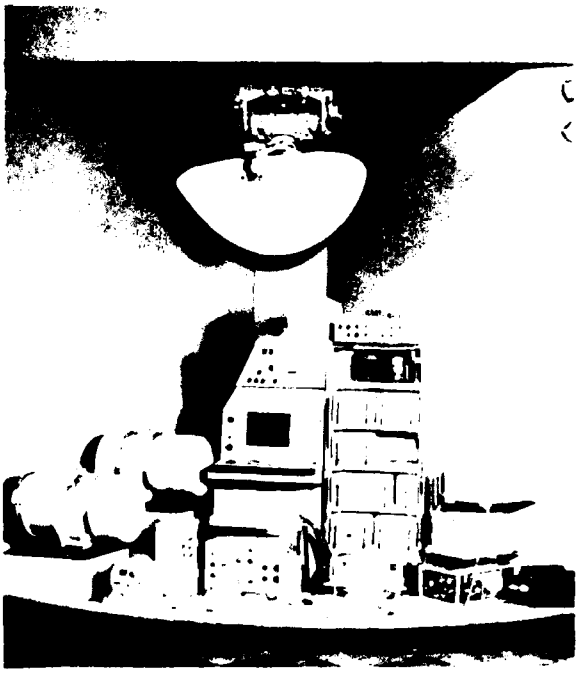

Fig 12 Searchwater

The TWT transmitter generates frequency agile chirp pulses in X-band. The stabilized 360° scanning aerial employs a cosec^2 elevation beamshape and incorporates IFF. Processing includes SAW pulse compression, adaptive thresholding, and integration using a digital scan converter. The detection threshold is continuously adjusted using a control signal derived from the instantaneous clutter level so that a constant false alarm rate is presented to the operator. In additon the radar has a multitarget automatic tracking capability. A-scan, B-scan, PPI, and file data outputs are present on a raster display with a bright phosphor. The radar has built-in test equipment which provides automatic detection and diagnosis of faults during flight.

MEL, a division of Philips Industries also manufacture a range of tactical maritime ASW and ASV radar systems. The para-military

Marec II, designed to meet the needs of airborne coastguard services, is currently in use with the Cameroun Air Force and being supplied to the Indian Coastguard on-board their Dornier DO228 aircraft. The radar has been demonstrated inside the envelope of the AD500 airship, see Fig 13. It operates at

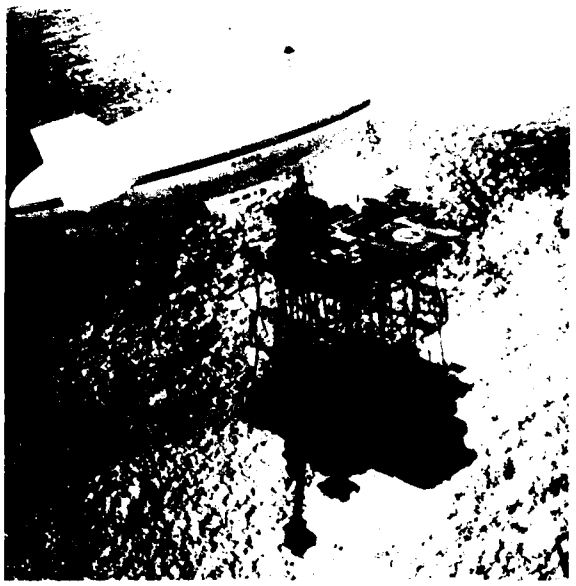

Fig 13 Airship Industries Skyship

X-band with a peak power output of 100 kW derived from a solid state modulator. A choice of 0.4 and 2.5 μs pulse lengths is available to the operator and, coupled with the use of horizontal polarization, a logarithmic receiver, STC and FTC, allows optimisation of the signal to clutter ratio on the display. A range of carbon fibre reflector aperture sizes is available from 42 x 16 inches to 22 x 10 inches in addition to a flat plate antenna having dimensions of 48 x 10 inches in addition to a flat plate antenna having dimensions of 48 x 10 inches. The antenna scans 360° in azimuth and has a built-in steerable sector scan with variable sector width. The radar beam is pitch and roll stabilised. A 17 inch diameter flat screen tactical display (Fig 14) is provided which can accommodate transparent overlay charts where graphics, such as coastal outlines, align with the displayed radar picture. Target range and bearing is displayed digitally and shown on the radar screen. Target range can be displayed as either height corrected or as slant range. The sensitivity is such that ships of 1000 tonnes are detected at ranges in excess of 100 miles and a submarine snort has been detected at over 15 miles. The total power demand is 1 kVA.

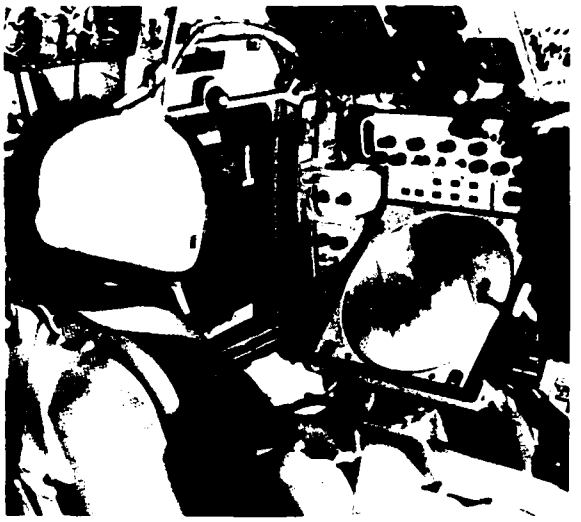

Fig 14 Marec display

Racal-Decca has reconfigured one of their marine radars into an airborne surveillance radar; it has been designated ASR-360. This X-band radar has a 30 in horizontal aperture and is in use on a Norwegian Navy Cessna 337 and a Piper Navajo. The antenna gain is 25 dB, beamwidth 3°, the polarizontal horizontal and the data refresh rate 3 s. The magnetron is nominally 25 kW peak and the pulse lengths 0.05 μs and 1 μs at a minimum PRF of 825 Hz. The signal processing includes a CFAR detector. The 12 in PPI has a choice of eight scales out to 95 nm range with options for off-centering and for true or relative motion.

Sideways looking airborne radar (SLAR) is another aspect of reconnaissance and EMI manufactured the P391 system as one of the sensors in the reconnaissance pod fitted to the Phantom RF4M. The radar is still in service with the French Mirage 3RD. It operates at 35GHz and employs a magnetron transmitter to generate 0.1μs pulses at 50 kW peak power. A multielement slotted array antenna produces a horizontal beamwidth of 3.5 mrad. The photographic record gives ground mapping information up to 16 km on both sides of the aircraft. Moving target indication (MTI) may be optionally selected. The use of synthetic aperture (SAR) techniques for reconnaissance is also being pursued. RSRE has developed a

real-time digitally processed, short range synthetic aperture radar. The radar was first demonstrated in 1976 and has subsequently completed a successful series of flight trials. It has a range of 8 km and a range and azimuth resolution of 3m. The meanpower of the transmitter is 4 W. The range resolution is achieved using pulse compression with a transmitted bandwidth of 100 MHz and a chirp compression ratio of 500. The success with the short range SAR has prompted a programme to build and fly a long range synthetic aperture radar. It utilizes ground based processing in conjunction with airborne recording and, at a later stage, will use an air-to-ground data link. This radar is essentially an upgrading of the short-range SAR by the addition of a higher power T/R and a new antenna. Research has also started on the investigation of short range high resolution millimeter-wave SAR for use in unmanned aircraft.

Helicopter Radars

A variety of helicopter radars have been developed in the United Kingdom. MEL developed the first of these, the ARI 5955, in the early 1960s and over 350 went into service in 12 countries on Westland and Agusta helicopters. The radar currently being fitted to the Sea King Mk 5 is the MEL SEA SEARCHER. The transmitter is in X-band and the specific frequency can be varied in flight. The stablized antenna has a gain of 34 dB and scans at 30 rev/min: a manual tilt range of ± 10° is available to the operator. The logarithmic receiver is matched to the transmitted pulse length (two options) and has a noise figure of 8.5 dB. STC is provided. The 17 in flat-screen projection display is employed as in MAREC:five range scales are provided from 0.5 to 16 nm/in. The display unit incorporates two tracking markers and interfaces with on-board navigation systems.

MEL's latest radar in production is SUPER SEARCHER which employs advanced digital radar signal processing techniques. It has a multiple pulse length and PRF, frequency-agile transmitter-receiver which maintains a maximum mean power on the target for optimum detection performance. This radar is currently being produced for the Westland Sea King Mk 42B (the first fully integrated ASW, ASV helicopter). Super Searcher is capable of interfacing with all "active" air to surface missiles and has recently been demonstrated successfully with the Sea Skua "semi active" missile. One of the benefits of this radar is its inherent radar signal processing techniques that enhances target detection whilst minimising the effects of sea clutter. It also incorporates a multiple track-while-scan system that employs a target prediction algorithm, essential in tactical "pop-up" manoeuvres. The system is configured as either an autonomous equipment complete with 14 inch colour raster scan display and keyboard, or as an integrated system being controlled via either an Arinc 429 or MIL 1553B data highway. It is designed to be able to form a central tactical control station, taking and processing other on-board sensor data. Current activities in this area include the combination of both tactical IFF and ESM data management within the same equipment. In addition to this the standard system includes high resolution synthetic coastal outlines and tactical data imagery which can be superimposed on the radar picture. The weight of this radar is 84 kg.

Ferranti manufacture the lightweight helicopter radar SEASPRAY. It was designed specifically to detect and track small surface targets at sea in high states and bad weather. Also it is designed to provide target illumination for Sea Skua missiles. Frequency agility using a spin-tuned magnetron, and monopulse technqiues are employed in this X-band radar. Total weight is 64kg. This display and control unit is shown in Fig 15. Track-while-scane and 360°

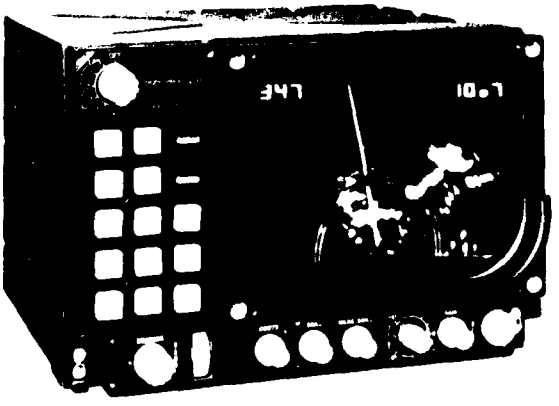

Fig 15 Seaspray display

azimuth coverage are provided in the Mk 3 version of this radar. Over 160 SEASPARY radars have been delivered to 7 navies: the SEASPRAY has also been fitted to the Lynx helicopter.

The BLUE KESTREL radar is in development for the Royal Navy by Ferranti and is suitable for the EH101 helicopter which is the Sea King replacement aircraft. Operating in X-band and using pulse compression, the antenna (Fig 16) can scan continuously through 360° or in a chosen sector. This is a high performance multimode radar with long range detection performance, flexibility in operating altitude, and multiple target track while scan. It can be fully integrated into an avionics suite through a MIL 1553B bus control interface.

Fig 16 Blue Kestrel Antenna

During the Falklands conflict it was clear that the British Naval task force without an airborne early warning radar capability was vulnerable to attack by low flying aircraft armed with air-to-surface missiles. By making use of the screening from the island, hostile aircraft could approach beneath the ship's radar cover to a range where they could launch their missile. THORN EMI modified the SEARCHWATER radar to provide an aircraft detection capability at ranges which would allow the effective deployment of combat air patrol aircraft or surface-to-air missiles. In order to provide a 360° uninterrupted view, the antenna is mounted on an arm projecting from the side of the Sea King (Fig 17) and protected from the elements of an inflatable radome. The reflector is larger than that of Searchwater and provides a pencil beam with circular polarization. The signal processor has been modified to remove the normal long term integration used for ship detection, while still providing false alarm rate control in the clutter limited range.

Fig 17 Sea King AEW

RSRE and Ferranti are working together on a rotor blade radar (Fig 18). This unusual X-band radar consists of a long antenna

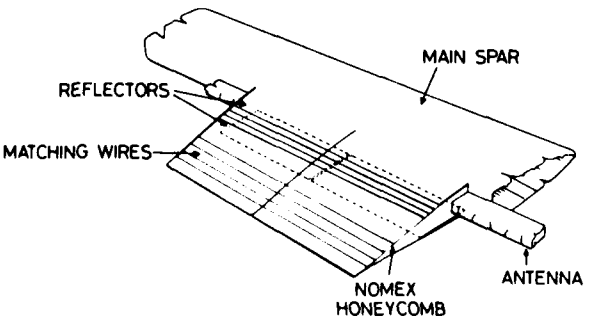

Fig 18 Rotor Blade Antenna

radiating from the trailing edge of a helicopter rotor blade. The narrow azimuth beamwidth coupled with a very short pulse at high PRF produces a clear, high definition radar picture. The system has been flying in a trials aircraft since 1980.

RSRE have actively supported and sponsored developments in the whole helicopter radar area for the UK.

Weather Radar

A wide range of weather radars have been made in the United Kingdom, including the EKCO range now handled by MEL. Here the technology used in these radars will be indicated rather than details of the many individual types. All operate at a wavelength of 3.2 cm (X-band) which has been found to produce adequate returns from the larger droplets in turbulent clouds while not suffering from excessive attenuation. Both two-axis and three-axis scanners are in use with vertical plane beam tilt available to the operator. A pencil-beam radiation pattern is provided for the normal weather mode and in some types beam spoiling is available as an in-flight option so that a ground mapping capability is available. Horziontal polarization has been preferred. Transmitter powers are in the range 10 to 70 kW. The RF pulse is obtained from a magnetron, both tube and solid-state (thyristor) modulators are in use. A PRF of 400 Hz or 200 Hz is employed locked to the aircraft ac power lines, and the pulse length is usually in the range 2 to 6 s.

Millimeter-Wave Efforts

In the millimetric field a significant amount of work is being undertaken in order to identify the potential performance of future weapons systems. For example, at British Aerospace a millimetric programme started several years ago with radar concept studies. This led to a measurement programme in order to identify real-world effects. Measurements on tactical targets, clutter of all types, and potential countermeasures are continuing. Three equipments in use are a monostatic noncoherent solid state radar which has been flown in the United Kingdom and Germany: a twin antenna ground based, noncoherent, radar which gives outputs of the orthogonal amplitudes of the received complex polarized wave, as well as the phase difference between them: and a solid state, pulsed radar which can operate in several modes - viz coherent fixed frequency, frequency agile on a pulse-to-pulse basis, chirp pulse compression to give narrow range gate widths, a range of fixed pulsewidths and pulse-to-pulse polarization agility for all linear and circular polarizations. Investigations are in hand to produce a radar which can be flown on a high speed aircraft in order to demonstrate the potential of such a sensor.

Antennas

To conclude this section particular mention must be made of UK efforts, largely RSRE sponsored, in airborne antennas. Design of airborne radar antennas is dominated by the needs for light weight, large angular scan range, and low sidelobes and also in some cases by requirements for broadband or multiple-band operation. Over the years, research has evolved techniques for providing these properties, though not necessarily all simultaneously. As antenna performance has improved, however, the degradations introduced by the radome have come to dominate installed performance by introducing transmission loss and angular boresight error and increasing the sidelobe level. Moreover, radomes have limited frequency passbands, not necessarily well matched to requirements, and often also carry additional hardware such as lightning diverters or pitotstatic tubes which exacerbate the degradations. Study of electromagnetic scattering by radomes is thus an important aspect of airborne radar antenna research in the United Kingdom. Prediction of scattering by detailed numerical modelling is being pursued by several groups. The problems are the establishment of techniques which are adequately accurate yet do not require excessive computing power, and the provision of experimental verification. Some success is being achieved with the technique of the method of moments. Investigations are also in progress on methods of designing microwave radomes with more control of frequency passbands than is offered by conventional structures. The use of dielectrics loaded by thin wires or other metallic structures appears to be a very

promising approach for modifying passbands, providing stopbands, and for making RF structures which are 'invisible' outside the frequencies of their primary function.

Seekers and Fuzes

Radar missile guidance has been undertaken for more than 30 years by Marconi Space and Defence Systems Ltd (MSDS). Their first monopulse semiactive radar seeker (40 cm diameter) was for Sea Dart, a long range surface-to-air missile providing area defence for ships. An improvement programme is currently underway.

The design of Sky Flash, a medium range air-to-air missile, was based on the existing Sparrow 7E wing, motor and warhead, but with a new British forebody, including an MSDS semiactive monopulse seeker (Fig 19). The effects of target glint have been made small and very low miss distances have been achieved; about 50 percent of the firings have been direct hits. Multiple target discrimination, using Doppler techniques, has significantly improved the kill probability against operational target groups. Sky Flash is in service with the RAF and Royal Swedish Air Force.

Fig 19 Sky Flash Seeker

A semiactive radar seeker has been developed for Sea Skua, a sea-skimming antiship missile which can be carried by the Lynx helicopter. The development firing trials were outstandingly successful. Sea Skua entered service with the Royal Navy in 1981.

Much work has been completed on active air-to-air seekers using both solid-state and tube devices. The development of digital detection, acquisition, and response to ECM threats all under the microprocessor control is at an advanced stage. A beneficial feature is the flexibility available for dealing with new forms of countermeasures. This programme has included the construction of a prototype 150 mm antiair seeker which has a wide angle of look to meet the requirements of short range engagements. This seeker is very much smaller than any active seeker in service and is suited to the NATO ASRAAM program. Considerable research has been undertaken on millimeter wave systems and from this has stemmed an active seeker suitable for use in a terminally guided submunition (TGSM) in an antiarmour application such as the multiple launch rocket system.

The development is well advanced of the active radar seeker for Sea Eagle (Fig 20) a long range sea-skimming missile capable of being launched from the Buccaneer, Tornado and Sea Harrier. The design of this 375mm diameter seeker uses an advanced concept of software control by means of an on-board computer to provide autonomous operation in fire-and-forget engagements.

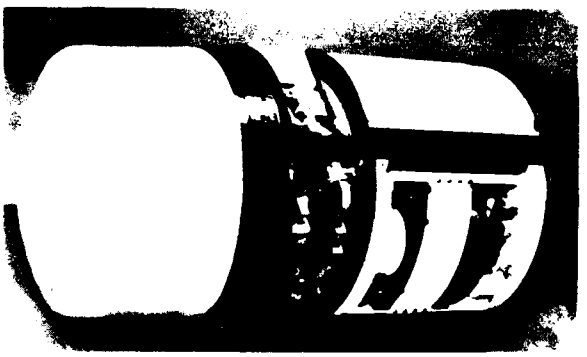

Fig 20 Sea Eagle Seeker

Radar proximity fuzes have been developed and manufactured by Thorn-EMI Electronics Ltd for most of the UK antiaircraft missile systems and for antisurface target applications. Each specific fuze needs to be matched to the characteristics of the missile which carries it, to those of the guidance system, to the warhead, and to the type of target. Its basic requirement is the need to generate a precisely timed output trigger pulse in response to the immediate proximity of the target without compromising the mission by premature operation. Detection of a target is achieved by the use of a hollow conical beam

from an antenna mounted on the skin of a missile, typically 4 slot arrays equally disposed around the missile body diameter. The manufacture of electronic circuits is based on hybrid thick-film technology, which permits the high component packaging density needed in missiles to ensure a low volume and weight. The electronic circuitry, for a representative in-service fuze, occupies a volume of approximately 350 cc. Microwave stripline and microstrip both have relevance to fuzing, but stripline circuits offer an overall volume-saving because of the elimination of the air space associated with microstrip circuits. Proximity fuzes currently in service include those in the Bloodhound, Sea Dart, Seawolf, and Sky Flash missiles.

Close

In this short article it has not been possible to mention every item of radar work that is under way in the United Kingdom. Furthermore, new advances and developments were being announced throughout the preparation period of the material, so it is not possible to claim that this review is definitive. However, this paper does give a representative picture of the wide range of radars that are in production or being developed. This may be taken as the backcloth against which the scientific endeavours at RSRE take place.

For the future, the increasing power of digital signal processing will be exploited in flexible programmable processors, relieving or even eliminating operator workload. The use of planar antennas, broadband components, and other features will continue to improve the ECM resistance of military radars. Wide bandwidth and low sidelobes are considered important, and there is a growing interest in multiple beam radars compatible with future multistatic concepts. Increasingly self-test functions will be provided as a major contribution to lowering operating costs.

The whole of the UK radar community looks forward to the future with confidence in its own abilities.

Acknowledgements

Many colleagues in the radar industry supplied material for this article. I am particularly grateful for the close collaboration of Prof D E N Davies, UCL; Mr M Radford, Marconi Research Centre; and Mr K F Slater, ASWE. Much of this material was published by the Aerospace and Electronic Systems Society, IEEE in September 1984.

The Author

John Clarke joined the Airborne Radar Group directly after submitting his Doctoral thesis on "Synthetic Aperture Radar" to the University of Birmingham. Throughout his career he has undertaken applied research on reconnaissance and surveillance radars and in recent years has taken a particular interest in Airborne Early Warning. He has published numerous papers on his work and has edited 3 books. The 1980 Military Conference was chaired by Dr Clarke and he has served the organising committees of all recent international radar conferences. He edits the radar, avionics and EW portion of IEE Proceedings and has been Chairman of the IEE Microwave Devices and Techniques committee. Within the IEEE Aerospace and Electronic Systems Society he is a member of the Radar Panel.

AN EXPERIMENTAL PHASE-CODED RADAR FOR THE MILLIMETRE BAND

P A Jefford, D E Lloyd and J C Parker

Introduction

The cost of RF hardware is of major concern in future solid-state radars and the key to exploitation of the higher frequency bands lies in the use of relatively low-cost integration technologies for applications requiring large quantity production. Applications requiring solid-state transmitters also suffer from semiconductor device limitations on the available transmitted power and this becomes more of a constraint at the higher frequencies. A CW transmitted waveform can be used in order to achieve maximum mean power from the simplest (and cheapest) of solid-state RF sources using single devices such as the Silicon IMPATT. State of the art results for IMPATT (single) devices approach 1 W CW at frequencies up to 100 GHz while pulsed results achieve in the region of 100 mW mean power at the same frequencies. It is important to examine the alternative CW modulation options for solid-state radars, particularly when low unit cost is a major consideration.

FMCW radars offer flexibility in waveform tailoring but suffer from difficulties in implementation and from range-doppler coupling. The problems in achieving sufficiently close control of frequency sweep in a source which will supply adequate prime transmitter power at an appropriate cost should not be underestimated. An alternative to FMCW is pseudorandom code (PRC) modulation implemented by means of phase-shift or frequency-shift keying on a CW carrier.

This paper describes an experimental radar head for tracking and guidance applications which was designed with the aim of achieving simplicity and potentially low unit cost in the RF hardware while maintaining adequate performance and versatility in the complete system. The technique of PRC (or maximal length sequence) modulation using a PIN diode phase reversal modulator allows 'repeatable' implementation, appropriate for integrated systems, and provides for the use of doppler information in target discrimination. However, PRC radars suffer the disadvantage of range sidelobes whose average level remains fairly constant over all range cell positions and the work described here has concentrated on the measurement of these range sidelobes. A further advantage of PRC radars is that a multiplicity of codes are available and this feature is useful when a number of radars are to be operated in close proximity.

The Radar Design

The basic features of the radar design are shown in the block diagram of Figure 1. The

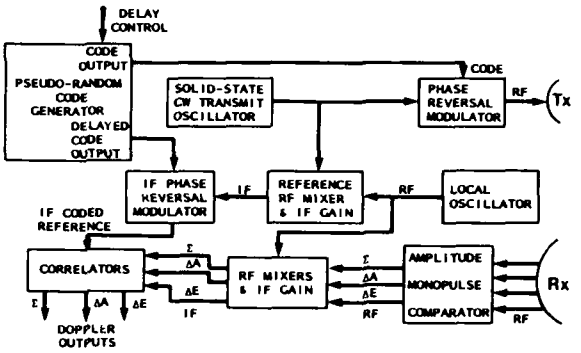

Fig 1 Block Diagram of Radar

transmitter section consists of a free-running CW IMPATT oscillator and a PIN diode phase reversal modulator switched by the master code output. The coded CW carrier is then transmitted via a single beam illuminating antenna. A small portion of the unmodulated oscillator output is coupled off to provide a phase reference for the receiver. The four beam monopulse receive antenna connects to a conventional amplitude monopulse comparator giving sum, azimuth difference and elevation difference output channels which are processed in 3 parallel receive channels to provide angle tracking information. The received RF signals are downconverted in separate balanced mixers to an intermediate frequency given by $f_{IF} = (f_T - f_{LO}) + f_d$ where f_T is the transmitter frequency, f_{LO} is the frequency of the free-running local oscillator and f_d is the doppler frequency corresponding to an approaching target. After IF amplification these signals are fed into the 3 correlators to produce the sum, azimuth difference and

elevation difference doppler outputs. The local oscillator output power is split 4 ways to drive the 3 receive mixers and the reference channel mixer which downconverts the unmodulated coupled output from the transmitter to the reference IF frequency (= $f_T - f_{LO}$). After amplification this reference signal is phase reversal modulated by the delayed code waveform to provide drive signals for the 3 correlators. Thus the code correlation function can be achieved by means of a double balanced mixer at the IF frequency and the amplitude of the doppler outputs corresponding to a target at a certain range is controlled by setting the programmable code delay appropriate to that range cell position. Target and clutter returns from other range cells are suppressed according to the range sidelobe level (or ratio of sidelobe to correlation peak). Control of the code delay facilitates range sweeping for target acquisition and also range tracking of an identified target.

The theoretically ideal range sidelobe level for an N bit repetitive maximal length sequence is given by $-20 \log_{10} N$ (dB). Two code generators have been used with the experimental radar based on 8 and 10 stage shift registers with feedback giving 225 bit and 1023 bit code repeat lengths respectively. Each generator provides a delayed code with time delay programmable in one bit increments and the 255 bit code delay can also be controlled in 1/10th bit steps. The radar waveform parameters are shown in Table 1.

The code parameters can be changed to suit particular applications and within the waveform parameters different code sequences are available by changing the feedback connections, thus reducing interference problems encountered when operating several radars simultaneously in close proximity. Note that doppler ambiguities can arise for f_d greater than half the code word repetition frequency and that severe degradation of the range sidelobe level occurs for doppler frequencies greater than (say) 1/4 of the code repetition rate [1]. These problems can be overcome for high doppler applications by artificial reduction of the difference frequency occuring at the correlator by means of a shift in the IF reference frequency before the phase reversal modulator. This technique also raises the possibility of a clutter locking system able to discriminate targets moving relative to ground clutter from a radar on a moving platform.

The range sidelobe of the radar, measured as a function of code delay, is degraded from the ideal 1/N ratio due to many factors such as code risetimes, timing errors, amplitude and phase errors from the RF and IF bi-phase modulators, and gain and phase variations in the IF amplifiers across the bandwidth of the received signals. We are interested in the peaks of this function, which can appear as false target indications at different ranges, and in the average range sidelobe level which provides rejection of all unwanted targets and clutter over the whole field of view of the radar. Typical millimetre-wave applications may require a -40 dB, or better, average sidelobe to cope with rain backscatter, ground clutter and transmit-to-receive antenna leakage from adjacent apertures.

Details of the Experimental Radar

A 35 GHz prototype radar has been built using metal waveguide components in order to demonstrate the techniques described above without attempting to integrate the various component functions. The radar head is shown in the photographs of Figure 2 complete with transmitter, antenna system, monopulse comparator, RF balanced mixers, local oscillator and IF panel. Shown on the

TABLE 1 RADAR CODE WAVEFORM PARAMETERS

Length of Code (bits)	Bit Length	Range Resolution (ns)	Code Word Length (ms)	Maximum unambiguous Range (m)	Code Word Repetition Frequency (KHz)	Ideal Range Sidelobe Level (dB)
255	66	10	16.8	2550	60	-48
1023	13	2	13.3	2046	75	-60

IF panel are 3 receive channel amplifiers, reference channel amplifiers, power splitter, and the 3 correlators.

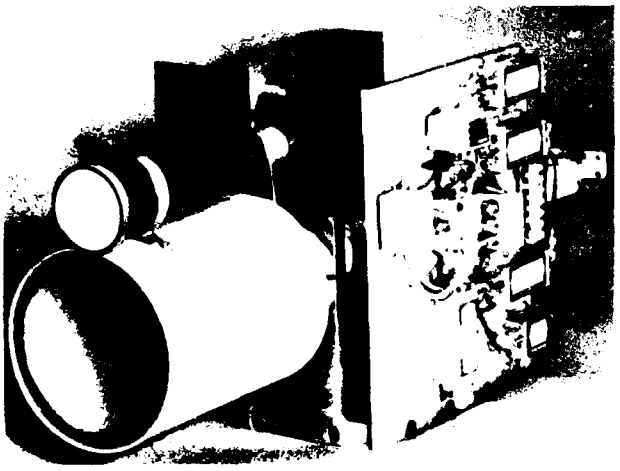

Fig 2 Experimental Equipment

The overall aperture dimension including both transmit and receive antennas is 180 mm and the diameter of the monopulse receive antenna is 120 mm. The aerial system and the RF monopulse comparator were designed and manufactured by Thorn-EMI Electronics Ltd (Wells, UK). The linearly polarized antenna assembly incorporates a 12° transmit beamwidth with a 5° sum pattern from the four beam monopulse receive antenna using a lens and corrugated four port feed structure. Isolation between transmit and receive antenna (sum port) was originally specified at 70 dB and better than 90 dB was achieved in practice with either plane of polarization. Flat sheets of dielectric placed ~10 cm in front of the aerials degraded this isolation but a figure of 75 dB could still be achieved with some materials. Figure 3(a) shows the antenna patterns for the sum and azimuth channels

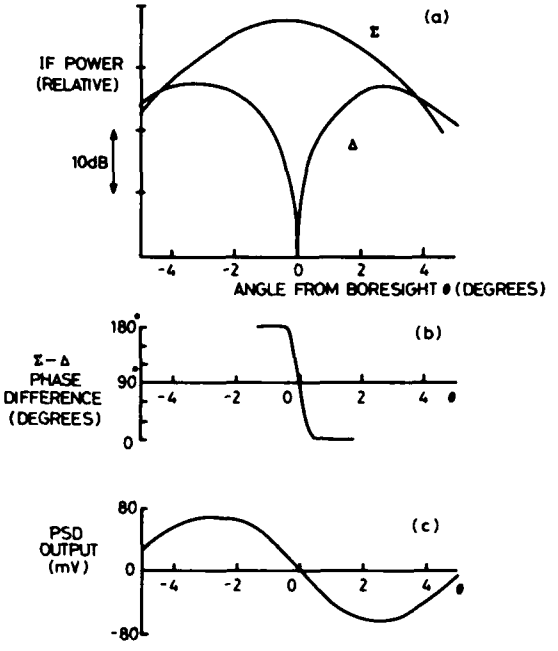

Fig 3 Azimuth Measurement Characteristics

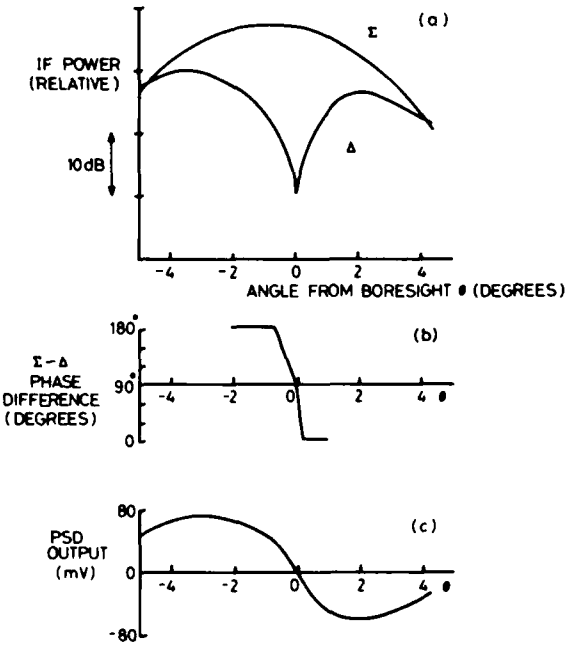

Fig 4 Elevation Measurement Characteristics

measured at the IF frequency (post amplification) using a stationary corner reflector and Figure 3(b) shows the phase difference between the two IF channels leading to the phase sensitive detector output as a function of antenna angle in Figure 3(c). Plus or minus steering feedback is available over an angle of>10°. Similar curves for the elevation channel are shown in Figure 4. (Note that these curves were measured after trimming IF lead lengths to compensate for small phase errors in the RF and IF channels).

The transmitter consists of a 200 mW CW Si IMPATT oscillator followed by a coupler, isolators and the waveguide modulator. The coupled output is approximately 66 dB down on the total oscillator output power. It was found that good isolation was required in order to prevent significant pulling of the oscillator frequency by the modulator and two 25 dB isolators were used to maintain a reasonable transmitted spectrum. (Lower isolation could be used if the modulator input was better matched at this frequency). The modulator (whose design originated from the British Telecom Research Laboratories, Martlesham, UK) [2] consisted of a coaxially mounted PIN diode in a waveguide cavity connected to one port of a 3-port circulator to provide 180° phase switching. The switching time was of the order of 1 ns and insertion loss was between 2 and 3 dB (although a lower insertion loss had been achieved in the same circuit). The modulated output power of the transmitter was approximately 75 mW indicating a total insertion loss >4 dB, between oscillator and antenna, which could be improved by careful design.

The Gunn local oscillator frequency was ~400 MHz below the transmitter frequency and the E-plane mixers were followed by 60 dB gain in each channel at the 400 MHz IF. The 3 correlators (double balanced mixers) were driven at LO power level by the reference channel IF signal after bi-phase modulation with the delayed code. The amplitude of the doppler output from the sum channel correlator was measured, after filtering, using a programmable voltmeter with averaging facility, and dc steering information was obtained using phase sensitive detectors between the sum and difference doppler channels.

The spectrum of the transmitted waveform using the 255 bit code is shown in Figure 5(a) and for the 1023 bit code in Figure 5(b). Note that the former is a much cleaner spectrum than the latter because the code risetimes and timing errors in the modulator and code drive circuitry are proportionately much larger in the 1023 bit code compared to its shorter bit length. The difference is between 66 ns and 13 ns bit lengths where the switching times and timing errors are of the order of 1-2 ns.

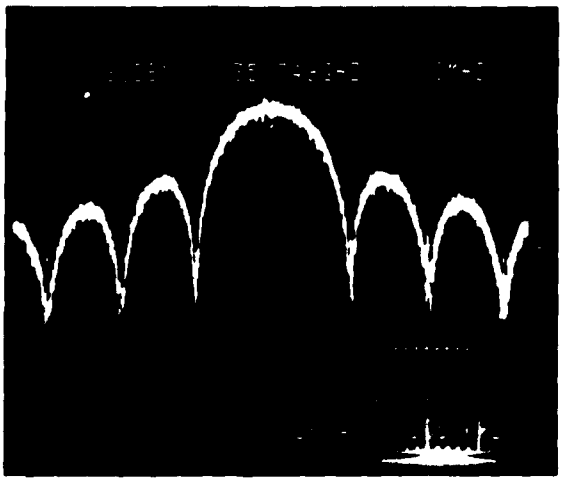

(a)

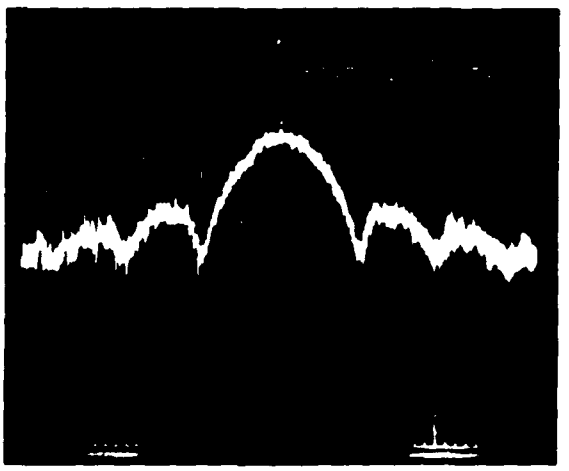

(b)

Fig 5 Transmitter Spectrum

Similar degradation occurs in the spectrum of the IF coded reference signals for the longer code with shorter bit lengths. Furthermore, the faster 1023 bit code sequence produces a phase-modulated carrier

with a wider signal bandwidth than the 255 bit coded waveform and this leads to worse distortion due to gain and phase variations across the IF amplifier band. The consequences of these effects on the radar performance will be seen in the measurements of range sidelobes.

Experimental Results

A single target moving with constant velocity was simulated using a 1.4m diameter rotating cylinder with radially mounted vanes developing tangential speeds of up to $\sim 20\ ms^{-1}$. Range sidelobe measurements were performed by setting the target speed constant and measuring amplitude of the doppler signal voltage in the sum channel, after passing through a bandpass filter centred on the 2.2 KHz doppler frequency, as a function of code delay. The voltage readings were sampled and averaged over time in order to reduce the effect of the fluctuating target and the results are normalised to the maximum peak and plotted against range (Range = No. bits delay x range cell width). In the case of the 255 bit code the delay was stepped in $\frac{1}{2}$ bit increments (5m steps) and for the 1023 bit code in 1 bit increments (2m steps).

The distance from the radar to the target was approximately 35m and Figure 6(a) shows a measured result for the 255 bit code where the true target return appears at a range of $\sim$ 30m. (There is a constant range offset error due to propagation delays around the RF, IF and code circuits which is different for the two codes but can be calibrated out). The average sidelobe level is approximately-40 dB compared with the ideal theoretical limit of -48 dB for a 255 bit code. A second peak occurs at $\sim$65m range which is -24 dB down on the real target peak and all other peaks are below -33 dB. The basic structure of the curve and the peak positions can be measured repeatably. Secondary peaks occur for a number of reasons and can appear as false target indications. Figure 6(b) shows a different result for a similar measurement but where the transmit oscillator bias current was changed very slightly to reduce the amplitude of the peak at 65m and now all peaks are below -30 dB with an average level better than -42 dB. This is a rather better result than shown in Figure 6(a) and indicates the sensitive interaction between the IMPATT oscillator and the modulator and it is felt that this is an area worthy of more careful attention to design. (The design of the modulator used in this experimental radar was not optimised for a good match to the oscillator at the particular RF frequency). However, these results show a very useful performance for many applications.

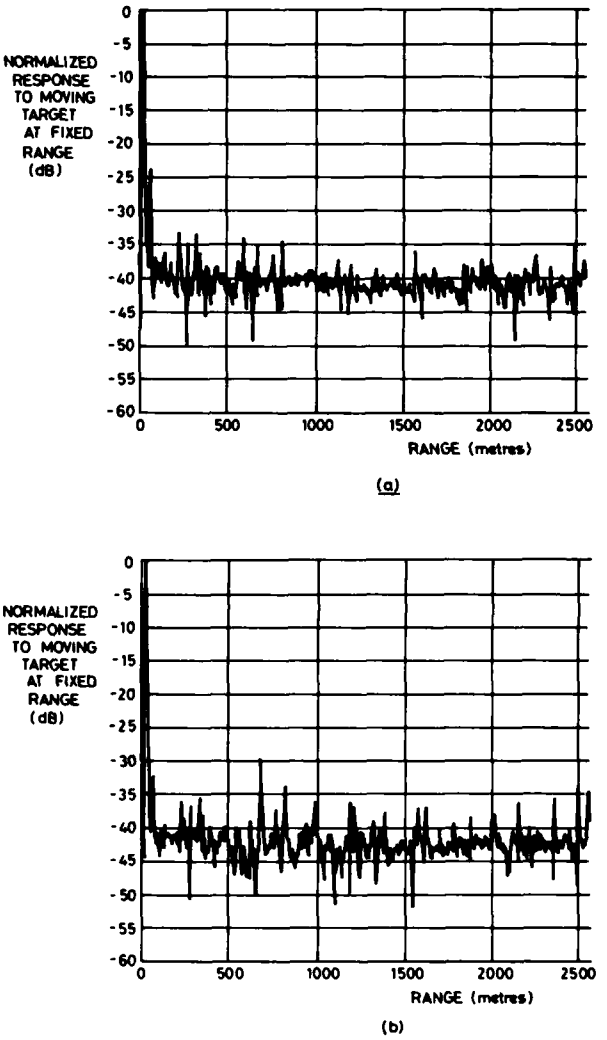

Fig 6 Range Sidelobes, 255 bit code

Figure 7(a) shows the result of a measurement using the 1023 bit code with 2m range resolution and the target peak occurs at $\sim$40m range (20 bits delay). The average sidelobe level is of the order of -38 dB and 3 main peaks appear at 96, 967 and 742 bits delay (192m, 1934m and 1484m respectively). The peaks at 96 and 967 bits delay are paired echoes about the real target peak at

20 bits and are probably due to gain and phase variations across the signal bandwidth in the IF amplifiers. The peak at 742 bits is sensitive to IMPATT bias and is therefore due to oscillator-modulator interaction. Changing the position of the IF bi-phase modulator in the reference channel amplifier chain (so that the modulation is applied to a higher level signal) gave the result shown in Figure 7(b) where the paired echoes are reduced in amplitude. In this measured result a secondary peak, which was bias sensitive, appeared close to the real target peak. The ideal range sidelobe level for the 1023 bit code is -60 dB and it is believed that the measured average level is degraded from the ideal, more than in the case of the 66 ns bit length code, due to the larger proportional switching times and timing errors in the 13 ns bit code modulation [1]. Further attention to the timing accuracy in the code generators and modulator circuits could significantly improve the average sidelobe level.

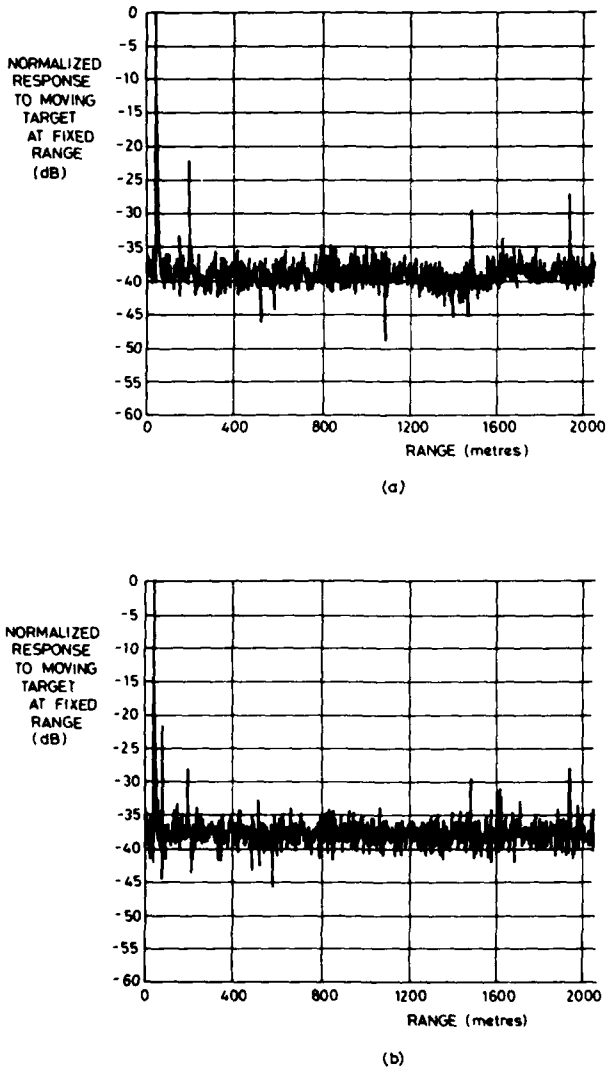

Fig 7 Range Sidelobes, 1023 bit code

Conclusions

An experimental phase coded radar has been used to demonstrate techniques relevant to the need for low-cost integrated microwave and millimetre-wave systems. The technique is particularly useful in solid-state systems for tracking and guidance applications where sufficient transmitter power is not available from pulsed devices. The design exploits the simplicity and low cost of a single device IMPATT oscillator as a transmitter together with repeatable implementation of the RF hardware while providing adequate performance for many applications.

Angle tracking is provided by means of a monopulse receive antenna and range discrimination is achieved using maximal length or pseudorandom code sequences which are modulated onto the transmitted CW carrier by means of a phase reversal switch. A programmable code delay in the reference channel is used to define range cell position and correlation is performed at the IF frequency in a mixer which preserves doppler information at its output. A 35 GHz radar has been demonstrated with an overall 180 mm diameter aperture using 66 ns and 13 ns bit length codes to provide 10m and 2m range resolution respectively. Range sidelobe measurements have shown that average sidelobe levels of the order of -40 dB are easily achieved which may be adequate for some applications. Further attention to code timing errors and changes in code waveform parameters could lead to improved average sidelobe levels for the radar. Peaks in the range sidelobe pattern arise from a number of causes and careful attention to design of the RF modulator is needed to minimise the effects of interaction between transmit oscillator and modulator.

The technique described can provide fine range resolution in a potentially low-cost radar which could radiate several hundred mW of CW power at frequencies up to 100 GHz. The PRC modulation scheme avoids the

problems of frequency control, implementation difficulties and range-doppler coupling which occur in FM CW radars.

References

1. D. Silber "Performance of a Pseudorandom Binary Phase Code with Errors and Doppler-Shifted CW" IEEE Transactions on Aerospace and Electronic Systems Vol AES-17, No 6, November 1981.

2. I.S. Groves, D.R. Borley, B.L. Clark "A Four-level HighSpeed Millimetre-wave PIN Diode Phase Modulator".

   Post Office Telecommunications Headquarters Research Memorandum No 76 R7/1 February 1976 (now British Telecom Research Laboratory, Martlesham, UK).

The Authors

Dr P A Jefford joined RSRE in January 1980 and was engaged in millimetre-wave subsystems research until 1984/5. This work aimed to exploit the emerging millimetre-wave device and circuit technologies into demonstrator subsystems and to devise techniques which were appropriate for low cost RF integrated circuit applications. D E Lloyd and J C Parker have worked in support of this research programme. More recent research has been associated with microwave phased array techniques and in particular the exploitation of Gallium Arsenide technology and optical fibre links for the distribution of microwave signals in transmit/receive array systems. Dr Jefford is now with the GaAs Unit, STC Components Limited, Paignton, Devon.

BISTATIC RADAR FOR LONG RANGE APPLICATIONS

C Pell

Abstract

A brief summary of the main characteristics and properties of bistatic radar as applied to long range air target detection is presented. The main system functions are highlighted and indications are given of the processing tasks required. An example of a bistatic system is included and this is used to illustrate the likely detection performance and surveillance coverage that could be achieved.

Introduction

It is clear from the number of papers presented in the open literature over the past 10 years that there is considerable interest in the subject of bistatic and multistatic radar detection systems. The reported work has covered both system concepts, as exemplified by Ewing and Dicken [1], several techniques issues including synchronisation by Retzer [2] and beamforming by Schoenenberger et al [3]. The applications have included both the short and long range requirements as discussed by Milne [4] and the long range, experimental Sanctuary system reviewed by Fleming and Willis [5]. The Sanctuary programme is particularly noteworthy, since it is a highly complex system, employing a moving airborne illuminator and a fixed ground-based receiver. Also, it is one of the few examples where systems and techniques concepts have been taken through to a complete experimental system, perhaps indicating the level of complexity of bistatic systems.

The bistatic detection principle can offer worthwhile performance advantages, both for surface-based and airborne sensors. In addition to the military applications indicated in the published work, it is possible that civil radar applications may also exist. These might take advantage of the bistatic geometry to compensate for tangential MTI (moving target indication) fades, to allow autonomous receive-only radar elements and to generally reduce the signal dynamic ranges encountered. Bistatic radar is not the ideal system solution for every requirement and it is necessary to carefully study individual requirements in relation to bistatic, monostatic and netted monostatic sensor solutions.

System Characteristics

It is necessary at the outset to define bistatic radar as covered in this short treatment. It will be defined as an active radar system in which significant spatial separation exists between the illuminator (transmitter) and receiver subsystems. "Significant" is defined as many times the effective aperture of the antennas employed. For example, a spatial separation of say, 10 Km associated with antenna apertures of 15 m falls within the definition. However, a system employing two contiguous antennas separately used for transmit and receive (as sometimes used for a CW monostatic configuration) does not fall within this particular definition of bistatic.

The specific signal and data processing functions that are required within any bistatic system depend upon the configuration and application of that system. For the surface-based sensor applications, the sensor (transmitter and receiver) element positions are invariant over the processing intervals considered. However, a "hybrid" system [5] employing a combination of fixed surface sensor elements and moving airborne elements is a viable concept. A more complex architecture is the totally airborne bistatic system with both receiver and transmitter elements in (independent) motion with respect to both targets and the surface. Clearly, a hybrid or completely airborne system necessitates processing functions that are additional to those required by the surface-based system.

In the airborne case, dynamic derivation of accurate sensor position information, antenna directionality information and general system control are required. Furthermore, whilst in the majority of surface-based systems, coherent processing for sub-clutter visibility and general clutter control is needed, the requirement

is more complex in the airborne case. In addition to the Doppler-shifted ground clutter and clutter spectral spreading caused by platform motion, the airborne bistatic system must accommodate sensor platforms having different velocity vectors as well as antennas exhibiting differing directionality characteristics.

An issue that is to be considered in any bistatic system design is the optimal receiver and transmitter antenna configurations. The antenna option selected not only affects the antenna function, but also has a substantial impact on the subsequent signal and data processing. Ewing and Dicken [1], for example, consider a combination of a static, floodlight transmitter (wide angular beamwidth) in combination with a sequentially scanned or multi-beam receiver. Milne [4] considers a wider range of transmitter and receiver antennaconfigurations including space-orthogonal scanning, directionally-decorrelated beams and interferometric receive processing. All of these fairly complex options significantly affect the processing functions required.

System Processing Functions

In common with all future radar systems, bistatic radar for long range defence applications will require new transmitter techniques, enhanced survivability optimisation of waveforms and covertness (both in the electromagnetic and physical senses). However it is suggested that it will be the system processing functions that will be most demanding and differ most from future monostatic radars [6]. The main processing functions required are:

a. Antenna Array Processing

A consequence of bistatic operation at other than very short baseline lengths (pseudo-monostatic) is the difficulty in achieving effective volumetric surveillance coverage. A single-beam, fast sequentially scanned receive antenna can be considered with simple waveforms but efficient operation can generally only be achieved with a multi-beam antenna configuration. In some cases the synthesis of a limited number of independentlycontrolled, angularly-agile beams is satisfactory. The synthesis of a fully populated sector of independent contiguous beams, however, allows superior flexibility. This is shown in figure 1 for an azimuth sector. For practical

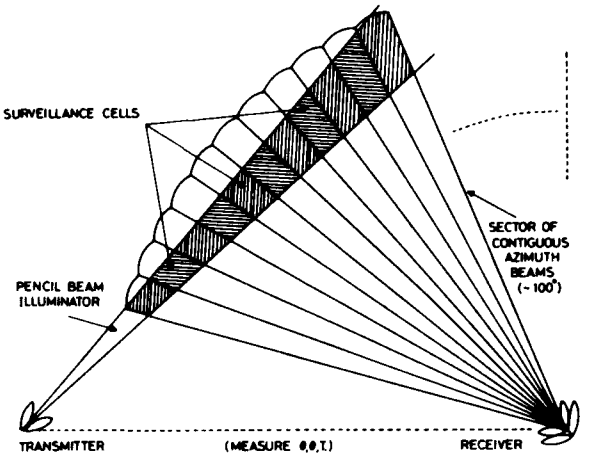

Fig 1 Multiple, contiguous beam receiver configuration

beamforming over a useful coverage sector, array antennas are dictated using RF, IF or baseband digital beamforming. On the grounds of efficiency, intrinsic performance and cost, IF analogue beamforming is a strong contender using today's technology. However, in addition to the basic beam construction, beam control is equally important, where the real-time control of perhaps 100 individual beams is required. For the future digital beam control or digital beam forming may find the bistatic receive antenna a fruitful application area.

b. Matched Filtering

The most important aspect of matched filtering for bistatic radar is the degree of flexibility needed to support the potentially wide range of waveforms encountered. These range from unencoded waveforms to coded large time-bandwidth product waveforms for high resolution pulse compression. If only limited waveform flexibility is required, then classical analogue pulse compression can be implemented using SAWS. For greater flexibility and superior performance, a programmable digital matched filter employing a pipelined, indirect convolution processor is necessary.

c. Coherent Processing

In some applications, bistatic operation

allows a greater freedom of choice of waveform, resulting from the spatial separation of the receiver and transmitter. Waveforms more optimally suited to the particular surveillance function and environment may be selected. Such waveforms and modes include CW Doppler, Pulse-Doppler, MTI and Adaptive MTI. A characteristic of bistatic Doppler that must be considered is the increased geometrical sensitivity of performance over the monostatic case [7].

d. Plot Extraction

Strictly speaking the plot extraction function embodies a large number of individual processes, operating in both a serial and parallel architecture. The majority of the processes operate in non-real time, being based upon data manipulation, hypothesis testing, conditioning and association. The major processes are Adaptive thresholding, Incoherent integration, Peak detection, Ambiguity resolution, Data association and Formatting.

In addition to the derivation of the usual sensor output data parameters, extraction of bistatic data must incorporate

- Geometrical transformation from bistatic co-ordinates to a defined R, θ, Φ reference.

- Suppression of sidelobe detections from spurious illuminator main-beam to receiver sidelobe coupling.

- Correction for bias errors that are illuminator-dependent.

e. Synchronisation Processing

An important distinction between a bistatic and monostatic radar system is the need for system synchronisation between the receiver and transmitter. Parameters such as time, frequency and phase are not self-consistent. Some degree of communication, perhaps by the direct path signal in the simplest case, is needed. Generally temporal synchronisation is most demanding and a surprisingly large degree of frequency error can be tolerated without significant performance degradation. However, phase stability remains important in order to achieve a high degree of sub-clutter visibility.

A more extensive treatment of bistatic radar processing functions is given in [8].

Generally, the bistatic radar processing is fairly similar to a modern monstatic radar processor with three major differences:

i. Since, ideally, operation with a wide variety of illuminators is desirable, a high degree of flexibility and reconfigurability of the processing is required.

ii. The characteristics of the bistatic geometry must be taken into account. This applies in particular to the elliptical surfaces of equal transmitter/target/receiver propagation time and the hyperbolic loci of maximum Doppler.

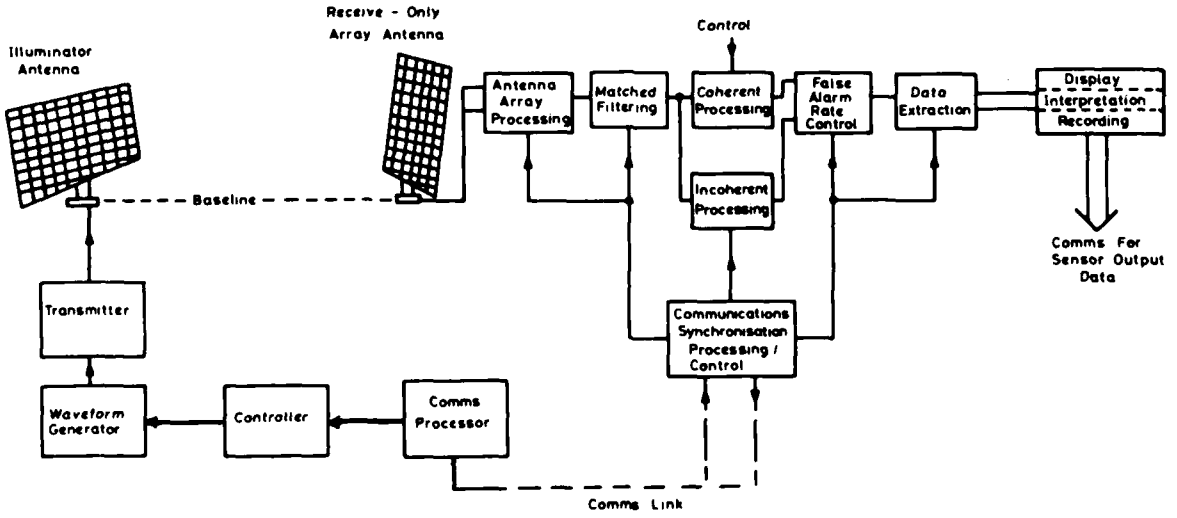

Fig 2 A basic bistatic radar system

iii. The computation, communication and processing of parametric data such as sequence timing, transmission frequency, mode of operation and coherency information may be needed. These are not automatically self-consistent as with a monostatic radar.

A functional represenation of a complete bistatic radar system is shown in figure 2.

System Performance

To complete this short paper, a simple performance and coverage assessment for a candidate bistatic radar system is included. It is assumed that a microwave frequency is selected and the radar detection performance is conveniently expressed in terms of $\sqrt{R_T \cdot R_R}$, where R_T and R_R are the target to transmitter and target to receiver distances. Assuming typical long range ground-based radar parameters and a target (bistatic) radar cross section of 5 m^2, the example of the surveillance coverage obtained is given in figure 3. In this case, the bistatic baseline length is 275 Km. The salient points to note are:

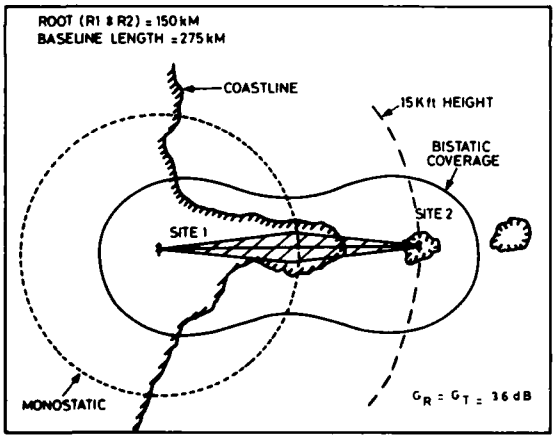

Fig 3 Bistatic coverage

- The coverage contour is considerably distorted from the ideal, monostatic, circularly symmetrical contour and it takes the form of a particular oval of Cassini. Although complex in shape, it allows the characteristic to be exploited by giving a large increase in forward surveillance coverage (at the expense of loss coverage in other regions. Of course certain applications will require a more uniform coverage characteristic, which can be achieved using a shorter baseline than the fairly extreme case shown here.

- Low-level coverage around the receiver site is only afforded if the illuminator is in an elevated position (eg on an aircraft platform at a height of ~15K ft).

- There is no real spatial discrimination (ie detection performance) close to the line joining the transmitter and receiver sites.

- For comparison, the equivalent monostatic radar detection performance (assuming similar system parameters) is shown as the dotted circle centred on Site 1 position.

Conclusions

Bistatic radar is significantly different to monostatic radar in terms of its characteristics, complexities and system architecture. It is not possible to directly answer the question "Is bistatic radar superior to monostatic radar?" The question is over simplistic and it is necessary to address the question on an application specific basis. Certainly, bistatic radar has some characteristics and properties that could be effectively exploited in various applications and it is a fruitful area for continued systems and techniques research.

References

1. Ewing E F and Dicken L W, "Some Applications of Bistatic and Multi-Bistatic Radars". Paris Intl Radar Conference, December 1978, pp 222-231.

2. Retzer G, "Some Basic Comments on Multistatic Radar Concepts and Techniques". Colloquium on Ground and Airborne Multistatic Radar, IEE London, December 1981.

3. Schoenenberger J G, Forrest J R and Pell C, "Active Array Receiver Studies

for Bistatic/Multistatic Radar". Proceedings of Radar 82 Conference, IEE London, October 1982, pp 174-178.

4. Milne K, "Principles and Concepts of Multistatic Surveillance Radars". Proceedings of Radar 77 Conference, IEE London, October 1977, pp 46-52.

5. Fleming F L and Willis N J, "Sanctuary Radar". Proceedings of Military Microwaves 80 Conference, London. October 1980, pp 103-108.

6. Pell C, Fairhead A C and Thomas M B, "VHPIC for Radar". Proceedings of IEE Intl Specialist Seminar on Advanced Signal Processing, Univ of Warwick, September 1984.

7. Hanle E, "Distance Considerations of Multistatic Radar". Proceedings of IEEE 1980 Intl Radar Conference, Arlington Va, April 1980, pp 100-105.

8. Pell C and Crossfield M D, "Signal and Data Processing Architectures for Multistatic Surveillance Radar". Proceedings of Intl Conference "Radar 84", Paris, 1984.

The Author

Chris Pell joined the Ground Radar Group at RSRE in 1979 following a period in the UK defence electronics industry. Prior to that time he was conducting research into millimetre wave radar astronomy in which he obtained his PhD. Since coming to Malvern his responsibilities have been in the field of systems and techniques research for future ground-based radars. His particular technical interests are radar signal processing, future system concepts and future technology for radars including VLSI and GaAs MMICS.

NEW ANTENNAS FOR SECONDARY SURVEILLANCE RADAR

J M Shaw

In the past, when SSR was thought of as just a labelling device for primary radar, there was little interest in producing improved antennas for SSR. Only recently, with the increased reliance on SSR and the higher expectation of performance especially with the advent of monopulse, has it been fully realised that there is a need for better antennas. It is particularly important to reduce the signal from the ground which causes the now familiar problems of reflections, vertical lobing and beam distortion. To shape the beam in elevation, an antenna with a larger vertical aperture (LVA) is required.

New LVA antennas, capable of long range performance, have been designed by Cossor and Marconi. Prototypes were built in 1983 and were made available to the Civil Aviation Authority for trials. A trials programme was started with the objective being to see how the antennas performed when installed at CAA radar sites. The training siteat Bletchley was used for monopulse trials, having been equipped with a Cossor 950 interrogator/receiver with monopulse plot extractor and recording system. Sliding window trials were done at Burrington, using the standard Stansaab plot extractors. At each site the performance of the new antennas was compared to the earlier hogtrough antennas.

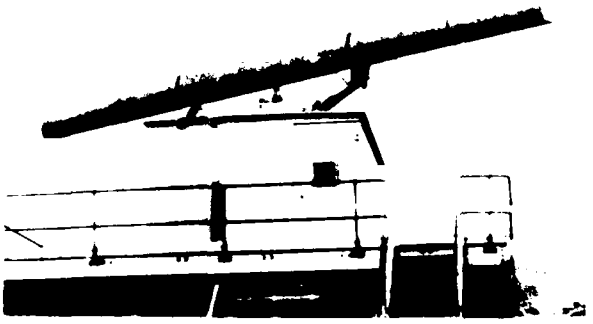

Photo A

An old HOGTROUGH antenna

Photo B

A new LVA antenna

Antennas

Photos A and B show the old hogtrough and one of the new LVA antennas. The important feature of an LVA antenna is the vertical beam shape and the typical form of the radiation pattern is illustrated in Fig 1.

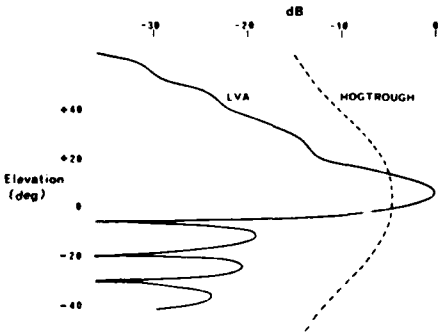

Fig 1 LVA Antenna - Typical Vertical Pattern

Trials

At Bletchley, recordings were made from the monopulse equipment and the performance analysed using the facilities developed for the monopulse plot extractor. This site, being amongst many buildings, provided a useful test for the reflection performance of the antennas. At Burrington, plots were recorded from the Stansaab plot extractors. A series of test flights were flown by

CAAFU, these being similar for each antenna. As expected, the performance of the two LVA antennas was broadly similar. The small sample of results presented here are intended to show the improvements over a hogtrough antenna and can be taken to apply to either LVA antenna.

Reflections

The test aircraft flew an orbital track around the radar at Bletchley. There was a spectacular contrast in the number of reflected plots seen by the LVA and hogtrough antennas, as is illustrated by Figs 2 and 3. Obviously Bletchley is a very bad site for reflections but ideal to demonstrate the effectiveness of an LVA antenna.

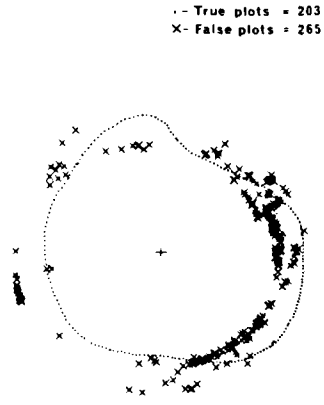

Fig 2 Orbital track - HOGTROUGH

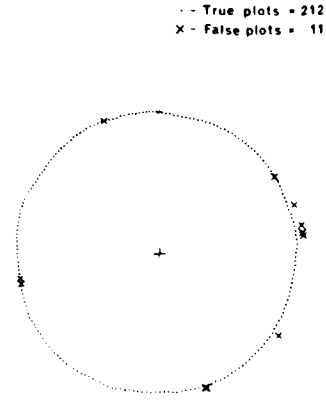

Fig 3 Orbital track - LVA

Similar proportions of reflected plots were seen in the general air traffic and typical percentages of false plots are given in the table below for various values of swept gain (GTC).

	GTC (dB at 1 nm)			
	0	30	36	42
HOGTROUGH	37	31	21	11
LVA	6	4	2	0.5

Percentage of reflected plots at Bletchley

Track Quality

The test aircraft flew radial tracks, the azimuth jitter on the monopulse positions was then analysed. For these tracks, the jitter with the LVA antennas was very small typically 0.03 degrees standard deviation and measurements were limited by the 12 bit shaft encoder at the site. The same tracks seen from the hogtrough antenna had standard deviations two or three times greater.

The improvement in track jitter is mainly due to the attenuation of the multipath signals from the many objects around the site. However, the multipath experienced at Bletchley did not produce the severe or regular distortions like those experienced from the sloping ground at Clee Hill. At a bad site, such as Clee Hill (without the screen), the improvement in azimuth measurement provided by an LVA antenna should be many times greater than a hogtrough.

Vertical Lobing

The amplitude of the plots seen by the hogtrough antenna for one of the radial test

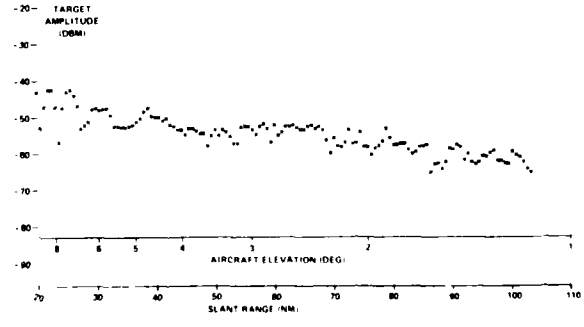

Fig 4 Radial Test Flight Amplitude - HOGTROUGH Antenna

flights is shown in Fig 4. Because the foreground at the site is not uniform, being littered with various structures, the ground signal is decorrelated and consequently the regular lobing expected from a flat foreground is destroyed. Nevertheless, large and rapid fluctuation in received amplitude can be seen. The amplitude of plots seen by an LVA antenna showed relatively little perturbation and consequently the loss of cover caused by vertical lobing is very much reduced by an LVA antenna.

Sliding Window Results

The results from Burrington showed that there was a significant improvement in azimuth jitter of the sliding window plots when using the LVA antennas. Standard deviations of about 0.08 degrees were obtained for the test tracks with the LVA antennas, whereas the hogtrough gave values about twice as much.

The plots of the test tracks as seen by Clee Hill were also recorded and it is interesting to note that the azimuth jitter, from a screened hogtrough antenna, was about the same as the LVA antennas. In effect, a hogtrough with a ground screen is about equivalent to an LVA antenna.

Conclusions

Obviously the new antennas provide a considerable improvement in performance over the old hogtrough antenna and it is unfortunate that they were not available a few years ago. The differences in beam shapes between Cossor and Marconi designs will gain advantage to one or other for various situations and at a particular site one or other may have a slight advantage. Other considerations such as mechanical design, which is significantly different, and cost will, of course, be important factors in the choice.

The Author

J M Shaw joined RSRE in 1968 and has since worked mainly on radar data processing and computing. His recent work has been concerned with improvements to secondary surveillance radar for the Civil Aviation Authority (CAA). In particular, he has been involved with the development of advanced plot extraction techniques using monopulse direction finding. This RSRE work, sponsored by the CAA, has culminated in the successful development of monpulse plot extractors which lead the world in performance and for which the manufacturer, Cossor, have received very many export orders.

COHERENT AND NON-COHERENT PROPERTIES OF K DISTRIBUTED SEA CLUTTER

C J Baker and K D Ward

The prediction and optimisation of radar systems where detection is limited by radar echo from the sea surface (sea clutter) requires a thorough understanding of the nature of the clutter. Statistical fluctuations in the echo often obey the central limit theorem and can be modelled by the well known properties of Gaussian thermal noise, giving a Rayleigh distribution after envelope detection and well defined spectral and correlation properties. However, when the radar resolution is sufficient to resolve the largest spatial fluctuation present in the illuminated surface, the statistical properties of the clutter deviate from Gaussian thermal noise, and non-Gaussian models (or non-Rayleigh after envelope detection) must be developed, from measurements and theory, for processing assessment application. Great care must be taken to avoid tacit assumptions, only valid for Gaussian thermal noise, in the development and application of non-Gaussian models. In this paper a model based on the compound K-distribution is described and related to coherent as well as non-coherent processing.

Non Coherent Processing

Where non-coherent processing is used for detection a number of amplitude distributions have been proposed to describe non-Rayleigh clutter. Lognormal and Weibull distributions have found the most applications. As these distributions fit well to measured amplitude distribution of sea clutter, their use in prediction of single hit detection with a fixed threshold is well founded. However, since they do not address the correlation properties of the clutter, prediction of systems using either spatial or temporal processing may incur large errors. In addition an analysis that includes a determination of the autocorrelation function (or spectrum) can also be misleading since for non-Gaussian processes this does not provide a full description of the clutter and in consequence can mask problems that occur in processing.

Observations of high resolution sea echo at near grazing incidence have shown [1] that the non-Rayleigh nature of the clutter arises principally from the bunching of electromagnetic scatterers caused by large dimension sea waves and swell patterns. This bunching produces a modulation of the usual speckle pattern obtained from the coherent addition of scatterers. Analysis reveals that the speckle component obeys the central limit theorem, is Rayleigh distributed and behaves in all ways like thermal noise; temporally decorrelating in approximately 10 mS (for a transmitter frequency of 10 GHz) or from pulse to pulse if frequency agility is used, and displaying a range correlation commensurate with the illuminated pulse length. The underlying modulation, when expressed in power, has a Gamma distribution and correlation properties very much dependent upon the sea conditions, wave structure and radar parameters and yet is unaffected by frequency agility. Bringing the two components together results in a K distribution for the amplitude distribution of the clutter [1,2].

The strength of this model is not the fit of the amplitude distribution to data, since other models fit equally as well. The advantage is in its treatment of the correlation properties, through the separation into two multiplicative components. It has been demonstrated [1] that the application of this model provides much more realistic prediction and optimisation of signal processing.

Coherent Processing

Measurement of the phase of a received radar signal gives the fine positioning of a target (ambiguous to a radar wavelength) and the time variation of the phase describes its motion. Coherent processing uses this information to discriminate targets from clutter by their velocity. Simple forms of processing include MTI (moving target indication), where signals are cancelled if there is no phase change over a given number of echoes, and Pulse Doppler processing, where the received signal is Fourier

analysed into separate spectral components for thresholding and detection.

Modelling coherent clutter usually consists of measurement of the average power spectrum followed by matching to a suitable analytical expression. For clutter that has Gaussian noise properties this is sufficient, since the fluctuations within each frequency cell will be Gaussian, of random phase, and independent from all the other cells. When considering non-Gaussian clutter the first step is to measure the distribution in each frequency channel. This allows detection and false alarm probabilities for individual range-Doppler cells to be evaluated, but before combining these or evaulating spatial or inter-frequency processing, correlation properties must be considered.

The existence of correlation from frequency to frequency can easily be detected by performing the complex convolution of all the individual frequency cell probability density functions and comparing with the unprocessed or non-coherent distributions. In the case of the K distribution this simply involves summing the shape parameter, ν. For other distributions either moment matching or numerical integration is necessary. If the unprocessed and convolved pdf's are different, correlation must exist and be accounted for in processing assessment. Data presented in [3] of ground clutter can be manipulated to clearly demonstrate the presence of correlation.

For high resolution sea clutter, the separation into two components as used for the non-coherent model [1] provides the easiest method to formulate a practical useful model as demonstrated in the final section.

Coherent High Resolution Sea Clutter

The data to be discussed is from an experimental, coherent, pulsed I band radar with a pulse length of 28 nS (4.2 m range resolution) and a beamwidth of 1.2°. 170 consecutive range gates separated by 3 m provide a range profile centred at a range of 3 Km from a clifftop site, 75 m above sea level. Figure 1 shows a typical Range-Doppler map generated from a 1024 point FFT, using a pulse repetition frequency of 1 kHz. The radar polarization is vertical, the sea state 3 and the aspect approximately across wind. Figure 1 shows the bunching of scatterers, evident in non-coherent records [2], here visible from a variation of mean intensity (averaged over frequency) at each range. The frequency spread at each range is due to the internal motion of scatterers contributing to the echo. A mean Doppler offset, varying with range, is also evident. These properties are demonstrated quantitatively in Figure 2 where the mean power, the mean, standard deviation and skewness of the spectra are plotted versus range. Figure 3 demonstrates in a scatter plot an interesting inverse relationship between the skewness and mean Doppler that is evident on the across wind records. This changes to a direct relationship upwind.

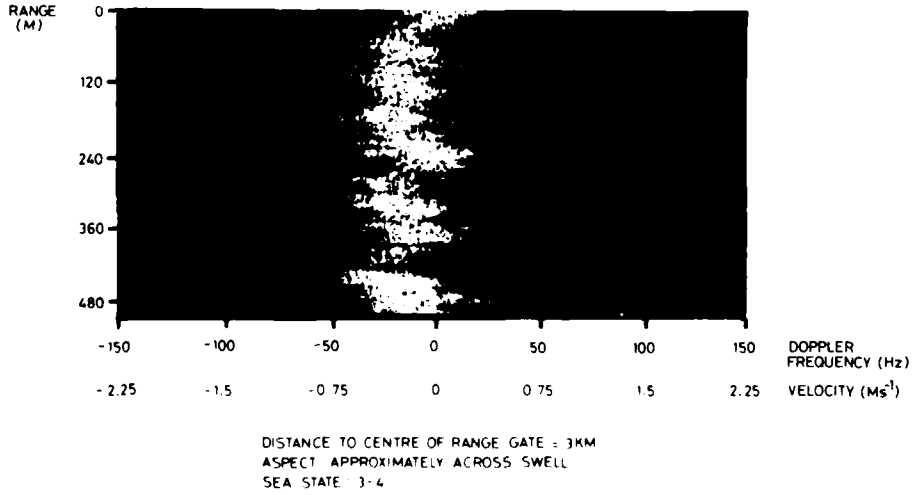

Fig 1 Range-Doppler map of sea clutter

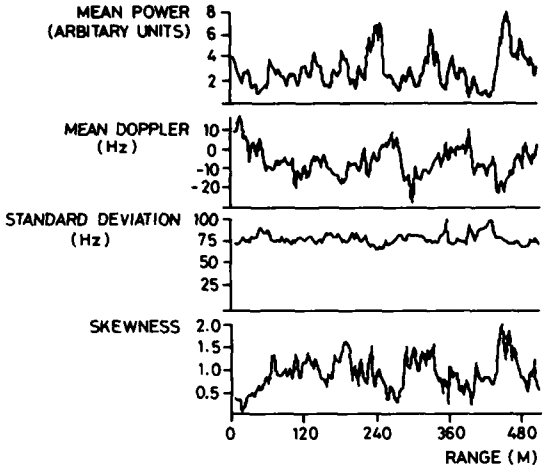

Fig 2 Variation of mean power, mean doppler, standard deviation and skewness of spectra with range

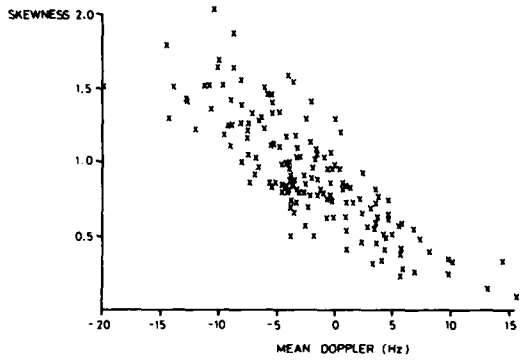

Fig 3 Scatter plot of skewness versus mean doppler

Of interest here, with relation to the earlier discussion on modelling non-Gaussian coherent clutter, is that the amplitude statistics of the power spectrum (derived from either range or time ensembles) would certainly yield non-Rayleigh probability density functions (pdfs) but not indicate the detailed correlation in the frequency domain that generates the effects.

Current work is aimed at quantifying effects described here and towards providing further physical insight into the processes.

References

1. Ward, K D, "A Radar sea clutter model and its application to performance assessment", IEE Conference 'RADAR 82', 203-207, 1982.

2. Ward, K D, "Microwave backscatter from the sea surface", in 'Wave Propagation and Scattering' proc IMA conference, Academic Press, 1984 (to be published).

3. Sekine, M, Tomita,Y,Hagisawa T, Kiuchi E and Irabu T, "Suppression of clutter and detection of targets", IECE Conference ISNCR-84, 279-284, 1984.

The Authors

Chris Baker graduated with a BSc degree in Applied Physics from the University of Hull in 1980. He subsequently spent three further years at Hull researching into RF excited CO_2 discharge lasers. Since joining RSRE, in early 1984, his research interests have centred around maritime radar and in particular scattering from the sea surface.

Keith Ward read Natural and Electrical Sciences at Queen's College, Cambridge University receiving a BA degree in 1977 and an MA in 1980. Since 1977 he has worked at the Royal Signals and Radar Establishment. His main interests are Maritime Radar, signal processing and in particular radar echoes from the sea surface. He is the author of a number of technical papers in these areas.

SYNTHETIC APERTURE RADAR

T M Mason

Summary

The best resolution in reconnaissance radars is obtained by the Synthetic Aperture Technique. This paper reviews the introduction of this type of radar and the development of modern digital SAR systems. Aspects being studied at RSRE are mentioned.

Historical

The need for a radar system which would provide a map of the terrain below a bomber aircraft was recognised early in the Second World War and experiments took place at Bawdsey and St Athan using modified AI sets operating on wavelengths of about 1.5 metres. Although transmitter pulse widths of 100-200ns were achievable giving 50-100 foot range resolution, the azimuth resolution was aperture limited. At the end of the war H2S Mk VII was in use, operating at X-band (10 GHz) with an aerial beamwidth of 1.3 degrees. This gave an azimuth resolution of 690 feet at 5 nm.

Improvements in resolution in post-war equipments were obtained by moving to higher frequencies and increasing the aerial aperture, one significant factor being the change to sideways looking radars with long aerial arrays placed on the fore-and-aft axis of the aircraft. In 1954 RRE had an X band equipment flying in a Valetta aircraft, using a 14 ft aerial aperture which gave a resolution of 100 yards along track and 32 yards across track at a range of 5 miles, when the aircraft was flying at a height of 5000 feet.

Proposals for TSR2 and for supersonic drone aircraft in 1962 using Q band (35 GHz), could not aim at a better along track resolution than about 75 ft at a range of 3 miles.

To achieve high cross track resolution demands a wide instantaneous bandwidth. For early pulsed radars employing a magnetron transmitter, this drove the pulse width down to 100 ns or less with a subsequent reduction in mean power. The advent of power amplifiers such as the TWT and Klystron as transmitter tubes opened up the possibliity of using wide band broad pulse transmission coupled with matched filter pulse compression on reception. Range or across track resolution of 3m and less can be readily achieved with Surface Acoustic Wave (SAW) devices offering pulse compression ratios of greater than 500:1.

Need For SAR

Given the requirement for a long stand off range, along track resolution is governed by the radiated wavelength and antenna length. For all weather performance the shortest useable wavelength is about 3 cm (X band). Coupled with a maximum sideways-looking antenna length of 6 metres, the best achievable real aperture resolution is about 0.3 degrees. That is 48m at 9Km (5nm) range. To achieve a resolution of a metre at 100Km would demand an antenna length of 3Km.

What is SAR

For a conventional real aperture sideways-looking radar, the along track resolution is determined by the amplitude history as objects pass through the aerial polar diagram. However, with a coherent radar, objects passing through the beam also have a phase history determined by the aircraft velocity, the range to the object and the radar wavelength. (Fig 1). This phase history is completely predictable and therefore a matched filter processor can be designed. Just as matched filter processing of a chirped transmitted pulse gives rise to

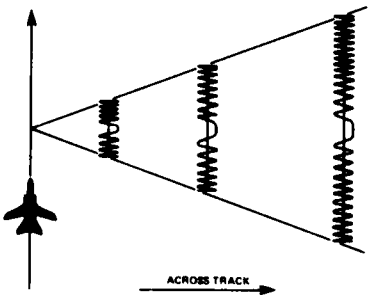

Fig 1 Synthetic Aperture Doppler Waveforms

enhanced range resolution through pulse compression, azimuth matched filtering gives rise to along track resolution improvement (Fig 2).

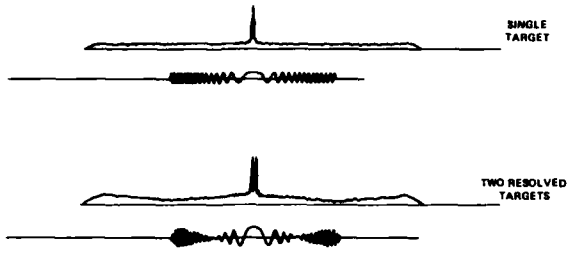

Fig 2 Synthetic Aperture Focussed Processing

Assuming the complete doppler history is processed over the real aerial beamwidth at all ranges, the system is known as focussed SAR. Its main features are listed at Table 1. In particular, the resolution is given

SAR – MAIN TECHNICAL FEATURES

1 RESOLUTION = HALF LENGTH OF REAL APERTURE

2 RESOLUTION INDEPENDENT OF:

WAVELENGTH

RANGE

AIRCRAFT VELOCITY

3 SIGNAL–TO–NOISE RATIO α (RANGE)$^{-3}$

TABLE 1

as half the length of the real aerial, implying that for 1 metre resolution the aerial must not exceed 2m in length. For continuous mapping this is true, however for high resolution mapping of a small selected area, a technique called "spotlight" can be used. A large high gain aerial is made to track the desired area as the aircraft flies past. The radar therefore dwells for longer, permitting higher resolution to be obtained.

A simpler process known as unfocussed SAR essentially low pass filters the doppler history. Whilst giving a resolution improvement over a real aperture system, it retains a range dependency and is therefore not appropriate to very long range systems. When squinted forward, this technique is also known as Doppler Beam Sharpening (DBS).

SAR Processing

Matched filter processing of the doppler histories can be performed in the time or frequency domain. For frequency domain processing, the phase/time history is first transformed into a signal spectrum. The signal spectrum is then multiplied by a reference spectrum and the resulting image spectrum is transformed back into the time domain.

Frequency domain processing was initially implemented using optical lenses as transform devices. Optically processed SAR has been in service with the USAF (Goodyear UPD-4) for several years.

With the advent of cheap high speed logic circuits in the early 1970s, the digital processing of SAR signals became a possibility. The main advantages of digital processing are essentially real time processing by elimination of the need to process signal and image films, rugged, reliable and flexible processing and the availability of a very wide dynamic range output.

Digital processing also opened up the possibility of using time domain processing.

Matched filtering in the time domain is a correlation process where the discrete phase samples constituting a signal phase history are multiplied by reference samples. The results of the multiplications are summed to give each output picture point.

Although time domain processing has been implemented on many digital SAR processors, advances in the implementation of time/frequency transformation algorithms and the advent of array processors has made the choice of frequency or time domain processing far less distinct.

SAR Requirements

a. Radar Coherence

To generate a large synthetic aerial it is often necessary to generate an accurate phase history over a period of several seconds. This requirement reflects on the radar coherence, demanding highly stable crystal locked oscillators and a wide

band microwave power amplifier such as a Travelling Wave Tube (TWT) in the transmitter.

b. Motion Compensation for SAR

When processing SAR data it is assumed that the aircraft flies in a perfectly straight line, giving a quadratic target phase history. In practice there will always be deviations from straight flight which, if not compensated, will lead to image degradations including defocussing, contrast reduction and multiple images. It can be shown that the maximum permissible uncorrected flight perturbation is a function of the frequency of that perturbation, the most stringent requirement being at frequencies around the reciprocal of the coherent integration time. To achieve 3m resolution at 100Km an acceleration of 10^{-4}g can be tolerated at a frequency of around 1Hz. This value is proportional to the square of the resolution, hence going to 1 metre resolution would decrease this limit by a factor of 9. Accelerations experienced by aircraft in flight are typically several orders of magnitude greater than those which the SAR processing can tolerate, thus some form of motion compensation is required.

There are two approaches to the problem, one being to measure the aircraft motions and apply corrections. The other is to use partly processed data to provide an estimate of the phase errors present. This process is known as autofocus. Combination of these techniques permits the production of high resolution SAR images.

SAR Systems

Since the 1960s considerable effort has been expended on SAR research.

In the US, systems such as the Goodyear UPD-4 and its derivatives have gone into service offering 3m resolution at X band out to ranges of around 60Km. Seasat was a civil L band satellite SAR giving 25m resolution. This radar gave detailed images of the sea surface showing internal waves, ocean waves and bathymetric effects. The most advanced known SAR is the Hughes ASAR-2 system.

The UK SAR programme started in the late 1960s and by 1973 RSRE had successfully demonstrated one of the world's first real time in flight digitally processed 3m resolution SARs. In 1982, RSRE started flight trials on a SAR giving high resolution out to long range (Figs 3,4).

Fig 3 RSRE SAR Research Canberra

Fig 4 RSRE SAR Image
Range = 40 Km

Post Processing Image Enhancement And Understanding

a. SAR Autofocus

In practice aircraft motion is uncertain leading to discrepancy between the reference and the actual data. This results in defocussing of the SAR image, often by factors of 5 to 10 times. RSRE have used an adaptive reference which is varied until the sharpest focussed image is obtained. In this way the full theoretical resolution limit of the SAR may be obtained consistently.

b. Terrain Classification

Since typical SAR images at full resolution consist of about one million pixels per second, it is essential to have a high degree of automatic image classification to aid the operator in his selection of targets of military significance. With this aim, work at RSRE on terrain classification and image segmentation based on local statistics, map matching and terrain modelling is producing promising results.

c. Resolution Enhancement

The achievable resolution of practical SAR systems is still inadequate for detailed study of targets of military significance eg vehicles. By exploiting other sources of information about the nature of SAR images, it is possible to introduce this information into target reconstruction leading to a significant improvement in the effective resolution. This is another area where RSRE have demonstrated some of the benefits which can be achieved.

Uses Of SAR

Applications of SAR range over both the military and civil sectors. Civil applications include studies of the ocean surface and large area mapping and classification of sea ice. Some geological and archeological features have also been exposed by SAR mapping.

Military uses range from the mapping of high value strategic targets such as airfields and fixed missile sites to the detection of battlefield targets either for cueing other short range sensors or for direct targetting.

Satellites are attractive platforms for SAR, they do not in general require sophisticated motion compensation. With a steerable antenna and suitable orbits, they can give access in war and peace to large areas of the earth. However, satellites are extremely costly and, once launched, do not have rapid flexibility. The launch of a number of satellites could however overcome this shortfall.

For stand-off battlefield surveillance, a high flying aircraft can give mapping out to very long range. Such systems are the US ASAR and the proposed UK CASTOR and US JSTARS. These systems give coverage of the forward battle area and are also able to direct Follow On Forces Attack (FOFA).

Short range surveillance from a penetrating RPV is assumed to be available from optical or infra-red sensors as proposed for Phoenix. However, low cloud and the necessity to fly high enough to avoid terrain obscuration of the data link may demand a longer wavelength sensor. A potentially low cost SAR may well be appropriate.

Apart from SAR as a stand alone sensor, it is also available as a switched mode option in such systems as the F-15 radar.

Future SAR Systems at RSRE

Current airborne SAR systems are able to produce high quality imagery and although this represents a remarkable angular resolution (<0.05 mrad), more information is required to permit recognition of small battlefield targets. Some of the potential techniques are:

a. Higher Spatial Resolution

With improvements in motion compensation, and the possible use of 'spotlight' mode, SAR is capable of giving even better along track resolution (< 1 metre) out to very long ranges. However, atmospheric inhomogeneity can limit the achievable resolution in some circumstances.

Comparable across track (range) resolution is also achievable though it demands more sophisticated pulse compression techniques.

b. Multi-frequency

To 'smooth' the specular image produced by a single frequency coherent radar, the summation of images produced by several different frequencies should produce a more 'optical like' image.

c. MTI

Any object passing through the real aerial beam has an associated doppler history. Thus, given knowledge of a target's motion, a matched filter can be designed to focus that particular target.

Using iterative processing techniques, together with reduced spatial resolution, some MTI performance has been demonstrated with SAR.

d. Polarimetry

A lot of work on polarimetric effects as a target discriminant has been carried out in connection with smart munition homing. This work may well have relevance to a fully polarimetric SAR as an aid to battlefield target identification.

In support of the above performance improvements and as an ECCM technique, various radar waveform designs and implementation techniques eg digital phase coding, for pulse compression will be investigated. The aim is for a high PRF, Low Probability of Intercept (LPI) transmission.

The application of next generation VLSI processors such as the ICL DAP and subsequently mil DAP, under development as part of the VHPIC programme, are being considered to permit either more sophisticated real time processing or compact airborne and spaceborne processors.

In parallel with work leading to long range SAR systems, the advent of microwave integrated circuits and low priced digital processing has opened up the possibility of producing a compact, low priced short range SAR. Such a system could offer an all weather high resolution capability to small air vehicles such as surveillance RPVs or Weapon bus vehicles.

Conclusions

SAR emerged from the research laboratories in the 1970s. Coupled with elaborate, delicate yet massive optical processors, it produced imagery with a few metres resolution out to ranges of a few miles. This represented an order of magnitude improvement over previous real aperture systems.

The digital revolution together with advances in wide band pulse compression and inertial sensing for motion compensation have led to the achievement of even higher resolution out to very long ranges. Coupled with techniques such as polarimetry, multi frequency and MTI, it is likely that identification of many small battlefield targets will be possible.

Advances in microwave miniaturisation and integration techniques, coupled with powerful signal processing offer the potential for a compact low priced SAR giving all weather visibility to small air vehicles.

SAR is a very powerful technique which permits the collection of high resolution imagery in conditions which preclude the use of any other imaging sensor.

The Author

T M Mason graduated in Electronic Engineering from Hull University in 1970. He has been employed at RSRE since then working on centimetric and millimetric SAR systems, infrared threat warning for aircraft and mm radiometry. He is a Principal Scientific Officer leading a section on airborne microwave reconnaissance research.

TRANSIENT FIELD GENERATION AND MEASUREMENT

D M Parkes and P D Smith

Introduction

In this paper we present the mathematical modelling and numerical computation of the electromagnetic field radiated by a biconic antenna which is excited by a transient waveform such as a pulse, and the experimental verification of the predicted results. The aim of the work is to develop an antenna which faithfully radiates the transient signal supplied to the system and which is easily portable. Such a system can then be taken to a site where EMC or EMP testing of equipment is required.

Our biconic antenna is shown in Figure 1: it consists of a spherically capped cone fed by a coaxial cable whose outer conductor is attached to a grounded earth plane. The impedance of the coaxial cable is matched to that of the cone, the cable supplies a travelling wave - such as a pulse - whose peak value is taken as 1 Volt, and whose shape as a function of time t will be denoted by V(t).

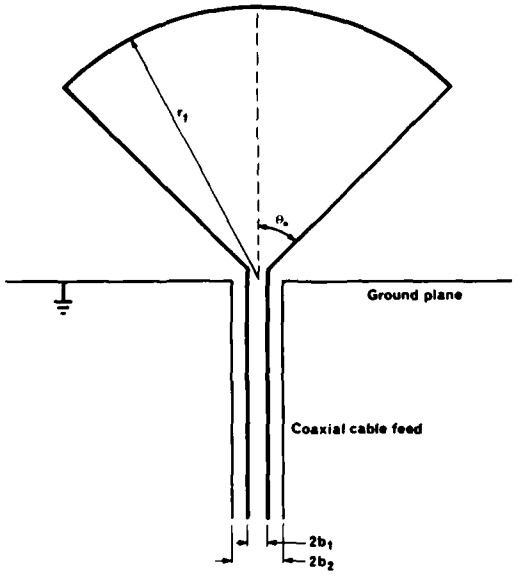

Fig 1 The Bionic Antenna

Experimentally, the ground plane is effectively infinite in extent. Making the same assumption and applying image theory, one obtains an equivalent model, in which the ground plane has been removed and the opening therein replaced by an annular frill of magnetic current of twice the original strength.

The transient radiated field is then obtained by computing the total field scattered from this equivalent model's surface by the pulsed magnetic current frill. To do this, an integral equation on the surface of the body is numerically solved to find induced surface currents; these surface currents are subsequently employed in an integral representation of the field to calculate the total scattered field.

Previous theoretical [1] and experimental work [2] has shown that at large distances R in the equatorial plane, the leading edge of the radiated electromagnetic field faithfully reproduces the shape of the exciting function V(t), according to the formula

$$E^{rad}(t) = \frac{Z_{ofs}}{Z_{ant}} \frac{1}{2\pi R} V(t) \qquad (1)$$

where Z_{ofs}, Z_{ant} denote free space and antenna impedance respectively. This formula is only valid for a limited period - there is a time τ_o for which (1) holds at all times $t < \tau_o$. This result is reproduced in our calculations, for a pulse width of t_w. The duration τ_o of faithful reproduction increases as the parameter r_1/ct_w increases (for a cone of fixed angle θ_o), where r_1 is the conecap radius. From a practical point of view, one desires r_1 as small as possible but τ_o as large as possible, so that the shape of the exciting waveform is clearly seen in the radiated field, ie $\tau_o/t_w \approx 6$.

Results

A Gaussian pulse of the form

$$V(t) = \exp[-(t/2a)^2] \text{ (Volts)}$$

was used to stimulate cones of impedance

79 Ω (θ_o = 30°) and 50 Ω (θ_o = 47°). (The impedance of the biconic is the "high frequency" limit $Z_{ant} = Z_{ofs}/2\pi \ln \cot \frac{1}{2}\theta_o$.) This pulse has full width at half weight $t_w = 4a\sqrt{\ln 2}$.

The radiated electric field E in the equatorial plane at large distances R has only one non-zero component E_θ which was obtained from the radiated magnetic field $\underset{\sim}{H} = H_\phi \hat{\underset{\sim}{\phi}}$ (since radiation conditions imply $R(E_\theta - Z_{ofs} H_\phi) \to 0$ as $R \to \infty$).

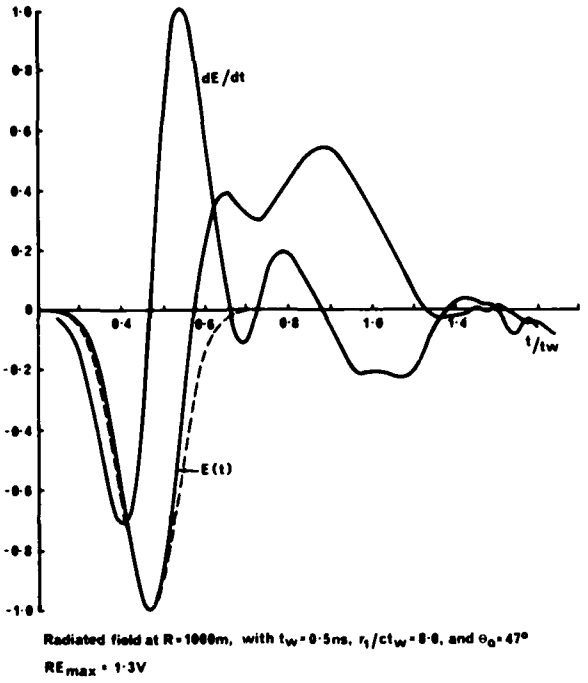

Radiated field at R=1000m, with t_w=0·5ns, r_1/ct_w=8·0, and θ_o=47°
RE_{max} = 1·3V

Fig 2

Figure 2 shows E_θ as a function of time with r/ct_w equal to 8. Note that the faithful reproduction of the incident waveform shape is clearly demonstrated. The peak value of $R\,E^{rad}(t)$ is in good agreement with [1] and is not significantly effected when R is reduced to 10 metres.

Description Of The Method

We begin by considering the scattering problem for a perfectly conducting body illuminated by an incident electromagnetic field $\underset{\sim}{E}_0(P,t), \underset{\sim}{H}_0(P,t)$. Let S represent the boundary of the body and S_+ the exterior domain. The total magnetic field $\underset{\sim}{H}(P,t)$ can be expressed as

$$\underset{\sim}{H}(P,t) = \underset{\sim}{H}_0(P,t) - \int_S \left\{ \underset{\sim}{j}(q,T) + \frac{|\underset{\sim}{x}_p - \underset{\sim}{x}_q|}{c} \frac{\partial \underset{\sim}{j}}{\partial t}(q,T) \right\} \times \text{grad}_q \Psi(P,q)\, dS_q \qquad (2)$$

where $P \in S_+$, $\Psi(P,q) = 1/4\pi|\underset{\sim}{x}_p - \underset{\sim}{x}_q|$, the retarded time $T = t - |\underset{\sim}{x}_p - \underset{\sim}{x}_q|/c$, $\underset{\sim}{j}$ is the surface current on the body and c is the velocity of light (see [3, p548]). Thus where the surface current j is known, the total magnetic field can be evaluated from (2). The surface current is found by solving the following integral equation obtained by considering the limit as P approaches a point p on S:

$$-\tfrac{1}{2}\underset{\sim}{j}(p,t) + \underset{\sim}{n}_p \times \int_S \left\{ \underset{\sim}{j}(q,T) + \frac{|\underset{\sim}{x}_p - \underset{\sim}{x}_q|}{c} \frac{\partial \underset{\sim}{j}}{\partial t}(q,T) \right\} \times \text{grad}_q \Psi(p,q)\, dS_q = \underset{\sim}{n}_p \times \underset{\sim}{H}_0(p,t) \qquad (3)$$

where $\underset{\sim}{n}_p$ denotes the outward normal vector at p, and the integral is to be evaluated as a principal valued integral (see [3, p549]).

Equation (3) is a time dependent integral equation for the surface current $\underset{\sim}{j}$ in which the values of $\underset{\sim}{j}$ in the integrand correspond to times T strictly less than t except at p = q: this observation forms the basis of a "marching in time" solution method. The surface S is split up into a set of patches $S_1, \ldots S_n$ and the time variable is discretised into a sequence $t_0, t_1, t_2, \ldots$ Since the incident field - from the ring current source - is a pulse, we begin the process at a suitable time t_0 before the pulse strikes the body (so that all fields and currents are identically zero for $t \leq t_0$) and proceed as follows.

Suppose the solution is known at all points and at each time step $t_i \leq t_r$ for some r, and the value $\underset{\sim}{j}(p,t_{r+1})$ is desired for some $p \in S$. Let $\hat{\underset{\sim}{t}}_q$ be a unit tangent vector in the direction of $\underset{\sim}{j}(q,t)$, so that $\hat{\underset{\sim}{t}}_q$ may be taken as one of $\hat{\underset{\sim}{r}}_q$, $\hat{\underset{\sim}{\theta}}_q$ or $\hat{\underset{\sim}{k}}$ ($q \in S$) and

write $\underset{\sim}{j}(q,t) = j(q,t)\hat{\underset{\sim}{t}}_q$. Then if the patch S_p containing p is small enough, equation 3 may be represented by

$$(\underset{\sim}{n}_p \times \oint_{S_p} \hat{\underset{\sim}{t}}_q \times \text{grad}_q \Psi(p,q) dS_q - \tfrac{1}{2}\hat{\underset{\sim}{t}}_p) j(p,t) =$$

$$\underset{\sim}{n}_p \times \underset{\sim}{H}_0(p,t) - \underset{\sim}{n}_p \times \int_{S-S_p} \left\{ j(q,T) + \right.$$

$$\left. + \frac{|\underset{\sim}{x}_p - \underset{\sim}{x}_q|}{c} \frac{\partial j(q,T)}{\partial t} \right\} \times \text{grad}_q \Psi(p,q)\, dS_q \qquad (4)$$

If the time increments are chosen small enough, the values of $\underset{\sim}{j}(q,t) = \underset{\sim}{j}(q, t - |\underset{\sim}{x}_p - \underset{\sim}{x}_q|/c)$ required over the rest of the surface patches $S-S_p$ are known, and $\underset{\sim}{j}(p,t)$ can be found from (4). Thus to solve (3) we start at t_0 and "march forward" in time, calculating the solution at selected points $p_i \in S_i$ $(i = 1,\ldots,n)$ at each time step using an appropriate numerical integration over the previous values of $\underset{\sim}{j}$.

It is essential that the values of $\underset{\sim}{j}$ used in the integration on the RHS of (4) correspond to previous time steps, so that $t_{r+1} - |\underset{\sim}{x}_p - \underset{\sim}{x}_q|/c < t_r$ for all values of q which we use in carrying out the numerical integration.

Finally, the source term $\underset{\sim}{H}_0(P,t)$ is evaluated from the electric vector potential expressed in terms of the (retarded) magnetic current.

$$Z_0 \underset{\sim}{H}_0(P,t) = \hat{\underset{\sim}{\phi}} \frac{2b_3}{4\pi} \int_0^{2\pi} \frac{1}{c} \frac{V'(t-\Lambda/c)}{\Lambda} \cos\phi\, d\phi \qquad (5)$$

where $\Lambda^2 = r^2 + b_3^2 - 2rb_3 \sin\theta \cos\phi$.

The integral equation (3) responds badly to discontinuities in V" and V' if the waveform V is obtained from numerical data, it should be interpolated by a cubic spline (for example) and the derivative values calculated from the spline formulae.

This method of solving the magnetic field integral equation is applicable for arbitrary surfaces S and magnetic current sources which have the described rotational symmetry. Changes to the surface S or the source require relatively minor programming changes; in particular a variety of source driving functions can be examined. Further computation details can be found in [4], [5] and [6].

Experimental Transient Radiation Field Measurements

To show experimentally that the computer predictions obtained were correct it was of use to try to radiate a pulse from a biconic antenna with approximately the same dimension as the one used in the model. Detection of the radiative waveform requires special equipment, because of the time history of the pulse, and the amplitude available in the far field of the radiating antenna.

A value of the radiation field available is given by (1).

For the case where Z_{ant} = 50 ohms, V(t) = 56 Volts and R = 10 metres the expected maximum field would be 6.72 Volts/metre. If this is the case, then using a small biconic sensor as the receiving element the expected maximum detected signal is given by:

$$e = h_e C_{ant} Z_o \frac{d(E_{rad}(t))}{dt} \text{ Volts}$$

where h_e is the equivalent height of the sensor, C_{ant} is the capacitance, and Z_o the termination impedance.

For a sensor with a radius vector r_o, and biconic half angle θ_o, then for a 50 ohm network [1]

$$e = n\left(\frac{d(E^{rad}(t))}{dt}\right) \text{ Volts} \qquad (6)$$

where

$$n = \frac{3}{2} r_o^2 \frac{\cos\theta_o}{c} \qquad (7)$$

Radiation

The pulse was obtained from a capacitive sampler placed in a coaxial transmission line situated between the output of a ferrite line pulse sharpener [7] and a

terminating matched load. The initial pulse is produced by a Cardon Instruments 3151 pulse generator [8] operating at 1 kHz prf.

The pulse has a peak amplitude of 5 kV and a duration of 11 nanoseconds. The rise time of the leading edge of the pulse being 3.5 nanoseconds. A second sampler is placed between the generator and the line to provide a trigger to the sampling oscilloscope.

The output pulse was connected to a special case of the biconical antenna, the bottom element forming the earth plane.

The transit time of the antenna should be long compared to the rise time of the pulse and is given by

$$\tau_a = \frac{r}{c} \times \sqrt{\varepsilon_r}$$

where, for an airfilled antenna, $\varepsilon_r = 1$

The antenna used had the following parameters $\theta = 46.9^{o}$ and r = 0.5 m which gives Z_{ant} = 50 ohm and τ_a = 1.67 nanoseconds.

Detection

The receiving element must be small compared to the rise time of the radiation field. In the case of the 9 mm radius cone used it can be shown that the element will act as a capacitive pick up and will produce the derivative of the radiation field [1].

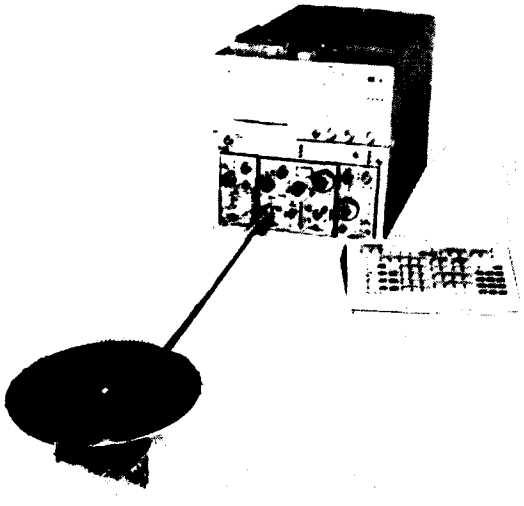

Fig 3 Receiving System

To ensure that cable distortion is minimised the receiving element is connected to the input of the sampling oscilloscope by a 1 metre section of air filled transmission line (Figure 3).

In order to allow processing of the received waveform on line, a Tektronics 7854 waveform processing scope was used, with a 7S12 TDR/sampling plug in. The sampling unit used was a Type S4 which has a rise time limitation of 20 picoseconds. An S53 pre-trigger pulse generator was used to complete the sampling system.

Experimental Results

The waveform from the sampler after the pulse sharpener (Figure 4) was monitored to check on the amplitude and full width at half height (FWHH). The receiving element

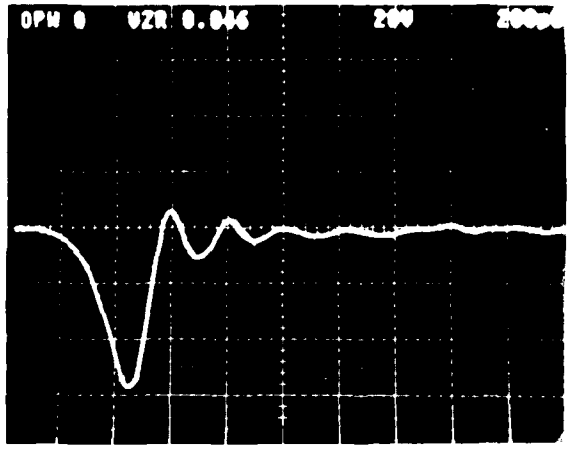

Fig 4 Input Pulse to Antenna

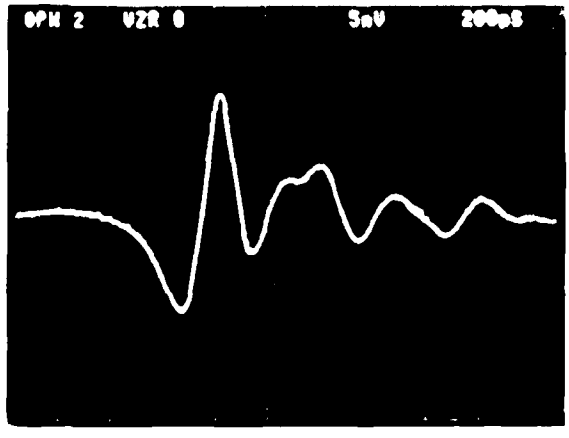

Fig 5 Received Signal

Fig 6 Integral of Received Signal

was placed 10 metres from the radiating antenna and the received waveform (Figure 5) was acquired using the slowest sweep speed on the sampler. As this is the differential of the radiation field the 7854 was used to integrate the waveform. This resulted in a waveform (Figure 6) which showed very good agreement over the major part of the pulse, with the radiating stimulus.

Analysis Of Results

For a sensor having r_o = 9 mm and $\theta_o = 46.9^o$ (ie Z_{sensor} = 50 ohms) then from (7)

$$n = 2.754 \times 10^{-13} \text{ pS m}$$

E(t) is given by

$$\int_{t_0}^{t_1} (e/n)\, dt$$

where t_1 is the time interval where the first "zero crossing" of the observed sensor waveform occurs.

From Figure 6 the numerical value of the integral is 1.75×10^{-12} Volt picoseconds. (This value is obtained either directly as a property of the Tektronics Waveform Processing Oscilloscope, or by transferring the waveform to a Cubic Spline Waveform Analysing Programme.)

The magnitude of the radiation field E(t) is given by

$$\frac{1.75 \times 10^{-12}}{2.754 \times 10^{-13}} = 6.36 \text{ Volts/metre}$$

As the maximum field available is 6.72 V/m, allowing for instrument tolerance of $\pm$ 5%, there is very good agreement with the theoretical amplitude of the radiation field using this method.

Conclusions

Because of advancements in pulse generator techniques, it is now possible to produce transient fields which have a significant amplitude at useful ranges, and are not limited to very low repetition rates.

Techniques have been developed to allow accurate measurement of the monopolar field to be made remotely. As a result of these advancements, it has been possible to validate the predictions of the model.

Very good agreement between the model and experiment has been achieved for the time history of the radiated pulse and the amplitudes of calculated field strengths are within engineering tolerances. It is now possible to predict the type of field and its amplitude, which will result, when any variant of biconic antenna is excited by a given input pulse, since the time marching method of solving integral equations has been shown to be successfully implemented on a computer.

Because the system is not limited to single shot events the measurement of induced currents which occur inside target equipments when they are illuminated by the radiation field is made very much easier, since sampling technology can be employed.

Predictions of current waveforms which occur in antennas can also be predicted by the model.

References

[1] Harrison, C.W. and Williams, C.S., "Transients in wide-angle conical antennas", IEEE Trans on A&P 13 (1965) 236-246.

[2] McQuillin, J.D.R., "Transient radiation field measurement", RSRE Unpublished BS3 Research Note, January 1982.

[3] Jones, D.S., "Methods in Electromagnetic wave propagation", Oxford University Press (1979).

[4] Mittra, R. (ed.), "Computer techniques for electromagnetics", Pergamon Press, See 4, (1973).

[5] Smith, P.D., "Computation of transient radiation from finite biconic antenna", MOD Research Report, University of Dundee, June 1984.

[6] Parkes, D.M. and Smith, P.D., "Transient Field Generation and Measurement", Colloquium Digest on "Protection of Communications Equipment against EMP and other Hazards", March 1985.

[7] Katayev, I.G., "Electromagnetic Shock Waves", Iliffe Books Ltd, 1966.

[8] Kitchin, H.D., "A fast rise time, high PRF pulse generator using a hydrogen thyratron", Bournlea Instruments Ltd, 1985.

The Authors

David M Parkes was born in Birmingham, England on August 30th 1944. He received an HNC in Electrical and Electronic Engineering from the College of Electronics, Malvern in 1965. He has worked on high power radar systems for the detection of Clear Air Turbulance and recently been involved in research into fast rise time high voltage pulse generators.

Paul D Smith was born in Adelaide, Australia on January 9th 1955. He received an Honours BSc degree from the University of Adelaide in 1976 and the PhD degree from Cambridge University in 1981. In 1980-81 he was Lecturer in Mathematics at Brunel University; since then he has been Research Fellow in Department of Mathematical Sciences at Dundee University, working on acoustic and electromagnetic scattering and radiation problems.

COMMUNICATIONS AND COMPUTING

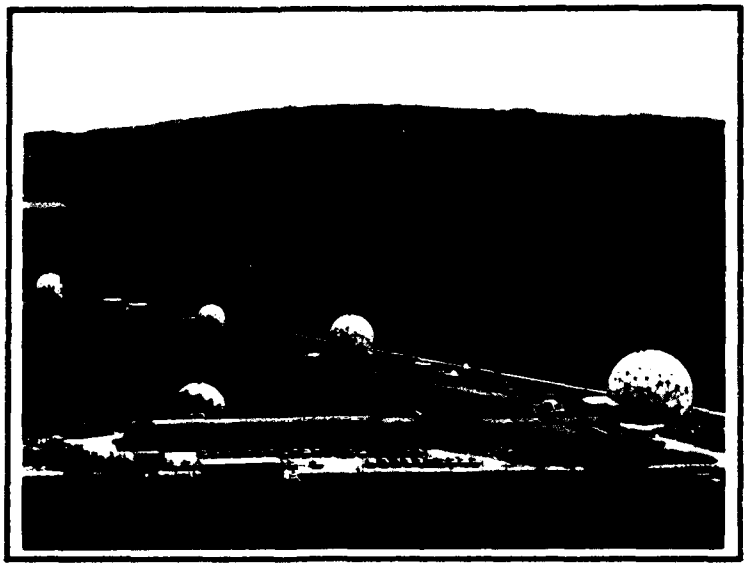

SLOW SCAN TELEVISION VIA TACTICAL SATCOMS

P Wells

Introduction

An early experimental system is described which enables near real time moving picture information in redundant scenes to be transmitted over a low data rate tactical satellite communication link. The RSRE prototype equipments were designed to operate from Landrover based satcom terminals (UK/VSC 501) using the 16 kilobit per second tactical voice links. With the advent of more powerful satellites (SKYNET 4) the equipment should be able to be used with manpack type satcom terminals such as the UK/PSC 504. The video codec operates at a constant 16 kilobit per second data rate and is therefore compatible with any 16 kilobit per second digital communications link.

Near real time movement of objects in redundant scenes can only be achieved by reducing the resolution of a standard 625 line television frame to enable transmission at low data rates. The analogue bandwidth of a conventional monochrome television signal is 5.5 MHz maximum. Using pulse code modulation this would require a digital data rate in the order of tens of megabits per second. To achieve a reasonable picture refresh rate over a 16 kilobit per second data link a picture format of 128 by 128 pixels is used, each pixel being coded using four bit pulse code modulation.

The system has two distinct modes of operation; conventional slow scan television to build up the television frame and conditional replenishment to send the moving picture information. The majority of information in a moving picture scene is stationary and is therefore redundant information. The system was also required to operate at the low signal to noise ratios incurred on 16 kilobit per second tactical satcom links.

Picture Format And Operation of the Video Codec

In the conventional slow scan television mode of operation a standard 625 line monochrome television picture is sampled using 4 bit PCM and the information is stored in a frame store (of size 128 x 128 x 4 = 65,536 bits). The information is then read out from the store a line at a time, progressing from the top to the bottom of the picture. The information is read out as 4 bit data which is then converted to a serial data stream. At the end of each line a sync pulse composed of 16 bits (corresponding to 4 pixels) is added. Each of the 128 lines is transmitted in this way. When the bottom of the frame is reached two complete lines of the sync pulse are sent to indicate a frame sync. Upon completion of this cycle a new fast scan (standard 625 line television picture) frame is sampled and the process is repeated. The frame refresh rate, at a 16 kilobit per second data rate, is one frame every four seconds.

On receive the sync pulses are used to format the picture and store it in a frame store. As this is being performed the received frame is being sampled and displayed as a standard 625 line television picture. Circuitry is provided on receive so that the frame format is held, even under very noisy conditions.

For the conditional replenishment mode of operation only information that has changed in the picture is transmitted. The fast scan television signal is sampled using 4 bit PCM and the information (A) stored in the frame store. Information from the next fast scan frame of the input video (B) is compared with that in the frame store using the following algorithm.

$$| A - B | > 1$$

This is necessary to overcome problems introduced by quantisation effects that give more change information than is actually necessary to convey moving information.

If a difference, according to the above expression is detected, then the new pixel information (4 bits) is put in the frame store and a separate pointer store is used to indicate the address in the memory where the change has occurred. This is carried out for the whole frame. Upon completion of

this the pointer store is scanned until the first change pixel is detected enabling the change pixel information and its address in memory (which corresponds to its position on the screen) to be stored in a latch. This information consists of four bits for the new pixel information and fourteen bits for the address information. This is converted to serial data and has a start and stop bit added to help resynchronisation at the receiver. This is repeated until all the change information has been transmitted then the next frame of the fast scan input is compared with that in the frame store and the whole process is repeated.

Thus the frame refresh rate is proportional to the amount of information changing in the input signal.

On receive the four bit data is placed in the relevant location in the frame store using the fourteen bit address information. As this happens the information is displayed as fast scan video on the receive monitor.

Using the conditional replenishment mode of operation when only a small proportion of the scene moves (ie the majority of the frame is stationary and therefore redundant information), near real time picture movement has been shown to be possible.

Performance And Applications

The RSRE prototypes have been used in both modes of operation and have shown a number of applications including:

a Video conferencing (full Duplex).

b Transmission of battle map information or personnel identification.

c Remote surveillance via satellite.

Figures 1 and 2 show typical pictures received at a Landrover based satcom terminal via the Indian Ocean DSCS satellite. The received signal to noise ratio (referred to unity bandwidth) was about 56 dBHz in both cases. The video codec has been used with signal to noise ratio's as low as 46 dBHz giving pictures in the slow scan television mode. In the conditional replenishment mode the receive modems lose lock before the viewed picture becomes objectionable, (ie less than 45 dBHz).

Fig 1 An example of the picture resolution of the SSTV system – personnel identification

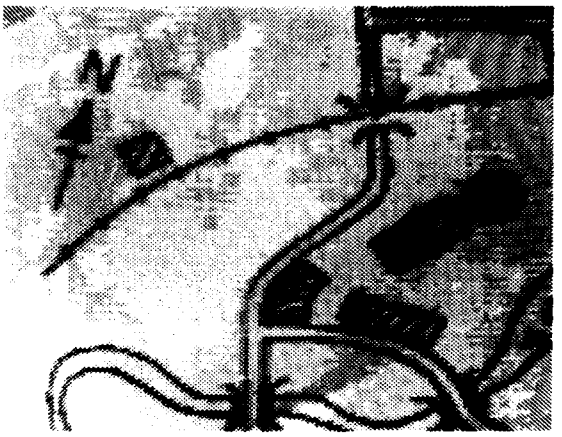

Fig 2 A further example – a hand sketched map

The next phase of this work will result in the production of engineered, miniaturised, man portable versions of the video codec to demonstrate remote surveillance, using secure, low probability of intercept/ detection links from manpack based satcom terminals. Also the use of transform coding techniques for higher resolution pictures as described in reference 1 will be investigated.

Reference

1 Compact Low Power Coder for Extreme Bit Rate Reduction of Television Pictures.

J G McWhirter, J B G Roberts, R F Simons, D J Watson IEEE Proc. Vol 127 Pt. f No 5 October 1980.

The Author

Paul Wells joined RSRE in 1983 after graduating from the University of Salford with an honours degree in Electronic Communication. At present he is working in the field of Satellite Communications at RSRE Defford. He is currently studying for the Diploma in Engineering higher degree and is aiming to be a Chartered Electronic Engineer.

DEMAND ASSIGNED MULTIPLE ACCESS CONTROL FOR TACTICAL SATELLITE COMMUNICATIONS TERMINALS

P W Braddock, A C Smith and S J Perkins

Abstract

Multiple Access (MA) techniques have the general objective of enabling traffic to be passed between many SATCOM system subscribers in an efficient manner when satellite resources are limited. Demand Assigned Multiple Access (DAMA) techniques automatically allocate resources as, and when, required by the subscriber.

This paper describes two distinct approaches to the DAMA problem for tactical terminal operation. In one implementation a central control station monitors traffic and allocates resources. In the second, a distributed scheme is under development whereby all terminals are of equal importance. This scheme is inherently less vulnerable since there is no reliance on a central control remaining operational.

Introduction

Currently military satellite use is based on the allocation of dedicated preassigned channels for communications between users. This scheme is wasteful in terms of satellite bandwidth, effective isotropic radiated power (EIRP) and management resources.

As the number of users increases the inefficiency of this scheme soon becomes apparent and a more automated and efficient management scheme is called for. With the demand for satellite capcity showing no signs of abating, particularly for many users who make intermittent use of the resources, efficient management becomes essential rather than desirable. DAMA techniques can provide an effective solution to this problem.

DAMA is a system for organising a relatively large number of intermittently used circuits to be passed over a smaller number of channels. It results in substantial economies of satellite resources compared to the dedicated channel system. The quality of the SATCOM link is unaffected since only the Resource Management is modified (reference 1).

RSRE's DAMA Route

The organisation of current SATCOM resource allocation and the requirements of existing equipments dictate that we should base our research effort on frequency division DAMA schemes. Future equipment development may alter this view and it is by no means clear what schemes should be used for future systems.

We have taken two approaches as being relevant to military SATCOMS and have, initially, concentrated on 16 kbits^{-1} speech rather than telegraph or secure links.

Our "centralised" experimental system enables a limited number of user accesses from small earth stations to be connected together, via an Anchor Station, which monitors and allocates satellite resources. Although attractive for C^3 reasons, we feel that this is inherently vulnerable due to the importance of the Anchor Station remaining operational.

Our "distributed" experimental system is currently under development and will enable a limited number of small earth stations to be connected together without the intervention of a central station. This makes the entire system less vulnerable because each user will be of equal importance. Any damage to users will not impair the facilities offered to the rest.

Implications On Existing Equipment

The centralised DAMA requires additional equipment at the Central Control Station. This could be as extensive as a modem for each simultaneous field equipment access. Both schemes require an additional "black-box" to be incorporated in each user equipment participating in the DAMA scheme. To monitor resource allocation and user activity a dedicated computer monitor would represent a minimum Central Control station addition. In essence we have sought to develop "add-on" units to existing equipments rather that evolve completely new designs.

Central Control DAMA

Use of the Anchor Station as the Central Control Station (CCS) figures prominently in this scheme. All traffic between terminals in both controlled and routed via the CCS. In addition to the channels required for the links to and from the mobile terminals there are two control channels, making 4N + 2 channels in total. The control channels comprise a Broadcast Channel (BC) and a Request Channel (RC). The RC is a common channel used by the remote terminals to inform the CCS that a link to another remote terminal is requested. All remote terminals are continually tuned into the BC. It is on this channel that instructions from the CCS are transmitted to them. In our current hardware the BC also transmits information relating to whether the RC is busy. This reduces the clashing probabilities of two or more terminals accessing the RC simultaneously.

The CCS equipment comprises a microprocessor control unit including an associated visual display and one modem per simultaneous remote terminal access. The remote terminal (figure 1 - excluding scanning receiver) contains another microprocessor control unit for recognising its own call sign and for controlling its accessing of satellite resources under CCS management.

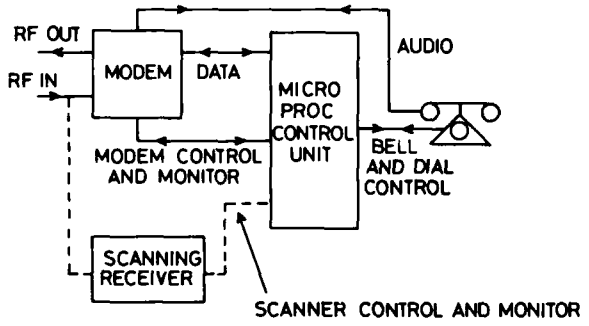

Fig 1 **Major components of the small station for centralised control. The dotted lines indicate the extra circuitry needed for distributed control**

Distributed Control DAMA

This scheme acts independently of a CCS (although there is a provision in our equipment for CCS monitoring and control, if necessary). Because of its independence from the CCS the system's organisation and architecture are somewhat simpler. Links are established directly between mobile terminals - which, naturally, must have system parameters capable of point-to-point operation. The number of channel accesses is reduced to 2N + 2, including two controlling channels called the Request Channel (RC) and a Reply Channel (RYC).

All inactive terminals will normally be tuned to the RC. The terminal wishing to establish a link will transmit his own and the destination's call signs. The called station, upon hearing its own call sign, will respond on the RYC. There then follows an exchange of information to determine which frequencies are to be used for communication purposes.

Each terminal keeps a record of which channels are occupied by making use of a scanning receiver. This is no more than a scanning envelope detector, scanning the band of frequencies over which this equipment works (figure 1).

When agreement has been reached their microprocessors re-tune their receivers and transmitters to the appropriate channels and the telephone bell at the destination address is rung. Replacement of the telephone handset at either end of the link causes the communication channels to be vacated and the receivers to be re-tuned to the RC again.

Request Channel Clashing Probabilities

Clashing of signals should only occur on the Request Channel and this is entirely due to the probablistic nature of call initiation. Because of the organisation of the two schemes outlined above it is possible for every terminal to monitor the activity of the RC and only transmit in periods of inactivity. If there is a remote terminal monitoring the RC and begins to transmit immediately the RC becomes clear then the fact that this channel is now occupied will not become known to others until about 240mS (ie. one up and down path delay to a geosynchronous satellite) later. It is during this time period that clashing may occur.

We have taken a simplistic model of clashing, based on Poissonian statistics, to give us some idea of the magnitude of the problem. In figure 2 we plot the

probability, p(n,M), of there being zero, one or greater-than-or-equal-to-two requests occuring within a period of 2 x 240mS. The absicissa represents the mean number, M, of users using the RC at any time where

$$M = \frac{Nt}{T} \quad .$$

N is the total number of users, t is the time during which clashes can occur (2 x 240mS) and T is the average time between an individual's call initiation. Both N and T have yet to be determined. Values of N = 20 and T = 600s give P ($\geq$2) of about 10^{-4}.

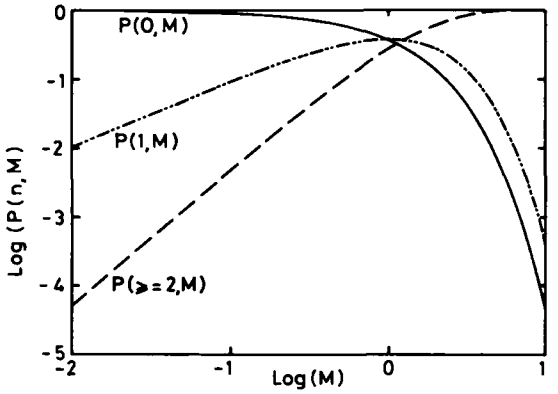

Fig 2 **The logarithm (base 10) of the probability for *zero, one and greater-than-or-equal-to-two* users occupying the Request Channel versus the logarithm of the mean number of occupiers of the channel**

Conclusions

The two schemes outlined in this paper represent extremes of frequency division DAMA.

The distributed approach gives no overall authority to one station and has no connection to any fixed ground stations where land lines can be accessed. The Central Control system has the advantage that the central station has overall authority and can use land lines. However, by routing links through the CCS more satellite accesses are used than in the distributed case by about a factor of two. The central control system is also heavily reliant on the CCS remaining operational.

We feel that a useful DAMA system for tactical satellite terminals will be a compromise of the two schemes with the CCS retaining some monitor and control functions.

Other features which need to be addressed are the management of priority accesses and the handling and control of subscribers with multiple traffic capabilities. These would include simultaneous clear and spread spectrum links and the subsequent routing to different destinations. These, and more, are to be the subject of future investigation.

Reference

1 Kota, S L, Demand Assignment Multiple Access (DAMA) Techniques for Satellite Communications.

Proc IEEE National Telecommunication Conference, New Orleans. 1981, 2, C8.8.1 - C8.5.7.

The Authors

Wayne Braddock (an 'Old Veseyan') read physics at Brighton College of Technology and Birmingham University. Since 1970, at RSRE, he pioneered work on solid state microwave amplifying devices and integrated circuits; became the Development Project Officer for a weapon location radar and is now head of R&D on tactical satellite communications terminals at Defford.

Alan C Smith read Physics at Durham University. He is a Fellow of the Royal Astronomical Society and is also a Chartered Physicist. Since 1978 he has worked at ARE (Portland) on acoustic aspects of Anti-Submarine Warfare. Now his interests embrace antennas for satellite communications and adaptive arrays.

Steve Perkins joined SRDE in 1968 and gained his HNC in Electrical and Electronic Engineering in 1975. He has been associated with many aspects of UK military satellite communications research since 1971. Steve is also a keen radio amateur.

MALVERN'S PROGRAM ANALYSERS

B D Bramson

In 1972, the computer scientist Edgser Dijkstra remarked that the exhaustive testing of a machine, claiming to perform the fixed-point multiplication of a pair of 27-bit numbers, would take 10,000 years. How then can we hope to certify the wide and growing range of systems whose safety depends, at least in part, on the correct behaviour of programmable machines, examples of which may be found in chemical factories, steel mills and avionics systems? In particular, what can be done to assess safety critical software?

First and foremost, we need soundly based production tools. Formal mathematical methods must be used to express our requirements for safety and to specify the software at every stage of its design. Such methods should be able to resolve issues of ambiguity and completeness and to guarantee conformity between different levels of specification. Secondly, we need formal methods for assessing the implementation of the software; which brings me back to Dijkstra's multiplier.

Now the avionics software of a modern aircraft performs tasks more complicated than mere multiplication. Exhaustive testing is neither theoretically nor financially possible: indeed, only a tiny proportion of the total flight envelope could ever be exercised. At the same time, manual review is both tedious and error prone. Thus we are faced with an enormous problem of certification. The solution lies in the mathematical theories of directed graphs and regular algebras.

A decade of activity at RSRE and at Southampton University has culminated in a suite of programs, the Malvern Program Analysis Suite (MALPAS), for the automatic, static analysis of safety critical software. Prior to analysis, a given text is translated into a standard Intermediate Language (IL), thus obviating the need for a new set of analysers for each programming language. IL is a strongly typed language with deliberately primitive control constructs; so that both high and low-level languages may be modelled. Many types are in-built; but new types, functions and procedures may also be declared without elaboration.

For each procedure, including the outermost program, six types of analysis are performed.

1. The Control Flow Analyser examines the topological structure of the software and identifies: all possible starts and ends; unreachable code and "black holes"; and the locations of loops with their entry and exit points. It also reveals the high-level control structure of the software and helps the analyst assess its engineering quality.

2. The Data Use Analyser is concerned with the sequential reading and writing of data and, in particular, with unset variables and unused values.

3. The Information Flow Analyser reveals the influence between input and output. For example, in an avionics application, the *analyser might declare*

"The position of the flaps (an output variable controlling an actuator) depends on the angle selected by the pilot and the *indicated airspeed*".

The dependence relations also point the way to constructing an intelligent test harness. (It helps to know that the position of the flaps depends on only two of all possible sensed inputs.)

4. The Partial Programmer decomposes the software into a set of sub-programs, one for each output or class of outputs in turn. (Inside every large program is a small one trying to get out - Hoare's Law.)

5. The Semantic Analyser converts the sequential logic of the software into the parallel logic of sets and maps by providing a path condition and consequent action for each program path. Thus semantic analysis yields the functional relation between input and output.

6. The Threat Analyser employs semantic

analysis to compare the software with its specification, expressed in predicate calculus. If a program does not imply its specification, those inputs, the threat, that lead to erroneous outputs are calculated explicitly.

All this applies to a wide class of programs but, of course, decidability is assumed.

I now turn briefly to how MALPAS works. The analysis tools are based on the mathematical theories of directed graphs and regular algebras, though recursion can also be handled. The system transforms a given IL text into a directed graph whose nodes indicate statements and whose arcs, labelled with the elements of an alphabet A, represent the effects of executing statements. By eliminating nodes and combining arc labels using three operators, x (composition), + (alternation) and * (repetition), the graph is reduced to a set of regular expressions in A, one for each procedure. At the same time, control flow analysis is performed.

To analyse the software further, the system calculates each regular expression by applying a homorphism from the algebra of languages over A into a suitably chosen, finite, regular algebra. The choice of algebra depends on the type of analysis being performed while the image of each arc label is governed by the program under analysis.

I conclude with an example that illustrates, via the Threat Analyser, what can go wrong when the requirement for a piece of software is not fully understood. A software procedure ADD was required to run on an 8-bit processor employing two's complement arithmetic. ADD was to satisfy the following properties:

"x and y are input and z is output. Data represents the range of integers from -128 to 127. z is to be the arithmetic sum of x and y unless there is overflow or underflow in which case the values 127 and -127 are to be returned respectively. It is dangerous for z to take the value -128."

After resolving the ambiguities in the informal requirement, the following specification emerged, written in predicate calculus (+ is the arithmetic sum):

```
    (-127 <= x+y <= 127 implies z =  x+y)
and (        x+y >  127 implies z =  127)
and (        x+y< -127 implies z = -127).
```

The procedure, written in an assembler, took the form:

```
[max = 127, min = -127]
1  LD x   JN 2  LD y   JN 4  AD x  JN 5  J 7
2  LD y   JN 3   J 4
3  AD x   JN 7   J 5
4  AD x    J 7
5  LD x   JN 6  LD max  J 7
6  LD min
7  ST z
```

whereupon the response of MALPAS was

```
THREAT:= x<= -1 AND y<= -1 AND x+y = -128
OR       x  =  0 AND y  = -128
OR       y  =  0 AND x  = -128.
```

Thus problems arose whenever the arithmetic sum of the inputs was the most negative number in the machine. Indeed, semantic analysis showed that z took the dangerous value -128 under those conditions. It is worth adding that errors of this type can remain opaque to countless hours of software testing.

Experience to date confirms that in MALPAS we have a most exciting software tool, on the brink of commercial exploitation, that will play a vital role in the certification of safety critical software. Early indications suggest that its use should be highly cost effective.

The Author

The author joined RSRE in 1979 following his Research Fellowship at Merton College, Oxford. He currently holds the position of Principal Scientific Officer.

FLEX: RSRE'S CAPABILITY COMPUTER

J M Foster

Introduction

Flex is a new computer architecture which has been developed at RSRE. It is based on capabilities. A number of implementations of the architecture have been made, including one using the ICL Perq2 hardware, and this version is available for evaluation outside RSRE. Flex has been in use for more than four years, and a considerable amount of software exists. It supports a multi-language environment, and compilers exist for Algol68 and Pascal. An Ada compiler is being completed.

The essence of all architectures based on capabilities is that the hardware or the microcode controls access to data at the finest level of detail so as to make sure that only legal operations are performed. This ensures that only operations of the right kind are applied to the data and that only data which is legally accessible can be reached. A main feature of such computers, therefore, is the ability to control access to data. It is clearly important to be able to arrange that certain data can only be read by the appropriate people, and equally important to arrange that it can only be altered by them. But the idea of capabilities can go much further than that. It is possible to arrange that data can only be used in the appropriate way, that is through the use of particular procedures, special to the kind of data. So we may be able to ensure that information is updated consistently, or only at particular times, or only by people having access to other information, and indeed any kind of check or control that can be programmed can be applied. Furthermore, we can make sure that this is the only way to reach the information. Earlier capability computers, such as the Plessey PP250 (1), the Cambridge CAP computer (2), the Intel iAPX432 (3) and the IBM System 38 (4), did not offer these possibilities in full.

Flex has extended the notion of capabilities in these earlier machines in three ways. First, the idea of capabilities is used on backing store as well as main store, so that all kinds of structured object which can be held in main store can also be held on any of the backing stores with the same degree of protection. There are two points here: the data is structured, and it is protected by the capability mechanism. On the Flex file store we can hold any kind of data with the same kinds of data structuring as are available in Algol68 or Pascal; this includes the ability to hold procedure values on the backing stores. Such a file store is in contrast to one which holds only vectors of characters, unstructured binary and directories. It gives Flex a powerful means of expressing database programs. The backing store data also has the capability protection, including the ability to access data only through procedures, which may be themselves stored on the file store. Flex has an explicit idea of many file stores, it does not treat file store as an extension of the main store but as a separate object in its own right.

The second extension of capabilities is to use them across a network of Flex computers, so that capabilities for data in one machine may be passed to and held in another. Once again Flex allows structured data to be passed across the network, again using the same kinds of data structure as in Algol68 or Pascal and again allowing procedure values to be passed. This means that Flex can not only use a remote procedure call protocol like Courier (5), but also pass new procedures around, as parameters or results, so that new dynamically created procedures can be remotely called by the same protocol.

Third, Flex uses true procedure values in the sense of Landin (6). Procedures in most machines are not free values, they can only be used in a particular context or environment and are not defined outside it. This means that the full benefits of capabilities are not achieved, for, though a procedure may control access to data, the environment necessarily also has access to it. In a system using true procedure values, where the procedure can be cut loose from an environment, this no longer applies, and the procedure can contain the only pointer to an object in the computer. So this allows Flex fully programmed sole

control of access to data. In fact, Flex also uses procedure values as the mechanism for providing an object-oriented machine architecture. Indeed Flex does not use the notion of programs, but uses procedures throughout, programs being merely the special case where a procedure has no parameters and no result.

There is an additional benefit of using capabilities for addressing which helps the designers of interactive systems. It is possible to arrange that the data for many procedures should coexist in the store and to allow values from one to be used freely in the other, provided that the capability rules are met. So in the middle of running an interactive procedure, the user can pick up some of his data, apply some completely unanticipated procedure to it in order to investigate or modify it, and deliver results which can be incorporated in his original data. It is the essence of interactive programming that the course of action is not totally foreseen when the user starts, so this consistency of data addressing combined with the security given by the capabilities is one of the most noticeable features to someone who is using, rather than programming, Flex.

On top of this architecture has been built a programming support system of considerable size and power. About three hundred modules are available to users, varying from large ones, like the compilers, to small ones, like the conversion of integers into their character representation.

This programming support uses a universal system of types, similar to but more powerful than that of ML. These types are sufficient, not only to describe all the values of the compiled languages (Algol68, Pascal and Ada) but also accomplish the much more challenging task of describing the values used in the command language. So all operations are type checked. The same system of types controls the display of values, that is, any value can be examined and displayed in a standard way. This is particularly useful in run-time diagnosis, where any value can be picked out of a run-time environment and displayed or otherwise used.

The same types again control the movement of data across the network between computers. As in Courier, Flex uses a remote procedure call protocol and can send structured data across the network. But the sending of the structures in Flex is controlled by the Flex type system, so the objects which can be transmitted consist of those which can be used in the command language and a fortiori those which can be used in Algol68, Pascal or Ada.

Procedure Values

One of the less familiar notions in Flex is the use of true procedure values. Consider a brief illustration. We suppose that we want to make a channel for the communication of integers. We can write a procedure to generate a channel, using a slightly extended Algol68.

```
PROC make-channel =
STRUCT(PROC(PROC(INT)VOID in,
PROC VOID out):
BEGIN REF INT i = HEAP INT:
     ( (INT j) VOID: BEGIN i: = j END,
       INT: BEGIN i END)
END
```

Any number of calls of make-channel can be made, each of which results in a new pair of procedures with a new common reference. No external program has access to that common reference: there is no notion of environment or display to hold onto the reference secretly. Then each pair of procedures so generated can be used to communicate from one to the other, without any possibility of interference externally. Clearly the bodies of the two procedures could be much more complex. They could carry out any programmed checks on the validity of the transfers which are taking place. So by introducing these true procedure values we have obtained the ability to write arbitrarily programmed controlled access to data, and the data concerned is entirely subject to procedures in question, there is no access at all to the data from anywhere else.

References

1. D M England. "Capability concept mechanisms and structure in System 250" Rev Fr Autom Inf Rech Oper (France) September 1975, Vol 9, p47-62.

2. M V Wilkes, R M Needham. "The

Cambridge CAP computer and its operating system" North-Holland 1979.

3. Symposium on Architectural Support for Prog Languages and Operating Systems. Sigplan Notices Vol 17, No4.

4. V Berstis. "Security and protection of data in IBM System 38". 7th Annual Symp on Computer Architecture 1980 p245-252.

5. "Courier: The remote procedure call protocol". Xerox Corporation XSIS 038112, December 1981.

6. P J Landin. "The mechanical evaluation of expressions". Computer Journal Vol 6, No 4, p308-320 (January 1964).

The Author

Dr Foster joined RSRE in 1961 and worked on computation techniques, producing an early Algol 60 compiler. In 1966 he went to Aberdeen University where he worked on dataflow languages and later to a Chair at the University of Essex. In 1973 he rejoined RSRE where his research has been into computer architecture and formal methods.

SIGNAL AND DATA PROCESSING

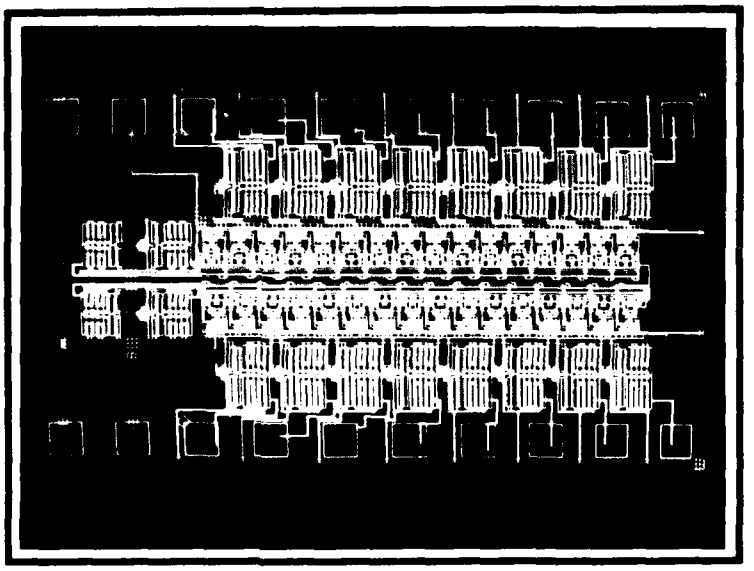

AN OVERVIEW OF OPTICAL SIGNAL PROCESSING TECHNIQUES

M F Lewis

Introduction

The invention of the laser in 1960 led to renewed interest in optical communications with its inherent advantages of enormous bandwidth and low propagation loss, and this has in turn resulted in the 'fibre optic revolution' in telecommunications. In parallel with these developments, interest has grown anew in numerous other aspects of optical signal processing, ranging from image processing to optical computing, where the principal advantages offered are high speed parallel processing with negligible crosstalk. In this review I shall provide a 'snapshot' view of the rapidly-changing optical signal processing scene as a whole. In particular, I shall attempt to highlight the achievements to date, and the remaining challenges in 'established' areas, to indicate the opportunities and obstacles to progress in other areas, and to discuss some of the problems of competing with and interfacing with other technologies.

Table 1 lists some of the principal signal processing operations performed in a modern communications or radar system, and it is interesting to note that optical techniques have been devised which are capable of performing each of these functions. Some are already being exploited, principally solid state sources and fibre optic transmission lines, while the use of acousto-optic spectrum analysers seems imminent. Other workers, eg Stern[1] use a much narrower definition of signal processing, comprising essentially only item 6 of table 1. I have made deliberate reference to Stern's article because the message he conveyed to the audience of the Ultrasonics symposium is equally applicable to the Optics community. A succinct version of this message is that a new technology is only adopted if it offers significant advantages over existing technology taking into account such factors as interfacing and peripheral costs. In particular almost all systems ultimately require to interface with digital electronics which is currently the preferred technology of systems designers because it is familiar, proven, versatile and accurate. This view may help us to find a sensible path through the jungle that is the optical research scene today.

Let us first look at the advantages offered by optical signal processing, table 2. These advantages are impressive, and item 2 is largely responsible for the success of fibre optic communications in which the distance between repeaters has been increased from ~2 km (using coaxial cable) to ~30 km, with projected separations > 150 km[2]. Item 5 of table 2 has long been exploited in numerous fields such as microscopy, photography and photolithography, some more recent examples being (i) the Phillips compact disc (audio) and laservision disc (video), and (ii) in laser rangefinders [3] where the small wavelength results in high 'antenna gains', with full illumination of the 'target' and a negligible clutter return.

It is, however, a sobering thought that one of the greatest strengths of optics, its enormous potential bandwidth (>10^{12} Hz), has not yet been exploited primarily because of the difficulty of <u>interfacing</u> with conventional electronics with bandwidth 10^9 Hz. Current efforts to partially recoup this situation mainly hinge on wavelength division multiplexing (WDM) using dispersive optical elements such as prisms and diffraction gratings. In the <u>time-domain</u> the large bandwidth of optical signals can result in ultranarrow pulses of potential value in signal processing, principally in sampling circuits[4, 5, 6]. Items 3 and 4 of table 2 are exploited in optical imaging, and in Fourier Transformation using coherent light[7], and many current activities in optical computing also aim to exploit these features.

The <u>disadvantages</u> of optics for signal processing form an equally impressive list, table 3. Points 1 and 2 are emphasised by Stern[1]. Point 3 concerns the modest dynamic range of most optical systems (typically 30 dB) which have necessitated the use of digital modulation techniques in telecommunications, although this is hardly a major limitation in this digital age. For single channels we only require 'point'

interfaces. The input interface is often achieved by direct intensity modulation of laser diodes at rates up to several GHz, or of LEDs up to a few hundred MHz. The most common output interfaces are with PIN diodes, avalanche photodiodes (APD) or PIN-FETs, all of which employ the creation of carriers in a semiconductor to detect the incident photons. A current trend in telecommunications is towards coherent detection, which offers significantly improved sensitivity and hence repeater separation, but which presents great technological challenges[2]. The input interface problems are far more severe in 2-dimensional optical systems where a variety of approaches have been devised, but none of which is anywhere near ideal in all respects. This absence of a viable spatial light modulator, SLM, has been the major obstacle to the exploitation of 2d optical signal processing schemes for many years. The problem also affects image processing because the Fourier Transform relationship (eg of a lens) obtains between complex quantities, so it is necessary to employ an incoherent-to-coherent converter (ie an optically addressed SLM) in Fourier Optics.

Returning to table 3, item 4 concerns mechanical stability which, in conjunction with the physical size of many conventional optical systems is a major deterrent to their use, even when they perform a sophisticated function such as SAR processing. No-one willingly employs an optical bench in a terrestrial application, let alone on board an aircraft, but satellites may provide a more benign environment in this respect. Item 5 of table 3 is currently a significant factor, but there is every prospect of continuous improvements in various aspects of the performance of solid state sources in the future, eg by exploiting developments in very high technology. Item 6 (scattering and wavefront distortion) can occur through dust in the laboratory, defects in solid state media and waveguides, and especially during atmospheric propagation. Some techniques have been devised to minimise these effects in specific cases, eg the use of polarisers in anisotropic Bragg Cells to discriminate between deflected and scattered light[8], and phase-conjugation to correct for wavefront distortion[9].

In the following sections we discuss the signal processing applications of fibre optics, integrated optics, acousto-optics and Fourier optics, and conclude with some comments on current trends in optical computing.

Signal Processing Applications of Fibre Optics

The principal application of fibre optics to date is in telecommunications. This is a continuously developing activity with a strong drive at present towards the use of single mode fibres at $\lambda = 1.3\ \mu m$ where the propagation loss and dispersion in SiO_2 are very low. Fibre optics have also been considered for signal distribution in phased array radars (PAR) where they offer advantages in size and weight over coaxial cables. Although not the subject of this review it should also be mentioned that fibre optics are under active investigation for numerous sensor applications, most notably the fibre-optic gyroscope[10]. Of course the low-loss propagation characteristics of fibre optic links are highly desirable in their own right, but they do not use the delay incurred in the process. The simplest exploitation of this delay would be in the use of fibre optics for analog or digital storage eg in radar for testing purposes and MTI applications, and in recirculating serial stores. Using single mode fibre at $\lambda = 1.3\ \mu m$ a time-bandwidth product $TB > 500000$ seems possible[10], and far exceeds the capability of acoustic delay lines. Further, the absolute delays ($\sim 100\ \mu s$) and bandwidths ($\sim$1 GHz) are well suited to the requirements of modern radar and communications systems.

An interesting signal processing application of fibre optics concerns the use of fibre bundles as bandpass filters, Fig 1. The input signal is imposed on the source (laser diode or LED) as amplitude modulation. For bundles with equal incremental delays, τ, the detected optical output has a sinx/x modulation-frequency response, being somewhat analogous to the response of an optical diffraction grating. For example, if $\tau = 1$ ns, this sinx/x response is centred on 1 GHz, and harmonics thereof, including zero. Further, by interposing a spatial light modulator (eg liquid crystal-based) at the input or output of the bundle this microwave filter may be made pro-

grammable[5,11]. The potential applications of such devices include their use as programmable notch filters to reject interference.

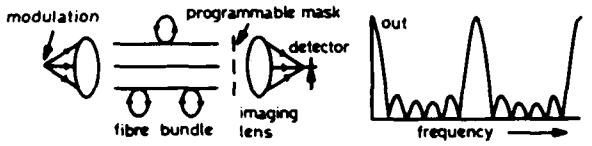

Fig 1 Schematic fibre optic filter and its frequency response

Integrated Optic Devices for Signal Processing

Integrated optic devices comprise a planar (2-dimensional) or ridge (1-dimensional) waveguide in the form of an optically slow medium (high dielectric constant) on a lower-index substrate. The waveguide is invariably designed to be single-mode at the wavelength of interest, and is often employed with a fibre optic input and output. Various layer/substrate combinations have been employed, the most common being Ti-diffused $LiNbO_3$, which is used mainly because of its relatively high electro-optic coefficient. A typical integrated optic component is the Mach-Zehnder interferometer, Fig 2a. This splits an incoming signal into 2 equal paths, one of which can be externally modulated, before recombining them to form the output. A variable applied voltage, V, causes a linear variation of the relative optical phase, leading to a periodic variation of the output signal, Fig 2b. In this device the untransmitted energy is lost into the substrate. An alternative device comprises coupled input and output waveguides lying side-by-side and can be used as a modulator or as a switch for routing purposes. A slightly more complex structure with two modulation inputs in quadrature can be used to implement a single sideband mixer, and is of considerable interest for use in fibre optic gyroscopes[10].

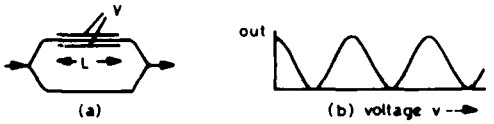

Fig 2 Schematic integrated optic interferometer and its response

Another potentially important use of integrated optics is in the very high speed A-D converter proposed by H F Taylor[5]. This device comprises a parallel array of Mach-Zehnder interferometers with electrode lengths (L in Fig 2a) in a binary sequence to provide variable sensitivities to the common analog input voltage, V. The outputs form a series of periodic waveforms, Fig 2b, which when applied to electronic comparators generate an output in the form of a parallel digital word in Gray-code format. (This is readily converted to conventional binary code). The optical input is a pulse train from a mode-locked laser, and performs the function of a fast sample-and-hold circuit free from electrical interference. A 4-bit version of this device has been operated at 1 gigasample/sec on a 500 MHz bandwidth analog input signal[6]. Although this achievement is most impressive, a number of technolgical problems remain to be solved before it can be exploited.

For completeness we mention two other possible future applications of integrated optics. Firstly, it is possible to separate different optical wavelength components by Bragg reflection from a chirped reflector array[12], Fig 3. This is of potential use in wavelength division multiplexing. Secondly, Taylor[5] has shown that all the binary logic gates employed in a digital computer can be realised in integrated optics - this is one of many current and highly speculative ideas on realising an 'optical computer'.

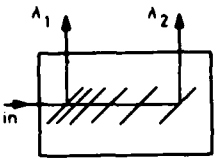

Fig 3 Schematic integrated optic demultiplexer

It is apparent that integrated optics has considerable potential for realising many important functions in signal processing. Despite this, nagging doubts remain on various aspects such as the physical size (cms), reproducibility, optical power handling capability, and long term ageing properties of $LiNbO_3$ devices. Recent progress has however been made on another problem, namely the mechanical interface between fibre optics and integrated optics; it appears that ion-milled slots in the substrate facilitate assembly and produce a more reliable mechanical structure[13].

Several other substrates have certain attractions. In particular, the III-V semiconductors offer the possibility of integrating lasers, detectors, multiplexers and high-speed electronics with integrated optics[14]. However they also present great technological challenges since they work at short wavelengths (~0.85 μm) on substrates of high dielectric constant (~3.5) so require extremely high definition, close to the practical limits of e-beam technology.

Acousto-Optic Devices - For Signal Processing

The basic physical phenomenon employed in acousto-optic devices is the change in refractive index induced by a mechanical strain, eg a compression. A simple picture of the interaction is as follows: a light wave is strongly reflected from the acoustic wavefronts when the Bragg condition is satisfied, Fig 4. During this process the optical frequency is Doppler shifted since the wavefronts are moving at the acoustic velocity. This description is consistent with a full coupled-wave treatment of the interaction, in which ω and k are naturally conserved. Numerous applications of acousto-optics have been devised and a succinct but readable review of their applications to signal processing has recently been provided by Gatenby and Sadler[15]. The principal application is the spectrum analyser which employs an array of detectors to measure the angular spectrum of deflected light, which is itself a measure of the frequency (or wavelength) spectrum of the acoustic wavetrain. Countless versions of this scheme have been described, a currently favoured version employing shear bulk acoustic waves in $LiNbO_3$ in the anisotropic mode in which the optical polarisation is flipped through 90° in the interaction[8]. An important parameter in any acousto-optic cell is its time-bandwidth product (TB) since this determines the number of resolvable frequencies in a spectrum analyser (or the number of resolvable spots in a laser deflection scheme etc). Current best performance figures are T ~1 μs, B ~ 1 GHz, TB ~ 1000, with a dynamic range of ~45 dB and limited by intermodulation effects. In the past much effort was expended on the integrated acousto-optic spectrum analyser (IAOSA) in which a guided optical wave interacted with a surface acoustic wave (SAW), and the whole device could be fabricated on one chip. Unfortunately despite numerous attractive features this device suffered from fabrication and other practical difficulties and its performance has been surpassed by recent developments in bulk acoustic wave devices. Ironically the IAOSA is likely to suffer less from intermodulation problems, since acoustic dispersion is readily introduced to destroy the phase-matching condition needed for the intermodulation to occur[16].

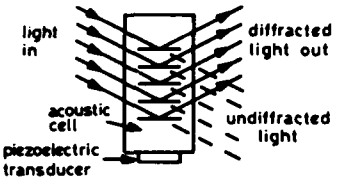

Fig 4 Schematic acousto-optic Bragg cell

One variation on the acousto-optic spectrum analyser described above is to mix the frequency-shifted deflected light beams with an undiffracted beam at each output detector. This heterodyne scheme provides improved dynamic range, and also ensures that the output of each detector is at a beat frequency equal to the input signal/acoustic frequency, so the device functions as a filter bank.

A variety of other applications of acousto-optics have been devised, and below we describe their use in correlators for spread spectrum communications[17]. Before describing the devices it is worth briefly recalling the principles involved. It is well known that the only parameter of importance in detecting a signal in the presence of Gaussian white noise is the ratio E_o/kT where E_o is the signal's energy and kT is the noise power per unit bandwidth. Thus, always assuming that the optimum receiver is employed, the detectability is independent of the precise waveform used. The situation is quite different, however, in the presence of a jamming signal of fixed power, for by spreading our signal over a great bandwidth we can reduce the jamming power per unit bandwidth and so reduce the effectiveness of the jammer. The optimum receiver for such a 'coded' or spread spectrum waveform is either a correlator or a matched filter. The former operates by multiplying the received signal by an identical reference

waveform and integrating the product; this requires precise fore-knowledge of the signal timing. By contrast the matched filter provides an output (correlation peak) for any signal arrival time, ie it is asynchronous. (A quite analogous situation arises in the spatial domain when we employ a matched filter for optical pattern recognition). Clearly, the matched filter is preferable to the correlator. An acousto-optic matched filter configuration was described as long ago as 1967[18] for use in pulse compression radar. However, this device has long been replaced by the much simpler SAW dispersive delay line. The principal difficulty with matched filters is that they become impracticable for long waveforms since their impulse response has the same duration as the signal (it is actually the time-reverse). One solution to this dilemma is to use multiple correlators with staggered reference timings, eg derived from a multiply-tapped SAW delay line[19]. The acousto-optic time-integrating correelator, TIC, is an extreme example of this concept in which the signal is applied to a coherent light source as amplitude modulation, while the reference waveform (in acoustic form in a Bragg cell) is imaged on to a linear detector array containing up to 1000 closely-spaced elements, so that the system covers ~1000 different arrival times simultaneously, a great aid to synchronisation.

The final acousto-optic device considered here is a 2-dimensional processor containing a linear array of acousto-optic Bragg cells, and this will lead naturally into the next section on 2d optical processing. The particular device we shall describe can be used to process the return signals in a phased array radar (PAR) and has one receiving antenna element connected to each input transducer of a linear array of Bragg cells, Fig 5. In this figure a plane input optical beam from above (ie with wavefronts parallel to the plane of the page) will be deflected in the y-direction dependent on the direction of arrival, θ, and in the x-direction dependent on the Doppler shift of the returned waveform. The output of the device (in the Fourier plane of a lens below the plane of the paper) therefore contains direction-of-arrival information along its y-axis and Doppler information (proportional to the target velocity) along its x-direction.

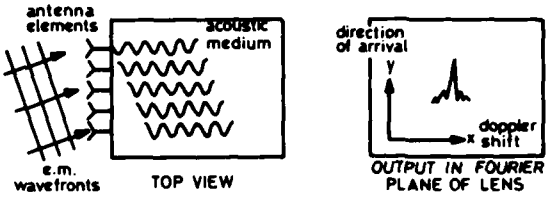

Fig 5 Schematic acousto-optic processor for phased array radar

Such schemes often have great simplicity as they exploit the common wave propagation properties of (i) the em communications or radar signal, and (ii) the signal processing medium be it acoustic, optical or other. Nevertheless they have not been widely exploited, at least partly because of the limited dynamic range and accuracy of the computations performed. Similar remarks apply to a much simpler planar SAW transducer array for PAR beamforming and reception, ref 16, Fig 9.

2-Dimensional Optical Signal Processing

We shall begin this section with the topic of coherent optical processing, which invariably exploits the Fourier Transform properties of an optical lens, i.e. the Fourier Transform relationship between the complex amplitude distributions of monochromatic light in the front and back focal planes of a lens. An attractive application of this property is to implement a two-dimensional (2d) matched filter for use in optical pattern recognition, the advantages of such a device being analogous to those of the 1d matched filter for spread spectrum receivers discussed earlier, but in the spatial domain[7]. We shall not discuss this topic further here as **image processing** is a major field in its own right. However we should mention that schemes can be devised to employ this 2d arrangement as a bank of 1d matched filters, eg to decode a 1d time-domain spread spectrum waveform. Another potentially powerful application of Fourier optics is in spectrum analysis. In particular it is possible to exploit the techniques of folded spectrum analysis to process a long time-duration waveform in a 2d optical processor. In effect, if the incoming 1d waveform is written in 2 dimensions line-by-line as in a page of text, it turns out that the output spectrum appears in a similar 2d format with coarse frequency information in one dimension, and fine resolution in the orthogonal dimension.

An example of the power of this scheme is the work described by Casasent[20] which shows a processor with TB-product $\sim 3.10^5$, and which is capable of a spectral resolution of 40 Hz in a 12 MHz bandwidth. In most such demonstrations the input waveform has been pre-recorded on film (eg by using a z-modulated CRO), although 'real-time' operation has been demonstrated by the use of a complex arrangement of SLM and Bragg cells[21]. In the author's view this is one of the systems that could most benefit from fast viable SLMs.

It should also be mentioned that various incoherent optical techniques have been devised for signal processing applications. For example Goodman et al have described the use of the 'Stanford matrix-vector multiplier' to perform discrete Fourier Transforms on 1d data input through a linear array of LEDs[22]. Although this scheme is extremely elegant and fast, its disadvantages are its limited accuracy, and the need to triplicate the linear dimensions and to employ peripheral electronics in order to handle complex numbers.

Before leaving this section, some comment is in order on the use of optics to process synthetic aperture radar, SAR, signals. This extremely sophisticated processing (described for example in ref 20, Ch 4) was an early example of the power of optical signal processing. However as time passes it is being steadily replaced by digital processing which offers greater accuracy and flexibility; in this latter category comes the ability to compensate for unwanted aircraft motion. Any remaining role for optical processing will probably be confined to providing a rapidly processed low-fidelity image, e.g. as a preliminary survey of a large terrain, or to provide the aircraft crew with a real-time scene in conditions of adverse illumination.

The topics of 4-wave mixing and phase conjugation[9] rightly belong in this section, but we have not discussed them here as their signal processing capability is basically similar to that of Fourier optics.

Optical Computing

In this final section we briefly comment on the potential role of optics in computing, a topic which, like many of the others discussed here, was conceived over 2 decades ago[23]. In the meantime digital electronic computers have advanced through many stages of increasing complexity and processing power, from discrete components, through integrated circuits and LSI to VLSI, with the future propsect of VHPIC and VHSIC. It is fascinating to note that today VLSI digital processors are facing two significant problems, each of which can in principle be solved by the use of optical techniques. The first concerns the desirability of extending the memory base and reducing its access time, the second concerns the problems of interconnection density, speed (i.e. slowness!), and crosstalk. Concerning the former, optical storage is one of many techniques that have been and are being actively investigated to implement large, cheap, rapidly accessible memory units for peripheral use in computers and elsewhere. On the second point, the possibility of employing optical interconnections within computers was mooted by O.A. Reimann as long ago as 1964 (ref 23, ch 14), and has recently been discussed in greater detail and in a modern context by Goodman et al[24]. One especially simple and useful such application would be to broadcast the clock signal optically to a distributed array of on-chip photodetectors in order to avoid the problem of clockskew. Thus optical techniques could beneficially provide two forms of 'bolt-on' improvement to conventional digital computers. To extend further the use of optical interconnections in computers would appear to require major design changes involving for example, the use of direct-gap semiconductors (e.g. GaAs instead of, or as well as Si), and the imposition of optical tolerances on the overall structure. In these circumstances it is pertinent to enquire whether optical techniques could be employed to perform the entire processing function. The widespread interest in such a possibility is evidenced by many recent publications, e.g. ref (25). Earlier investigations into optical computing, eg the Stanford matrix-vector multiplier[22], were mainly the counterparts of analog electrical computers and suffered the same limitations in accuracy (in the optical case through the sources and detectors, and doubtless by the SLM's if they existed!). Some recent attempts have been made to minimise these limitations by the use of more subtle analog approaches requiring a

limited dynamic range, e.g. residue arithmetic[26] and multiplication by analog convolution[27]. In the author's view such halfway measures introduce so many complications that they are doomed from the outset; certainly their simpler CCD and SAW predecessors have not yet been exploited. The remaining possibility is to implement all-optical digital computing. Various approaches to this task have successfully used optical non-linearities to demonstrate logic gate functions and bistability[28], a more recent example being the work of Smith et al[29]. Perhaps surprisingly, the power budget does not seem to present an inherent problem in such devices[28]. In this context it is interesting to note that the energy carried by a single photon is of order 1 eV, roughly the same as that of an electron in a semiconductor device. In the author's view a successful outcome to this work will need to exploit simultaneously all the advantages of optics (parallel processing, high-speed low-crosstalk interconnections, and large memory bases) and will doubtless require the development of new languages, algorithms and architectures, such as the systolic array[30] and wavefront array processors[31] currently being devised for VLSI.

Conclusion

Optics have many potential applications in signal processing but to date only a few have been exploited, principally fibre-optics for low loss data transmission, and acousto-optics in spectrum analysis. In each case the performance of the optical device greatly surpasses that of alternative technologies, in agreement with our opening remarks. The principal limitations of most other applications of optics concern their accuracy and dynamic range, and the problem of interfacing with electronics. The most obvious and important problem concerns the non-availability of a cheap, reliable, reproducible spatial light modulator (SLM); to date this has precluded the exploitation of many clever 2d optical processors. The attraction of all-optical computing is given a boost by the problems currently being encountered in VLSI, although being realistic, it is likely to be many years or decades before we see such devices seriously competing with digital electronics.

Acknowledgement

I am indebted to numerous workers in Industry and the Universities for discussions which have helped formulate the views expressed here. Within RSRE, I am especially grateful to Dr C West.

References

1. STERN, E., 'Comparison of New Analog Device Technologies for Signal Processing' Proc. 1983 IEEE Ultrasonics Symposium, pp 129-136.

2. MIDWINTER, J.E., 'Coherent Optical Communications', Proc. 7th IEEE Topical Meeting on integrated and guided wave optics (1984), paper ThA5.

3. STITCH, M.L., Laser Handbook (North Holland, 1972), pp 1745-1804.

4. WANG, S.Y. and BLOOM, D.M., '100 GHz Bandwidth Planar GaAs Schottky Photodiode', Electronics Letts. 19, (1983) pp 554-5.

5. TAYLOR, H.F., 'Fibre and Integrated Optical Devices for Signal Processing', SPIE 176 (1979), pp 17-27.

6. BECKER, R.A., WOODWARD, C.E., LEONBERGER, F.J. and WILLIAMSON, R.C., 'Wideband Electro-Optic Guided-Wave Analog-to-Digital Converters', Proc. IEEE 72, (1984) pp 802-819.

7. GOODMAN, J.W., 'Introduction to Fourier Optics', McGraw-Hill, 1968.

8. BAGSHAW, J.M. and WILLIATTS, T.F., 'Anisotropic Bragg Cells', GEC Journal of Research, 2 (1984), pp 96-103.

9. PEPPER, D.M., 'Nonlinear Optical Phase Conjugation', Optical Engineering 21 (1982), pp 156-183.

10. CULSHAW, B., 'Optical Fibre Sensing and signal Processing', Peter Peregrinus Ltd., London, 1984.

11. HANSON, G.J., 'Optical Filtering of Microwaves', IEE Colloquium on 'Manipulation of Microwave Signals', 10 December 1984.

12. LIVANOS, A.C., KATZIR, A., YARIV, A. and HONG, C.S., 'Chirped-grating demultiplexers in dielectric waveguides', App. Phys. Lett. 30 (1977), pp 519-521.

13. NUTT, A.C.G. BRISTOW, J.P.G., McDONACH, A. and LAYBOURN, P.J.R. 'Efficient Fibre-Chip Coupling using Ion-Milled Alignment Grooves on Lithium Niobate at $\lambda = 1.3\ \mu m$', Proc. 7th IEEE Topical Meeting on integrated and guided wave optics (1984), paper ThC3.

14. CARTER, A.C., FORBES, N. and GOODFELLOW, R.C., 'Monolithic Integration of Optoelectronic, Electronic and Passive Components in GaAlAs/GaAs multilayers', Electronics Letters 18 (1982), pp 72-4.

15. GATENBY, P.V. and SADLER, R.J., 'Acousto-Optic Signal Processing', GEC Journal of Research 2 (1984), pp 88-95. A more extensive coverage will be found in a recent book edited by N.J. BERG and J.N. LEE, 'Acoustic-Optic Signal Processing' (Marcel Dekker Inc. 1983).

16. LEWIS, M.F., WEST, C.L., DEACON, J.M. and HUMPHREYS, R.F., 'Recent developments in SAW devices', IEE Proceedings 131 (1984), pp 186-215.

17. CAFARELLA, J.H., 'Device requirements for spread-spectrum communications', SPIE 209 (1979), pp 53-56.

18. COLLINS, J.H., LEAN, E.G.H., and SHAW, H.J 'Pulse compression by Bragg Diffraction of Light with Microwave Sound', Applied Phys. Lett. 11(1967), pp 240-242.

19. DARBY, B.J. and MAINES, J.D., 'The Tapped Delay Line Active Correlator: a neglected SAW device', Proc. 1975 IEEE Ultrasonics Symposium, pp 193-6.

20. CASASENT, D., 'Optical Data Processing', Topics in Applied Physics 23 (Springer-Verlag 1978).

21. ANDERSON, J.L., BROWN, H.B. and MERKEVITCH, B.V., 'Wideband real-time Fourier analyser using folded spectrum techniques', SPIE 180 (1979), pp 128-133.

22. GOODMAN, J.W., DIAS A.R. and WOODY, L.M., 'Fully parallel, high-speed incoherent optical method for performing discrete Fourier Transforms', Optics Letters 2 (1978), pp 1-3.

23. TIPPETT, J.T. et al (Eds.) 'Optical and Electro-Optical Information Processing', Proc. Boston Symposium 1964, MIT Press.

24. GOODMAN, J.W., LEONBERGER, F.J., KUNG, Sun-Yuan, and ATHALE, R.A., 'Optical Interconnections for VLSI Systems', Proc. IEEE 72 (1984), pp 850-866.

25. Proc. IEEE 72 (1984), Special Issue on Optical Computing.

26. HUANG, A., TSUNODA Y., GOODMAN, J.W. and ISHIHARA, S., 'Optical Computation using Residue Arithmetic', Applied Optics 18 (1979), pp 149-162.

27. CAULFIELD, H.J., NEFF, J.A. and RHODES,W.T 'Optical Computing: The coming revolution in optical signal processing', Laser Focus (Nov 1983), pp 100-110.

28. GIBBS, H.M., McCALL, S.L. and VENKATESAN, T.N.C., 'Optical Bistable Devices; the basic components of all-optical systems?' Opt Eng 19 (1980), pp 463-8.

29. SMITH, S.D., MATHEW, J.G.H., TAGHIZADEH, M.R., WALKER, A.C. and WHERRETT, B.S. 'Room Temperature Visible Wavelength Optical Bistability in ZnSe Interference Filters', Opt. Comm. 51 (1984), pp 357-362.

30. KUNG, H.T., 'Why Systolic Architectures?', IEEE Computer (Jan 1982), pp 37-46.

31. KUNG, Sun Yuan, ARUN, K.S. GAL-EZER, R.J. and RAO, D.V.B., 'Wavefront Array Processor: Language, Architecture and Applications', IEEE Trans. C-31 (1982), pp 1054-66.

Table 1

Some Signal Processing Operations

1. Signal Generation
2. Multiplexing/Demultiplexing
3. Transmission
4. Storage
5. Switching/Routing
6. Bandpass Filtering/Matched Filtering
7. Fourier Transformation/Spectrum Analysis
8. Frequency Conversion or Direct Detection
9. A - D Conversion
10. Digital Processing

Table 2

Advantages of Optical Signal Processing

1. Great Bandwidth
2. Low-Loss Propagation
3. Parallel Processing
4. Low Cross-Talk
5. Small Dimensions, $\lambda \sim 1$ μm.
   This feature is commonly exploited, e.g. in
   (a) Aerial reconnaissance and optical storage on film.
   (b) Photolithography for IC production.
   (c) Highly directional antennas (laser beams).
   In the future it may be exploited to perform interconnections between semiconductor chips.

Table 3

Disadvantages of Optical Signal Processing

1. 'New' Strange Technology
2. Electronic Interface (In and Out)
3. Poor Dynamic Range
4. Mechanical Stability
5. Coherent Source Requirement (Cost, Reliability, Temperature Instability)
6. Light is prone to (Rayleigh) Scattering and Wavefront Distortion, especially during Atmospheric Propagation

The Author

Meirion Lewis was born in 1939, and received his B.A. and D.Phil degrees in Physics from Oxford University in 1960 and 1964 respectively. From 1964 to 1972, as a member of the G.E.C. Hirst Research Centre, he worked on Microwave Acoustics and Delay Lines, Paramagnetic Resonance and Relaxation, Thermal Conductivity, Spin Wave propagation and devices, and SAW devices. He has worked at RSRE since 1972 on numerous aspects of SAW and SSBW devices and their applications, principally oscillators and synthesisers, convolvers, low-loss filters, and filter banks. His attention is currently directed towards optical signal processing. He is a Fellow of the Institute of Physics.

ANDIE

M Barraclough

ANDIE, (AEW Nimrod Data-handling Interoperability Evaluator) is a data handling rig which is being used to support the development of the Nimrod AEW and to carry out studies on potential enhancements to the UK Air Defence System.

ANDIE has been designed to permit tests and trials to be performed under as realistic conditions as possible, an essential step in the development of complex software based systems for air defence where it is hoped the full specified performance will never have to be met in the real world.

A very important requirement of Nimrod AEW is that it should interoperate effectively with other elements in the Air Defence System. Such interoperation involves complex interactions between these elements in order to produce a clear and unambiguous representation of the current position to the users of the Air defence System. ANDIE provides the AEW element in trials involving more comprehensive simulation of Air Defence systems on the Air Defence Test Bed at RSRE and other ground based rigs. Such trials allow the complex interactions to be studied early under controlled conditions. This obviates the need to involve operational units until the final validation stage and thus provides a cost effective development by reducing the protracted, expensive and wasteful use of operational equipment and trained service manpower at too early a stage.

An essential step in the research and development of potential enhancements is that of testing and demonstrating to operational staff the benefits the new ideas have to offer. The versatility of ANDIE makes it admirably suited to this task and allows ideas to be refined well before full development is undertaken.

ANDIE has at its heart the Nimrod AEW Data Handling, and Display System, in which is run the Operational Flight Program (OFP) as written for the airborne system. Data to exercise the OFP can be provided from a number of sources to meet the needs of any particular assessment task. These include

a. simulated data from a DEC 10 computer,

b. Link 11 data from a Data Terminal Set and communication equipment,

c. IFF/SRR data from a live secondary radar system,

d. recorded data from mission flight tapes and other sources.

Fig 1 RSRE rig for performance assessment interoperability and research

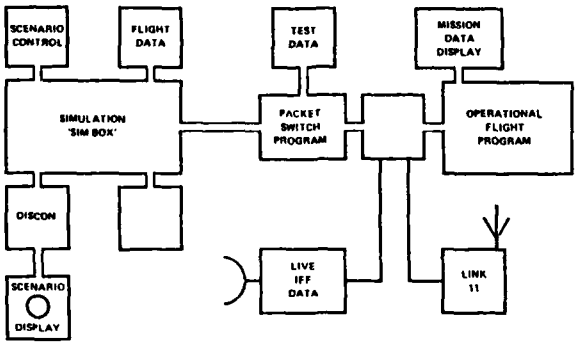

Fig 2 AEW Nimrod data-handling interoperability evaluator

Three main programmes are being conducted on ANDIE. The first is concerned with the performance of the AEW as a self-contained entity and includes assessment of:

1. the performance limits of the OFP;
2. system behaviour under full load and overload conditions;
3. operator loading and procedures;
4. the validity of acceptance criteria;
5. potential software changes and enhancements;
6. factors causing problems during flights.

The second is to study the interoperability of the AEW with other components of the Air Defence System and includes:

7. interoperability with RN and NATO units through the Link 11 data link;
8. interoperability with UKADGE via data link buffers;
9. factors affecting interoperability such as multi site report correlations;
10. command and control problems in the overall defence system.

The third programme is the assessment of system enhancements by implementation of the results of theoretical studies and off line simulation of new concepts and techniques.

The major part of the assessment of AEW performance is conducted with simulations of realistic scenarios created by the simulation tool SIMBOX run on a DEC 10 computer. With SIMBOX, 'objects' eg ships, aircraft, radars etc can be inserted into a 'box' in space and all the interactions between them are computed in real time. The data appropriate to any particular assessment is obtained by means of a SIMBOX 'user program' that in conjunction with SIMBOX generates real time data streams very closely resembling those produced by the surveillance radar, communications and data link subsystems in the Nimrod AEW. On line control of any parameter which affects the operation of any object is also available by means of an interactive display and control system, DISCON, which gives the user a view of the simulated 'real world' and the means of control by keyboard, joystick etc. The data provided by SIMBOX and the 'user program' could be for example the radar and navigation data of a Nimrod AEW. This would be sent over from the DEC 10 to an interface computer, in which runs a purpose-built Packet Switch Program whose function is to send data at the right time down the right channels to the inputs to the 'Data Handling System'.

Assessment can be carried out either qualitatively by observation of the console displays or quantitatively, in which case data, eg track data, provided by additional software in the OFP is fed back to the DEC 10 for either on line or off line analysis. A comprehensive analysis package has been written to provide detailed statistical data on the OFP performance by comparison of track data with the simulated target data.

Investigation of interesting conditions observed during flights have been carried out using recorded flight data and also by setting up simulations to reproduce accurately the conditions noticed during flight. Such investigations will continue as the aircraft enter service.

The second programme, interoperability trials, using the Link 11 data link, was started initially in conjunction with other ground rigs including the Air Defence Test Bed at RSRE and a naval rig at ARE Portsdown. Further trials have involved the display and analysis of Link 11 data either recorded during operational exercises or received directly by use of the comprehensive HF and UHF voice and data communications system. Most recently use

has been made of the ability of ANDIE to produce Link 11 messages based on the data derived from the IFF/SSR sensor system attached to ANDIE and thus operate as a participating unit in a Link 11 net.

The third use of ANDIE, assessment of performance enhancements, is at an early stage. A number of studies including raid tracking, kinematic ranging and improved Man Machine Interface are in progress and some are reaching the stage where implementation on ANDIE is the next step.

As well as these three in-house programmes extensive use has been made of ANDIE by Development Flight Trials crews from A & AEE and the Nimrod Training Squadron. These activities have ranged from initial familiarisation with the operation of the AEW system from the operator's point of view prior to actual flights to the development of trials scenarios on the ground to meet particular flight trials objectives thus allowing cost effective use of actual flight trials resources.

The versatility of ANDIE has allowed and continues to allow this wide range of different activities to be carried out in an effective manner. Its construction is such as to permit proposed enhancements to the Air Defence System to be assessed under both realistic simulated conditions and using live sensors and communications with live operational units. It supports research into new methods of data handling for AEW systems easing the problem of demonstrating the value of such research to operational staffs. It is making a significant contribution to UK Air Defence Development on all aspects involving AEW systems.

The Author

M Barraclough joined RSRE (then RRE) in 1959 to work on digital circuits and computers with emphasis on novel storage devices. From 1971 to 1977 worked on the man-machine aspects of Air Traffic Control. This period included 2½ years attachment to the Civil Aviation Authority. Since 1977 he has worked on the Nimrod AEW project with responsibility for the Data Handling Aspects including the development of the ANDIE rig at RSRE.

APPLICATION OF SEMI-MARKOV MODELS TO AUTOMATIC SPEECH RECOGNITION

M J Russell and R K Moore

Introduction

One of the most successful approaches to automatic speech recognition to emerge in recent years is a statistical pattern recognition technique called hidden Markov modelling (see for example [1]). With this technique each word in a vocabulary is represented as a probabilistic function of a Markov process, or hidden Markov model.

A hidden Markov model consists of an underlying Markov chain, of the type depicted in figure 1, plus a set of multivariate probability density functions, one for each node of the Markov chain, which are called the states of the model. Intuitively the states describe variations in the pronunciation of different regions of a word while the underlying Markov chain describes the temporal structure of that word. Thus in hidden Markov modelling a speech signal is treated as the output of a sequence of stationary stochastic processes.

Fig 1 State transition diagram representing a 5 state Markov model

Such an approach has several attractions. First, it has been shown that dynamic time-warping, the most significant speech pattern-matching methodology of the 1970s, is a special case of hidden Markov modelling [2]. Second, a hidden Markov model provides a formal statistical framework for modelling spectral and temporal variability in speech signals. Finally, hidden Markov models are mathematically sufficiently simple to enable rigorous optimisation and recognition strategies to be applied.

However, it is also clear that many properties of hidden Markov models are inappropriate in the context of speech. For example it is well known that transitory regions in speech signals can have contrastive significance, but transitory information is not accommodated in conventional hidden Markov models. Furthermore, the Markov property, which contributes greatly to mathematical simplicity, has undesirable consequences for the way in which temporal, and in particular durational, structure is modelled.

This paper describes some of the problems which arise in first-order Markov modelling of temporal structure in speech signals and shows how they can be alleviated by generalising the concept of hidden Markov model to incorporate an underlying semi-Markov process.

Modelling State Durations

Temporal structure in a hidden Markov model is determined by the underlying Markov chain which, in turn, is completely specified by a state transition probability matrix. The time spent in states is modelled by the diagonal elements of this matrix while the off-diagonal elements model sequential structure.

More precisely, if the probability of a transition from a particular state to itself is denoted by p, then the probability d(n) of remaining in that state for precisely n time-units is given by:

$$d(n) = p^{(n-1)}(1-p)$$

In other words, the statistics of state duration in a hidden Markov model are described by a geometric probability density

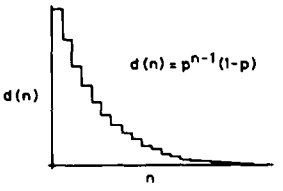

Fig 2 Geometric probability density function

function, of the type shown in figure 2.

It is unlikely that such a function is an appropriate model for duration in speech signals. Instead, one would expect each state to have a most probable 'target

duration' with lower probabilities assigned to shorter or longer durations. By contrast, a geometric probability density function is biased towards short state durations. Consequently it can be difficult to discriminate between words for which durational structure provides a primary cue for discrimination. These problems are accentuated in connected word recognition, where the absolute durations of words are not known in advance. In this case the bias in the geometric probability density function can cause states to assume their minimum duration, giving rise to an over estimation of the number of words that were spoken.

This suggests that improved performance would be achieved by ignoring the diagonal elements of the state-transition probability matrix and modelling state duration directly with more appropriate forms of probability density function. In this case the appropriate model of temporal structure is a semi-Markov process.

Hidden Semi-Markov Models

A semi-Markov model [3] consists of an underlying Markov chain, together with a sequence of 'state duration' probability density functions. A typical semi-Markov model is represented in figure 3. Notice that 'loop transitions', from a state to itself, are absent since state duration is modelled explicitly by the state duration probability density functions.

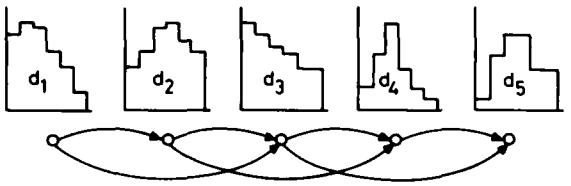

Fig 3 Diagram and state duration pdfs for a semi-Markov model

The concept of hidden Markov model can be extended to incorporate an underlying semi-Markov process. The resulting model is called a hidden semi-Markov model [4]. Intuitively the stochastic process associated with such a model can be described as follows. At some time the process enters a state. It then remains in that state for a period of D time units during which time a sequence of D vectors is generated. The duration D is drawn randomly from the state duration distribution and the observed vectors are determined randomly (and independently) according to the state. At the end of the period the process moves on to another state which is determined randomly by the underlying Markov chain. The cycle is then repeated.

In a hidden semi-Markov model speech recognition system, recognition is performed according to a maximum likelihood classification rule. Each word in the recogniser vocabulary is represented by a suitable hidden semi-Markov model and an unknown utterance is assigned to the class of the model for which its likelihood, conditioned on the model, is greatest.

Parameter Estimation

The preceding section shows how hidden semi-Markov models can be applied to the task of automatic speech recognition. However, the critical problem of model parameter estimation has not been addressed. The key to the successful application of these techniques is the ability to automatically construct an effective model for each word in a vocabulary.

The most common approach to hidden Markov model parameter estimation is founded on a theorem of Baum (see [1]). Given a set of examples of a particular word and a hidden Markov model, Baums theorem shows how a new model can be generated which has the property that the likelihood of the set of words conditioned on the new model is greater than or equal to their likelihood conditioned on the original model.

Hence the standard hidden Markov model parameter estimation procedure for a particular word, represented by a set of training utterances, is as follows. First an initial estimate of the model parameters is obtained. This estimate might be chosen randomly, derived from one or more example utterances, or compiled using prior knowledge of the structure of the word. Baums theorem is then applied repeatedly until the increase in the likelihood of the set of training utterances between successive models falls below some threshold. This process is commonly called

the Baum-Welch or Forward-Backward algorithm. Because the forward-backward algorithm is simply a 'hill climbing' technique, the process is only guaranteed to find a hidden Markov model which is locally optimal. Hence the choice of the initial model can be crucial.

Fortunately, Baums theorem can be extended to the case of hidden semi-Markov models, provided that suitable constraints are placed on the forms of the state duration probability density functions [5]. Hence hidden semi-Markov model parameter estimation can be achieved using a generalised version of the forward-backward algorithm.

Recognition Experiments

The following experiments were conducted in order to compare the performance obtained using hidden Markov and hidden semi-Markov models for the task of speaker dependent isolated word recognition. Three different vocabularies, V_1, V_2 and V_3 were considered.

Vocabulary V_1 contains recordings of isolated digits from five speakers. Each speaker recorded ten samples of every digit for training and fifteen for recognition. The second set, V_2, contains five training examples and ten test examples of each letter in the orthographic alphabet, spoken by a single speaker. The final set, V_3, was chosen to test the performance of both types of model on pairs of words for which duration is important for discrimination.

V_3 contains ten training examples and one hundred test examples of each word from the pairs "pod-pot", "league-leek" and "close(door)-close(near)".

Results

The results of the experiment are displayed in table 1. It should be stressed that the experiment is comparative and that it is the relationship between the scores rather than their absolute values which is of interest.

On tasks V_1 and V_2 the performance of both methods are comparable. The most interesting result occurs in task V_3, where the overall error rate for hidden semi-Markov models is significantly less than that for hidden Markov models. This demonstrates the ability of semi-Markov models to capture durational structure, since accurate modelling of durational structure is essential for discriminating between the words in this test set.

	Hidden Markov Models	Hidden Semi-Mrkov Models
Digits		
(Speaker 1)	6.7	6.3
(Speaker 2)	0	0
(Speaker 3)	0.3	0
(Speaker 4)	0.7	0.7
(Speaker 5)	5.7	9.0
Alphabet	6.9	8.1
Word-pairs	26.5	14.7

Table 1 Percentage error rates for the experiment described in the text

Conclusion

Hidden semi-Markov models are a natural extension of current approaches to automatic speech recognition based on dynamic time-warping and hidden Markov modelling. They offer a more flexible framework for modelling temporal structure, but at the same time maintain sufficient mathematical simplicity to allow proven training and recognition strategies to be applied. They represent the most recent development in a continuing programme of research at RSRE which is directed towards high accuracy automatic speech recognition through the identification and characterisation of important sources of variability in speech signals.

References

1. S E Levinson, L R Rabiner and M M Sondhi, "An introduction to the application of the theory of probabilistic functions of a Markov process to automatic speech recognition", Bell Syst Tech J, 62, 1035-1074, 1983.

2. J S Bridle, "Stochastic models and template matching: different techniques for automatic speech recognition:, Proc Institute of Acoustics, Autumn Conf, 1984.

3. L Kleinrock, "Queueing systems. Volume 1: Theory", Wiley, 1975.

4. M J Russell and R K Moore, "Explicit modelling of state occupancy in hidden Markov models for automatic speech recognition", Proc IEEE Int Conf Acoustics, Speech and Signal Processing, 5-8, 1985.

5. M J Russell, "Maximum likelihood hidden semi-Markov model parameter estimation for automatic speech recognition", RSRE Memorandum Number 3837, in preparation.

The Authors

M J Russell joined RSRE in 1980 with a background in Pure Mathematics. He is a member of the team working on Automatic Speech Recognition, and is mainly concerned with research into pattern recognition techniques for speech processing. Dr Russell has published several papers in the field.

R K Moore joined RSRE in 1980 in order to lead the research on "Automatic Speech Recognition". Dr Moore has published more than 30 papers in this field and is chairman of the Institute of Acoustics Speech Group, the Speech Technology Assessment Group and the NATO Research Study Group on Speech Processing, RSG10.

PRIOR KNOWLEDGE IN SYNTHETIC APERTURE RADAR (SAR) PROCESSING

S P Luttrell and C J Oliver

Introduction

All that we know of the world about us has been deduced from data collected by our senses (eyes, ears, etc), and those of our ancestors. Usually we employ sophisticated transducers (microscopes, telescopes, radars, etc) to transform signals into a form which our senses can "see", therefore we require an accurate model of the transducer(s) if we are to know how our sensory data is acquired. Furthermore we require a model of the source of the signals being transduced in order to "make sense of" this data. We shall call this model "prior knowledge", because it exists in advance of acquiring the data. Such prior knowledge manifests itself with various degrees of complication. In some cases the model may leave very little undetermined, and it remains to determine the values of a finite number of parameters from the data. This type of situation arises when we take measurements of a well known and controlled phenomenon. In other cases the model may provide only a weak constraint on the source of the signal. This may be for two basic reasons: we are ignorant of what we are observing, or we have a detailed model but it contains a large number of parameters. It could be argued that these are the same reason! In all cases however the model is essential if the data is to be interpreted at all.

Information Theory And Prior Knowledge

The basic theory of information was formulated by Shannon. His interest lay in the transmission of information over noisy communication channels. Fortunately the theory is expressed in very general terms, and so we may use it to analyse the information which is acquired by sensors.

In the previous section we pointed out that data may be interpreted only in the light of a model. In other words the information content of sensor data is measured with respect to a model, and so it is not an absolute quantity! The only truly meaningful information measure is thus "relative information". In this spirit it is meaningless to speak of the information content of data ALONE; it is always necessary to refer to the model being used to interpret the data. Our intuitive notion that an image (a radar picture, say) alone conveys information to us, holds true only because we have a prior notion of what we expect to give rise to such an image - there is an implicit model.

This view of models and data interpretation may seem unduly philosophical! However if we wish to perform a disciplined analysis of what information is, where it comes from, and where it goes to, it is absolutely necessary to identify ALL the information sources (and sinks!): prior knowledge is the most important implicit information source.

Data Acquisition And Prior Knowledge

A striking way in which prior knowledge may be used is to optimise the way in which data is acquired. In order to understand how this is achieved, the meaning of data *redundancy must be understood.* Data is redundant if the signal is oversampled: there will not be much potential signal information present (which is undesirable), but what information is present is robust with respect to the effects of data noise (which is desirable). As the redundancy is decreased the amount of potential signal information is increased at the expense of reducing the data's robustness to noise. Clearly we cannot maximise potential signal information AND robustness with respect to noise simultaneously - a tradeoff must be sought. Information theory provides a framework for solving this problem. Thus *the net level of signal information in the* data may be calculated as the potential information content LESS the amount of information lost in data noise; both of these quantities have rigorous definitions within the framework of information theory. However the POTENTIAL information content is the signal information measured relative to the prior knowledge of the signal source (the model), and so the NET information also depends on the prior knowledge. Thus in seeking the optimum way in which to acquire data we must bear in mind that the

optimisation is prior knowledge dependent. We must therefore "match" our transducer/sensor system to the available prior knowledge. This statement is intuitively obvious, but its expression in information theoretic terms is subtle.

The simplest type of data acquisition schemes are well represented as point samples of a continuous "field". Optimisation of the net information (for a given prior knowledge) is then achieved by finding those positions at which it is best to place the samples. In practice there is a cost associated with each sample, and so we should place constraints on the sampling possibilities which are to be considered in the optimisation. The great advantage of this information theoretic approach is that it rigorously combines prior knowledge and data into a composite pool of information. Thus all sources of information are treated on the same footing as required in a unified approach to the problem of sensory data acquisition and interpretation.

Application To Synthetic-Aperture Radar

Let us next discuss how the concepts of prior knowledge may be applied to the interpretation of synthetic-aperture radar (SAR) surveillance imagery. A SAR is a coherent radar which synthesises a large effective aperture by combining the signals which are received at well separated points. The large synthetic aperture gives a radar image with very high resolution when compared with conventional radar imagery. For simplicity we shall assume that such surveillance data is acquired by a conventional sampling scheme (eg Nyquist sampling). These images comprise an enormous quantity of data, eg 300,000 samples per second, of which the principal component is map-like terrain imagery, which we shall call CLUTTER, within which may be set a few significant objects, termed TARGETS. The clutter requires interpretation in the form of segmentation and classification into a comparatively restricted set of features, eg woodland, fields, rivers, roads, built-up areas etc. Targets within such a scene would then be viewed against a background represented by the different categories of the model.

The observed SAR image could arise from an enormous number of different scatterer configurations all of which would be indistinguishable. If we introduce additional information in the form of prior knowledge about the scatterer properties, then the number of feasible scatterer configurations is reduced to a manageable size. It is necessary to devise a suitable means of representing this prior information. One approach is to formulate models which represent the scatterer configuration and then interpret the image in terms of the parameters of these models. The models contain any prior knowledge we possess about the scattering process and the microscopic or macroscopic structure of the objects which can aid our interpretation of clutter and targets within SAR images.

Clutter Models From Prior Knowledge

A striking feature of SAR images is speckle, which occurs for the same reasons as laser speckle. Speckle arises because coherent illumination preserves phase detail in the scattered field, which in turn permits constructive and destructive interference to occur between the various scattered waves. Such interference gives rise to images with a characteristic granular, or speckled, appearance. A suitable model for speckle production is one in which a large number of scatterers are randomly positioned within each resolution cell. For a constant scatterer cross-section the received field has complex Gaussian statistics with Rayleigh-distributed envelope and negative-exponential intensity (the so-called Gaussian speckle). The image of uniform grass typically demonstrates this type of statistics. More generally we may use a model in which the underlying cross-section fluctuates from resolution cell to resolution cell. The total field would then result from the convolution of the underlying fluctuation with the Gaussian speckle. The underlying fluctuations would then be obtained by deconvolving the speckle. Unfortunately the number of feasible solutions is very large, and so despeckling algorithms cannot provide unique solutions. This is because the effective signal to noise ratio in a speckled image is of order of unity. We shall discuss later (super-resolution) how small regions of the image "speckle" contain valuable information on targets.

In order to progress beyond the simple

scattering model above we need to introduce knowledge about the terrain structures themselves. Indeed, it is the correlations within the image, containing the structure of the scene, which convey the most information about the terrain. Our brains are capable of using this information for segmentation and classification. In principle, measurement of all the correlations between pixel intensities could be used in automatic classification. However the computational task for such a multi-dimensional approach is not feasible, so we are forced to consider simpler models which use only, for example, the spatial autocorrelation function and the single-point moments to represent the different classes of terrain.

The observed structures in the image may be either microscopic or macroscopic in scale. For example, microscopic terrain statistics could be used to represent the structural properties of a single class of terrain. In a wooded area one might represent the local structure in terms of the autocorrelation function of the image which would in turn be related to the underlying spatial scales and fluctuations. The spatial scale would be related to quantities such as tree size and separation, whereas the depth of fluctuation would depend on the extent of shadowing between trees and their variability of cross-section. In principle, the exact positions of individual trees and their sizes could be used in such a model but it seems more sensible to treat the cross-section within the feature as a random statistical variable with appropriate statistics and correlation properties. Thus a model which allows us to include arbitrary spatial spectra and a parameter which describes the spikeyness of the fluctuations is called for. One such model is that in which the surface cross-section is gamma-distributed, arising from regarding the local scatterer density as being the result of birth-death-migration process. In addition to defining the single-point statistics, correlations within the surface cross-section are also introduced. Following coherent imaging the resultant clutter then consists of correlated K-distributions.

The microscopic structure model treats the surface cross-section as a statistical random variable. It makes no use, therefore, of deterministic information on the positions of the boundaries of the different features which make up the image. In many cases such information is readily available from maps or other types of image. The microscopic model implies that the total cross-section is made up of the incoherent summation of individual cross-section contributions. Each feature may thus be treated separately. The total image intensity may be calculated by simply summing the intensities generated by each type of terrain within the resolution cell when imaged with the appropriate imaging response function. Therefore combining these three types of prior knowledge enables us to predict expected clutter properties for arbitrary distributions of terrain features and system resolution.

Super-Resolution From Prior Knowledge

Having separated the SAR into target and clutter components by using a suitable threshold derived from the clutter model explained in the previous section, we may introduce further target-specific prior knowledge in order to analyse the target data. An effective way to proceed is given by SUPER-RESOLUTION theory. This technique is used to process the target data so that detail which was not originally apparent becomes clear. This is not a trivial filtering of the data to remove the effects of noise, rather the technique goes further and performs an inversion (or deconvolution) of the data acquisition process to provide us with an estimate of the distribution of scatterers within the target. The extent to which this inversion can be achieved depends on the "strength" of the target prior knowledge. In particular a useful degree of inversion is achieved if this prior knowledge states that most of the received signal derives from a source signal that has a restricted spatial (and/or temporal) extent, which is usually the case for targets. The use of such prior knowledge is intuitively clear since we can then discount the possiblity that the inverse contains any pieces which lie outside the a priori admissable region; the inversion process may then concentrate on the admissable region ALONE. In practice the source signal is never completely constrained to lie in such a restricted region because the target data will contain contributions from the surrounding clutter, and so it is false to

assert that all the energy comes from the target alone. However we have generalised the basic super-resolution technique to allow for this effect. Furthermore we have formulated a more general version of the technique which permits prior knowledge of internal target structure to be systematically incorporated into the super-resolution algorithm. In practice this technique may be applied with increased effect as the signal to clutter ratio of the SAR data rises beyond the minimum level required for target detection. The output of the super-resolution algorithm can be used as the input to a more general target recognition algorithm, which in turn could feed its conclusions back to control the super-resolution algorithm as necessary. Thus our technique should be viewed as one step in an integrated approach to data interpretation.

The super-resolution algorithm thus performs a simultaneous noise filtering and inversion of SAR target data. It exhibits the desirable property of "graceful degradation"; weakening the prior knowledge merely reduces the extent to which the inversion is taken. In the trivial case when no prior knowledge is supplied the output is merely an interpolation of the data. More generally the output is the same as would be produced by a suitable Wiener filtering of the data. The particular choice of Wiener filter is subtle, and it is made according to what prior knowledge, data acquisition system and data noise are present. Such a filter uses the detailed form of the "speckle" in the vicinity of a target to deduce the target structure.

Some typical super-resolution results are shown in the figures. A composite object made up of four components, each with the same cross section but random phase, is combined with a clutter background in figure 1. The corresponding data set (image) is shown in figure 2; note that the target detail has been blurred into a single broad peak. Figure 3 shows the output of the super-resolution algorithm without feedback control, and figure 4 shows the output after a small amount of feedb control has been introduced. Both of these outputs exhibit an enhancement of resolution when compared with the original data set in figure 2, and feedback control is seen to provide the better output as expected. The types of feedback which we can introduce are varied and depend in detail on the particular application, so figure 4 should not be taken as an exhaustive example of the types of result which we can obtain.

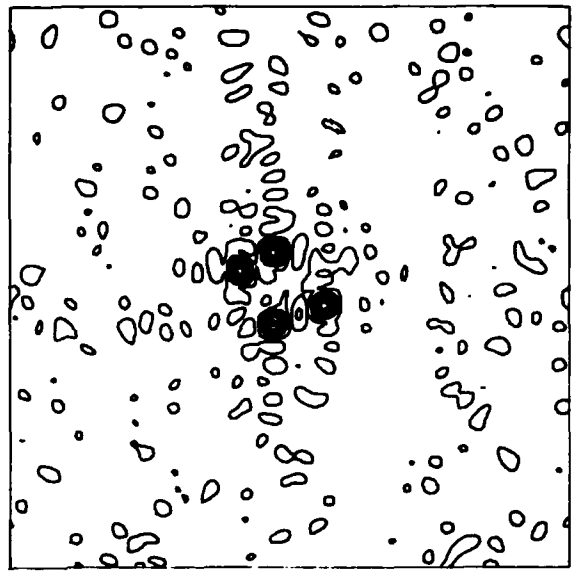

Fig 1 Composite object in clutter

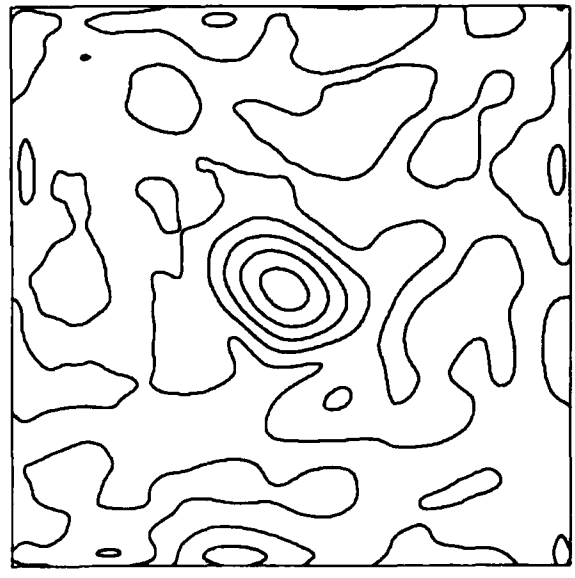

Fig 2 Data set

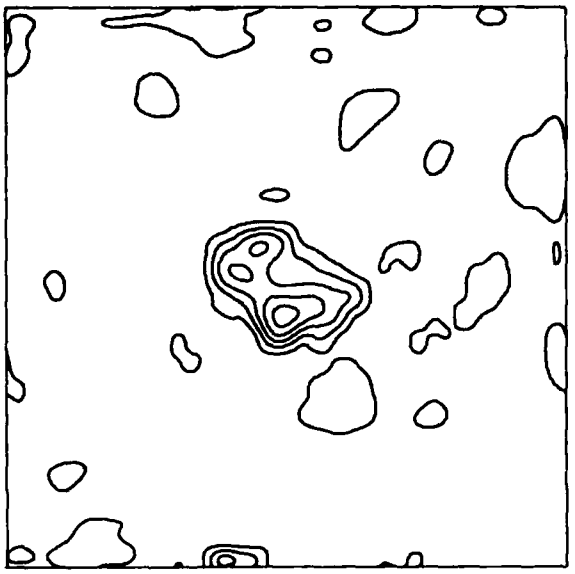

Fig 3 Super-resolved data (no feedback control)

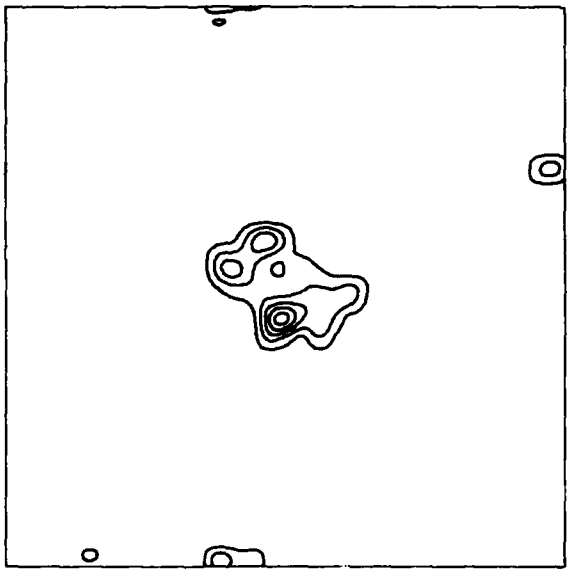

Fig 4 Super-resolved data (with feedback control)

Conclusions

We have shown how both data acquisition and data interpretation must be conducted in the context of whatever prior knowledge is at hand. Thus the choice of how we should "deploy" a set of sensors in order to acquire the maximum amount of useful information must depend on what we already know. Information theory provides a means of making this choice in a systematic fashion. For an image which has been acquired by a SAR sensor the problem of interpretation is subtle. This can only be conducted if a model (prior knowledge) of what caused the image is available. A model with correlated gamma-distributed cross section fluctuations fits the clutter which is observed in SAR data. Such a model can be augmented by the inclusion of collateral map data of the scene which the SAR is surveying. Thus the map may be used to determine the clutter model parameters in advance of receiving the SAR image data. Regions of the SAR image which are inconsistent with this clutter model (typically small bright regions) are called targets; a different model is needed for these regions. A general method of interpreting such target data is provided by super-resolution. Thus prior knowledge of the general properties of targets is introduced in order to extract the maximum amount of target structural detail from the image. The effect of such processing is to enhance the resolution of the target image.

All our SAR data processing operations are conducted within an information theoretic framework. This is crucial because there are many ways of processing data to produce APPARENT detail out of nothing! Thus we explicitly identify all prior knowledge sources (ie models) and their implications for image processing. Such a unified approach to image processing is necessary for systematic information extraction.

The Authors

Dr Luttrell joined RSRE in 1982 on completing his PhD work in the field of quantum chromodynamics. Since then his role has been to conduct basic theoretical research into various aspects of data acquisition and interpretation. His fields of interest include information theory, sampling, physical model building, resolution enhancement, and learning.

Dr Oliver joined RSRE in 1967 to conduct research on photon statistics. He shared the MacRobert Award for this work in 1977. Since then he has investigated aspects of image coding and coded laser rangefinding before becoming involved in the interpretation of coherent synthetic-aperture radar images. Here his particular interests are in clutter modelling and resolution enhancement.

INFRARED AND LASERS

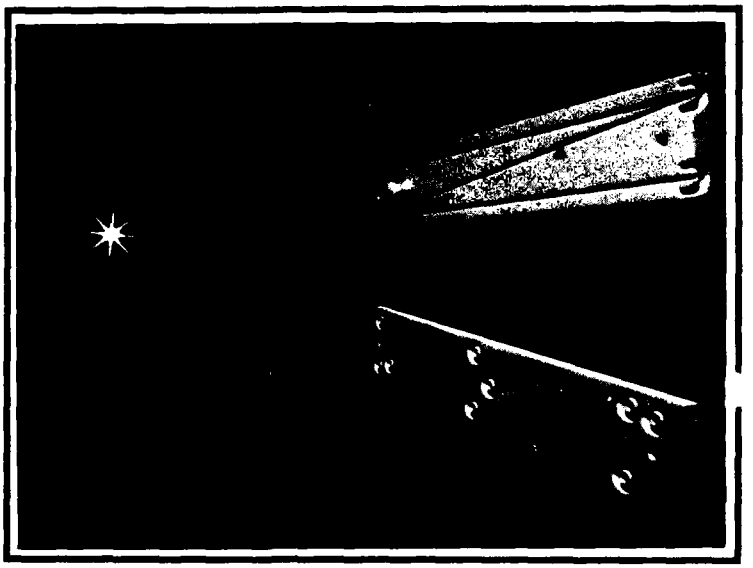

THE INFRARED APPLICATIONS OF CHALCOGENIDE GLASSES

J Savage

Abstract

In the past 20 years chalcogenide glasses have been actively researched in order to determine their suitability as passive bulk optical component materials for 3-5 μm and 8-12 μm infrared applications and as active electronic device components in photocopying and electronic switching applications. Much theoretical and experimental work has been done which has led to a greater understanding of the glass forming and general physical properties of these materials. This review concentrates upon the optical and general properties of these bulk chalcogenide glasses.

Introduction

The chalcogenide glasses are so named because they contain one or more of the chalcogenide elements S, Se or Te together with one or more of the elements Ge, Si, As, Sb and a number of others. They are mainly covalently bonded materials with room temperature resistivities between 10^3 and 10^{13} ohm cm. For instance As_2S_3 has a resistivity of 2×10^{12} ohm cm (130°C), As_2Se_3 a resistivity of 1.5×10^8 ohm cm (130°C), Se a resistivity of 2×10^4 ohm cm (120°C) and As_2SeTe_2 a resistivity of 3.5×10^3 ohm cm (130°C). The conductivity activation energy of these glasses varies from 0.3 eV to 1.25 eV while the optical energy gap approximates to that of the crystalline analogues where these exist (Edmond 1968).

For optical applications the chalcogenide glasses possessing the higher resistivities mainly sulphides, selenides, and mixed selenide tellurides are utilised and during the 1950s major work first centred on arsenic trisulphide as an optical material for the near and middle infrared. This work led to commercial exploitation and arsenic trisulphide is now well known as an optical component material. During the early 1960s to the early 1970s it was shown that selenide glasses and mixed selenide-telluride glasses were suitable for optical component applications in the far infrared and the commercial exploitation of these glasses is now established. Generally the sulphides offer some limited visible transmittance, while the selenides and tellurides are opaque in the visible part of the spectrum. For useful thicknesses of a few millimetres, sulphides offer transmittance from 0.7 to 12 μm, selenides from 1.0 to 15 μm and tellurides 2.0 to 20 μm. The infrared refractive indices are in the range 2 to 3 and the reciprocal dispersive power V_{8-12} ranges from around 100 to 200 depending upon the glass composition. Reported infrared absorption coefficients range from 4×10^{-1} to 7×10^{-3} cm^{-1} depending upon the wavelength, purity and chemical composition. Extrinsic absorption can be a problem with these optical glasses and in particular oxygen impurity must be kept $\leq$ 1 ppm in the final product to avoid excessive absorption particularly between 8 and 12 μm.

While the optical and electrical properties of the chalcogenide glasses are reasonably well known, other properties such as thermal conductivity, hardness, the elastic moduli and the mechanical properties are less well known. There is some information on how these latter properties vary with chemical composition amongst the sulphide (Tsuchihashi *et al* 1968) and selenide glasses (Tille *et al* 1977) (Michels and Frischat 1982). For instance Hilton *et al* (1975) have shown that amongst Ge-As-S glasses Knoop hardness can vary from 200 to 280 kg/mm^2 while Young's Modulus varies from 20×10^9 Nm^{-2} to 41×10^9 Nm^{-2} and amongst the selenide glasses the knoop hardness can vary from 100 to 200 kg/mm^2, while Young's Modulus varies from 14×10^9 Nm^{-2} to 27×10^9 Nm^{-2}. The fracture toughness of Ge-As-Se glasses ranges from 5.5 to 9.4 $Nmm^{-3/2}$ (Michels and Frischat 1981a) while the four point bending strength varies from 1 to 2.5×10^7 Nm^{-2} (Michels and Frischat 1981b). The thermal conductivity can vary from 14×10^{-4} W cm^{-1} $^oC^{-1}$ for pure selenium glass to 38×10^{-4} W cm^{-1} $^oC^{-1}$ for a glass of composition Ge35 As40 S25 (Hilton *et al* 1975). Clearly these glasses are much less physically and thermally robust than oxide glasses but nevertheless still retain sufficiently acceptable thermal and mechanical

properties to be used as optical components with the exception of window components interfacing with rugged environments.

The Need For Infrared Optical Materials

It is fortunate that the two most common gases in the atmosphere, nitrogen and oxygen, are homopolar and possess neither a permanent nor an induced dipole moment, and hence do not exhibit infrared molecular vibrations which would result in the absorption of infrared radiation. In the region of the infrared spectrum from 0.75 μm to 14.0 m the absorptions of the minor atmospheric constituents, water vapour and carbon dioxide result in three main 'windows' in the atmosphere (Kruse et al 1962), one from 0.75 μm to 2.5 μm (near infrared), another from 3.0 μm to 5.0 μm (middle infrared), and a third from 7.5 μm to 14.0 μm (far infrared). From the black body spectral emittance curves shown in Fig 1 it is clear that to detect relatively hot objects the 3.0 μm to 5.0 μm window is most suitable and to detect objects at room temperature the 7.5 μm to 14.0 μm (8 μm to 12 μm hereafter) window is most suitable.

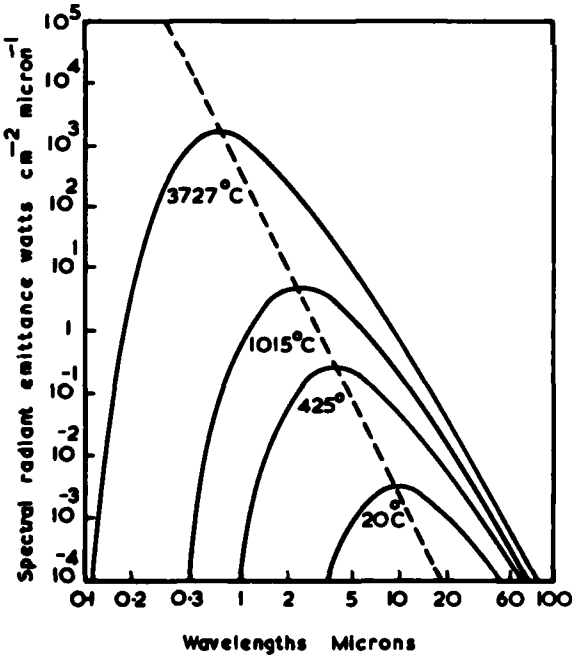

Fig 1 Black-body Spectral Emittance Curves

There is a major interest in thermal surveillance systems at present and these practical uses of infrared radiation are concerned with wavelengths up to about 12.0μm. In order to focus this infrared radiation onto detection systems, windows lenses and telescopes are required made from materials exhibiting adequate infrared transmission in this wavelength region. Generally the requirements for infrared transmitting materials are set primarily by the atmospheric transmission and secondly by the operational wavelength range of the sources and detectors and by the power handling requirements of particular systems. For surveillance or thermal imaging applications where chalcogenide glasses are useful, materials are required in sizes up to 150 mm diameter and up to 20 mm thick. At present the requirements for optical component materials tend to be for single thermal band operation ie 3-5 μm or 8-12 μm but it is possible that future requirements may call for multi thermal band operation eg 3-5 μm and 8-12 μm. Thus the reader so far will have gained some insight as to how requirements for infrared optical materials arise and the likely component sizes necessary. The next points to consider are those governing the transparency of insulators and semi-conductors to understand why chalcogenide glasses are suitable as infrared optical materials.

Loss Mechanisms In Infrared Materials

Metallic materials not exhibiting an energy gap possess a high density of free electrons in their structure. These electrons are of such low inertial mass that they can freely respond to electromagnetic radiation over a wide frequency range and thus metals are opaque in significant thicknesses. Insulators and semiconductors with energy gaps $>$ 0.1 eV will exhibit some near, middle and far infrared transmission within their transparency range. The short wavelength cut off frequency in these solids is determined by electronic transitions across the band gap while the long wavelength cut off results from lattice absorptions due to the vibrational modes of the atoms or ions of the solids. The chalcogenide glasses can be classified amongst this latter group of substances.

When electromagnetic radiation is incident upon and passes through an insulator various loss mechanisms operate. Some of the radiation is reflected at the interfaces between a solid and its environment. The amount reflected is determined by the

refractive index of the solid and that of the medium in which it is immersed. This is a basic property of the material but may be partially overcome by means of anti-reflection coatings applied to the surfaces of the solid. Some of the radiation may be scattered at the surface of the solid and/or in the bulk. The surface scattering is likely to be due to lack of adequate care in surface preparation, but bulk scatter can arise from defects, inclusions or perturbations in the refractive index particularly in a complex solid consisting of several atoms of different mass as is the case with chalcogenide glasses. Some of the radiation may be absorbed at the surface of the solid or in the solid. The mechanisms which give rise to bulk absorption may be classified as intrinsic or extrinsic ones. The intrinsic absorption mechanisms are those which result in electronic and vibrational structural absorptions in vitreous material of specific chemical composition. Extrinsic mechanisms are those associated with impurity atoms and molecules and deviations from stoichiometry. The intrinsic mechanisms define the region of transparency to electromagnetic radiation in a solid and the ultimate transmission achievable within this region, while the extrinsic mechanisms generally determine the percentage of the theoretical level of transparency achievable in practice within this region.

Intrinsic Absorption Mechanisms

Intrinsic absorption mechanisms in a solid define its region of transparency to electromagnetic radiation. In order to transmit infrared radiation a solid must be an insulator or a semiconductor exhibiting an energy gap eg (ie the nominal energy to excite bound electrons to a conduction band). Only materials possessing a band gap larger than the equivalent of the infrared wavelengths of interest (0.75 to 14.0 μm) need to be considered since it is the band gap that sets the transmission limit at the short wavelength end of the spectrum of a solid as illustrated in Fig 2. This short wavelength cut off λ_c isgiven by the relationship shown in equation 1.

$$\lambda_c = \frac{hc}{E_g} \qquad (1)$$

where h = Planck's constant and c = velocity of light and E_g is the band gap.

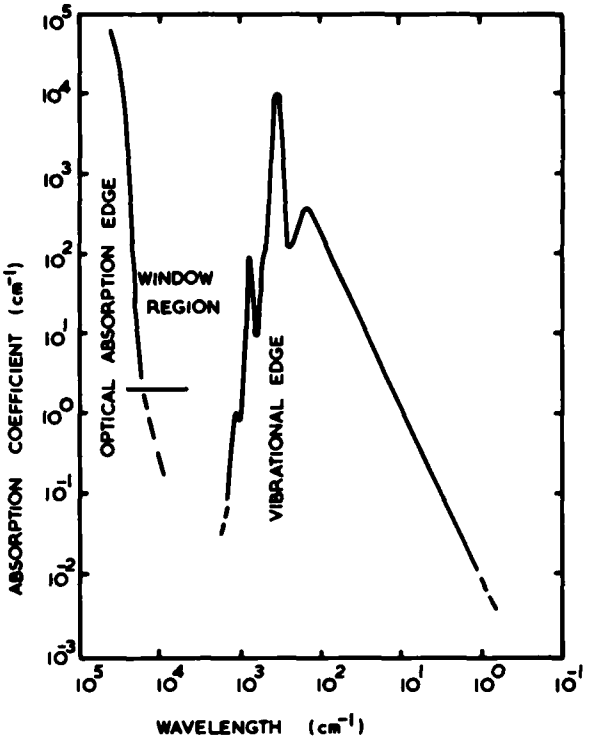

Fig 2 A plot of absorption coefficient against wavelength showing intrinsic absorption in As_2S_3 glass

The low frequency tail of this short wavelength cut off extends slightly into the transparent region of the solid. This is known as the Urbach tail (Urbach 1953) (Hopfield 1968) and is of the form shown in equation 2.

$$\beta \alpha e^{c\omega/kT} \qquad (2)$$

where ω = frequency, k = Boltzmann's constant, T = absolute temperature and β = absorption coefficient.

This exponential tail would only be of major significance for most infrared applications if it was very close to one of the infrared atmospheric 'windows' discussed in para 2. An explanation of this exponential tail in the UV interband edge has been recently put forward. It is known that the random structure in glasses gives rise to varying local electric fields on a microscopic scale. Theoretical work by Dow and Redfield (1971) (1972) and by Tauc (1975) provide evidence that such local microfields cause intrinsic absorption in chemically pure materials in what is normally the transparent region below the fundamental interband absorption edge. The mechanism is due to local field induced broadening of

exciton levels which are created in optical absorption energies close to but below the interband edge.

The long wavelength cut off in a solid is set by lattice absorptions. These lattice absorptions result from the vibrational modes of the atoms in the solid. In ionic crystals vibrations of large amplitude will occur when incident radiation is of the same frequency as the resonant frequency of the atomic units and this is termed the reststrahl frequency. These atomic units must possess a permanent dipole moment which can be activated by the oscillating electric field of the incident radiation. Non polar solids would be expected to be infrared inactive but usually exhibit induced dipole effects. For example a non ionic solid can have an effective charge and thus a dipole moment if the atoms are not identical. The fundamental absorption frequency can be calculated for a linear polar diatomic molecule consisting of two point masses m_1 and m_2. The frequency of vibrations V, of the simple harmonic motion of the two masses along a line joining them is given by equation 3 (Kittel 1956).

$$V = \frac{1}{2\pi}\left(\frac{K}{M}\right)^{\frac{1}{2}} \qquad (3)$$

where K is the force constant and M is the reduced mass of the cation-anion pair. If an anharmonic oscillator is considered then in addition to the fundamental frequency a series of overtone vibrational bands arise. The long wavelength cut off in a solid is usually set by the first overtone of the fundamental lattice absorption. In the case of multi element chalcogenide glasses of somewhat indeterminate structure equation 3 can be used to provide general rules as to the likely long wavelength transmission limit. For instance it is clear that the smaller the force constants or the weaker the bonding in the glass, and the larger the atomic masses in the glass and the higher the co-ordination number then the lower will be the frequency of the fundamental absorption. Thus other things being equal selenide glasses will transmit farther into the IR than sulphide glasses and telluride glasses will transmit farther than sulphide or selenide glasses.

Recently several investigations have shown how the infrared absorption decreases as the frequency becomes much greater than the fundamental lattice absorptions and overtone frequencies in alkali halides (Mitra and Bendow 1975) and semiconductors (Deutch 1975). Highly purified samples of these materials exhibit an absorption coefficient, β, which reduces exponentially (Bendow 1975). This exponential tail can be represented by the expression shown in equation 4.

$$\beta(\omega) \approx Ae^{-\gamma\omega} \qquad (4)$$

where β = absorption coefficient, A and γ are material dependent parameters and ω = frequency.

In such materials multiphonon absorption takes place when a high energy phonon couples weakly with a transverse optical mode of the material. This transverse optical mode decays into two or more lower energy phonons of frequencies corresponding to fundamental vibrational modes. The most probable multiphonon absorption process involves production of the minimum number of final state phonons (Pohl and Meier 1974). For the alkali halides the one phonon density of vibrational states is sizeable over a broad range of frequencies and this has been shown (Pohl and Meier 1974) to lead to a predicted exponential absorption spectrum in the multiphonon region at ambient temperature in agreement with the experimental results. In the case of chalcogenide glasses such as As_2S_3, As_2Se_3 and GeS_2, a molecular model for the vibrational properties has been proposed (Lucovsky and Martin 1972). In this model it is presumed that the AsY_3 pyramidal groups or the GeY_4 tetrahedral groups are only loosely coupled to one another by the bridging chalcogenide atoms. As a consequence of this the infrared spectra are expected to correspond to those of isolated AsY_3 or GeY_4 molecules superimposed on less intense spectra due to the bridging As-Y-As or Ge-Y-Ge groups. The one phonon density of states is predicted by this molecular model to consist of a collection of discrete vibrational modes broadened slightly due to the amorphous state. This means that the multiphonon absorption processes in chalcogenide glasses should be analogous to combination and overtone bands in isolated molecules and experimental results have been shown to be in agreement with this model (Mitra and Bendow 1975).

Thus the fundamental absorption processes that limit the transparency range of chalcogenide glasses are due to electronic transitions across the band gap at short wavelengths and lattice vibrations at longer wavelengths. A sufficiently wide spectral window exists between these two limits, where these materials are usefully transparent as shown in Fig 2 where the absorption coefficient of As_2S_3 is plotted as a function of frequency. The first region of Fig 2 shows a sharply rising absorption at the electronic band edge followed by a relatively transparent region ($\sim$ 2000 to 10,000 cm^{-1}). Multiphonon absorption occurs between 500 cm^{-1} and 2000 cm^{-1} and one phonon peaks occur between 100 cm^{-1} and 500 cm^{-1}. This is followed by a region extending up to microwave frequencies where the absorption varies approximately as the frequency squared (Strom et al 1974). Within the window illustrated by Fig 2 the transparency is limited by the tails of the optical and vibrational absorption edges, possibly free electron absorption in some chalcogenide glasses and by intrinsic scatter.

Intrinsic Scatter Mechanisms

From thermodynamic considerations some degree of intrinsic scatter is likely in all homogeneous infrared optical glasses due to the natural perturbations in the refractive index caused by compositional fluctuations frozen in during the glass synthesis. Scattering theory is complex (Stacey 1956) but three cases of wavelength dependence can be distinguished. If the size of the scattering centres is $<\lambda$ then Rayleigh scattering theory can be used and the backward scatter is $\propto \lambda^{-4}$; if the scattering centres are $\approx \lambda$ Mie forward scattering theory which is a complex function of λ can be used; and if the scattering centres are $>\lambda$ then scattering can be described as non selective and is independent of λ. It can often be difficult to identify and distinguish between scatter inducing defects in materials but a number of informative measurements can be made. The wavelength dependence at a fixed angle can provide data on the size of the inhomogeneity responsible for the scatter. The angular dependence of the scatter may alsc aid in identifying the relative size and shape of the inhomogeneity. Measurements of polarised scattering can provide data on strain induced inhomogeneities. Much useful data on scatter problems is published and referenced in SPIE (1982).

Extrinsic Loss Mechanisms

Extrinsic loss mechanisms determine the fraction of the theoretical level of transparency achievable in a glass in practice at certain wavelengths within its available window region. These mechanisms are scatter and absorption arising from the fabrication process employed and the chemistry of the glass in relation to certain specific impurities. For instance OH, hydrocarbons and oxygen in chalcogenide glasses can give rise to unacceptable absorptions at specific wavelengths and inadequately homogenised glass can give rise to unacceptable scatter in the high frequency regions of the near and middle infrared. Chalcogenide glasses can be synthesised from the melt or by a

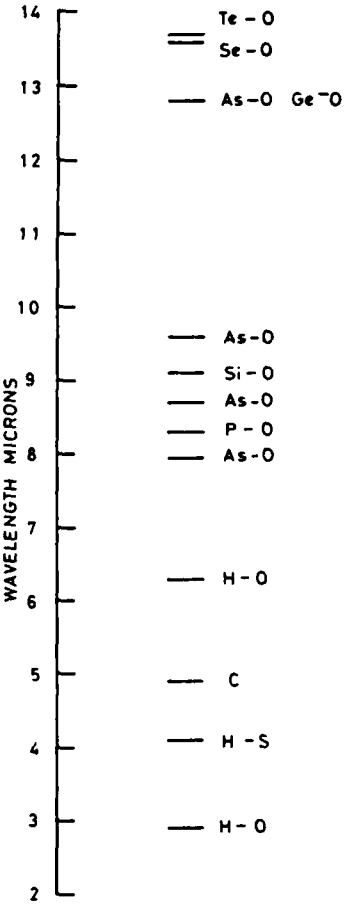

Fig 3 *An indication of the extrinsic absorptions seen in chalcogenide glasses*

distillation process and components can be manufactured by a pressure slumping or cutting and grinding process utilising a variety of containment vessels such as silica, carbon or metal. Since the extrinsic loss mechanisms are specific to a particular glass or family of glasses and the method of synthesis they will be discussed for individual materials. In this way an appreciation of the problem of extrinsic loss in relation to particular applications will be obtained. An indication of the likely absorbing species is given in Fig 3 and their effects on the transmittance of chalcogenide glasses is shown in Fig 4. Useful works of reference to find the absorbing frequencies of these impurities are Miller and Wilkins (1952), Nyquist and Kagel (1971) and Nakamoto (1963).

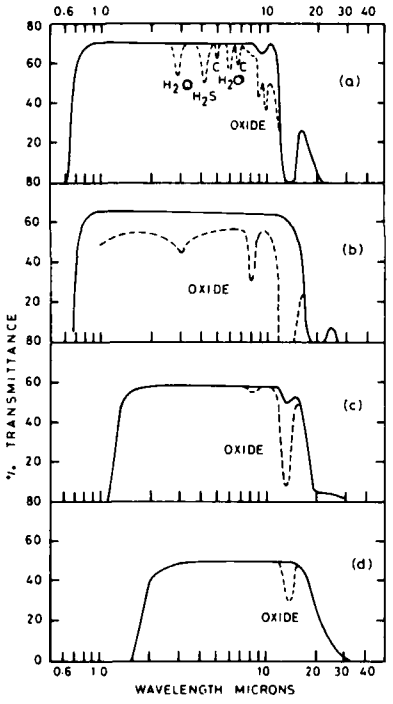

Fig 4 The infrared transmittance of chalcogenide glasses

(a) Sulphide Glass Ge30 As20 S50 1.86 mm thick

(b) Selenide Glass Ge34 As8 Se58 1.80 mm thick

(c) Selenide-telluride Glass Ge30 As13 Se27 Te30 2.3 mm thick

(d) Telluride Glass Ge10 As50 Te40 1.62 mm thick

The effect of extrinsic impurity is indicated by the dashed curves

Sulphide Glasses

Most commercial optical glasses produced for use in the UV and visible region of the spectrum exhibit effective transmission in the 0.75 μm to 2.5 μm wavelength region hence there is no need to develop special materials for this region. However these optical glasses are not effectively transparent beyond 2.5 μm due to the Si-O bond vibration (Adams 1960), and special materials have been developed for use in the 3-5 μm spectral band which are also transparent in the near infrared and sometimes completely or partially transparent in the visible. The need for these special materials for optical application first stimulated research on sulphide glasses and resulted in arsenic trisulphide being developed as a bulk optical material.

Arsenic trisulphide is the most widely known and used sulphide glass. It was manufactured in the USA (USP 1957) and in the UK during the mid 1950s and has been found useful ever since that time as an optical component in many 3-5 μm optical systems. The manufacture of this glass to optical standards set new technical problems since arsenic and sulphur are toxic and volatile and their oxides act as major extrinsic impurities thus reducing the infrared transmission of the material. In a bold departure from the then current glass technology pratice the volatility of these elements was used to advantage in that the raw arsenic metal and sulphur were first pre-reacted in a closed steel or silica vessel to form a crude solid which was broken to a small particle size and then heated in silica apparatus under an inert atmosphere to such a temperature ($\geq$700°C) that final reaction, melting and distillation took place. The vapours were condensed at a low enough temperature (300-500°C) to maintain the As_2S_3 in a liquid state but high enough ($\geq$193°C) to keep As_2O_3 in its vapour state. Thus the bulk of the oxide contamination present in the starting materials was swept out of the still as SO_2, SO_3 and As_2O_3. This synthesis was operated as a batch process with batches of 3-5 Kg being collected, mixed by stirring at 625°C, then finally annealed. Components were either cut or heat slumped from the glass boules. This material being required for low power applications was not produced to a very high standard of purity. Commercial grade arsenic and sulphur were

used so that cation impurities were present in the material as well as traces of H_2S and oxides. Nevertheless the quality was adequate for 3-5 μm low power applications and a stock is still available (Billard and Cornillault 1962). A particular production problem in such a distillation process was maintaining constancy of chemical composition and therefore of optical properties in the finished product. The material produced by the ICI company in the UK was designated A or B (Billard and Cornillault 1962) depending upon whether the distillate was collected at the beginning or end of a batch distillation. Fibre optic components such as fused faceplates and light pipes have been made from As_2S_3 with a cladding glass containing a different sulphur concentration to provide the required refractive index difference. These have demonstrated effective transmission ($\geq$40%) in lengths up to 8 cm between 1 and 5μm (Kapany 1967). The full potential of the material was not realised since the glasses contained extrinsic impurities such as Fe, H_2O and H_2S. Some of the physical properties of type B As_2S_3 are given in Tables 1 and 2 and refractive index data on USA material is given in the literature (Rodney et al 1958). Details of the vibrational absorption edge in As_2S_3 are reported by Onomichi et al (1971) and these are broadly in agreement with the data shown in Fig 2. V_{TO} is given as 301 cm^{-1} and V_{LO} as 339 cm^{-1}. A number of other uses have been proposed for As_2S_3 glass such as the moisture passivation of NaCl components (Young 1970), and as a transparent optical film on $LiNbO_3$ active substrates for integrated optics applications (Klein 1974).

For those interested in glass formation data the following indicates some of the information available for sulphide glasses; As-Tl-S (Flaschen et al 1960a), As-I-S (Flaschen et al 1960b), Ge-As-S (Savage and Nielsen 1965a), As-Te-S (Kolomiets 1964), Ge-P-S, Si-Sb-S (Hilton et al 1964) and Ge-Sb-I-S (Turjanitsa et al 1972). The optical properties of sulphide glasses depend markedly upon chemical composition. Hence for the present purposes it has been decided to take the example of the Ge-As-S system which is one of the most useful from the point of view of bulk optical glass manufacture. It has been shown that Ge-As-S glasses (Savage and Nielsen 1965a) demonstrate excellent infrared transmission from 1.0 to 11.5 μm as indicated in Fig 4 and that the wide composition range allows glasses with differering optical, thermal and mechanical properties to be prepared. Binary sulphide glasses can be made containing 10% to 40% As or 15% to 30% Ge and ternary sulphide glasses can be made containing as little as 30% S. Compositions containing more than 60% of sulphur are transparent in the visible, the position of the cut on wavelength depending upon the arsenic germanium/sulphur ratio. Glasses containing less than 60% sulphur show little infrared fine structure between 7 and 13 μm, but still show the strong Ge-S or As-S absorption between 11 and 15 μm as is seen in Fig 4. Materials containing more than 60% sulphur show a complex infrared spectrum. Between 7 and 15 μm the number of absorption bands increases as the sulphur content of the glasses increases. There is good agreement between the positions of these absorption bands when extrinsic oxygen absorption has been removed and the absorption bands observed in crystalline sulphur due to combination tones of the S_8 fundamental absorptions (Bernstein and Powling 1950). Glasses from which to manufacture optical components would be best chosen from those containing $\leq$ 60% of sulphur. These materials are likely to yield a transmission curve similar to that shown in Fig 4. The dashed curve in this figure shows clearly the problem of extrinsic absorption due to water, oxide and carbon impurities. If a typical component is say 10 mm thick then an examination of Fig 4 shows that the level of impurity indicated by the dashed curve would destroy the useful infrared transmission of the component. Impurities such as these need to be controlled at $\leqq$ a few ppm wt in order to achieve an adequate transmission. Fuxi et al (1983) have reported devitrification and property studies in the Ge-As-S glass system. They found that because of the stable glass formation in this system devitrification was difficult mainly occurring at low ($\sim$10%) As content. The frequency of the main IR absorption peak (cm^{-1}) was given for several ternary glasses, Ge30 As10 S60 378(s) 330(m), Ge30 As15 S55 375(s) 325(m), Ge25 As15 S60 378(s) and Ge20 As20 S60 375(s) 330(s). Some optical property data for four ternary sulphide glass compositions is given in Table 1 and some other physical property data is given in Table 2. Structural and

physical property data for other glasses in the Ge-As-S system is reported by Andreichin et al (1976). Three useful general reviews of the optical properties of chalcogenide

TABLE 1 OPTICAL PROPERTIES OF CHALCOGENIDE GLASSES

Class atomic %	n_2	n_3	n_4	n_5	V_{3-5} +	n_8	n_{10}	n_{12}	V_{8-12} *	dn/dT °C x 10^{-5}
As40 S60 type B	-	2.395	2.390	2.386	154	-	-	-	-	-1
Ge15 As25 S60	2.30	-	-	-	-	-	-	-	-	-
Ge25 As15 S60	2.22	-	-	-	-	-	-	-	-	-
Ge30 As15 S55	2.25	-	-	-	-	-	-	-	-	-
Ge40 As15 S45	2.30	-	-	-	-	-	-	-	-	-
As40 Se60	-	-	-	-	-	2.7789	2.7789	2.7728	159	-
Ge20 Se80	-	-	-	-	-	2.4071	2.4027	2.3973	143	-
Ge10 As20 Se70	-	-	-	-	-	2.4649	2.4594	2.4526	119	-
Ge10 As30 Se60	-	-	-	-	-	2.6254	2.6201	2.6135	135	-
Ge10 As40 Se50	-	-	-	-	-	2.6108	2.6067	2.6016	176	-
Ge20 As10 Se70	-	-	-	-	-	2.5628	2.5583	2.5528	156	-
Ge30 As10 Se60	-	-	-	-	-	2.4408	2.4347	2.4271	104	-
Ge30 As15 Se55	-	-	-	-	-	2.4972	2.4914	2.4840	113	-
Ge30 As20 Se50	-	-	-	-	-	2.5690	2.5633	2.5560	120	-
Ge33 As12 Se55	-	-	-	-	-	2.5002	2.4942	2.4867	111	-
Ge28 Sb12 Se60	-	2.6263	2.6200	2.6165	165	2.6083	2.6002	11.0 µm 2.5962	99	+8
Ge30 As13 Se57	-	2.4936	2.4887	2.4859	193	2.4784	2.4724	2.4650	110	+7
Ge30 As13 Se47 Te10	-	2.6118	2.6057	2.6024	171	2.5952	2.5897	2.5829	129	+7
Ge30 As13 Se37 Te20	-	2.7412	2.7342	2.7305	162	2.7229	2.7178	2.7117	154	+11
Ge30 As13 Se27 Te30	-	2.8818	2.8732	2.8688	144	2.8610	2.8563	2.8509	185	+15
Si25 As25 Te50	-	-	-	2.93	-	-	-	-	-	+1
Ge10 As20 Te70	-	-	-	3.55	-	-	-	-	-	-
Si15 Ge10 As25 Te50	-	-	-	3.06	-	-	-	-	-	+17

$$+ V_{3-5} = \frac{n_4 - 1}{n_3 - n_5} \qquad * V_{8-12} = \frac{n_{10} - 1}{n_8 - n_{12}}$$

TABLE 2 THERMAL AND MECHANICAL PROPERTIES OF CHALCOGENIDE GLASSES

Glass Composition Atomic %	Tg °C	Thermal Expansion Coefficient x 10^{-6}/°C	Density Kg/m^{-3} x 10^3	Hardness K=Knoop V=Vickers Kg/mm^2	Thermal Conductivity Cal/cm Sec °K	Rupture Modulus MPa	Young's Modulus GPa	K_{Ic} N mm$^{-3/2}$	Viscosity Fulcher Equation $10^5 - 10^{13}$ P
As40 S60 type B	-	26.1	3.15	109 (K)	-	-	-	-	-
Ge15 As25 S60	-	19.4	3.05	159 (K)	-	-	-	-	-
Ge25 As15 S60	425	12.8	3.00	200 (K)	-	-	-	-	-
Ge30 As15 S55	400	9.6	3.17	216 (K)	-	-	-	-	-
Ge40 As15 S45	-	7.7	3.53	276 (K)	-	-	-	-	-
As40 Se60	178	21.0	4.62	-	-	-	-	-	$\log_{10}\eta = -4.44 + 2764/(T°C - 22.25)$
Ge20 Se80	154	24.8	4.37	147 (V)	-	-	-	-	-
Ge10 As20 Se70	159	24.8	4.47	154 (V)	-	-	16.5	6.7 ± 0.4	-
Ge10 As30 Se60	210	19.0	4.51	176 (V)	-	-	18.0	7.1 ± 0.6	-
Ge10 As40 Se50	222	20.9	4.49	173 (V)	-	-	15.9	7.4 ± 0.8	-
Ge20 As10 Se70	209	20.5	4.41	186 (V)	-	-	16.1	-	-
Ge30 As10 Se60	345	13.7	4.36	236 (V)	-	-	18.6	7.7 ± 0.4	-
Ge30 As15 Se55	351	12.8	4.42	245 (V)	-	-	-	-	-
Ge30 As20 Se50	361	11.7	4.47	266 (V)	-	-	21.3	-	-
Ge33 As12 Se55	-	13.0	4.40	170 (K)	0.60	17.2	22.1	-	-
Ge28 Sb12 Se60	277	15.8	4.67	150 (K)	0.72	17.3	21.8	-	$\log_{10}\eta = -4.97 + 2824/(T°C - 122.41)$
Ge30 As13 Se57	342	13.0	4.40	237 (V)	-	-	-	-	$\log_{10}\eta = -4.71 + 4070/(T°C - 116.13)$
Ge30 As13 Se47 Te10	308	13.2	4.56	234 (V)	-	-	-	-	$\log_{10}\eta = -5.91 + 4627/(T°C - 67.49)$
Ge30 As13 Se37 Te20	285	12.9	4.77	228 (V)	-	-	-	-	$\log_{10}\eta = -9.74 + 6466/(T°C - 5.06)$
Ge30 As13 Se27 Te30	262	12.8	4.91	226 (V)	-	-	-	-	$\log_{10}\eta = -8.19 + 4868/(T°C - 35.52)$
Si25 As25 Te50	-	13.0	4.76	167 (K)	-	-	-	-	-
Ge10 As20 Te70	-	18.0	-	111 (K)	-	-	-	-	-
Si15 Ge10 As25 Te50	-	10.0	-	179 (K)	-	-	-	-	-

AD-A163 899 RSRE (ROYAL SIGNALS AND RADAR ESTABLISHMENT) 1985 2/3
RESEARCH REVIEW(U) ROYAL SIGNALS AND RADAR
ESTABLISHMENT MALVERN (ENGLAND) A J GRANT ET AL. 1985
UNCLASSIFIED DRIC-BR-98221 F/G 17/9 NL

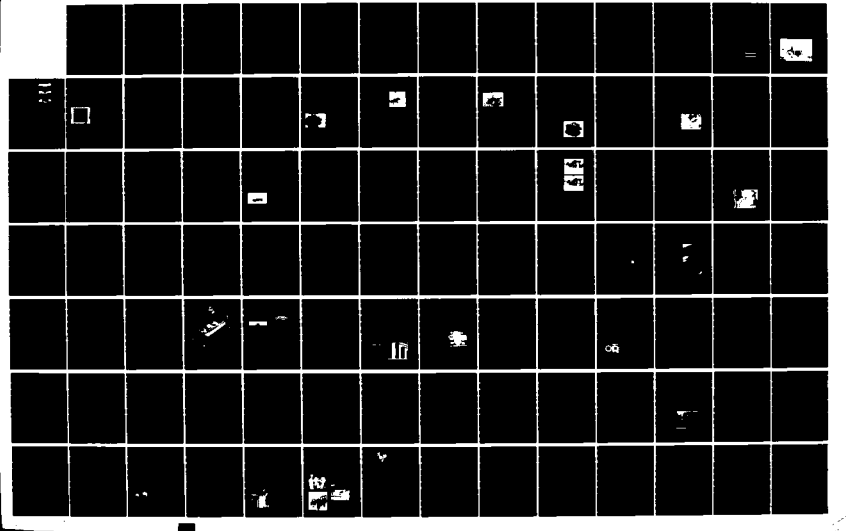

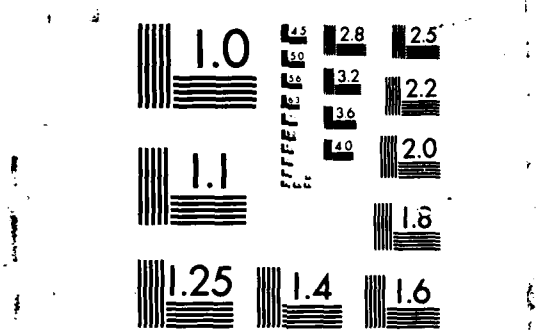

MICROCOPY RESOLUTION TEST CHART
NATIONAL BUREAU OF STANDARDS-1963-A

glasses including sulphide glasses appear in the literature (Savage and Nielsen 1965b) (Hilton 1966) (Hilton 1970).

Silica fibres for optical communications have been developed to their practical limit of ~ 0.2 dB/km in the wavelength range 1.3 to 1.55 μm. Residual intrinsic losses are due to Rayleigh scatter proportional to λ^{-4} and particularly due to the increasing phonon loss in SiO_2 based materials. The use of an alternative material with a phonon loss edge situated farther into the infrared would allow fibre operation at longer wavelength and also result in lower Rayleigh scatter losses thus offering the promise of losses perhaps as low as 0.001 dB/km (Tebo 1983). Thus there is a major drive to develop a mid IR (~4μm) optical communications glass fibre from the recently discovered fluoride glasses reviewed by Drexhage et al (1982). However a number of workers are considering sulphide glasses for this or shorter length applications in the mid infrared. The first glasses to be considered (Kapany 1967) were arsenic sulphides particlularly As_2S_3 glass but as previously mentioned the purity of these was insufficient for them to be considered for anything other than very short length applications such as fused faceplates. Vasiliev (1983) has reported that the minimum optical loss wavelength of As_2S_3 is near 5.15 μm and that the material dispersion is zero at 4.89 μm and does not exceed 20 ns/nm km in a wide spectral region around this zero dispersion wavelength. Hence this and other sulphide glasses are promising candidates for mid infrared optical communications applications. Dianov (1982) has considered the Rayleigh scattering and the infrared absorption loss of As_2S_3 glass and has predicted a minimum loss of ~0.05 dB/km in the wavelength region of 4 to 5 μm. CO laser calorimetry of high purity bulk glass indicated the absorption losses in glass to be ~70 dB/km. Miyashita and Terunuma (1982) have drawn unclad fibre from high purity rods of As_2S_3 glass and have found that the optical loss was limited by impurity absorption (eg S-H at 4.1 μm) but nevertheless a loss of 170 dB/km was measured at 5.25 μm. Kanamori et al (1983) have reported fibre losses of 64 dB/km at 2.4 μm for As_2S_3 glass and Katzir and Arieli (1982) indicate that losses of 10^3dB/km at 5μm have been measured in a Ge-S glass. Shibata et al (1980) have shown that optical losses in Ge-P-S glass may be as low as 10^{-1} to 10^{-2} dB/km at 5.5 μm. Thus it remains to be seen whether there is sufficient further interest in these chalcogenide glasses for mid infrared applications to allow their theoretical loss levels to be realised.

Selenide Glasses

As can be seen from Fig 4 bulk sulphide glasses do not fully cover the far infrared spectral band. Hence the attention of researchers looking for glasses for use in this band was directed towards selenides. Elemental selenium was known to be a glass former and to transmit over the required spectral range. Further work on the absorption and reflection spectra (Vasko 1965) of pure selenium glass confirmed this. Selenium and its derivatives in thin film form have been used in a multi-billion dollar photocopying industry and this glass must be regarded as the single most important chalcogenide in terms of commercial exploitation. It has also been used in rectifying applications and as a photovoltaic detector for visible radiation. However, because of its poor general physical properties it was found wanting for bulk optical applications. This stimulated research on selenide glass formation and an indication of some of the information available is as follows: As-Tl-Se, As-S-Se (Flaschen et al 1960a), As-Sb-Se, As-Tl-Se (Kolomiets 1964), Ge-As-Se (Kolomiets 1964) (Savage and Nielsen 1964), Ge-P-Se, Si-Sb-Se (Hilton et al 1964) and Ge-Sb-Se (Hilton et al 1966a). The physical properties of selenide glasses, like those of sulphide glasses, depend upon the chemical composition (Hilton and Hayes 1975) but the most work has gone into glasses in the Ge-Sb-Se and Ge-As-Se systems from which commerical bulk optical materials have been manufactured. Hence this review will mainly concentrate on the bulk optical properties of these glasses. First of all it must be borne in mind that when compared to oxide optical glasses, the chalcogenide glasses are classified as weak materials with low softening temperatures. Therefore it is particularly important that the thermal and mechanical properties are optimised. During the mid 1960s a useful review was published (Savage and Nielsen 1965b) which indicated that selenide glasses with acceptably high glass transitiontemperatures (T_g) >150°C could be made. It was also established that

the majority of the absorptions exhibited by chalcogenide glasses between 1 and 6 μm and 8 and 13 μm resulted from traces of H_2, H_2Se and oxide impurities all of which could be eliminated from the glasses if sufficient care was taken during the preparation and processing of these materials. The transmission curve of a Ge-As-Se glass showing the positions of some of the oxide impurity bands is given in Fig 4. Further reviews were published yielding much more detailed information on physical properties (Hilton et al 1966a), additional information on absorption by oxide impurities (Hilton and Jones 1966) and investigations of the atomic structure of selenide and other chalcogenide glasses (Hilton et al 1966b). At the time these four reviews neatly summarised the general physical property data of most known chalcogenide glasses and indicated that in principle, glass compositions with physical properties suitable for 8-12 μm requirements were possible. In addition the requirement was for an optical glass to correct chromatic aberration in 8-12 μm germanium lens systems. The refractive index of the glass was required to be $\sim$2.5, the reciprocal dispersive power, $V_{8-12} = (n_{10} - 1)/(n_8 - n_{12})$, was required to be $\sim$100. Other requirements were that the refractive index be maintained within the range $\pm$ 0.005 to $\pm$0.0001 in a batch of material and from batch to batch of material, the $T_g \geq 150°C$, the mechanical strength and hardness were required to be high and the thermal expansion was required to be low. Hence work was done to establish the detailed physical properties of Ge-Sb-Se (Hilton and Hayes 1975) (Savage et al 1978) and Ge-As-Se (Webber and Savage 1976) (Savage et al 1977) glasses to enable industrially makeable materials to be identified. From this work it became clear that all of the requirements could only be met by a glass containing of the order of 30% Ge and 10 to 20% As or Sb. The refractive indices of several Ge-As-Se glasses are given in Table 1 so that the effect of As/Ge content and ratio on the refractive index and reciprocal dispersive power can be seen. Other physical properties are given in Table 2. However much work has been done particularly in relation to extrinsic absorption problems on the glass Ge28 Sb12 Se60 in the USA and glass Ge30 As15 Se55 in the UK both of which have been produced commercially. Selenide glasses are synthesised from the elements inside sealed evacuated silica tubes at temperatures of the order of 950°C (Ford and Savage 1976) in quantities of 25-100 gm in research and in quantities up to several kilogrammes in production. The glasses are then annealed and cooled to room temperature for use, or heat slumped into particular component shapes followed by further annealing and cooling. This sealed tube process has the merit of retaining compositional integrity, but requires extrinsic impurity free starting materials. An alternative technique of distillation of lower grade elemental material in hydrogen gas was investigated and proved to be practical for a Ge-As-Se ternary glass (Kettlewell et al 1977) for batches of 1.5 kg. However the batch to batch compositional variation and hence refractive index variation was too great for the present requirement so that emphasis was placed on solving the extrinsic impurity problems associated with the sealed tube process.

Inspection of Fig 4 reveals the importance of oxide removal from the raw materials and reaction vessel surfaces in the sealed tube process. A synthesis technique was evolved which reduced the oxide impurity level in Ge-As-Se glasses to the order of 1 ppm wt. Essentially, this was to remove surface oxide from the silica reaction tube and the Se and As raw materials by baking them in a vacuum. The reactants and tube together

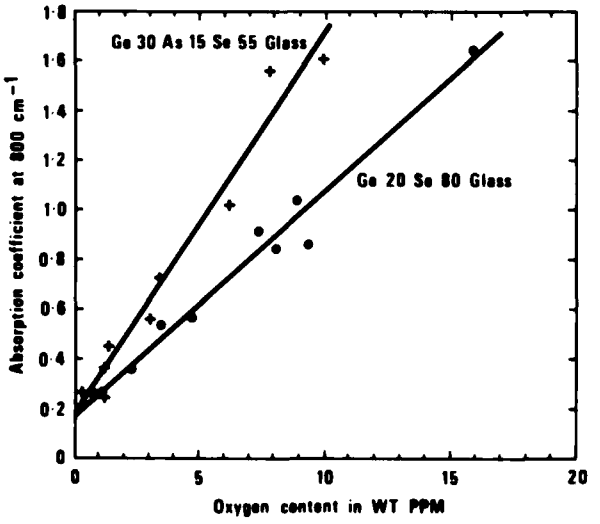

Fig 5 A plot of absorption coefficient at 800 cm^{-1} against oxygen extrinsic impurity content for two selenide glasses

with the germanium were then subsequently handled in an argon glove box until the reaction tube was finally evacuated and sealed prior to glass melting (Savage et al 1977). The effect of oxygen impurity on the absorption coefficient of two selenide glasses is shown in Fig 5. The oxygen levels were measured by a gamma photon activation analysis technique (Savage et al 1977).

Similar purification techniques were adopted for Ge28 Sb12 Se60 glass but with this material the purification process was taken further to establish the absorption limit for the glass and to lower the absorption at 10.6 μm (Hilton et al 1975). After removal of oxygen and carbonaceous matter it was shown that the transmission was limited by "silica" in the glass originating from the ampoule sealing process. In further studies (Rechtin et al 1975) after eliminating extrinsic absorption effects it was shown that by reducing the fraction of Ge-Se bonds in the glass composition to those in Ge23.5 Sb18 Se58.5 glass a value of absorption coefficient at 10.6μm of $8 \times 10^{-3} cm^{-1}$ could be achieved.

Russian workers have provided refractive index data for Ge-As-S-X glasses where X=Se, Sn, Te, Tl, Pb and Sb and came to the conclusion that the experimental results support the view of chalcogenide glasses as covalently bonded polymers with saturated valence bonds (Aio et al 1978). In an interesting quantitative study of infrared absorption in the 250-4000 cm^{-1} region of As_2Se_3 glass (Moynihan et al 1975) it was demonstrated that three distinct oxide impurity species existed in the glass from the relative intensities of the extrinsic absorption bands. Oxide bands at 1125 cm^{-1} and 650 cm^{-1} were assigned to oxide incorporated in the As_2Se_3 network, bands at 1050, 1265, 1340 and 785 cm^{-1} were assigned to As_4O_6 molecules dissolved in the glass and a band at 965 cm^{-1} was considered to be separately but not unambiguously assignable. It was also concluded that the absorption at 10.6 μm was limited by intrinsic multiphonon processes to a value of the order of 10^{-2} cm^{-1}. Selenide glasses in the Ge-As-Se and Ge-Sb-Se systems were considered to be sufficiently structurally similar to possess similar multiphonon absorptions and hence similar absorption coefficients at 10.6 μm. This is in broad agreement with the data given above for Ge-Sb-Se glasses and that below for Ge-As-Se-Te glasses.

Glasses Ge20 Sb12 Se60, Ge33 As12 Se55 (Hilton 1978) (Hilton et al 1975) and Ge30 As15 Se55 have been produced in batch quantities of several kilogrammes by the sealed tube method from semiconductor grade raw materials. After synthesis the glass boules are either annealed and cooled or sometimes subjected to a further homogenisation process (Hilton 1970) before annealing and cooling to room temperature. Components are then either cut from the glass or heat slumped to shape from slices of the glass. The main problem in achieving optical homogeneity requirements has been found to be in maintaining chemical compositional homogeneity after synthesis and mixing during the subsequent cooling process. This is due to the fact that the vapour composition is not necessarily the same as that of the liquid glass. While this is not a problem for experimental melts of the order of 100 gm it becomes more serious for melts of several kilogrammes since the available vapour space above such melts is greater and the temperature gradients tend to be larger. If any condensate of different chemical composition to the bulk is allowed to contaminate the liquid glass after homogenisation during the cooling process before annealing, then the viscosity of the glass is still sufficiently low for limited intermixing and hence local compositional variations to occur. Such variations in composition can lead to refractive index variations of the order of 3×10^{-3} or greater. However, these problems have now been largely overcome (Worrall 1979). Large 200 mm dia and 50 mm thick cast glass plates of high quality for submarine window applications have recently been reported by Stachiw and Bertic (1982) made by the Hilton process (Hilton et al 1975). This indicates that there is no fundamental problem in attaining good optical homogeneity if good working practices are maintained.

Kapany (1967) reported that chalcogenide glasses were potential materials for fibre applications where transmittance up to 14 or 15 μm was required. Since that time much data on glass formation and physical property measurements has become available and a number of workers are now investigating selenide glasses as candidate fibre materials. Bornstein et al (1982)

synthesised As_2Se_3 glass by the sealed tube technique and unclad fibres 100-500 μm in diameter and up to 20 m long were drawn from the melt at speeds of 0.5 to 5 m/min inside a glove box containing an inert atmosphere. Using a CO_2 laser and pyroelectric detector the loss in the fibre was found to be 0.1 dB/cm. These authors considered that improved losses could be achieved by further reducing extrinsic absorption and by modifying glass composition to minimise intrinsic phonon absorption. Brehm et al (1982) have synthesised plastic clad fibres from Ge30 As15 Se55 glass. Rods 10 mm in diameter and 80 mm long were made from glass synthesised by the sealed tube technique and these were used for fibre drawing at 400°C in an argon atmosphere to avoid oxidation. Fibres 200μm in diameter and 100 m in length were drawn at a speed of 10 m/min. The fibres were coated in polyolefin plastic and placed in a heat shrinkable polyethylene tube to improve the handling characteristics. The packaged fibre either 1.8 or 3 mm OD had a minimum bending radius of 30 mm, a breaking strength >1 daN and an optical loss in the 4-11 μm band of ~10 dB/m. Takahashi et al (1983) have reported a loss of 4.5 dB/m at 10.6 μm for a selenide glass teflon FEP clad fibre of composition As38 Ge5 Se57 made from oxide impurity reduced raw materials.

Katsuyama et al (1982) have disclosed the synthesis of solid or hollow core fibre of high stability and low optical loss from selenide glass deposited by the Modified Chemical Vapour Deposition inside tube deposition process. An object of the work was to avoid contamination from impurities in the raw materials and from the containing vessel by avoiding prolonged melting. Argon gas carrying $GeCl_4$, $SbCl_5$, and Se_2Cl_2 was passed through a lead glass substrate tube of composition mole % SiO_2 57, Na_2O + K_2O 12, PbO 30 and of dimensions 12-13 mm ID, 14 mm OD. Heating to 600°C during deposition was achieved using a traversing oxyhydrogen burner. After a glass of composition mole % Ge 28, Sb 12, Se 60 was deposited in the tube it was collapsed and drawn into a conventional fibre or hollow core fibre at 800°C. The hollow core fibre had a measured loss of 0.7 dB/m at 10.6 μm and the conventional fibre had a loss of 0.1 dB/m. When a core glass of composition mole % Ge 28, Sb 12, Se 60 and a cladding glass of composition mole % Ge 23.5, Sb 12, Se 64.5 were deposited in a lead glass tube and drawn into a solid fibre as before, the measured loss at 10.6 μm was 0.01 dB/m. This patent claim represents a breakthrough in reducing the loss in chalcogenide glass. If this achievement can be repeated for a commercial cabled product, selenide glass fibres are very promising for far infrared applications.

Mixed Selenide Telluride Glasses

Having established basic industrial products in the Ge-Sb-Se and Ge-As-Se glass systems researchers turned their interest to examining the possibilities of extending the range of optical properties in terms of refractive index but particularly of increasing the reciprocal dispersive power, V_{8-12}. Clearly from Table 1 the composition As40 Se60 offers a useful increase in V_{8-12} but at the expense of rather poor thermal and mechanical properties. Edmond (1968) suggested that selenide and telluride glasses were compatible and that it would be possible to make high quality stable mixed selenide-telluride melts. Muir and Cashman (1967) also indicated that a glass of composition (Ge Se Te)92 As8 was thermally stable, and the refractive index at 10 μm was found to be approximately 2.71. Savage et el (1980) considered that work on mixed selenide-telluride glasses offered the most useful approach to extending the range of optical properties of the basic selenide glasses for 3-5 μm and 8-12 μm applications. Additions of tellurium to the Ge-Sb-Se system rapidly led to devitrification problems therefore it was decided that the Ge-As-Se system would offer the most stable glasses in which to substitute tellurium for selenium in order to retain sufficiently robust thermal and mechanical properties for the intended applications (Savage et al 1980). The glasses in the Ge-As-Te (Savage 1971) system possess lower values of T_g and are much less thermally stable than those in the Ge-As-Se system (Savage and Nielsen 1966). Hence tellurium additions to the latter glasses would be expected to decrease their glass transition temperatures and reduce their thermal stabilities so that very stable base glasses containing 20 to 30% germanium and 10 to 30% arsenic were initially chosen for tellurium substitution. About 40 glass melts were made and analysed by differential thermal analysis and on the basis of the thermal properties one base

glass Ge30 As13 Se57 was chosen for investigation of optical properties. It was found that ≤ 30% Te could be substituted for Se in this glass but amounts of Te > 30% caused devitrification. A further extrinsic impurity problem was encountered with these quaternary glasses in that Te cannot be purified from TeO_2 by thermal baking since the vapour pressure of the metal is greater than the oxide. In this case an acid etching technique (Savage et al 1980) was developed which allowed glass of adequate purity to be made by the sealed tube technique. Several melts of glass Ge30 As13 Se27 Te30 were analysed for oxygen by a gamma photon activation technique and within the measured range of 0 to 10 ppm wt the oxygen content of this glass was found to be related to the absorption coefficient by expression 5.

$$Y = 0.078 + 0.182\ x \qquad (5)$$

where x = oxygen content in ppm wt
Y = absorption coefficient at 780 cm^{-1}

An absorption coefficient of 7×10^{-3} cm^{-1} was obtained for this glass at 10.6 μm by laser calorimetry which correlates very well with the values given for Ge23.5 Sb18 Se58.5 and As40 Se60 glasses in 5.0. Refractive index and reciprocal dispersive power data are given in Table I where it can be seen that the range of V_{8-12} is 110 to 185 when the base glass is substituted with up to 30% Te for Se. All of these glasses possess very acceptable general physical properties for infrared optical applcations as can be seen in Table 2. The effect of Te substitution on the short wavelength end of the spectral window is to move the absorption edge from 0.6 - 0.7 μm for a glass containing no tellurium to 1.1 - 1.2μm for a glass containing 30% Te.

A good general review of mixed $As_2(Se\ Te)_3$ glasses containing some data on optical properties is given by Thornburg (1973), and this complements data already given in this review on As_2S_3 and As_2Se_3 glasses. McLauchlan and Gibbs (1977) have reported thin film data for mixed Se-Te glasses.

Telluride Glasses

In the early 1960s before selenide glasses had become established preliminary research was also conducted on telluride glasses as alternative materials for 8-12 μm applications. As is seen in Fig 4 telluride glasses were shown to transmit farther into the infrared than sulphide or selenide glasses and in the 8-12 μm spectral region appeared to be less prone to multi-phonon absorptions and in the case of Ge-P-Te and Ge-As-Te glasses also less prone to oxide absorptions. This work and the later work for switching glass applications in the early 1970s has resulted in much information on glass formation, an indication of which is as follows: Si-As-Te (Hilton and Brau 1963), As-I-Te (Peck and Dewald 1964), Ge-As-Te, Ge-P-Te (Savage and Nielsen 1966) (Hilton et al 1966a), Ge-Te, As-Te (Savage 1972a), Si-Ge-As-Te (Savage 1972b) and quater-naries based on Si-As-Te (Anthonis et al 1973/74). From this work some conclusions can be drawn concerning telluride glasses. The major glass forming region was found in the Si-As-Te system while the Ge-P-Te and Ge-As-Te systems only offered minor glass forming regions. The effect of oxygen extrinsic impurity on the transmission of Si-As-Te glasses (Hilton et al 1966c) was similar to that in the case of sulphide and selenide glasses. Trace oxide impurity has a much less deleterious effect on the transmission of Ge-As-Te and Ge-P-Te (Savage and Nielsen 1966) glasses as is noticeable in Fig 4. This was perhaps due to a restricted solubility in the case of Ge-As-Te glasses and a negligible solubility in the case of Ge-P-Te glasses. These latter facts are very advantageous but the limited glass forming regions means that commercial production is likely to be difficult and the achievement of a family of glasses with a range of optical properties unlikely. Germanium raw material can be incorporated in chalcogenide glasses readily at 950°C with no reaction tube corrosion problems. On the other hand silicon is difficult to incorporate into a glass melt in the sealed tube process since the glass melting temperature of around 1000°C is considerably lower than the melting point of silicon and in addition attack on the silica melt tube is observed. Therefore in spite of the fact that the Si-As-Te glass forming region is large these glasses are difficult to melt and homogenise and very difficult to make with low intrinsic oxygen impurity due to corrosion of the silica melt tubes. Due to these problems and the fact that selenide glass manufacture became established no further work was done towards telluride

glass production for optical applications. Comprehensive data on the properties and structure of As-Te glasses are given in the literature (Cornet and Rossier 1973a,b,c) and this complements the data already referred to on As_2S_3 and $As_2(SeTe)_3$ glasses.

References

Adams, R.V. 1960 The absorption of infrared radiation and the structure and constitution of various oxide glasses. PhD Thesis, Dept Glass Technology, Sheffield University.

Aio, L.G., Efimov, A M and Korkorina, V.F. 1978 J Non Cryst Solids 27 299.

Andreichin, R., Nikiforova, M., Skordeva, E, Yurakova, L., Grigorovici, R., Manaila, R., Papescu, M. and Vancu, A. 1976 J Non Cryst Solids 20 101-122.

Anthonis, H.E., Kreidl, N.J. and Ratzenback, W.H. 1973/74 J Non Cryst Solids 13 13.

Bendow, B. 1975 Multiphonon Infrared Absorption in the Highly Transparent Regime of Solids. A review AFCRL LQ Tech Memo 29.

Bernstein, H.J. and Powling, J.J. 1950 Chem Phys 18 1018.

Billiard, P. and Cornillault, J. 1962 Acta Electronica 6 Special IR Cahier No 3.

Bornstein, A., Croitova, N. and Marom, E. 1982 SPIE 320 Advances in IR Fibres.

Brehm, C., Cornebois, M., Le Sargent, C. and Parant, J.P. 1982 J Non Cryst Solids 47 251-254.

Cornet, J. and Rossier, D. 1973a J Non Cryst Solids 12 61.

Cornet, J. and Rossier, D. 1973b J Non Cryst Solids 12 85.

Cornet, J. and Rossier, D. 1973c Mat Res Bull 8 9.

Deutch, T.F. 1975 J Electronic Materials 4 663.

Dianov, E.M. 1982 SPIE 320.

Dow, J.D. and Redfield, D. 1971 Phys Rev Lett 26 762.

Dow, J.D. and Redfield, D. 1972 Phys Rev B5 594.

Drexhage, M.G., El-Bayoumi, O.H. and Moynihan, C.T. 1982 SPIE Proceedings 320 27.

Edmond, J.T. 1968 J Non Cryst Solids 1 39.

Flaschen, S.S., Pearson, A.D. and Northover, W.R. 1960a J Amer Ceram Soc 43 274.

Flaschen, S.S., Pearson, A.D. and Northover, W.R. 1960b J Appl Phys 31 219.

Ford, E.B. and Savage, J.A. 1976 J Phys E - Scientific Instruments 9 622.

Fuxi, G., Xilai, M. and Peihang, W.H.Y. 1983 J Non Cryst Solids 56 309-314.

Hilton, A.R. and Brau, M. 1963 Infrared Physics 3 69-76.

Hilton, A.R., Jones, C.E. and Brau, M. 1964 Infrared Physics 4 213.

Hilton, A.R. and Jones, C.E. 1966 Phys Chem Glasses 4 112.

Hilton, A.R., Jones, C.E. and Brau, M. 1966a Phys Chem Glasses 7 105.

Hilton, A.R., Jones, C.E., Dabrott, R.D., Klein, H.M., Bryant, A.M. and George, T.D. 1966b Phys Chem Glasses 4 116.

Hilton, A.R., Jones, C.E. and Brau, M. 1966c Infrared Physics 6 183.

Hilton, A.R. 1966 Applied Optics 5 1877.

Hilton, A.R. 1970 J Non Cryst Solids 2 28.

Hilton, A.R., Hayes, D.J. and Rechtin, M.D. 1975 J Non Cryst Solids 17 319.

Hilton, A.R. and Hayes, D.J. 1975 J Non Cryst Solids 17 339.

Hilton, A.R. 1978 SPIE 131.

Hopfield, J.J. 1968 Comments on Solid Stste Physics 1 16.

Kanamori, T., Terunuma, Y. and Miyashita, T. 1983 Integrated Optics and Optical Fibre Communications, Tokyo.

Kapany, N.S. 1967 Fiber Optics Principles and Applications. Academic Press NY.

Katsuyama, T., Matsumura, H. and Suganuma T. 1982 European Patent Application 82301088.9 Publication No 0 060 085.

Katzir, A. and Arieli, R. 1982 J Non Cryst Solids 47 149-158.

Kettlewell, B.R., Kinsman, B.E., Wilson, A.R., Pitt, A.M., Savage, J.A. and Webber, P.J. 1977 J Mat Sci 12 451.

Kittel, C. 1956 Solid State Physics. J Wiley and Son Inc NY.

Klein, R.M. 1974 J Electronic Materials 3 79-99.

Kolomiets, B.T. 1964 Phys Stat Sol 7 359.

Kruse, P.W., McGlauchlin, L.D. and McQuistan, R.B. 1962 Elements of Infrared Technology. J. Wiley and Son Inc NY.

Lucovsky, G. and Martin, R.M. 1972 J Non Cryst Solids 8-10 185.

McLauchlan, A.D. and Gibbs, W.E.K. 1977 NBS Publ 509 222-228.

Michels, B.D. and Frischat, G.H. 1981a J Amer Ceram Soc 64 C150-C151.

Michels, B.D. and Frischat, G.H. 1981b Glastechnische Berichte 54 302-306.

Michels, B.D. and Frischat, G.H. 1982 J Mat Sci 17 329-334.

Miller, F.A. and Wilkins, C.H. 1952 Anal Chem 24 1253-1294.

Mitra, S.S. and Bendow, B. (eds) 1975 Optical Properties of Highly Tranparent Solids. Plenum Press NY.

Miyashita, T. and Terunuma, Y. 1982 J Appl Phys 21 L75-L76.

Moynihan, T.C., Macedo, P.B., Maklad, M.S., M.S.,Mohr, R.K. and Howard, R.E. 1975 J Non Cryst Solids 17 369.

Muir, J.A. and Cashman, R.J. 1967 Optc Soc of America 57 1.

Nakamoto, K. 1963 Infrared Spectra of Inorganic and Co-ordination Compounds. J Wiley and Son Inc NY.

Nyquist, R.A. and Kagel, R.O. 1971 Infrared Spectra of Inorganic Compounds. Academic Press NY and London.

Omonichi, M., Arai, T. and Kudo, K. 1971 J Non Cryst Solids 6 362.

Peck, W.F. and Dewald, J.F. 1964 J Electrochem Soc 1 561.

Pohl, D.W. and Meier, P.F. 1974 Phys Rev Lett 32 58.

Rechtin, M.D., Hilton, A.R. and Hayes, D.J. 1975 J Electronic Materials 4 374.

Rodney, W.S., Malitson, I.H. and King, T.A. 1958 JOSA 48 633.

Savage, J.A. and Nielsen, S. 1964 Phys Chem Glasses 5 82.

Savage, J.A. and Nielsen, S. 1965a VII International Congress on Glass, Brussels.

Savage, J.A. and Nielsen, S. 1965b Infrared Physics 5 195.

Savage, J.A. and Nielson, S, 1966 Phys Chem Glasses 7 56.

Savage, J.A. 1971 J Non Cryst Solids 6 964.

Savage, J.A. 1972a J Mat Sci 11 121.

Savage, J.A. 1972b J Mat Sci 7 64.

Savage, J.A., Webber, P.J. and Pitt, A.M. 1977 Applied Optics 16 2938.

Savage, J.A., Webber, P.J. and Pitt, A.M. 1978 J Mat Sci 13 859.

Savage, J.A., Webber, P.J. and Pitt, A.M. 1980 Infrared Physics 20 313.

Shibata, S., Terunuma, Y. and Manabe, T. 1980 Japan J. Appl Phys 19 L603-L605.

Stacey, K.A. 1956 Light Scattering in Physical Chemistry, Butterfields.

Stachiw, J.D. and Bertic, S.L. 1982 NOSC Tech Report 634. ADA 119495.

SPIE 1982 362 Scattering in Optical Materials.

Strom, U., Hendrickson, J.R., Wagner, R.J. and Taylor, P.C. 1974 Solid State Commun 15 1871.

Takahashi, S., Kanamori, T., Terunuma, Y. and Miyashita, T. 1983 4th International Conference on Integrated Optics and Optical Fibre Communication, Tokyo, Japan.

Tauc, J. 1975 in Optical Properties of Highly Transparent Solids Eds Mitra, S.S. and Bendow, B. Plenum Press NY. 245-260.

Tebo, A.R. 1983 Electro Optics June 41-46.

Thornburg, D.D. 1973 J Electronic Materials 2 495.

Tille, U., Frischat, G.H. and Leers, K.J. 1977 J Non Cryst Solids Ed Frischat, G.H.

(Trans Tech Publications Aedermannsdorf, Switzerland) 631-638.

Tsuchihashi, S., Kawanato, Y. and Adachi, K. 1968 J Ceram Soc Japan 76 103-106.

Turjanitsa, I.D., Mihalinets, I.M., Kaperljas, B.M. and Kopinets, I.F. 1972 J Non Cryst Solids 11 173.

Urbach, F. 1953 Phys Rev 92 1324.

USP 2,804,378 27/8/57.

Vasco, A. 1965 Czechoslovak J Phys 15 170.

Vasiliev, A.V., Dianov, E.M., Plotnichenko, V.G., Sysoer, U.K., Bagrov, A.M., Baikalov, P.I., Devyatykh, G.G., Scripacher, I.V. and Churbanov, M.F. 1983 Electron Lett 19 589-590.

Webber, P.J. and Savage, J.A. 1976 J Non Cryst Solids 20 271.

Worrall, A.J. 1979 SPIE 163 8-12.

Young, P.A. 1970 Thin Solid Films 6 423.

The Author

Jim Savage joined RSRE in 1962 and has worked in the field of infrared optical materials for the past 20 years. He has been involved in the research and development of materials such as Chalcogenide Glasses, Germanium, Zinc Sulphide and Calcium Lanthanum Sulphide. He also has interests in infrared fibres and anti-reflection coatings and is the author of a recent book entitled "Infrared optical materials and their anti-reflection coatings". Adam Hilger 1985.

CADMIUM MERCURY TELLURIDE INFRARED DETECTORS

C T Elliott

Introduction

The alloy semiconductor cadmium mercury telluride is now well established as the most important semiconductor material for the fabrication of infrared detectors to operate in the wavelength range from about 3 μm to 13 μm, that is the range covering the important atmospheric transmission windows from 3 μm to 5 μm and from 8 μm to 13 μm. The particular feature of an alloy material is that one can choose its energy-gap and its long wavelength cut-off by selecting the alloy composition. In addition to its tunable, direct energy gap, the other fundamental properties of the CMT alloy are very suitable for fabrication of infrared detectors. For example, the electron mobility is very high, the electron-to-hole mobility ratio is high and the dielectric constant is modest. In consequence many different types of infrared device have been made from CMT despite its difficult materials growth problems. These include photoconductors, photodiodes, charge transfer devices and even transistor structures. It is not the purpose of this paper to attempt to review all of these devices, instead it concentrates on some recent developments which have taken place in the United Kingdom at RSRE and at Mullard Limited.

The three following sections of the paper describe CMT infrared detectors which are at very different stages of development. The first section is on SPRITE detectors which are used in high performance thermal imaging systems. These detectors and the systems based on them have been in production now for some time, and the emphasis here is on new developments which will be used in second generation systems with improved spatial resolution and improved temperature resolution.

The second section is concerned with electronically scanned two-dimensional arrays of CMT detectors which are still in the research and development phase. The topic of focal plane arrays is the subject of a great deal of research and many different approaches are being pursued. This paper will be concerned exclusively with the particular approach we have pursued in the UK, which is to use photovoltaic CMT detectors hybridised with silicon addressing circuits.

The topic of the third section is a very new piece of research based on some ideas to raise the operating temperature of infrared detectors. All of the high performance infrared detectors presently used in the 3-5 μm and 8-13 μm spectral regions require cooling to cryogenic temperatures. For the shorter wavelength band this is typically around 200K, and for the longer wavelength band typically around 80K. Cooling adds very considerably to the expense and the inconvenience of using the detectors and is the principal obstacle to the more widespread use of infrared systems, particularly in the civil field.

Recent Developments in SPRITE Detectors

The principle of operation of the SPRITE detector has been outlined in several papers [1,2,3,4]. It is a three-lead photoconductive CMT detector and the essential point of its operation is that the image scan velocity is matched to the ambipolar drift velocity of the photogenerated carriers. The device performs the same function as a serial-scan array of detectors together with the associated preamplifiers and time-delay-integration circuits, thereby considerably simplifying both the detector fabrication and the imager electronics.

Recent research has been aimed at modified and improved detector structures which will further improve both the temperature resolution and the spatial resolution of thermal imaging systems. The temperature resolution is improved by putting in more SPRITE detectors to increase the area of CMT on the focal plane. This has been achieved both by increasing the number of SPRITES in linear arrays and by the fabrication of two-dimensional arrays of SPRITES. The spatial resolution of the SPRITE detector, when the scan velocity and the carrier velocity is matched throughout the device length, is determined by the diffusion spread of the

photogenerated carriers and the spatial averaging in the read-out zone. This may be expressed through the modulation transfer function

$$MTF = \left(\frac{1}{1 + k_s^2 Q_a^2}\right)\left[\frac{2 \sin (k_s \ell/2)}{k_s \ell}\right] \quad (1)$$

where k_s is spatial frequency, Q_a is diffusion length, ℓ is the length of the read-out region. Alternatively, the equivalent expression for the impulse function is obtained from a convolution of the diffusion spread function with the rectangular response of the read-out zone.

$$F(t) = \int_{-\infty}^{\infty} \exp(-|vt-x|/Q_a)\ \mathrm{rect}(x|\ell)\ dx \quad (2)$$

The latter expression is used for comparison with the experimental data given below. The modifications to the device which have been carried out to improve the spatial resolution fall into two categories. The first is the correction of deficiencies in the original device which caused its performance to fall short of that predicted in equations (1) and (2), and the second is more fundamental modifications which allow the spatial resolution to be improved below the apparent limit set by the diffusive spread of carriers.

In the first category are the horn read-out device and the tapered drift-region device [5]. In the original SPRITE with bifurcated read-out geometry, which is illustrated in Figure 1a, the non-uniform electric field in the structure led to a significant transit-time spread for carriers drifting into the read-out region. The carrier illustrated as coming along the top of the device travels a longer path, and travels in a weaker field than a carrier which started at the same distance from the end but travels along the bottom of the device. This transit-time spread was considerably reduced by using the horn geometry illustrated in Fig 1b. A further benefit of the horn device is that the higher electric field at the negative electrode reduces the delay in the recombination of minority carriers at the contact, due to its finite recombination velocity.

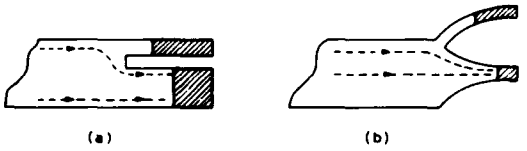

Fig 1 SPRITE read-out geometry (a) bifurcated, (b) horn

The second geometrical change which has been made to the SPRITE is to produce a slight taper on the drift region of the device. In operation a SPRITE element is exposed to the uniform background illumination from the ambient temperature scene, in addition to the signal radiation. This background flux is integrated in a similar way to the signal flux and produces an excess carrier distribution along the length of the device as illustrated in Figure 2a. Although this excess is only a small fraction of the extrinsic carrier density, it does produce a slight change in the carrier velocity along the length, both through the variation of resistivity (and electric field) and through a variation of the ambipolar mobility. The solution is to put a slight taper on the device which has been calculated to counter

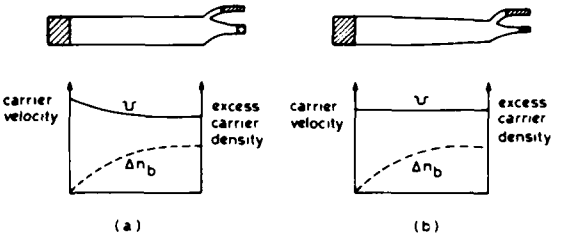

Fig 2 SPRITE drift-region geometry (a) straight, (b) tapered

the effect. This is illustrated in Figure 2b. An actual example of the device which includes both the taper and the horn read-out is shown in Figure 3. This is an 8 row device, the elements are 500 μm long overall and are 62.5 μm wide at the widest point. The effect of these geometrical changes on the impulse function width is illustrated in Figure 4, where the width or impulse function, at the 1/e height, is plotted against the measured minority carrier lifetime in the filaments. Theoretical line 1 is calculated from equation 2; theoretical line 2 shows the broadening of the impulse produced by the background integration effect; and theoretical line 3 shows the

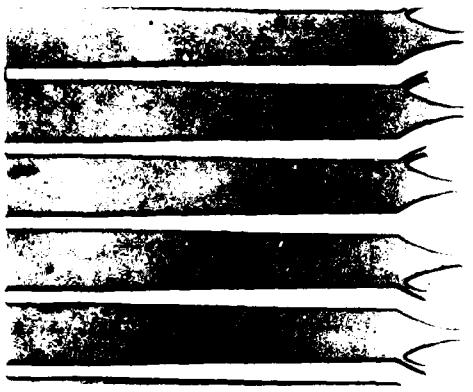

Fig 3 Eight row SPRITE with tapered-horn geometry. Courtesy of Mullard Ltd

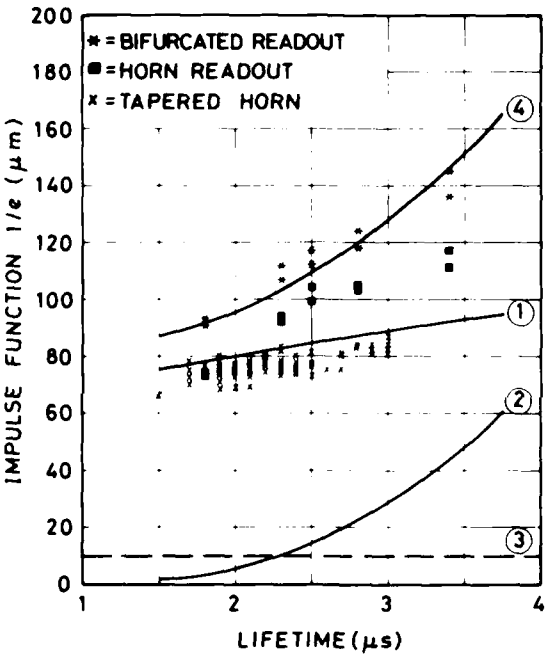

Fig 4 Impulse function width versus lifetime for SPRITE elements. *, straight/birfurcated; ■, straight/horn; X, tapered/horn

broadening of the impulse function produced by the read-out. The last component is difficult to predict accurately and for the purpose of calculation a value of 10 μm independent of lifetime is assumed. The basis of this figure was that in comparing experimental results for the bifurcated and horn geometries, at low lifetimes where the background effect is negligible, an excess contribution of 10 μm was observed. Theoretical line 4 represents the total of all of these effects. The theoretical results from the straight, bifurcated read-out devices can be seen to be in good agreement with line 4. The experimental results for the straight, horn read-out devices are shown to give reduced impulse function widths compared to the bifurcated read-out for all values of lifetime. The results for the tapered drift region, horn read-out devices can be seen to be in good agreement with the predictions of equation 2. The deficiencies of the original straight, bifurcated SPRITE have therefore been corrected.

The diffusive spread of carriers does not represent a fundamental limit to the spatial resolution of the device. The spatial resolution can be improved beyond this limit by means of a meander-path structure [4],or by means of a modification to the system optics to use an anamorphic detector lens [6]. A meander-path device is illustrated in the lower part of Figure 5, it has the same width as previous devices, typically 60 μm, but by cutting slots in it the carriers are forced to take a tortuous meander path. The bias field is increased so that the mean velocity of carriers along the long axis of the device remains matched to the image scan velocity, but the effective diffusion length of carriers along the long axis of the device is reduced in the ratio Y/W where W is the true width of the device, and Y is the width of the actual filament. The problem of fabricating these devices is that damage introduced at the cut flanks, during the element definition, introduces a finite recombination velocity and because of the very narrow filament width, typically 15 μm, this reduces the carrier lifetime to very small values. It is only through technological developments made very recently, that it has been possible to confirm the principle of this

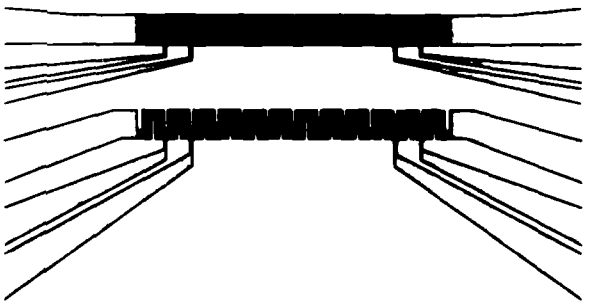

Fig 5 A meander-path SPRITE and a straight SPRITE

device [7]. A summary of measured data comparing the performance of a straight device and a meander-path device, like those shown in Figure 5, is given in Table 1.

Table 1 Meander Sprite Performance

Device	Lifetime (μs)	D* (500K) (cm $Hz^{\frac{1}{2}}W^{-1}$)	Pulsewidth (1/e)	
			Meas. (μm)	Calc. (μm)
Straight	9.5	$3.4\ 10^{10}$	135	124
Meander	7.0	$3.3\ 10^{10}$	97	81

This shows that the lifetime and detectivity are maintained in the meander-path device while the impulse width is improved. The device cut-off wavelength is 4.5 μm and is operated at 193K. W is 70 μm and Y is 20 μm.

The anamorphic optic is a modified detector lens in the system which gives increased magnification of the image in the scan direction. The detector length and scan speed are increased in the same proportion as the increase in magnification, but the diffusion length of the carriers remains constant so that the spatial resolution is improved. Since the SPRITE detectors remain background limited even in low background flux, the signal-to-noise ratio is unaffected and the improved spatial resolution is obtained without penalty in the thermal sensivitity of the system. Smith, Braim and Campbell [6] have described an anamorphic SPRITE system operating in the 8-13 μm band and have demonstrated the expected improvement in spatial resolution. An example of a thermal image obtained from this system is shown in Figure 6.

Electronically Scanned Two-Dimensional Arrays

There is currently a very large research activity in many research laboratories throughout the world directed towards the fabrication of two-dimensional arrays of detectors, which consist of several thousand elements and are addressed electronically so that they do not require mirrors and

Fig 6 Example of a thermal image obtained using an eight row straight/horn SPRITE operating in the 8-13 μm band with an anamorphic detector lens. White is hot in the picture

scanning mechanisms. The prospects for producing sufficiently large arrays to replace high performance thermal imaging systems, like those described in the previous section, are still remote, but staring arrays will find applications in a new generation of sophisticated missile homing heads, and perhaps also in simple, small light-weight imagers. One major attraction of these electronically scanned arrays is the elimination of the mechanical scanning which reduces the complexity of the system and is most important when space is at a premium. A second is the increase in sensitivity due to the longer integration period of detectors when compared with the scanned systems. This gives much longer detection ranges, or it may be traded for reduced optical apertures, and hence decreased system size.

We have chosen CMT/Silicon hybrid technology because of the broad range of cut-off wavelengths and the wide operating temperature range which it offers. A common technology based on this hybrid can provide arrays for both the 3-5 μm and 8-13 μm bands with operating temperatures of 80K, or even higher in the shorter wavelength band.

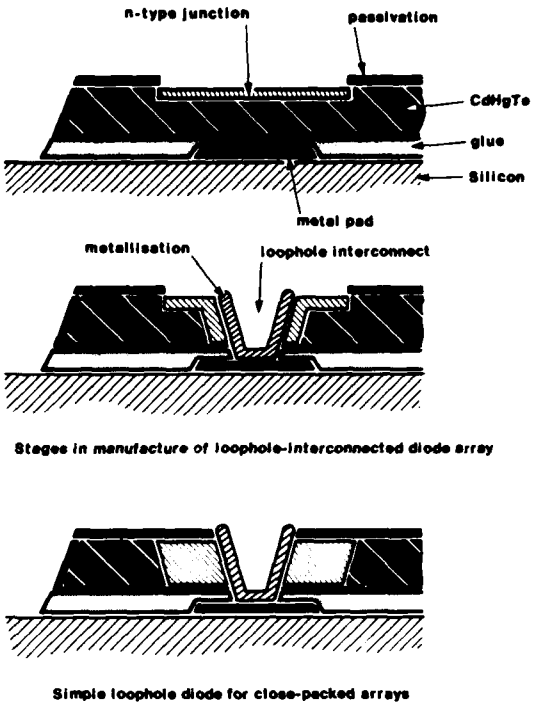

Fig 7 Schematic of hybrid technology (a) formation of planar junction, (b) hybrid interconnect for planar junction, (c) hybrid interconnect for lateral collection diodes

The loophole interconnect technology described previously by Baker et al [8,9] presently allows an array of up to 64 x 64 diodes to be interconnected with silicon circuits. This elegant technique gives a high fill factor, small unit cell (typically 40 μm x 40 μm at present) and high connection yield (greater than 99.8% currently). The fabrication steps involved are illustrated schematically in Figure 7. With reference to the upper part of the figure, the CMT monolith is polished to about 8 μm thick, passivated on both sides and then glued to the silicon chip. Using the chip as a substrate, a matrix of junctions is ion-implanted or diffused in the p-type CMT. The junctions are then individually connected to the underlying parts of the silicon by cutting 10 μm holes through the junctions, doping the exposed CMT in each hole, and then backfilling with metallisation. This is illustrated in the lower part of the figure. In high density two-dimensional arrays the first diffusion stage may be omitted, and the loophole diffusion driven deeper so that the photosensitivity is achieved by lateral collection to a cylindrical junction. Finally, an ohmic contact to the p-type monolith completes the structure. One of the advantages of the loophole technique is that it requires just one masking stage to achieve both the junction and interconnection to the silicon. The structure has been found to be both thermally and mechanically stable, and gives a high connection yield with a very small loss of sensitive area by obscuration, which is only 5%.

The two generic types of silicon addressing circuits which have been developed are CCD and FET switches [8,9,10]. The two-dimensional CCDs operate in the interline transfer mode and are twin-layer, buried channel devices which give large charge storage capacity together with high clocking speeds. These devices are used both in the 3-5 μm and in the long wavelength band at cut-off wavelengths to about 9 μm at 80K operating temperature. Longer wavelength operation of two-dimensional CCD hybrids awaits the development of higher quality CMT diodes with larger zero bias impedance. This is expected to follow from the development of modern epitaxial methods of

preparing the CMT, which will both yield higher quality material and give the possibility of more complex heterostructure devices. The greater flexibility in CCD geometry which is possible in linear arrays currently allows longer cut-off wavelengths than for area arrays. For example, high injection efficiency is obtained with 10 μm cut-off in F/1 field-of-view.

Longer wavelength operation of two-dimensional arrays is possible by use of FET switch addressed arrays. Each detector is connected through an N-MOS silicon switch to the Y lines of a co-ordinate addressed matrix. In operation, the shift register selects a row of detectors and switches each device to a line of integrating amplifiers which are then multiplexed. The diode impedance requirements for this type of addressing are reduced by more than an order of magnitude compared to CCD addressing. Also, the dynamic range of the amplifiers is

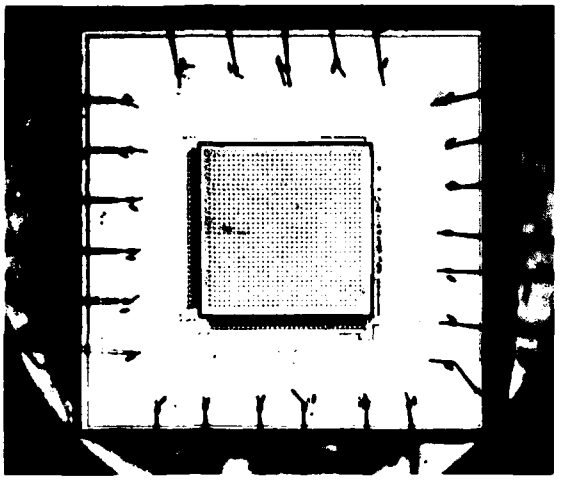

Fig 8 Photomicrograph of a 32 x 32 CMT/Silicon CCD hybrid array. Courtesy of Mullard Ltd

very large compared to the CCD. These simplifications have permitted the demonstration of imaging from two-dimensional arrays at wavelengths beyond 12 μm. The N-MOS technology used for the switches is simple, and potentially cheaper than the CCD and it also offers some benefits in terms of simpler uniformity correction for the following electronics. Random access can also be included if required. The disadvantage of the switch addressing, and the reason that it is not also used in the shorter wavelength band is that the detector integration period is of order a line period rather than a frame period. An example of a 32 x 32 CMT hybrid CCD array is shown in Figure 8.

Non-Equilibrium, Auger-Suppressed Devices for High Operating Temperature

The requirement for cooling long wavelength infrared detectors does not appear to be fundamentally necessary. The basic effect which limits the signal-to-noise performance of narrow-gap semiconductor detectors at near ambient temperature is the thermal generation of electron-hole pairs by Auger processes. These can be suppressed and consequently the need for cryogenic operation can be reduced by operating the device in a non-equilibrium mode, in which the carrier densities are held below their thermal equilibrium values. The objective is to make the material behave extrinsically at temperatures at which it would normally be intrinsic, ie at ambient temperatures for 3-5μm band devices and at around 200K for 8-13μm band devices. Provided that the reduction of carrier density can be achieved without significantly raising the electron temperature, the net Auger generation rate and the fluctuations in it will be reduced. The non-equilibrium situation can be achieved in either photoconductive or photovoltaic devices and the principle of each is described below.

An excluding contact photoconductor is illustrated schematically in Figure 9. At the top of the diagram a plan view of the device shows a long strip of near-intrinsic,

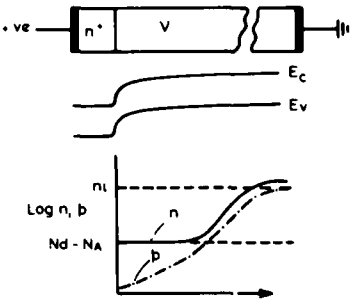

Fig 9 Schematic of an excluding-contact photo-conductive detector (a) plan view, (b) band diagrams, (c) carrier concentrations

but n-type so-called ν CMT. At the left

hand end we have an n^+ or heavy-light contact, the band diagram for which is sketched schematically underneath. The contact could alternatively have been a heterojunction of wider gap n material. The property of the n^+ contact is that it allows free flow of electrons across the contact but does not inject minority holes into the material, so that when the contact is biased positively no holes can be injected into the material to sustain the flow of holes in the bulk away from the contact. Plots of the carrier concentrations as a function of position along the device are shown in the lower part of the diagram. Before the bias is applied both the electron and hole concentrations are near the intrinsic value. When the bias is applied the hole concentration falls for some distance away from the contact and in order to keep space charge equilibrium the electron concentration also falls, close to the extrinsic level, N_d-N_a. The reduction in carrier concentration obtained in this way can be several orders of magnitude and the range over which it occurs can be some tens or even hundreds of microns. This reduction in the carrier densities, and in particular, the reduction in electron density is expected to considerably reduce the Auger generation rate and hence improve the signal-to-noise ratio. A second benefit of this type of device is that the resistance is increased and therefore responsivity is also considerably higher than is normally achieved in near intrinsic devices.

Exclusion effects have been investigated in long filaments of n-type CMT with carrier concentrations in the range 5 10^{14}-1 10^{15} cm^{-3}, and of dimensions 1 mm long and 100 μm wide. The type of device used is illustrated schematically in the inset of Figure 10. The excluding contact at the earthy end of the device is produced by ion implantation of the n^+ region. There are multiple side-arm potential probes along the length of the device which allow measurements of electric field, Hall effect and detector properties. The results shown on Figure 10 are for material with a cut-off wavelength of 5 μm operating at 275K. The current I flows through the length of the filament and the voltage V is measured between the pairs of probes as indicated by the labels on the graphs. A transition from a low impedance to a high impedance region may be seen in the lower left quadrant of

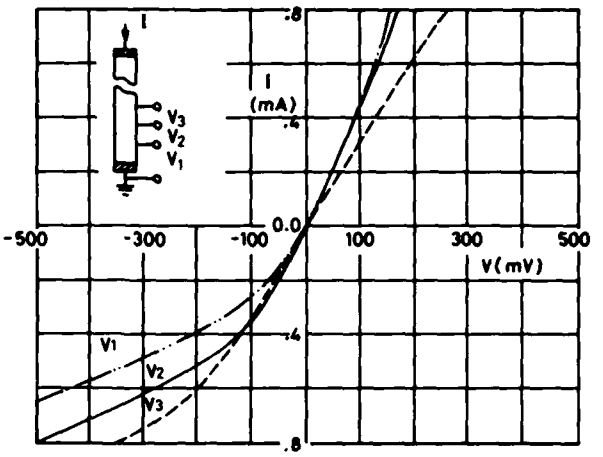

Fig 10 Current voltage characteristics for an excluding-contact photoconductor operating at 275K with a cut-off wavelength of 5 μm

the graph. It is in this high impedance region that the device is excluded. We refer to this as the reverse direction and to the positive bias as the forward direction. Not only is the exclusion effect seen between the end contact and the first probe but it can also be seen with higher knee voltages between the second pair and the third pair of probes. This demonstrates that the effect is not one that is localised at the contact, but it is distributed in the bulk of the material. In this particular device the ratio of the resistance in the forward and reverse directions is about a factor of five. Hall effect measurements confirmed that the carrier concentration is reduced below its equilibrium value in the excluding direction.

Detector measurements have been made by measuring the voltage between the n^+ end contact and the first potential probe, and by illuminating in this region, with a 500 K blackbody source. The responsivity is plotted in Figure 11 and in the reverse, or excluding direction it rises superlinearly with bias current and then tends to level off. The responsivity in the forward direction saturates at a much lower level, the ratio of responsivity in the saturated regions being typically more than a factor of ten. The problem with the devices at present is that the high levels of flicker noise are observed when they are biased in the excluding direction. This has so far prevented the conclusive demonstration of Auger suppression. Measurements carried out

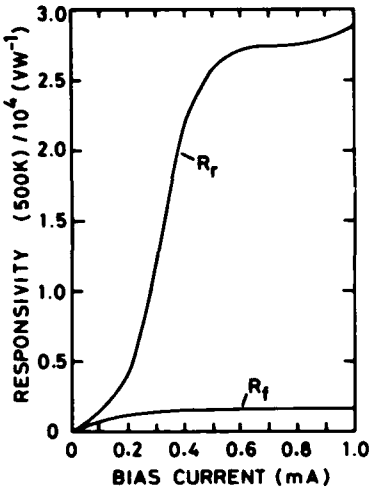

Fig 11 Responsivity versus bias current for an excluding contact photoconductor operating at 275K with a cut-off wavelength of 5 μm. R_r is reverse bias. R_f is forward bias

at high modulation frequencies above 100 KHz show small improvements in detectivity, of about a factor of two which could be consistent with the Auger suppression but further measurements are required when the level of flicker noise has been reduced.

There is another possibility for achieving the non-equilibrium operation which is shown schematically in Figure 12. The region of the device which absorbs the infrared radiation is a near intrinsic p or region. This makes a heterojunction contact with a wider gap n region. The contact at the other end of the π region is a heterojunction to a wide-gap p region, ie it is an excluding contact which will not inject minority electrons into the π region. Provided that the width of the π region is small compared to a minority carrier diffusion length we would expect to see

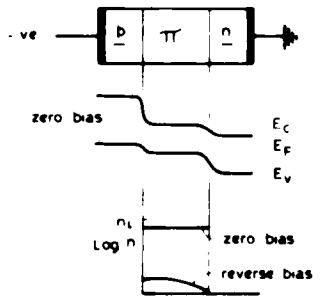

Fig 12 A schematic diagram showing the principle of operation of an Auger-suppressed diode

large reductions in the carrier densities below their equilibrium values in this region when the device is reversed biased. This occurs because the π to wide gap n junction acts as a sink for the minority electrons in the π region, they therefore diffuse to it and are lost. Since these cannot be replaced by injection from the wide gap p region, the carrier concentrations fall from the near intrinsic level to the very low values indicated in the lower part of Figure 12. The practical implementation of such devices will require a well established multilayer, epitaxial technology such as we may expect to see from MOCVD or MBE.

Acknowledgements

The author gratefully acknowledges contributions to this work from many colleagues at RSRE and Mullard Limited. Part of the work is supported by DCVD, MOD(PE).

The paper is reproduced by kind permission of Journal of Crystal Growth, in which it was first published.

References

1. Elliott C T, Electron. Letters 17, 312 (1981).

2. Elliott C T, Day D and Wilson D J, Infrared Phys 22, 31 (1981).

3. Blackburn A, Blackman M V, Charlton D E Dunn W A E, Jenner M D, Oliver K J and Wotherspoon J T M. Proc Int Conf on Advanced Infrared Devices and Systems, IEE Conference Publication No 204, 7 (1981).

4. Elliott C T, "Solid State Devices" eds Goetzberger and Zerbst, 175, Physik Verlag, Weinheim (1983).

5. Ashley T, Elliott C T, White A M, Wotherspoon J T M and Johns M D, Infrared Phys 24, 25 (1984).

6. Smith D A, Braim S P and Campbell A P, Proc of SPIE 28th International Technical Symposium, San Diego, 1984.

7. Dean R J, Elliott C T, Johns M D, Readhead J and Tarry H A - to be published.

8. Baker I M, Jenner M D, Parsons J, Ballingall R A, Blenkinsop I D and Firkins J H, 2nd International Conference on Advanced Infrared Devices and Systems, IEE Conference Publication 228, 12, 1983.

9. Baker I M and Ballingall R A, Proc of SPIE 28th International Technical Symposium, San Diego, 1984.

10. Ballingall R A, Blenkinsop I D, Elliott C T, Baker I M and Jenner D, Electronics Letters 18, (7), 285 (1982).

11. Ashley T and Elliott C T - to be published in Electronics Letters.

The Author

Dr C T Elliott is a Senior Principal Scientific Officer (Individual Merit) carrying out research on opto-electronic devices, with a particular specialisation on infrared detectors based on narrow-gap semiconductors. He graduated in Physics from the University of Manchester in 1960 and went on to carry out postgraduate research in the Electrical Engineering Department of that University, where he subsequently took up a lecturing post in 1963. He joined RSRE (then RRE) in 1967 and has remained since, except for a year on exchange to MIT Lincoln Laboratory during 1970/71.

NON-GAUSSIAN LIGHT SCATTERING EXPERIMENTS

E Jakeman

Abstract

A review of data acquired in light scattering experiments designed to investigate non-Gaussian fluctuations will be given. Systems investigated include dynamic scattering in liquid crystals, laboratory generated thermal plumes, mixing layers, rippled liquid surfaces and specially prepared solid diffusers. Comparison with theoretical predictions will be made where possible.

Introduction

Since the advent of the laser there have been a wealth of coherent light scattering experiments from a very wide range of scattering systems. Many of these experiments were designed to investigate or exploit the most familiar laser light scattering phenomena: "speckle", the pattern of bright and dark regions formed when coherent light is scattered by almost any kind of rough surface Fig 1. Speckle is the

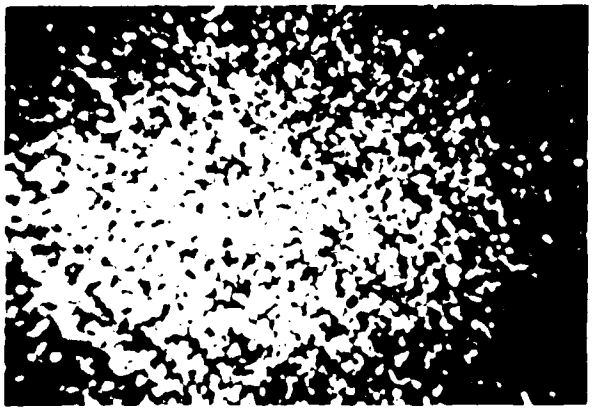

Fig 1 A Gaussian speckle pattern

optical analogue of Gaussian noise and arises when randomly phased contributions from many independent scattering centres add together coherently. The central limit theorem predicts that in this situation the resultant field vector is a circular complex Gaussian process with a Rayleigh distributed amplitude and negative exponential distribution of intensity fluctuations [1]. Gaussian speckle is now a thoroughly investigated and fully understood phenomenon which has found application in many areas of practical measurement such as surface roughness and anemometry. Many naturally occurring optical phenomena, however, are broadband (white light) effects visible to the naked eye and do not owe their existence to the coherence of the source. These are non-Gaussian effects and their statistical and correlation properties are on the whole not well characterised or understood [2]. In order to start to rectify this situation a programme of non-Gaussian light scattering experiments was begun at RSRE some ten years ago. Since then we have investigated a wide variety of simple scattering systems with the principle aim of gaining some insight into the statistical nature of non-Gaussian intensity patterns for noise modelling purposes. Many of these systems were generic ie typical of scattering systems encountered in practice, rather than artificially contrived to enable their characteristics to be measured by other techniques. However, a few specially prepared and characterised scatterers have been investigated and it is important to carry out more such experiments in the future as the aim of the programme shifts towards the development of remote sensing techniques.

In recent years a number of other groups have carried out non-Gaussian scattering experiments, in particular Professor Dainty's team at Rochester (now at Imperial College) [3,4] and Professor Asakura's Group in Japan [5]. However in this paper I shall restrict my historical survey to our own work on diffusing layers and surfaces at RSRE with which I am most familiar, and I would like to acknowledge at this point the invaluable support and encouragment of my experimentalist colleagues over the years, particularly Dr P N Pusey, Dr G Parry and more recently Drs J G Walker, D L Jordan and R C Hollins. Although many of the experimental results have been interpreted in the light of predictions made by solving Maxwell's equations for specific theoretical models, a more empirical approach: the two dimensional random walk model [6] has often provided much needed insight and has led to

one of the most useful outputs from this programme of research: a non-Gaussian noise model with wide applicability, namely, the class of K-distributions [7]. Thus in the next section we briefly review the predictions of the random walk model. Sections 3 and 4 are devoted to scattering by fluid and solid scattering systems respectively with some concluding comments in section 5.

The Random Walk Model

In the simplest random walk model the scattered wave field is represented as the sum of N randomly phased vectors of variable length:

$$\mathcal{E} = \sum_{n=1}^{N} a_n e^{i\phi_n} \qquad (1)$$

where the $\{\phi_n\}$ are uniformly distributed and independent of the $\{a_n\}$ which are also statistically identical and independent from each other. The mean intensity and second normalised intensity moment are then given by

$$\langle I \rangle = N\langle a^2 \rangle$$

$$\frac{\langle I^2 \rangle}{\langle I \rangle^2} = 2 - \frac{2}{N} + \frac{\langle a^4 \rangle}{N\langle a^2 \rangle^2} \qquad (2)$$

When $N \gg 1$ the second moment reduces to the Gaussian speckle value of two as predicted by the central limit theorem. When N is finite there is a deviation from this value which is inversely proportional to N. If equation (1) is used to model rough surface or diffuser scattering then it is reasonable to expect N to illuminated area so that the deviation from Gaussian statistics obtained by illuminating a small area should be inversely proportional to this area. Note that the random phase assumptions made in equation (1) presumes that the scatterer introduces phase fluctuations greater than 2π, which is the case of most interest. Also when N is finite equation (2) depends on the detailed statistical behaviour of the form-factors $\{a_n\}$ ascribed to the individual scattering centres. Thus the model will be highly sensitive to the detailed nature of the scatterer. It is usually found in practice (except for certain simple particle scattering systems) that the final term in equation (2) is much larger than the second term so that enhanced fluctuations are observed [8,9]. The pattern generated by a scatterer in such a non-Gaussian configuration may have a highly complicated structure as indicated in Figure 2 and, in the case of a moving pattern, the detected intensity will have a spikey structure quite distinct from Gaussian noise.

Fig 2 Intensity pattern due to a small illuminated area

The origin of the correlated regions of high intensity evident in Figure 2 can also be interpreted in terms of the random walk model through the coherence function

$$\frac{\langle I(x)I(x')\rangle}{\langle I(x)\rangle\langle I(x')\rangle} = \left(1 - \frac{1}{N}\right)\left[1 + \frac{\mathcal{E}(x)\mathcal{E}^*(x')}{\langle I(x)\rangle\langle I(x')\rangle}^2\right] + \frac{\langle a^2(x)a^2(x')\rangle}{N\langle a^2(x)\rangle\langle a^2(x')\rangle} \qquad (3)$$

where x and x' represent two space-time points. When N is large equation (3) reduces to the factorisation property of a complex Gaussian process and the second term in the square brackets represents the effect of interference or speckle in the pattern. The associated coherence time reflects the relative motion of scatterers whilst the coherence length will be just inversely proportional to the aperture (illuminated area) size. When N is finite, however, the final term becomes important. This is a single scatterer term characterised by the time constant of the motion of individual scatterers and by one or more length scales associated with their diffraction and focussing properties. It is evident that

all of these scales will be longer than those characterising optical frequency speckle, as indeed is observed in Figure 2. Because the single scatterer contribution may be geometrical in origin it may well be present with broadband (white light) illumination when the interference term vanishes.

Summarising then, the random walk model leads us to expect that when only a small area of the scatterer (comparable to the largest scale size present) contributes to the intensity at the detector we expect the second normalised moment of the intensity fluctuation distribution to exhibit a deviation from Gaussian statistics inversely proportional to the illuminated area. We expect the intensity coherence function to exhibit more than one length scale and more than one time scale and we expect residual fluctuations even in white light illumination.

The random walk model (1) can be solved exactly in a formal sense for the distribution of amplitude fluctutations ($A = \sqrt{I}$)

$$P_N(A) = A \int_0^\infty u\,du\, J_o(uA) \langle J_o(ua)\rangle^N \qquad (4)$$

However this result is not particularly useful as a noise model.

It is well known that

$$\lim_{N\to\infty} P_N(A) \sim 2Ae^{-A^2} \quad \text{for all } p(a)$$

and that

<u>if</u> $p(a) \sim 2ae^{-a^2}$

<u>then</u> $P_N(A) \sim 2Ae^{-A^2}$ for all N

Evidently neither of these results is useful in non-Gaussian noise modelling. However it is not difficult to show that [7]

<u>if</u> $p(a) \sim a^\nu K_{\nu-1}(a)$

<u>then</u> $P(A) \sim A^{\nu N} K_{\nu N-1}(A)$

for all N (5)

where K_ν is the modified Bessel function of the second kind.

These K-distributions have moments which lie between Rayleigh and log-normal and clearly have a number of attractive features. For example the coherent addition of vectors whose amplitude is K-distributed leads to a resultant whose amplitude is distributed according to a different member of the same class: no new parameter is introduced into the model.

Although K-distributions were introduced as an empirical class of distributions satisfying (4) they have proved to provide an excellent model for data from a wide range of scattering systems, particularly multiscale systems [10]. It has been conjectured that the modulation of small scales by an underlying larger scale structure leads to clustering or bunching of the scattering centres which result in non-Gaussian fluctuations even in the high scatterer density limit. It is not difficult to show that the negative binomial step number distribution

$$P(N) = \binom{N-\nu+1}{N} \frac{(\bar{N}/\nu)^N}{(1+\bar{N}/\nu)^{N+\nu}} \qquad (6)$$

leads to K-distributed amplitude fluctuations in this limit [11] ie

$$\lim_{\bar{N}\to\infty} \langle P_N(A)\rangle \sim A^\nu K_{\nu-1}(A)$$

where $\bar{N} = \langle N\rangle$ and $P_N(A)$ is given by equation (4). Thus the K-distribution model can arise as the combined result of scatterer density fluctuations and interference effects. Although the negative binomial model is only one particular cluster model, some kind of clustering property is more likely to be common to a large number of systems than the detailed behaviour of individual scattering centres ie p(a). It has been shown that the cluster-interference interpretation is indeed correct for one scattering model which leads exactly to K-distributed intensity fluctuation [12].

Experiments on Diffusing Fluids

1 Liquid Crystal Experiments

The first quantitative non-Gaussian scattering experiments were carried out on

25 μm layers of the negative nematic liquid crystal MBBA used in early liquid crystal watch displays etc [8,9]. When driven into a turbulent state by the application of a small potential difference this layer takes on the appearance of ground glass and under the appropriate polarisation conditions behaves as a random phase changing screen. The scattered intensity pattern was investigaated in a far field configuration as a function of illuminated area and

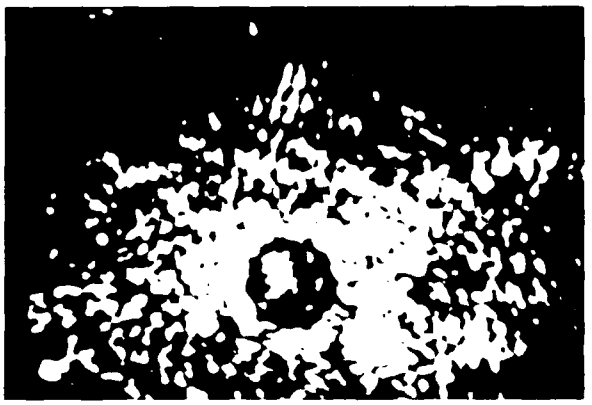

Fig 3 Pattern generated by dynamic scattering in MBBA

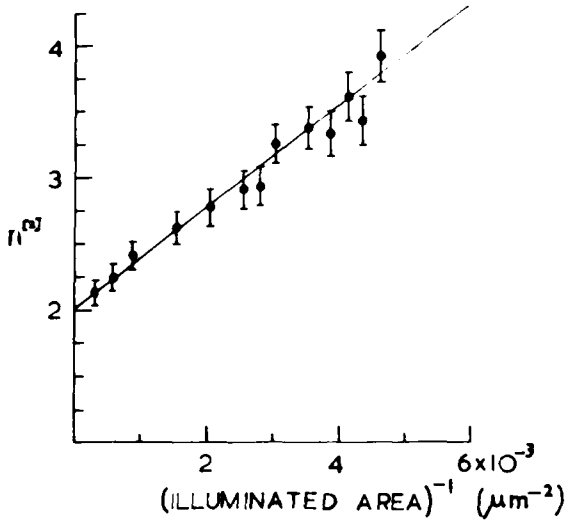

Fig 4 Dependence of second intensity moment on illuminated area

scattering angle. Figure 3 shows the appearance of the pattern. Figure 4 shows the second normalised intensity moment as a function of illuminated area and confirms the $(\text{area})^{-1}$ behaviour predicted by the random walk model. However it was estimated that the effective number of scatterers was still relatively large in these experiments (>16). Figure 5 shows a plot of the spatial coherence function of the intensity fluctuations and exhibits two well defined length scales as expected. By increasing the applied potential difference the size of the scattering structures could be reduced and it was then found that only the central rapid fall-off was preserved, indicating that this length scale related to interference effects or speckle.

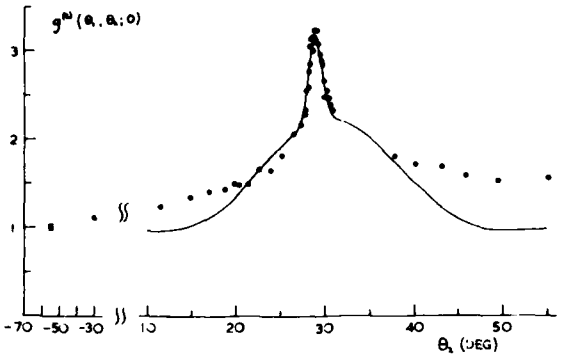

Fig 5 Dynamic scattering: spatial coherence function

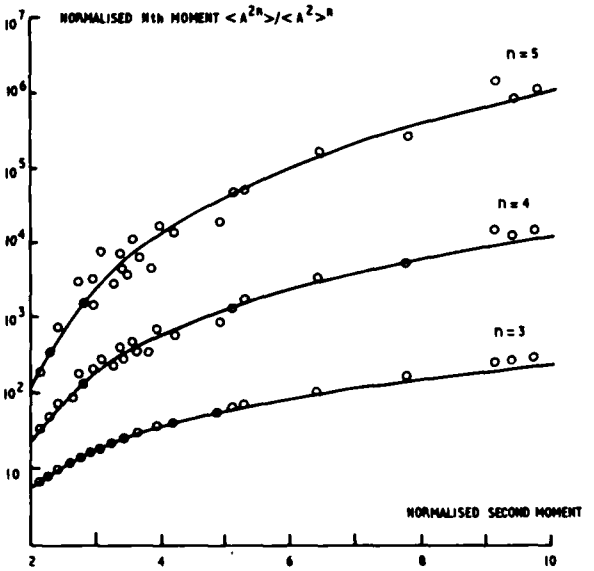

Fig 6 Dynamic scattering: statistical data compared with K-distributed noise

A number of other measurements were made on this system including the dependence of the

second normalised intensity moment on angle and the temporal coherence properties of the intensity. These could all be explained satisfactorily on the basis of the random walk model and are not reproduced here. An adequate model for the higher order moments of the intensity fluctuation distributions could not be found at the time of the original experiments but it was subsequently found that the K-distribution model was an excellent fit to the data (Figure 6).

2 Thermal Plume Experiments

Theoretical predictions for the intensity fluctuations in the Fresnel region of a phase changing screen appeared in the literature during the 1950's and 1960's. A number of simple experiments on thermal plumes and mixing layers were devised at RSRE during the mid 70's in order to test these predictions and also to gain insight into the more difficult but important problem of propagation through extended media. Figure 7 shows the focussing curve or scintillation plot for light scattered into the Fresnel region by a thermal plume generated by a heater between two baffles [13]. Note that enhanced non-Gaussian fluctuations occur in this scattering geometry as a result of the limited area of the scatterer which contributes to the intensity at the detector when this is sufficiently close. The limitation is typically caused by geometric considerations eg the finite tilts of the scattered wavefront, although diffraction plays the dominant role in the case of fractal scatterers. Comparison of the data with theoretical curves assuming a joint Gaussian phase function with Gaussian auto-correlation function indicates that the predicted focussing peak is too narrow, probably because a range of scale sizes focussing at different distances are present. This data was subsequently compared with the predictions of a two scale model [4] and more recently with the predictions of a sub-fractal model as shown in Figure 8 [15]. Much better agreement with the data is obtained using the latter model, the apparent deviation at large propagation distances being attributable to inadequate modelling of outer scale effects.

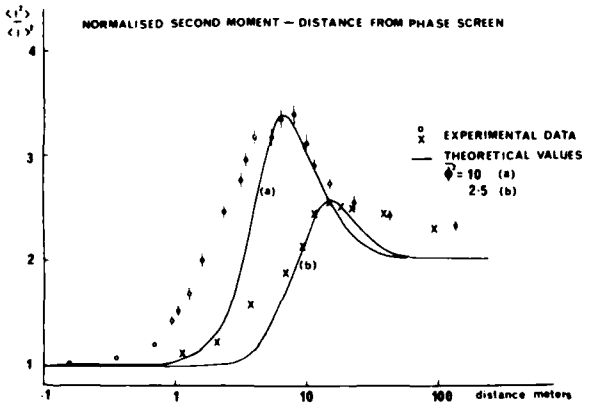

Fig 7 Focusing curve for propagation through a thermal plume

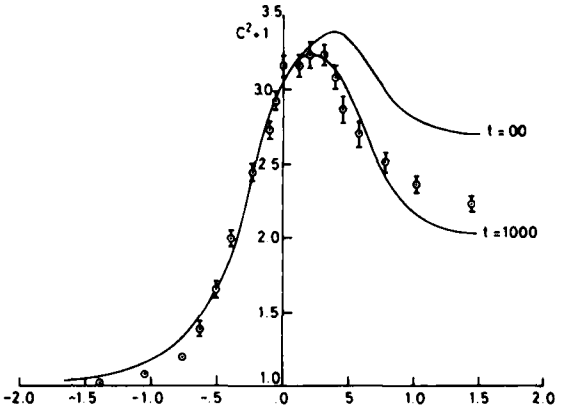

Fig 8 Thermal plume: comparison of data with theory
$C^2 + 1 = n^{[2]} = \langle I^2 \rangle / \langle I \rangle^2$

It was found experimentally that different focussing curves were obtained for plumes of different scattering strengths, thus ruling out a simple fractal description of the system. Indeed, geometrical effects are

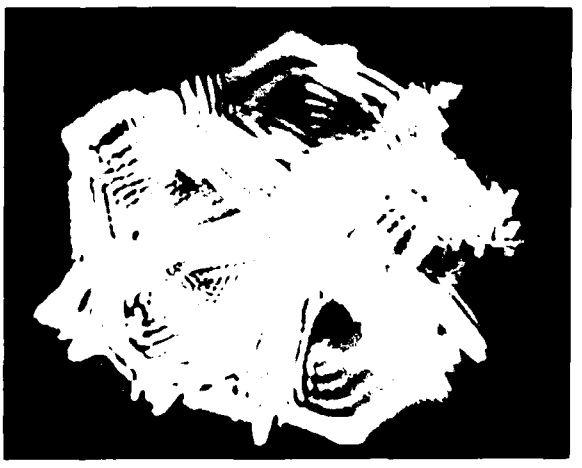

Fig 9 Thermal plume: intensity pattern in focusing region

clearly visible in the scattered intensity pattern (Figure 9).

Several other properties of the scattered intensity, including the spatial, temporal and spatio-temporal coherence functions have been measured for this system and the reader is referred to the literature for a full description of the experiments [16]. One interesting and important observation made was that close to the plume the intensity fluctuations were greater than log-normal (ie the higher moments were greater for a given second moment). At larger propagation distances a narrow region of log-normal behaviour was found but in the focussing peak region and beyond the intensity fluctuations were K-distributed. In a subsequent measurement of non-Gaussian stellar scintillation it was deduced on this basis that the observation was being made in a region preceding the focussing peak [17].

A number of measurements similar to the above have been made on mixing layers of hot and cold water and qualitatively similar results have been obtained. Strikingly different effects have been observed in the case of mixing layers of brine and water, possibly as a result of the smaller diffusion coefficient leading to smaller scale structures [18]. For example, the focussing curve in this latter system exhibited little or no peak despite the obvious strength of the scattering. Far field measurements indicate that geometrical optics effects are still important, however, and a sub-fractal model appears to give good agreement with data (Figure 10).

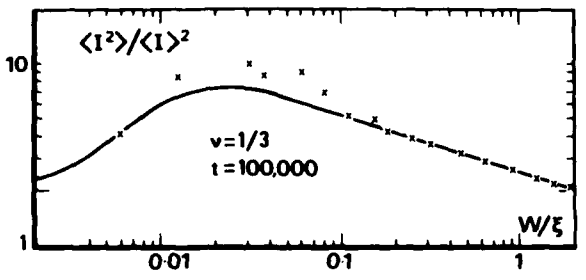

Fig 10 Brine/pure water mixing layer: comparison of far field data with theory

3 Rippled Water Surface Experiments

In these experiments a laser beam was propagated up through the surface of a wind-ruffled water surface [19]. The ripples so generated were typically less than 1 cm in size so that only the capillary wave spectrum was excited. The moments of the intensity fluctuation distribution were measured as a function of illuminated area for different "wind" strengths. Figure 11 shows a comparison of data with theoretical predictions based on joint-Gaussian phase statistics with Gaussian autocorrelation function. Good agreement is found showing that this scatterer is well described by a smoothly varying, single-scale model. The intensity fluctuations were not accurately K-distributed.

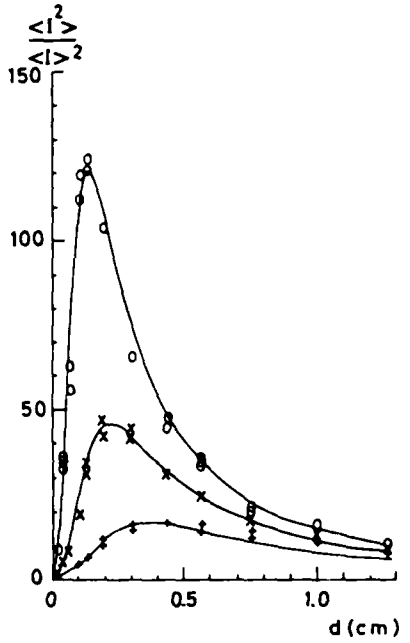

Fig 11 Far field scattering by a wind ruffled water surface: comparison of data with theory for various wind strengths

Experiments on Solid Diffusing Surfaces

1 Prepared Gaussian Diffusers

A number of experiments have been carried out in recent years on specially prepared and characterised diffusing surfaces. Figure 12 shows the focussing curve obtained with one such surface made by exposing photoresist to a super-position of many speckle patterns. Measurements showed that the resulting surface height was approximately Gaussian with Gaussian autocorrelation function [2]. Comparison with theory does not show perfect agreement, however. The intensity fluctuations were

not accurately K- distributed in any scattering regime.

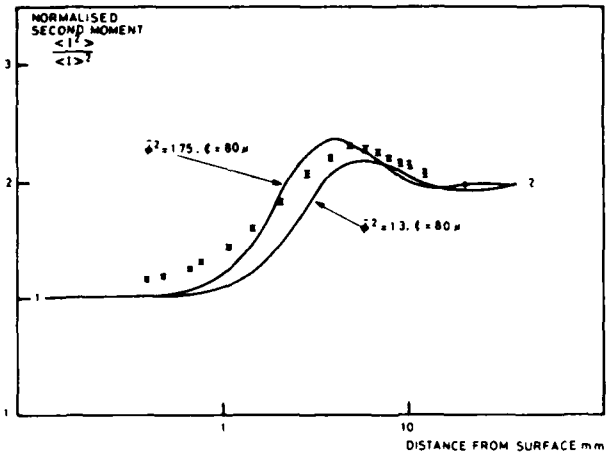

Fig 12 Scattering by a prepared Gaussian diffuser: comparison of theory with experimental data

2 IR Scattering from a Fractal Surface

Figure 13 shows the structure function for a randomly engraved Germanium surface measured using a "Talysurf" [20,21]. The power law

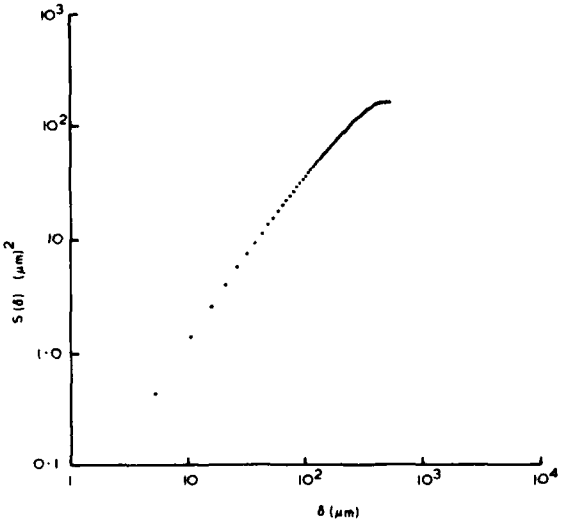

Fig 13 Structure function of a prepared fractal diffuser

dependence indicates a scaling behaviour over several decades and taken together with the observed Gaussian distribution of height differences suggests that this surface is fractal over almost three decades. The distribution of scattered intensity in the far field is very broad and in spite of height fluctuations of tens of microns only weak non-Gaussian peaks were observed in IR scattering experiments in both Fresnel and Fraunhofer configurations. Figure 14 shows a typical focussing curve exhibiting a peak only a little in excess of the Gaussian speckle value. Figure 15 shows the observed intensity pattern in the peak region of the Fresnel configuration visualised using a pyroelectric vidicon tube. Although the

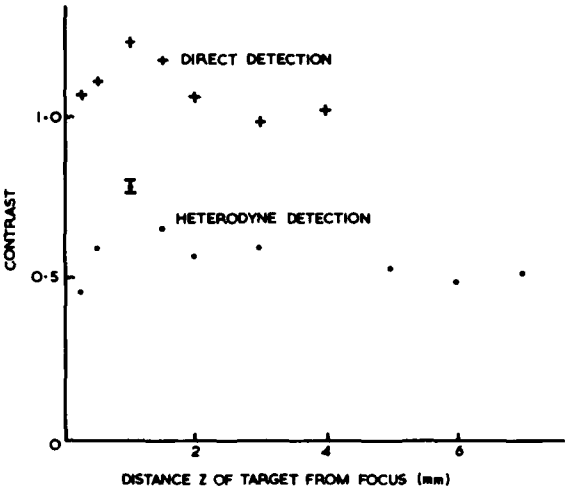

Fig 14 Focusing curves for a prepared fractal diffuser

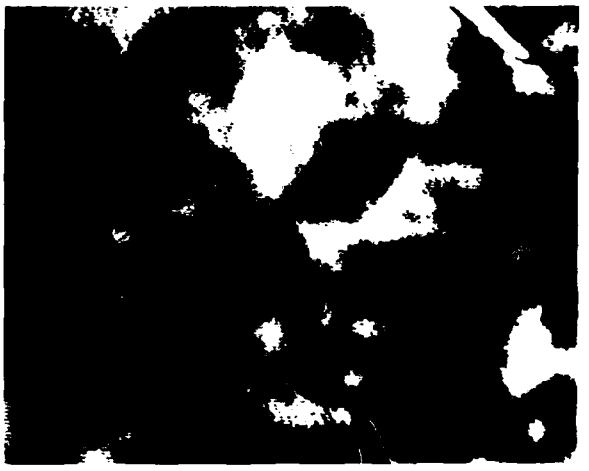

Fig 15 Prepared fractal diffuser: Non-Gaussian intensity pattern

picture quality is poor the pattern is evidently very different from those generated by "smoother" diffusers such as thermal plumes (Figure 9), showing little structure of the geometrical optics type.

Concluding Remarks

It is evident that optical frequency scattering experiments are playing an important role in advancing our understanding of non-Gaussian fluctuations in scattered waves. In particular the feedback of information between theory and experiments in which reliable and accurate statistical data can be acquired on laboratory systems operating in a controlled environment has led not only to the development of a widely applicable non-Gaussian noise model but also to a more general appreciation of the significance of the multiscale nature of many scattering systems. At a qualitative level, the visual appearance of a scattered intensity pattern can now be used to distinguish between smoothly varying and fractal scatterers. Solutions of Maxwell's equations for the appropriate model can then in principle be used to make quantitative comparisons with experimental data and thus obtain estimates of significant parameters characterising the scatterer. In practice a number of anomalies remain - for example, the observed strong geometrical optics features generated when waves are scattered by turbulent media which are usually considered to be describable in terms of the (fractal) Kolmogorov spectrum. Non-Gaussian optical scattering experiments on a well characterised turbulent system in which inner and outer scale effects are measured are thus a highly desirable objective for the future.

References

[1] Dainty, J.C. Ed. 1975 "Laser Speckle and Related Phenomena" Vol 9 of Topics in Applied Physics Springer-Verlag, Berlin.

[2] Jakeman, E. 1980 "Speckle statistics with a small number of scatterers" SPIE 243 9-19.

[3] Levine, B.M. and Dainty, J.C. 1983 "Non-Gaussian image plane speckle: measurements from diffusers of known statistics" Opt.Commun. 45 252-257.

[4] Chandley, P. and Escamilla, 1979 "Speckle from a rough surface when the illuminated region contains few correlation areas" Opt. Commun. 29 151-154.

[5] Ohtsubo, J. and Asakura, T. 1978 "Measurement of surface roughness properties using speckle patterns with non-Gaussian statistics" Opt. Commun. 25 315-319.

[6] Pusey, P.N. 1977 "Statistical properties of scattered radiation" in Photon Correlation spectroscopy and velocimetry ed by H.Z. Cummins and E.R. Pike, Plenum, New York.

[7] Jakeman, E. and Pusey, P.N. 1976 "A model for non-Rayleigh microwave sea echo" IEEE Trans Antennas Propag. AP-24 806-814.

[8] Jakeman, E. and Pusey, P.N. 1975 "Non-Gaussian fluctuations in electromagnetic radiation scattered by a random phase screen, I:theory" J.Phys.A 8 369-391.

[9] Pusey, P.N. and Jakeman, E. 1975 "Non-Gaussian fluctuations in electromagnetic radiation scattered by a random phase screen, II: Applications to dynamic light scattering in a liquid crystal" J.Phys.A 8 392-410.

[10] Jakeman, E. 1980 "On the statistics of K-distributed noise" J.Phys.A 13 31-48.

[11] Jakeman, E. and Pusey, P.N. 1978 "Significance of K-distributions in scattering experiments" Phys.Rev.Letts 40 546-550.

[12] Jakeman, E. 1982 "Fresnel scattering by a corrugated random surface with fractal slope" J.Opt.Soc.Am. 72 1034-1041.

[13] Parry, G. Pusey, P.N. Jakeman, E. and McWhirter,J.G. 1977 "Focussing by a random phase screen" Opt.Commun. 22 195-201.

[14] Jakeman, E. and McWhirter, J.G. 1981 "Non-Gaussian scattering by a random phase screen" Appl.Phys. 1326 125-131.

[15] Jakeman, E. and Jefferson, J.H. 1984 "Scintillation in the Fresnel region behind a sub-fractal diffuser" Optica.Acta 31 853-865.

[16] Parry, G. Pusey, P.N. Jakeman, E. and McWhirter,J.G. 1978 "The statistical and correlation properties of light scattered by a random phase screen" Coherence and Quantum Optics- IV. Eds L.Mandel and E.Wolf, Plenum, New York.

[17] Jakeman, E. Parry, G. Pike, E.R. and Pusey, P.N. 1978 "The twinkling of stars" Contemp.Phys. 19 127-145.

[18] Walker, J.G. and Jakeman, E. 1984 "Observation of sub-fractal behaviour in a light scattering system" Optica Acta 31 1185-1196.

[19] Walker, J.G. and Jakeman, E. 1982 "Non-Gaussian light scattering by a ruffled water surface" Optica Acta 29 313-324.

[20] Jordan, D.L. Hollins, R.C. and Jakeman, E. 1983 "Experimental measurements of non-Gaussian scattering by a fractal diffuser" Appl.Phys. B31 179-186.

[21] Jordan, D.L. Hollins, R.C. and Jakeman, E. 1984 "Infra-red scattering by a fractal diffuser" Optics Commun. 44 1-5.

The Author

Eric Jakeman graduated in mathematical physics at Birmingham University in 1960 and obtained his PhD on Superconductivity theory in 1963. After a year researching low energy nuclear physics at the University of California, Los Angeles, he joined RRE in 1964. He developed a strong interest in photon counting statistics, and also heat and mass transfer problems in crystal growth. Since the mid seventies his principal area of work has been the statistical analysis of propagation and non-Gaussian scattering problems. His work in statistical optics was recognised in 1977 when he was awarded the Institute of Physics' Maxwell Medal and Prize and he was a member of the team who received the McRobert Award for the development of the Malvern Correlator. He is a Fellow of the Institute of Physics and Vice Chairman of its Optical Group.

TUNABLE LASERS

M J P Payne, R C Hollins, D L Jordan, H W Evans and N A Lowde

Tunability, or frequency agility, has not to date been a feature of any major UK military laser system. Current systems, principally laser rangefinders and target designators, have little need of frequency diversity except as a means of overcoming jamming or similar countermeasures which have so far not proved militarily effective. Thus continued use has been made of the technically simpler, single wavelength lasers, using ruby or neodymium:YAG. New uses for lasers are now envisaged which require frequency diversity over quite large spectral widths (10% or more of the central frequency). Output energy, power and beam divergence requirements are similar to those of single frequency lasers generating beams for transmission over appreciable distances through the atmosphere, ie 100 mJ and more in energy and beam divergence of order one milliradian.

RSRE is addressing the science and technology of tunable lasers on a broad front. The range of applications and the number of known classes of possibly suitable tunable lasers renders it necessary to explore the potential for militarisation of a varied selection of lasers. The intra-mural programme includes research on tunable carbon dioxide lasers for the 10 micrometre spectral region, vibronic solid state lasers for the visible and near infrared, dye lasers and tunable excimer lasers. Extra-mural programmes support this work, for example in supplying materials for the vibronic laser research, but also serve to investigate other laser types and techniques perceived to be applicable in this area. Thus, contract work is in hand on Raman, dye, mercury halide, copper vapour and deuterium fluoride lasers. The techniques being pursued include the use of face pumped slab lasers and phase conjugate resonators, both of which offer improvements in output beam quality and pulse repetition rates. An important aspect of the extra-mural work is the study of the engineering and militarisation problems of the topics pursued.

Among the intra-mural research projects, the work on line tunable carbon dioxide lasers is furthest advanced. Previous RSRE work had demonstrated 30 Hz operation in a sealed-off CO_2 TEA laser. A solid catalyst was incorporated to prolong the gas life. This demonstration has been extended to line tunable operation by replacing the resonator total reflector with a diffraction grating. The grating is positioned by a computer controlled motor. This allows random selection, from shot to shot at 30 pulses/sec, of any of approximately fifty wavelengths in the range 9.2 to 10.9 micrometres, with pulse output energy greater than 40 mJ. Such operation is achieved with the use of 'ordinary' carbon dioxide, $^{12}C^{16}O_2$. Isotopic substitution of ^{13}C allows a considerable change in the accessible range of wavelengths. The possibilities have been partially demonstrated in the current equipment which, however, has characteristics not entirely compatible with the lower optical gain of the isotopic gas[1]. The design requirements of a laser employing $^{13}C^{16}O_2$ are somewhat clarified. The efficiency of the RSRE solid catalyst used with this gas has been proved.

The work programme on vibronic solid state lasers aims at the fabrication of tunable lasers based on transition metal ions. They will be similar in general form of construction and mode of operation to neodymium and ruby lasers. They will show output characteristics similar to those of lamp-pumped dye lasers but with the added possibility of Q-switched operation. Of the small number of materials at present known to possess good vibronic laser action, alexandrite and chromium:GSGG (gadolinium scandium gallium garnet) have been commercially exploited; the former material has demonstrated capability in high power lasers.

Work on vibronic lasers at RSRE is intended to assess the usefulness of known lasing materials and to discover new and improved ones. Among the known materials, large, laser quality crystals of chromium: GSGG have been grown in house and lamp-pumped operation has been demonstrated. Efficiency was initially very low, due to excited state absorption, colour centre

formation and thermal lensing, but matched that reported from Russian work[2]. Currently effort is being successfully devoted to efficiency improvement; continuous wave lasing has exhibited high differential efficiency[3]. Apart from laser operation, measurements have been made of the properties of a variety of candidate materials including crystals from in-house sources and glasses fabricated on a university contract. Present facilities include the measurement of absorption and fluorescence spectra and fluorescence decay. Variable temperature facilities are being added to aid, for example, the investigation of non-radiative decay processes. A capability for excited state absorption measurement will be established as soon as possible. Work to date has revealed no previously unknown good crystalline materials. Among the range of glasses available, the fluorescors showing greatest efficiency and suitable lifetimes have been identified with both copper (450 nm to 600 nm fluorescence) and chromium (650nm to 900nm) active species.

The search for new vibronic materials is hindered currently by the lack of a comprehensive set of criteria for guidance. For this reason two theoretical approaches to the prediction of materials properties are being pursued. The first is a derivation of some constraints on material parameters for efficient lasing based upon analysis of simple configuration co-ordinate diagrams. The second is a computation and analysis of the multi-dimensional configurational co-ordinate diagrams. This analysis is based on quantum mechanical principles and uses an X-alpha computational method.

Excimer laser research addresses the direct generation of broadly tunable and broad-bandwidth radiation. It is intended to demonstrate efficient discharge-pumped operation on visible laser transitions in rare gas halides. Species such as XeF and XeCl are well known as efficient ultraviolet laser media, and they are potentially also capable of laser action on wide bandwidth blue/green transitions. The blue/green C→A transition of XeF which competes with the familiar B→X transition at 350nm is a candidate for efficient laser action since the upper level is extremely efficiently formed under discharge conditions. Research centres around techniques of efficiently extracting the radiation from the low-gain transition. A high-pressure discharge laser has been designed and built, and initial measurements have been made in lower-pressure devices of the conditions under which a uniform discharge may be operated and the spontaneous fluorescence on the transitions maximised. Attempts at laser action are to follow.

Substantial progress has been made in studies of novel tuning configurations for pulsed dye lasers. A compact and efficient excimer laser-pumped device has been demonstrated which gives a simultaneous tunable output at three wavelengths widely spaced across the visible waveband. This laser provides spectral coverage over 120 nm of tuning range. Output energies of 10 mJ/pulse have been demonstrated, limited by the energy of the pump laser. Further studies will investigate configurations for overcoming inherent line-narrowing mechanisms in homogeneously-broadened dye lasers so as to achieve simultaneous directional output across the whole fluorescence bandwidth of a dye.

References

1. L I Freed, C Freed and R G O'Donnell, IEEE J Quantum Electron, QE-18 (8), 1229-36 (1982).

2. E V Zharikov et al., Sov J Quantum Electron, 13 (9), 1274-6 (1983).

3. B Struve and G Huber, J Appl Phys, 57 (1), 45-8 (1985).

The Authors

M J P Payne was born at Weymouth in 1940. He gained his BSc degree in Physics from Imperial College in 1962 and his PhD degree from the same college in 1966. He joined RSRE in 1967 and currently leads the work on tunable and solid state lasers.

R C Hollins was born in 1955 and joined RSRE in 1980 after completing his D Phil degree at Oxford University on studies of laser kinetics. His first research within MOD addressed the tuning and stabilisation of pulsed CO_2 lasers, and the scattering of radiation by fractal surfaces. He now works on tunable dye and excimer laser devices.

D L Jordan joined MOD in 1973 following research experience at Bristol and Liverpool Universities, and at GEC. He worked initially on electron gun design at SERL Baldock, and initiated studies of Leterodyne rangefinding techniques employing pulsed CO_2 transmitters on moving to RSRE Malvern in 1979. His research interests now include scattering of optical radiation, and tunable visible lasers.

H W Evans was born in Towyn in 1941. He was employed at RAE Aberporth before joining RSRE in 1966. He has worked on various types of lasers and rangefinders and is now chiefly concerned with tunable solid state lasers.

N A Lowde was born in London in 1928. After working with Nuvac and Mullard Research Labs, he joined RSRE in 1963. Following work on long life and tunable CO_2 lasers he is now engaged on the assessment of solid state laser materials.

A PYROELECTRIC LINEAR ARRAY INFRARED IMAGER

D E Burgess, P A Manning and R Watton

Two requirements for future IR systems have, during recent years, led to the growth of interest in uncooled thermal infrared detectors. These requirements are the freedom from cryogenic cooling, important if the sensor is to be used remotely for extended periods, and the need for inexpensive technologies for very large numbers of expendable sensors.

Whilst in general thermal infrared detectors using the pyroelectric effect have the first of the necessary attributes, room temperature operation, linear detector arrays in particular also have the other, low cost, since simple wire bonding techniques can be used to couple signals from the detectors into adjacent silicon circuitry. Linear detector arrays are particularly suitable for those applications where there is relative motion between the sensor head, containing the detector array, and the object to be imaged. Examples are intruder alarms, where movement in the scene must be sensed, and 'push broom' line scan where an aircraft platform pans the sensor in a continuous motion over the scene.

Pyroelectric linear arrays of up to 64 elements are now becoming available, and when mounted with good thermal isolation from their package they have a D* of 10^6 m $Hz^{\frac{1}{2}}$ W^{-1} in the 8 to 14 micron waveband at a few 10's of Hz readout rate (Ref 1). Translated into temperature sensitivity, this corresponds to a fraction of a degree NETD with f/1 optics. Performance above about 30 Hz falls with increasing sampling frequency, but the high sensitivity frequency decade from 10 to 100 Hz is just that range required for the intruder alarm and line scan applications mentioned above.

An imager has been built at RSRE to demonstrate the capabilities of pyroelectric linear detector arrays (Ref 2). The arrays, purchased from Plessey Research (Caswell) and based on the CVD funded VX9515 technology, have been coupled to minimal readout electronics to maintain the low cost aim. To this end, only a unity gain source follower FET connects the detector to the multiplexer, and the only filter to reduce aliassed noise is after the multiplexer. A focal plane chopper, synchronous with the multiplexer switching, enables stationary scenes to be observed; a digital image difference processor (IDP) subtracts the shuttered reference signal from the scene signal and completely removes fixed pattern noise.

Design

The overall sensor design is illustrated in figure 1. Infrared radiation is focussed on

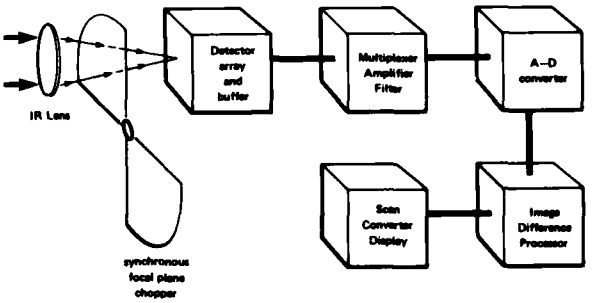

Fig 1 Overall schematic of pyroelectric linear array imager

to the detector array where it is periodically interrupted by a rotating chopper, synchronised to the readout electronics. An alternating voltage is produced from each detector element according to the radiation from the scene being viewed. Due to the small amplitude of these signals (typically 1 μV/K) and the large offsets (typically 2 volts) from the JFET source followers, even 12 bit A-D conversion and digital image processing is inadequate to give detector noise limited performance. The signals are therefore AC coupled at this point to remove the DC offsets. The multiplexed signal is amplified, band limited and digitised to 12 bits accuracy. The digital signals with chopper closed are subtracted from those with chopper-open, the result normalised, then outputted as 8 bit data words to a scan converter.

Results

The system sensitivity may be described in

terms of the noise equivalent temperature difference (NETD), which corresponds to that scene temperature difference producing an electrical signal equal to the r.m.s. of the electrical noise.

Table 1 presents results of signal response, measured NETD and predicted NETD based on the known detector and silicon parameters for three values of chopper frequency for a 20 element array. The agreement between theory and experiment is seen to be excellent.

Chopper frequency, Hz	20	30	50
Response, volts	0.16	0.10	0.07
Measured NETD, °C	0.07	0.12	0.16
Theoretical NETD, °C	0.067	0.11	0.16

Table 1. Detector sensitivity and measured and predicted NETD for 3 chopper frequencies.

A sample of imagery produced by the prototype sensor fitted with a 64 element array, using the vehicle's motion to produce the second image dimension, is shown in figure 2. This image was taken with a 25 mm f/1 lens and a chopper frequency of 30 Hz.

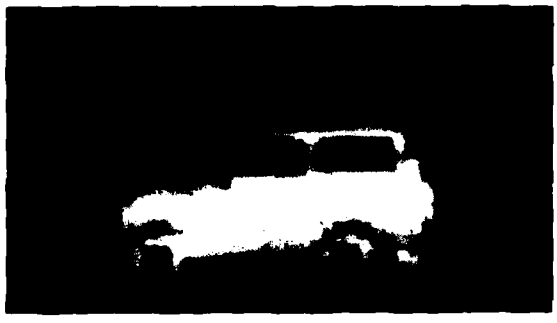

Fig 2 An example of imagery produced by the prototype equipment

Conclusion

A linear pyroelectric infrared detector array which has the attributes of room temperature operation and low cost required for future IR systems has been demonstrated in a prototype imager. Present work is investigating the use of uncommitted logic arrays and hybrid techniques to miniaturise the sensor head electronics. During 1985 the equipment will be trialled in the intruder detection and line scan roles described above.

References

1. Technologies and performance for linear and two dimensional pyroelectric arrays.
   Watton, Ainger, Porter, Pedder, Gooding. 28th SPIE Conf. Optics & Electro-Optics, 1984. paper 510-21.

2. Unpublished MOD data.

The Authors

Douglas Burgess and Rex Watton have worked on the development of Infrared Imagers, notably the Pyroelectric Vidicon Camera, for a number of years. Rex is responsible for research on new Detector Materials and Douglas is developing future low cost electro-optics. Paul Manning's responsibility is for the development of low noise preamplifier Electronics and Signal processing for Infrared sensors.

HIGH POWER FIBRE OPTIC LASER ANEMOMETRY

R G W Brown, D A Jackson, J D C Jones
and R K Y Chan

Introduction

The use of optical fibres in laser anemometer systems has become common, but cw laser powers of up to only a few tens of milliwatts have been used. However, for large scale flow facilities many watts of laser power may be necessary for adequate anemometer performance. To date, such facilities have employed conventional optical components on a grand scale. The potential ease of operation of a fibre optic solution is attractive, if the power handling and other properties of such fibres and necessary related components can be established.

Power Transmission Measurements in Monomode Optical Fibes

We have investigated the properties of a number of monomode fibres having both nominally circular and elliptical core cross-sections, with a wide range of design parameters and cut-off wavelengths. Power transmission, loss and back-scattering measurements have been made at two principal wavelengths: 488.0 and 514.5 nm. Of special interest in laser anemometry are polarisation-preserving fibres; for lack of space we describe here results from just one fibre of this kind: York Technology high-birefringence fibre, type HB 488/2, which is designed to operate at 488.0 nm, and has bow-tie [1] construction with an elliptical core cross-section of 4 x 5 microns. The core material is GeO_2 at 4 mol%. The fibre supports two orthogonal polarisation states (eigenstates) and propagates both 488.0 and 514.5 nm light monomodally.

Figure 1 shows the transmission characteristics of 90 and 10 m lengths of the HB 488/2 fibre. A Spectra Physics 165 argon ion laser was used without an etalon and in TEM_{00} mode. The observed saturation limit is <u>not</u> due to Stimulated Brillouin Scattering because of (i) the broad laser linewidth, and (ii) the observation of saturation in short fibres of lengths 10 m and 1 m (not shown). Cladding mode strippers were used at the input and output ends of the fibre; measurements of the optical power in the fibre cladding at these points showed linear and non-linear (saturation) transfer functions respectively, negating both the possibilities of higher order mode structure from the laser source with increased power output and intensity dependent refractive index change but pointing to an intensity dependent absorption process. Such a process might well be expected from the existence of GeO_2 in the core material and its known action as a colour centre. Research is in progress to understand the precise physical mechanism involved in this observation. Similar power limitations were discovered in other fibres, but it is possible that the absorption process could be removed by the use of - say - phosphorous as a dopant in the SiO_2 core, in place of GeO_2.

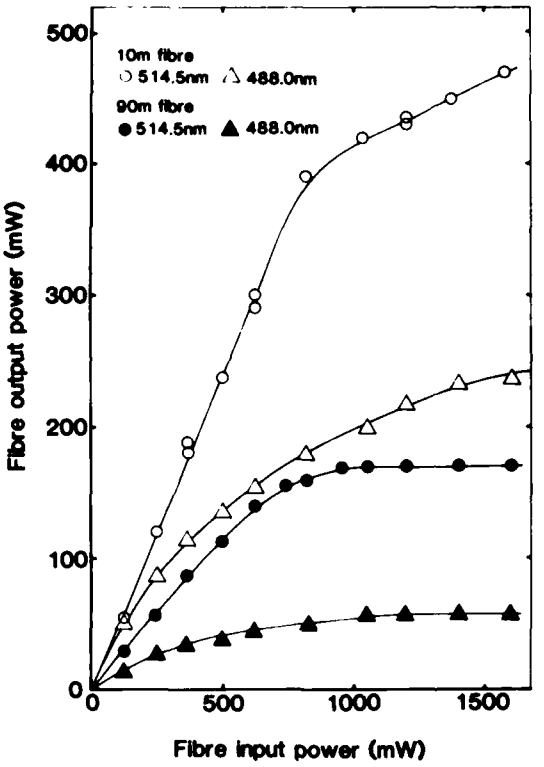

Fig 1 Power transmission curves for York HB488/2 high birefringence monomode fibre

The power limitations represent a serious problem for high power fibre laser anemometry, but a fibre optic laser Doppler anemometer (LDA) has been successfully

constructed capable of delivering 500 mW at 514.5 nm to the measurement volume [2]. The transmission optical system utilised a 10 m length of York Technology circular core fibre of design wavelength 633 nm, but which shows monomode performance at 514.5 nm. Similar experiments with Lightwave Technologies fibre were also conducted. In further experiments, beam division was achieved using a fibre directional coupler. This was fabricated from the York Technology circular core fibre using a twist-etch technique [3]. Using this component, the maximum optical power delivered to the measurement volume was 100 mW.

Necessary Considerations during High-Power Fibre Laser Anemometer Design

There are many potential hazards in the design and construction of a high power fibre laser anemometer:

(i) High power lasers often exhibit TEM_{01} "doughnut" mode output (in place of TEM_{00} desired) as the drive current is increased, reducing the efficiency with which power is coupled into a fibre as laser power output is increased.

(ii) Beam pointing stability of the laser is crucial to efficient and stable coupling of light into fibres. Furthermore, use of high laser power during alignment can physically damage a misaligned fibre.

(iii) Faraday isolation of the laser from the fibre may be needed to prevent feedback induced intensity fluctuations causing spurious results.

(iv) The maximum practical delivery power to a measurement volume using fibres is much less than with "bulk-optic" equivalent components, affecting anemometer data rate.

(v) Mismatch of the input polarisation plane to an eigenstate of polarising fibre with subsequent use of polarisation sensitive elements causes undesirable signal intensity fluctuations due to thermally induced polarisation changes within the fibre.

(vi) Elliptic cross-section LDA measurement volumes (created from elliptic core fibres) will yield irreversibly degraded velocity and turbulence estimates when only a few fringes are used.

(vii) Stimulated Brillouin scattering [4] (SBS) can limit power delivery to the measurement volume, but is reduced by removal of the laser etalon. SBS has been observed with only 80 mW of narrow-linewidth 5145 A^{o} light in 50 m of monomode SiO_2 core fibre of 20 dB km^{-1} loss.

(viii) Stimulated Raman scattering [4] (SRS) causes re-distribution of power between different wavelengths propagating in a fibre core, a potential problem in multi-colour/component LDA. SRS onsets if several watts of 0.5 micron wavelength light are launched into a few tens of metres of 20 dB km^{-1} loss, 4 micron core diamter fibre.

(ix) 3-wave mixing [5] occurs when the multi-longitudinal mode output of a laser containing no etalon used at high powers is launched into a suitable fibre. New frequencies are generated, beating between them could cause spurious LDA signals.

(x) Intensity dependent refractive index changes are possible in monomode fibres at moderate laser powers, causing loss of transmitted power to the cladding.

(xi) The intensity dependent absorption shown in our experimental results limits transmitted power in fibre cores containing colour centres (dopants) such as GeO_2. The effect is strongly wavelength dependent and difficult to predict. Fig 1 shows that it can limit power transmission to only 60 mW through a 90 m fibre at 4880 A^{o} wavelength.

Conclusions

Though potential hazards exist, many can be alleviated by judicious choice of lasers and fibre materials for high power fibre optic laser anemometry.

Monomode optical fibres capable of delivering hundreds of milliwatts of cw laser light over tens of metres to laser anemometer measuring regions will be developed in the near future. These will form the basis of a valuable new generation of multiplexable, miniaturised and relatively inexpensive laser anemometer optics.

Acknowledgements

We are grateful to Dr J M Vaughan of RSRE for assistance with spectroscopic measurements.

References

1 R D Birch, D N Payne, M P Varnham: Electron Letts, 18, (1982), 1036.

2 D A Jackson, J D C Jones, R K Y Chan: J Phys E, (1984), in press.

3 S K Sheem, T G Giallorenzi: Opt. Letts, 4, (1979), 29.

4 R H Stolen: in "Optical Fibre Telecommunications", S E Miller and A G Chynoweth, Academic Press (1970).

5 K O Hill, D C Johnson, B S Kawasaki, R I MacDonald: J Appl. Phys. 49, (1978), 5098.

The Authors

Robert Brown was born in 1953. He took a BSc in Physics and his PhD was concerned with photon correlation laser velocimetry. Early experience was gained with Marconi Ltd in infrared and LLTV systems analysis. He joined RSRE in 1977 to work on laser light scattering, primarily in laser velocimetry. He has authored over 35 papers (and some patent applications) in the areas of infrared systems design, photon correlation, laser velocimetry, biotechnology and fibre optics. Brown is a member of the IOP and OSA and an Organising Committee member of two 1985 National and International conferences.

D A Jackson, J D C Jones and R K Y Chan are staff members of the Physics Laboratory, University of Kent, Cantebury, Kent. This work is the result of an informal research collaboration.

HIGH SPATIAL RESOLUTION THERMAL IMAGERS

A P Campbell

Introduction

One of the aims of the UK Thermal Imaging Common Modules (TICM) stretch programme is to increase the performance of the Class II imager, TICM II, by improving its spatial resolution without degrading the thermal sensitivity or increasing the front aperture of the system. The horizontal spatial resolution of TICM II is determined primarily by the modulation transfer function (MTF) of the detector, Figure 1, and therefore, for maximum effectiveness, it is in the detector MTF that improvements must be made. Changes in the detector geometry could be, (and have been), used to improve the MTF, but improvements realised by such means are relatively small. Also, detectors are expensive so this route is inappropriate for the retrofit of existing imagers. However, substantial improvements in the effective detector MTF may be realised by the use of a new design of detector lens, [1], [2] offering a cheap retrofit option, as described below.

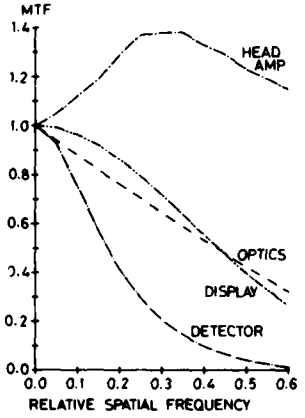

Fig 1 TICM II component MTFs

Effect of Anamorphic Detector Optics on Sprite Operation

The TICM II imager uses SPRITE (Signal Processing In The Element) detectors, (previously known as TEDs).[3] These consist of a filament of detector material along which the image is scanned. A bias voltage is applied to the filament and this causes the photogenerated carriers to drift along the filament to the readout at a speed matched to the scan speed, thereby achieving integration of the signal.

The MTF of a SPRITE detector is limited fundamentally by spatial averaging due to the finite size of the readout, and by the diffusive spread of the photogenerated carriers in the filament. The effects of both of these can be minimised by operating the detector at a longer focal length so that the image at the detector is magnified with respect to the diffusive spread and readout length. Whilst it would be possible to increase the focal length in both directions, vertical optical magnification is undesirable since it would necessitate a similar-fold increase in detector pitch to maintain the vertical field of view, without giving any increase in vertical resolution. Anamorphic optics, having a longer horizontal than vertical focal length, are therefore required. Horizontal scaling of the detector is not essential since use of the same length filament does not affect the field of view but merely reduces the integration time of the detector, leading to a slightly lower responsivity than would be obtained with a scaled detector. Figure 2 shows the calculated MTFs of a SPRITE detector operated with optics of various anamorphic ratios.

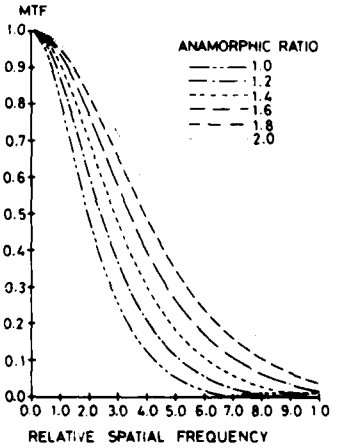

Fig 2 SPRITE detector MTF

The use of anamorphic optics of ratio R:1

has several effects on the operation of a SPRITE detector:

(i) the scan velocity increases by a factor R, so the bias voltage must be increased to raise the drift velocity by a similar factor. This increases the values of responsivity, noise voltage and detectivity. The increased bias current leads to a factor R^2 increase in the power dissipated in the detector (c.f. R^3 increase with horizontal scaling of the detector geometry, and R^4 increase with both horizontal and vertical scaling).

(ii) the increase in the horizontal cold shield f-number reduces the background photon flux falling on the detector. The ambipolar lifetime is consequently lengthened, while the ambipolar diffusion coefficient is reduced. The nett effect is to slightly increase the diffusion length. The longer lifetime and lower background photon flux result in a higher detectivity, providing the detectors remain background limited (which they should for anamorphic ratios of interest).

(iii) the increase in the horizontal cold shield f-number reduces the signal photon flux falling onto the detector. Thus, although the detectivity of the detector is increased as described in (i) and (ii) above, the actual signal to noise ratio at low spatial frequencies is very slightly reduced.

Thus, anamorphic detector optics enable a substantial improvement in horizontal detector MTF to be realised without requiring any detector geometry changes, and with a minimal loss in thermal sensitivity.

Incorporation of Anamorphic Optics in TICM II

Anamorphic detector optics have been designed for TICM II which are a form, fit and function retrofit to existing imagers. The only adjustment required is an increase in bias current, and this can be accomplished with the present bias supply circuits. The consequent increase in power dissipation is easily accommodated with the current detector and dewar combination.

Figure 3 shows a comparison of images taken using an imager with standard optics and an imager with anamorphic optics. This demonstrates the substantial improvement in spatial resolution that may be realised by a simple retrofit of anamorphic detector optics.

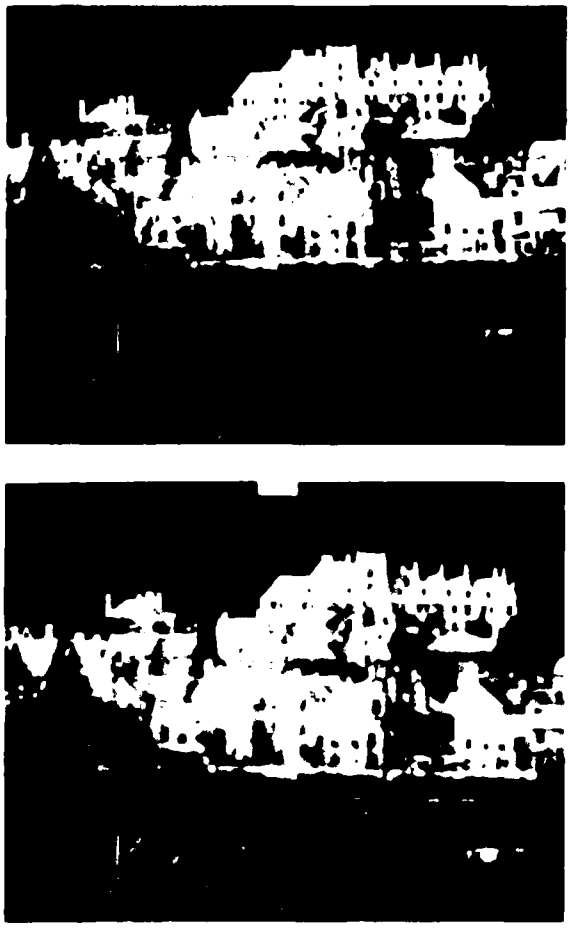

Fig 3 Comparison between anamorphic image (top) and standard image (bottom)
Note the Tower in the foreground

However, by making further adjustments to the imager, the performance may be improved still further. The anamorphic optics increase both the signal MTF and noise voltage spectrum, leading to aliasing errors and additional aliased noise. To fully realise the performance improvements possible with anamorphic optics, it is important that this aliasing be minimised by increasing the horizontal sampling rate and/or by the incorporation of anti-aliasing filters. Both of these modifications are currently being pursued.

Conclusion

A substantial improvement in the horizontal

spatial resolution of a TICM II imager can be achieved by the use of anamorphic detector optics, with minimal loss in thermal sensitivity. The new lenses are relatively cheap and are thus suitable for retrofitting to existing imagers. Future modifications to TICM II will permit the performance to be enhanced still further.

Acknowledgements

Acknowledgements are due to Rank Pullin Controls Ltd (Debden) for designing and making the anamorphic lenses, and to GEC Avionics Ltd (Basildon) for their incorporation in the imagers.

References

(1) C T Elliott. IEE 1st Int. Conf. on Advanced Infrared Detectors + Systems 1 (1981).

(2) A C Sleigh. IEE 1st Int. Conf. on Advanced Infrared Detectors + Systems 19 (1981).

(3) C T Elliott. Electronics Letters 17 312 (1981).

The Author

Ann Campbell graduated from Bristol University with a B.Sc (Hons) in Chemical Physics in 1976. After spending three years at Wilkinson Match Research Laboratories, she joined RSRE in 1979 and has since worked on thermal imager research.

SOLID STATE PHYSICS AND DISPLAYS

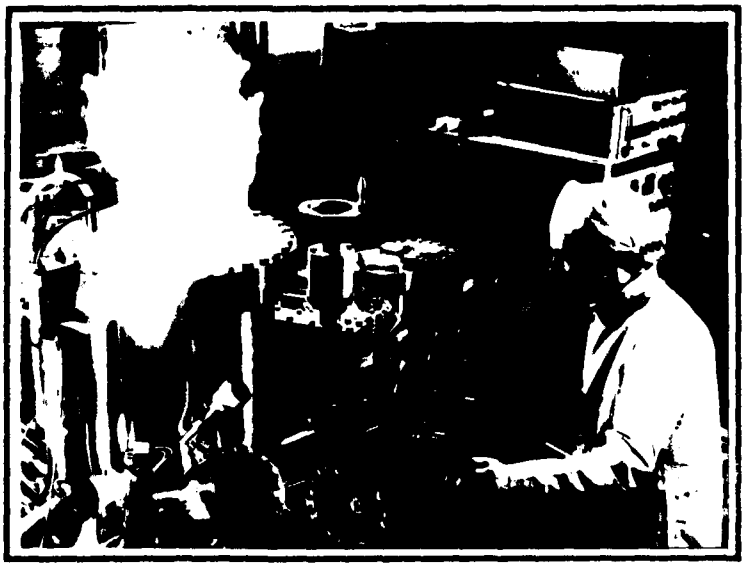

IDENTIFICATION OF IMPURITIES AND DEFECTS IN SEMICONDUCTORS BY OPTICAL SPECTROSCOPY

M S Skolnick

Abstract

A review is given of the information that can be obtained on defect centres in semiconductors by optical spectroscopy. Particular emphasis is given to donor and acceptor identification, and symmetry determination of transition metal and axial defect-complex centres. The information that can be obtained from isotope doping effects is discussed.

Introduction

Optical spectroscopy is a very widely employed technique for characterisation of the electronic properties of semiconductor materials. In the present paper, attention will be concentrated on several specific examples from the fields of photoluminescence (PL) and far infrared photoconductivity (FIRPC). These are chosen to demonstrate the type of detailed information that can be obtained as to the specific nature of defect centres and of their local symmetry environments. In the context of this discussion the term defect is taken to imply any chemical contaminant or native defect which introduces an observable optical transition in the material.

In the field of luminescence spectroscopy, specific identifications of impurity related recombination centres are normally obtained by means of careful back-doping of high purity materials. This is particularly true of the shallow donor and acceptor impurities which give rise to prominent near band edge luminescence lines. The specific chemical information is observed in the low energy satellites, termed two electron or two hole replicas[1], of the shallow donor or acceptor bound exciton lines [2]. Similar information on shallow impurities can be obtained from far infrared photoconductivity (FIRPC) experiments [3], where the internal excitations of the hydrogenic-like centres are observed directly. The two techniques of PL and FIRPC will be discussed and contrasted in section 2. Mention will also be made of the study of donor-acceptor pair transitions for acceptor identification.

Deduction of the actual symmetry of the centre giving rise to a PL or optical absorption spectrum can usually only be obtained in a reliable way by the application of an external perturbation to the sample. The most commonly employed techniques are those of magnetic field and uniaxial stress. In addition to the symmetry information, the angular momentum and spin quantum numbers of the states involved in the optical transition are also obtained. The use of such perturbation spectroscopy will be demonstrated by examples from the study of crystal field transitions of 3d-transition metal impurities in III-V semiconductors. It will be shown that the symmetry, and equally importantly the charge state of the centre, can be reliably deduced from such investigations, whereas simple examination of the form of the spectrum can lead to mistaken identifications.

In the absence of information from deliberate doping studies, specific chemical attributions can still be obtained if isotope shifts in the optical spectra are observable. This is obviously restricted to those elements which have different isotopes, and can be employed to most effect for light elements (eg B, Li, C, O) where the change in mass between the isotopes is most significant. In the present paper, examples will be taken from PL spectroscopy where specific identifications are obtained from the observation of isotope shifts in zero-phonon lines and their local phonon replicas.

One important point should be emphasised before closing the introductory section. This concerns the importance of optical spectroscopy in obtaining an understanding of those centres which control the electrical properties of semiconductor materials. For the case of shallow centers in sufficiently pure materials the nature of the dominant impurities and the relative concentrations of, for example, different acceptor species can be obtained from PL investigations. However, the technique is normally not quantitative, except in the case of Si where the detailed calibration

work of Tajima has enabled donor and acceptor concentrations to be deduced from study of the relative intensities of free and bound exciton recombination lines [4]. All the examples mentioned so far relate to cases where the phonon coupling of the centre is relatively weak, and where sharp zero phonon lines are observable. In cases of strong phonon coupling where the PL spectrum is a difficult to interpret broad band, techniques such as optically detected magnetic resonance (ODMR) and related methods can be employed to obtain detailed information as to the nature of the center involved in an optical transition.

The paper is organised in the following way. In the next section donor and acceptor identification by PL and FIRPC is discussed. This is followed by examples of the study of transition metal and axial defect centres by Zeeman and piezo-spectroscopy. Then the detailed information obtained from isotope doping effects is discussed, and finally the contents of the paper are summarised.

Identification of Shallow Donor and Acceptor Centers

The use of PL and FIRPC to identify shallow donor and acceptor impurities will be discussed in this section. The specific examples will be taken from the direct gap III-V materials InP and GaAs, (E_g = 1.424 eV and 1.519 eV respectively at 2K). Very large amounts of work have also been carried out on Si, Ge, GaP and II-VI materials such as CdS, ZnTe, ZnSe, CdTe, etc, but the basic principles of the techniques employed are the same for the different semiconductors.

i) Shallow-Donors

Identification of shallow donors is obtained by observation of the central cell corrections (chemical shifts) of the 1s ground state of the effective mass-like donors which vary with the chemical nature of the impurity. The effective mass binding energies of donors in InP and GaAs are rather small (7.3 meV and 5.7 meV respectively [5] and because of the large Bohr radii ($\sim$100 Å) of the 1s ground state wavefunctions the variations of the donor binding energies with the chemical nature of the donor are only of the order of 0.4 and 0.2 meV for the two materials respectively [6],[7]. This necessitates spectral linewidths of 0.05 meV or better in order to obtain donor discrimination.

The central cell corrections are observed by PL spectroscopy from study of the "two electron satellites" $(D^o,X)'$ of the neutral donor bound exciton transitions (D^o,X). In the (D^o,X) transition the bound exciton recombines leaving the donor in its 1s ground state, whereas in the $(D^o,X)'$ transition the donor is left in a 2s or 2p hydrogenic excited state. The energy difference between (D^o,X) and $(D^o,X)'$ is thus the 1s-2s,p energy separation of the neutral donor. The (D^o,X) recombination energy is only weakly sensitive to the nature of the binding center, but the full chemical shift is observed on the $(D^o,X)'$ satellites. The 2p state has no chemical shift since its wavefunction has a node at the impurity, and the 2s shift is 1/8 of that of the 1s state.

Chemical shifts on the (D^o,X) satellites have just been resolved at zero magnetic field in very high purity GaAs by Almassy et al [8] but this has never been achieved in InP, since the spectral linewidths ($\sim$0.1 meV in the best material) are of the order of, or greater than the central cell corrections. Great improvements are obtained in both materials by the application of magnetic fields of greater than $\sim$ 4 Tesla [9],[10]. The principal result of this is a reduction in linewidth by about a factor of four from 0.1 to 0.025 meV between 0 and 10T in InP [9]. This great improvement is due to a shrinkage of the donor wavefunctions in magnetic field which leads to a reduction of the dominant Stark effect broadening of the donor energy levels [11]. There is also an increase of central cell corrections with magnetic field, again due to the shrinkage of the donor wavefunction. However, this effect ($\sim$15% in InP at 10T) is less important than the line narrowing.

An example of well resolved central cell structure for InP in the $(D^o,X)'$ region is shown in Figure 1, for a high purity sample grown by the In-PCl_3H-$_2$ vapour phase epitaxy (vpe) process. Two electron satellites due to S and Si (labelled 1 and 2 on the figure) donors are observed. The identifications are obtained from back-doping of similar high purity material. The

improvement of the quality of the spectra with magnetic field is so great that central cell structure can be observed in material with $N_D+N_A \sim 5 \times 10^{15}$ cm^{-3}, where the $(D^o,X)'$ satellites are not even visible at zero magnetic field, as in crystals of Liquid-Encapsulated-Czochralski (LEC) InP[6]. The residual donors in vpe, LEC, metal-organic vpe and liquid phase epitaxial (lpe) InP have been obtained from such studies[6],[9],[12]. Similar information from PL studies in magnetic field has been reported for GaAs by Reynolds and co-workers[10].

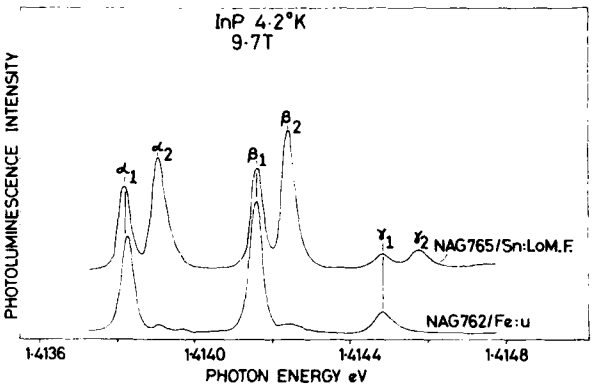

Fig 1 Donor identification in InP

Donor identifications in these direct gap materials can also be obtained by FIRPC studies of the 1s-2s,p transitions in magnetic field. In fact the FIRPC investigations for GaAs[3] predate those by PL by about 10 years. The observation of 1s-2s,p transitions in photoconductivity depends on the photothermal ionisation mechanism whereby the electron is thermally ionised to the conduction band following photo-excitation to the n=2 state[3]. As with the PL work, application of magnetic field is necessary to obtain well resolved central cell structure.

The two techniques of PL and FIRPC provide complementary information on donor identifications. Their relative merits have been compared in recent publications[9],[13]. One of the principal differences is that PL studies the ~ 1 μm surface region, as determined by the diffusion length of excitons created by the exciting laser beam, whereas the FIRPC signal arises from the whole thickness of the epitaxial layer. Spectra obtained from similar InP samples by PL and FIRPC are compared in Figures 2 and 3.

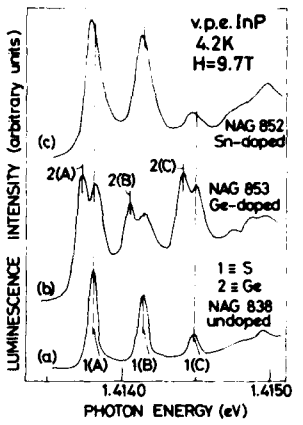

Fig 2 Ge and Sn doped InP

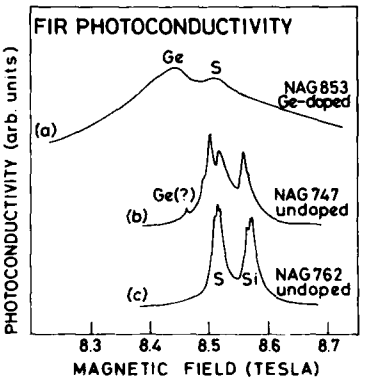

Fig 3 FIRPC of InP

The problem of donor identification is much less severe in wider direct gap and indirect band gap materials, where donor binding energies and the corresponding chemical shifts are significantly larger. In these cases (eg in CdS, ZnTe, ZnSe, GaP, Si, Ge, etc) central cell structure can be easily resolved without the application of external magnetic fields in both PL and FIRPC.

Marked improvement in the resolution of the "two electron" satellites can be achieved by excitation with a narrow laser line within the inhomogeneous linewidth of the (D^o,X) transitions. So long as diffusion of the excitation between donor sites does not occur before recombination, then significant narrowing of the $(D^oX)'$ satellites is obtained. This can lead to donor identification in materials of lower purity, without the application of magnetic field. This has been clearly demonstrated for the

II-VI materials ZnTe and ZnSe[14],[15] and in GaAs[16]. However, this technique was not successful in InP where the larger extent of the donor wavefunctions and the insufficient purity available leads to diffusion of the excitation between donor sites, and the loss of any potential line narrowing[17].

ii) Shallow-Acceptors

The general techniques for spectroscopic shallow acceptor identification are analogous to those already described for shallow donors. Central cell structure on the "two hole" satellites $(A^o,X)'$, where an exciton bound to a shallow acceptor recombines, leaving the acceptor in a $2s_{3/2}$ excited state, is observed in PL, whereas the $1s\text{-}2p_{3/2,5/2}$ acceptor state transitions are detected in FIRPC.

In GaAs and InP (and the other materials discussed previously) the central cell structure can be resolved without the application of magnetic field, since the acceptor effective binding energies are 27.0 and ~40.0 meV respectively, with central cell corrections in the range 0 to ~60 meV for the relatively shallow centres[5]. The intensity of the $(A^o,X)'$ satellites is strongly enhanced by resonant excitation into the principal acceptor bound exciton line [18]. This greatly enhances the utility of the technique in material with $N_D + N_A \sim 10^{15}$ cm^{-3} where the $(A^o,X)'$ satellites are not otherwise observable[18]. In such cases the donor-acceptor pair (DAP) transitions are commonly used for acceptor identification, but with a great loss in precision, due to the large linewidth of the DAP lines (~3 meV), as compared to 0.1 meV for the "two hole" satellites[19].

Symmetry information on the acceptor centre can be obtained from magnetic field studies. Most common acceptors are demonstrated by investigation of acceptor bound exciton lines in magnetic field to have the T_d symmetry expected for substitutional impurities. If the acceptor arises from an axial complex this is clearly shown by the anisotropic Zeeman splittings, as demonstrated for axial acceptors in eg ZnTe and GaP[20]. Similar work has been carried out for a deep axial donor in GaAs[21]. In cases where the axial field is very large, the valence band degeneracy itself is lifted, as exemplified by studies of excitons bound to Cu-related acceptor complex in GaAs[23],[24].

Identification of 3d-Transition Metal Centres

As for the shallow centres in the previous section, there is a very large literature on the investigation of 3d-transition metal ions. Specific examples will be taken from the III-V semiconductors, to demonstrate the sort of detailed information that can be obtained on the nature of transition metal centres. Transition metals normally give rise to deep levels in semiconductors, the two most technologically important cases probably being Fe in InP and Cr in GaAs which lead to mid-gap levels, and are employed in the manufacture of semi-insulating material. At the end of this section, investigation of radiation damage induced centres in Si will be mentioned briefly, as another class of deep centre studied by optical spectroscopy.

3d-transition metals give rise to very characteristic PL or optical absorption spectra, typically composed of sharp zero phonon lines, followed by a series of phonon sidebands to lower energy, as shown in Figures 4 and 5 for two well-studied cases of PL in GaAs:Cr[26],[27] and InP:V[28],[29]. The transitions occur between the localised energy levels of transition metal ions split by the crystal field of the host semiconductors. Identification of the symmetries of the centres, and deduction of the initial and final states of the transitions are

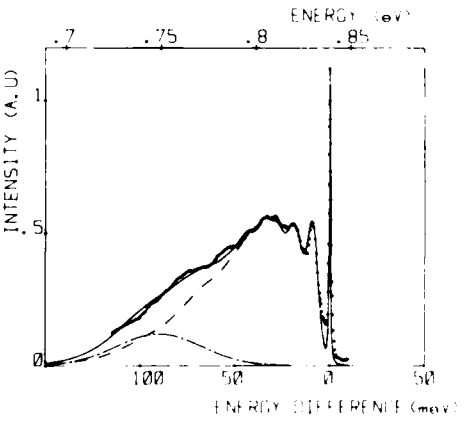

Fig 4 PL(4K) for Cr in GaAs

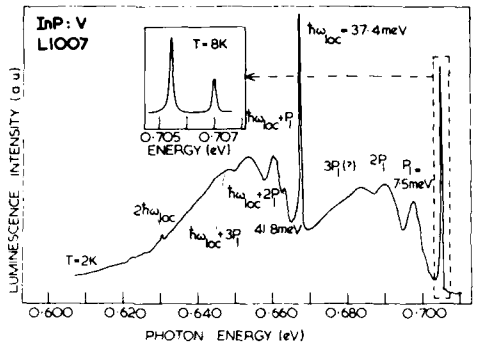

Fig 5 PL spectrum (2K) of V^{3+}_{In} in InP

difficult to achieve with any reliability simply by inspection of the form of the unperturbed spectrum.

The first example of Zeeman perturbation spectroscopy is that of the 839 meV zero phonon line which dominates the PL of Cr doped GaAs (see Figure 4). This PL spectrum was originally attributed to the ^5E-$^5T_2$ transition of Cr^{2+} substituting on the Ga site. White[30] and Picoli et al[31] suggested from a detailed examination of the structure of the zero phonon line that the recombination actually arose from a trigonal complex involving Cr. This was confirmed by the magnetic field investigations of Eaves and Uihlein[31],[32] and Killoran et al[33] (who deduced a slight distortion away from trigonal). The magnetic field anisotropy at 10T obtained by Eaves et al is shown in Figure 6. The most important point for the present discussion is that the C_{3V} (trigonal symmetry, <111> axes) of the centre is immediately apparent. The major splittings shown in Figure 6 arise from the lifting of orientational degeneracy of the <111> axial

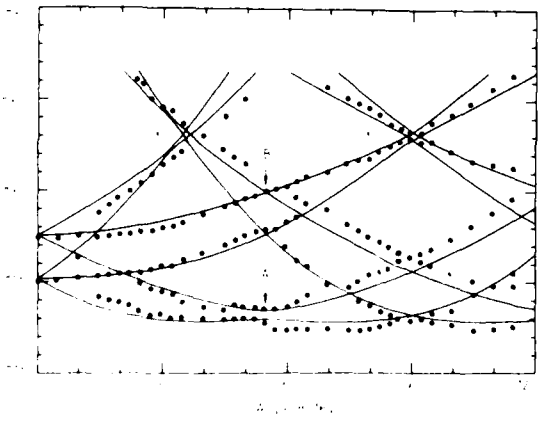

Fig 6 Anisotropy of Cr-X PL in GaAs

defects. For H ∥ [001] all the centers are equivalent, and so the Zeeman splittings are equal for this direction, as observed in Figure 6.

The symmetry of the centre is immediately deduced from such an anisotropy plot, for rotation of the magnetic field in the (110) plane. A detailed fitting of the magnetic field and angular dependences has led to the identification of the transition as the ^5E-$^5T_2$ transition of Cr^{2+} in trigonal symmetry, but there is still some dispute as to the relative magnitudes of the trigonal field perturbation and vibronic interactions[31],[32],[34]. The actual microscopic nature of the trigonal complex is not obtained from these experiments, except for the conclusion that Cr_{Ga} forms one member of what may be a defect pair, with the other component on the As sublattice. There has been much speculation in the literature as to the actual nature of thecentre with Cr-V_{As} (arsenic vacancy) or Cr-O the most likely possibilities[35],[36]. The observation of PL from Cr-Te_{As} pairs[38] at 844 meV indicates that the second member of the complex is probably a donor on the As lattice site. This example demonstrates one of the shortcomings of Zeeman or piezospectroscopic investigations of defect centres. The symmetry and the electronic nature of the transition are clearly determined, but full chemical information on the constituents of the centre may not always be obtained, in the absence of information from direct doping experiments. Finally, it should be noted that although the axial complex dominates the PL of GaAs:Cr, it is believed to contain <10% of the Cr in the crystal[35], the majority of the Cr being present as isolated Cr_{Ga}. The ^5E-$^5T_2$ transition of isolated Cr^{2+} has been observed in optical absorption[37] and very recently in PL using 1.2 eV laser excitation[38].

Such uncertainties do not exist for the second example discussed, in which the crystal field levels of vanadium in InP are investigated by Zeeman and piezo-spectroscopy. The zero phonon line at 704.5 meV and its accompanying phonon sidebands are shown in Figure 5[27],[39]. Similar spectra for GaAs and GaP had previously been interpreted as arising from the V^{2+} charge state[40],[41].

Zeeman spectroscopy unambiguously demonstrates that the spectrum arises from the $^3T_2$-$^3A_2$ transition of V^{3+}. The magnetic field splittings for the three principal crystallographic directions are shown in Figure 7. The three fold splitting seen most clearly for H ∥ [111] in Figure 7b with g = 1.95 arises from the lifting of the spin degeneracy of the orbital singlet, spin triplet (S=1) ground state. The only charge state of vanadium with spin of 1 is V^{3+} which has two electrons in the d-shell.

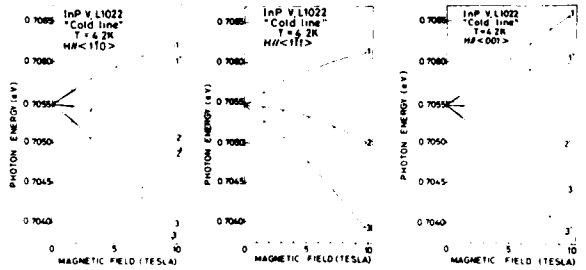

Fig 7 Zeeman splittings for V^{3+} in InP

Thus, the charge state of the centre involved in the transition is obtained in a very simple, direct way. The anisotropy of the Zeeman spectrum for rotation of the field in the (110) plane is shown in Figure 8. In this case a tetragonal anisotropy (D_{2d}) is observed, which arises from Jahn-Teller coupling of the $^3T_2$ excited state to distortion modes. A very good fitting to

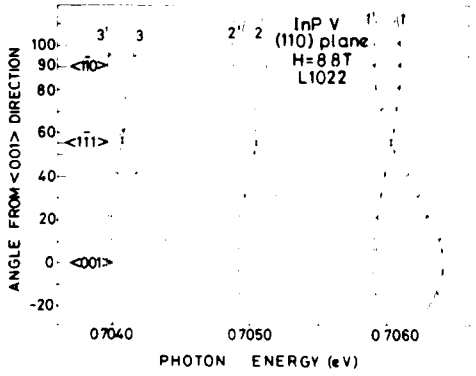

Fig 8 Zeeman anisotropy for V_{In}^{3+} in InP

all details of the magnetic field behaviour is obtained with a simple spin Hamiltonian for the excited state of the form

$$H = DS_z^2 + g\mu_B \underline{H}.\underline{S}$$

with S=1, where the DS_z^2 term gives rise to second order spin orbit splitting at a centre where the symmetry is lowered by the tetragonal Jahn-Teller distortion in the $^3T_2$ state. Further details can be found in [29].

The existence of the tetragonal distortion in the $^3T_2$ state has been confirmed by the uniaxial stress investigations of Nash et al[42]. The next crystal field transition to higher energy of V^{3+}, expected to be $^3A_2$-$^3T_1$ has been observed in PL excitation of the 705.5 meV band[39],[29],[42] and with higher resolution in optical absorption by Clerjaud et al[43]. It shows a zero phonon line at 993 meV. Nash et al studied this line together with the 705.5 meV PL line in their piezo-spectroscopic investigations. They found that the 993 meV line exhibited trigonal symmetry, which they attributed to Jahn-Teller coupling to τ_2 modes in the $^3T_1$ state. The observation of different symmetries for the $^3T_2$ and $^3T_1$ states of what is almost certainly the same centre (since one is observed in the PL excitation spectrum of the other), demonstrates that the symmetry lowerings arise from Jahn-Teller coupling to ϵ and τ_2 modes, for the $^3T_2$ and $^3T_1$ states respectively. If only one of the states had been studied the possibility that the lowered symmetry arose from an axial complex would have remained. Thus it is concluded with confidence that the transitions occur at an isolated V centre. The observation of the 3+ charge state (d^2), whereas the free atom has the $3d^34s^2$ configuration, implies that the vanadium must substitute on the In sublattice, with three electrons being given up to satisfy the bonding requirements for the substituted In atom. The other lattice position (apart from the P anion site) which could have T_d symmetry and where transition metals are observed (in Si[44] although not as yet conclusively in III-V materials) is the tetrahedral interstitial position. However, this possibility can be excluded since the d^4 or d^5 configuration would be expected in this case, as opposed to d^2 as actually observed. Similar arguments can be applied to substitution on the P site.

This case has been discussed in some detail since it provides a good example of the microscopic defect information which can be obtained from perturbation spectroscopy. The charge state, electronic configuration and lattice site of the defect are deduced from the Zeeman and piezo-spectroscopic

investigations. The same conclusions apply to vanadium in GaAs and GaP. Similar investigations have been carried out for a number of other transition metal systems eg GaP:Co, Ni (see Kaufmann and Schneider[45] and Clerjaud[46] for comprehensive reviews of transition metals in the III-V materials).

Excitons Bound to Isoelectronic Axial Defects

Low symmetry defect centres which are neutral relative to the surrounding lattice can often give rise to very prominent PL recombination bands. Such "isoloectronic" centres can bind an exciton, where one of the particles in the complex is bound by short range forces, and the second particle in the exciton is then bound in the Coulomb field of the first particle. This is the Hopfield-Thomas-Lynch model[47] for binding at isoelectronic centres.

In this section very brief mention is made of the symmetry information which can be obtained from Zeeman or piezo-spectroscopic investigations of exciton recombination at such neutral, axial centres. Additional microscopic information on such defects is obtained by observation of isotope effects (see section 5).

Most of the early work was carried out in GaP, the best known example probably being the Cd-O isoelectronic centre[48]. Zeeman spectroscopy conclusively demonstrated that the defect had C_{3V} axial symmetry, as expected for nearest neighbour substituents on opposite sublattice[49]. Similar studies have also been performed on Li-Li-O[50] and B-N[51] defects in GaP. The Zeeman anisotropy plot for the Li-Li-O centre, for rotation of the field in the (110) plane is shown in Figure 9. The splitting at [111] is due to lifting of spin degeneracy, whereas the extra splittings away from this direction arise from lifting of orientational degeneracy for the C_{3V} trigonal centers. In all these cases the valence band degeneracy is lifted by the axial field, with an $m_j = \pm 3/2$ state resulting at highest energy. It is the magnetic anisotropy of this state which is detected in the Zeeman effect. The initial state of the transition is the bound exciton, comprising just one electron and one hole, whilst the final state is the neutral binding centre, which shows no magnetic splittings. If on the other hand the $m_j = \pm\frac{1}{2}$ hole state lies uppermost, corresponding to quenching of the hole orbital angular momentum, then the hole g-value is close to 2, and the Zeeman spectrum is almost isotropic. If this is the case, as for several Cu-related centers in GaP then more sensitive ODMR techniques must be used to obtain symmetry information[52].

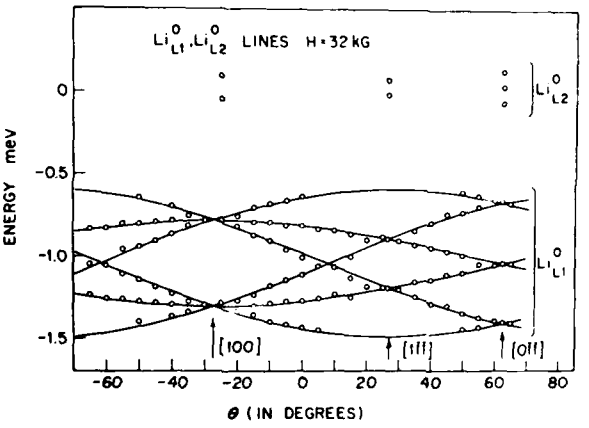

Fig 9 Zeeman anisotropy for Li-Li-O in GaP

Low symmetry radiation damage centres in Si have also been the subject of detailed Zeeman and piezo-spectroscopic studies in recent years[53],[54],[55]. These deep centres normally give rise to sharp zero phonon lines in PL and richly structured phonon sidebands to lower energy. Many of the bands have been shown to arise from singlet or triplet exciton recombination[56] at low symmetry, isoelectronic complexes. For details of the perturbation spectroscopy, and the methods of symmetry deduction, see references [53]-[55]. As for the GaP centres, great use has been made of studies of isotope effects to obtain more detailed information on the microscopic structure of the defects.

Identification from Isotope Effects

In this section the deduction of the constituents of defect centres from the observation of isotope shifts in optical spectra will be discussed. Isotope shifts can be observed in zero phonon lines and in local mode phonon replicas of electronic transitions. The study of local mode phenomena by direct infrared (local mode) absorption has been discussed in detail by

Newman.[57]

Isotope shifts in the energies of zero phonon lines (ZPL) can arise if there is a difference in the energy of the zero point motion in the initial and final vibronic (electronic plus vibrational) states of the transition. The shift in energy of a local mode phonon due to the change in mass ΔM between isotopes is given by

$$\Delta(\hbar\omega) = -F\left(\frac{\hbar\omega}{2}\right)\left(\frac{\Delta M}{M}\right)$$

in a simple harmonic oscillator approximation, where ω is the local phonon energy, and F is the fraction of the kinetic energy of the mode associated with motion of the ion mass M.

Both ZPL and local mode isotope shifts are observed for the Li-Li-O center[50]. There is a 0.80 meV shift of the ZPL to higher energy on O^{16} to O^{18} substitution. This is close to the isotope shift (0.72 mev[58] observed for $O_P^{\ o}$ and provides evidence for the participation of O on the phosphorus site in the defect. Doping with mixed Li^6, Li^7 isotopes gives rise to two extra local mode satellites as compared to Li^6 or Li^7 separately, demonstrating that the defect contains at least two inequivalent Li atoms. These observations lead to the model of Li_{Ga}-$Li_{interstitial}$-O_P for the defect, which is consistent with the requirement that the center should be isoelectronic with the Ga, P atoms replaced, and also has the overall trigonal symmetry found in the Zeeman studies[50].

A similar study has been performed for the Li saturated vacancy in Si, a four Li atom complex produced by electron irradiation of Li doped Si[59,60]. Zeeman and piezo-spectroscopy have shown that the PL band of Figure 10 arises from exciton recombination at an isoelectronic center with trigonal symmetry[54]. The effects of isotope doping (Li^6, Li^7 in the ratio 1.34:1) on two lines in the region are shown in Figure 11. Canham et al were able to fit the relative intensities of the five main groups of lines in Figure 11 to the five possible combinations of Li in a four atom complex. The additional structure visible in the upper trace of Figure 11 arises from the trigonal symmetry of the defect.

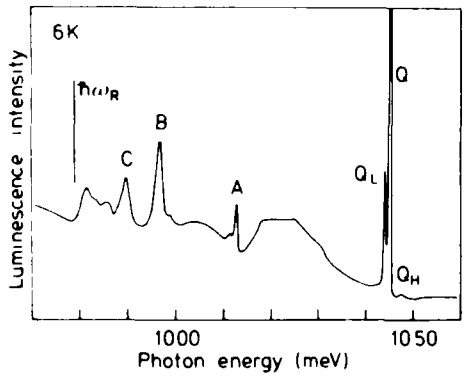

Fig 10 PL spectrum from electron irradiated Si:Li

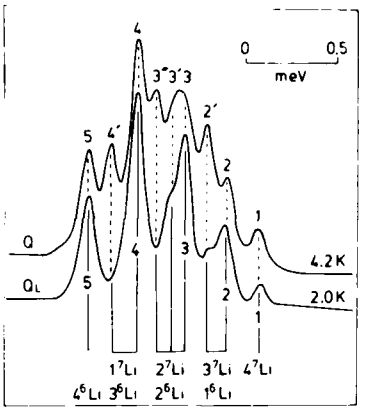

Fig 11 Isotope structure for Li centre in irradiated Si

The basic principles of the isotope shift work carried out on radiation damage centres involving C, O and Si in Si are very similar to those already discussed. Isotope doping work is proving of very great importance in this field, since many of the damage centres in nominally undoped Si which give rise to strong PL bands, have actually been shown to be C and O related [53],[54],[60-62].

Isotope shifts in electronic transition energies have been observed for hydrogen and lithium related shallow acceptor and donor centers in Ge in FIRPC investigations [63],[64]. Once again these observations have been crucial in obtaining detailed models for the defects.

Conclusion

The main aim of this paper has been to demonstrate the wide variety of situations where optical spectroscopy is a vital tool for defect identification in semiconductors. It is hoped that this has been demonstrated

by the particular examples chosen from the fields of both shallow and deep centres. Nevertheless, it should be emphasised that a full understanding of defects is often only achieved by a combination of the techniques described here together with complementary methods such as DLTS, Hall effect, EPR, ODMR and ENDOR.

Acknowledgements

I wish to thank G Davies, B Deveaud and L Eaves for permission to use figures from their published work.

Thanks are also due to M J Kane, K J Nash, B Cockayne, L L Taylor, W R MacEwan, G W Iseler, S H Groves, E Kuphal, Ch Uihlein and in particular the late P J Dean for their collaboration in the work on shallow and deep centers in InP described in this review.

References

1 P J Dean, J D Cuthbert, D G Thomas and R T Lynch, Phys Rev Lett 18, 122, 1967.

2 For a comprehensive review of bound exciton phenomena see P J Dean and D C Herbert in Excitons (edited by K Cho), Springer-Verlag, Berlin 1979, p55, 1979.

3 For review of FIRPC see G E Stillman and C M Wolfe, in Semiconductors and Semimetals, Vol 12, (edited by R K Willardson and A C Beer), Academic Press 1977, p169.

4 M Tajima, Appl Phys Lett 32, 719, 1978.

5 See Landolt-Bornstein Numerical Data and Functional Relationships in Science and Technology, Volume 17, Springer-Verlag (Berlin, Heidelberg, New York), 1982.

6 P J Dean, M S Skolnick, B Cockayne, W R MacEwan and G W Iseler, J Cryst Growth 67, 486, 1984.

7 K L Hess, P D Dapkus, H Manasevit, T S Low, B J Skromme and G E Stillman, J Electronic Materials, 11, 1115, 1982.

8 R J Almassy, D C Reynolds, C W Litton, K K Bajaj and G L McCoy, Solid State Commun 38, 1053, 1981.

9 P J Dean, M S Skolnick and L L Taylor, J Appl Phys 55, 957, 1984.

10 D C Reynolds, P C Colter, C W Litton and E B Smith, J Appl Phys 55, 1610, 1984.

11 D M Larsen, Phys Rev B13, 1681, 1976.

12 M S Skolnick, P J Dean, S H Groves and E Kuphal, Appl Phys Lett 45, 962, 1984.

13 M S Skolnick, P J Dean, L L Taylor, D A Anderson, S P Najda, C J Armistead and R A Stradling, Appl Phys Lett 44, 881, 1984.

14 P J Dean, D C Herbert and A M Lahee, J Phys C13, 5071, 1980.

15 P J Dean, D C Herbert, C J Werkhoven, B J Fitzpatrick and R N Bhargava, Phys Rev B23, 4888, 1981.

16 R G Ulbrich, N van Hieu and C Weisbuch, Phys Rev Lett 46, 53 1981.

17 P J Dean and M S Skolnick, J Appl Phys 54, 346, 1983.

18 R Dingle, C Weisbuch, H L Stormer, H Morkoc and A Y Cho, Appl Phys Lett 40, 507, 1982.

19 D Ashen, P J Dean, D T J Hurle, J B Mullin, A M White and P D Greene, J Phys Chem Solids 36, 1041, 1975.

20 P J Dean, R A Faulkner and G Schonherr, Proc of the tenth Conf on the Physics of Semiconductors, Cambridge 1970 (edited by S P Keller, J C Hensel and F Stern), p286.

21 J L Dessus, Le Si Dang, A Nahmani and R Romestain, Solid State Commun 37, 689, 1981.

22 M Ozeki, K Dazai and O Ryuzan, Solid State Commun 18, 1267, 1976.

23 F Willmann, D Bimberg and M Blatte, Phys Rev B7, 2473, 1973.

24 E F Gross, V I Safarov, V E Sedov and V A Maruschak, Fiz Tverd Tela 11, 348, 1969 (Sov Phys Solid State 11, 277, 1969).

25 H P Gislason, B Monemar, Z G Wang, Ch Uihlein and P L Liu, to be published 1985.

26 W H Koschel, S G Bishop and B C McCombe, Solid State Commun 19, 521, 1976.

27 G Picoli, B Deveaud and D Galland, J Physique 42, 133, 1981.

28 M S Skolnick, P J Dean, M J Kane, Ch Uihlein, D J Robbins, W Hayes, B Cockayne and W R MacEwan, J Phys C16, L767, 1983.

29 M J Kane, M S Skolnick, P J Dean, W Hayes, B Cockayne and W R MacEwan, J Phys C17, 6455, 1984.

30 A M White, Solid State Commun 32, 205, 1979.

31 L Eaves and Ch Uihlein, J Phys C15, 6257, 1982.

32 Ch Uihlein and L Eaves, Phys Rev B26, 4473, 1982.

33 N Killoran, B C Cavenett and W E Hagston, Solid State Commun 35, 333, 1980.

34 J Barrau, M Brousseau, S P Austen and C A Bates, J Phys C16, 4581, 1983.

35 M S Skolnick, M R Brozel and B Tuck, Solid State Commun, 43, 379,, 1982.

36 Y Fujiwara, T Nishino and Y Hamakawa, Jap J Appl Phys 21, L727, 1982.

37 P J Williams, L Eaves, P E Simmonds, M O Henry, E C Lightowlers and Ch Uihlein, J Phys C15, 1337, 1982.

38 B Deveaud, B Lambert, G Picoli and G Martinez, J Appl Phys 55, 4356, 1984.

39 B Lambert, B Deveaud, Y Toudic, G Pelous, J C Paris and G Grandpierre, Solid State Commun 47, 337, 1983.

40 U Kaufmann, H Ennen, J Schneider, R Worner, J Weber and F Kohl, Phys Rev B25, 5998, 1982.

41 V V Ushakov and A A Gippius, Fiz Tech Poluprovodn, 14, 336, 1980 (Sov Phys Semicond 14, 197, 1980).

42 K J Nash, M S Skolnick, B Cockayne and W R MacEwan, J Phys C17, 6199, 1984.

43 B Clerjaud, C Naud, C Benjeddou, G Guillot, P Leyral, B Deveaud and B Lambert, 3rd Conference on Semi-Insulating III-V Materials, Warm Springs (edited by J S Blakemore and D C Look), p484.

44 G W Ludwig and H H Woodbury in Solid State Physics, edited by F Seitz and D Turnbull (Academic Press), Vol 13, 1962.

45 U Kaufmann and J Schneider iin Festkorperprobleme XX, (Advances in Solid State Physics) ed J Treusch (Vieweg, Braunschweig 1980), p87.

46 B Clerjaud, J Phys C 1985, to be published.

47 J J Hopfield, D G Thomas and R T Lynch, Phys Rev Lett 17, 312, 1966.

48 T N Morgan, B Welber and R N Bhargava, Phys Rev 166, 751, 1968.

49 C H Henry, P J Dean and J D Cuthbert, Phys Rev 166, 754, 1978.

50 P J Dean, Phys Rev B4, 2596, 1971.

51 P J Dean, D G Thomas and C J Frosch, J Phys C17, 747, 1984.

52 H P Gislason, B Monemar, P J Dean, D C Herbert, S Depinna, B C Cavenett and N Killoran, Phys Rev B26, 827. 1982.

53 K Thonke, J Weber, J Wagner and R Sauer, Physica 116B, 1983.

54 G Davies, L Canham and E C Lightowlers, J Phys C17, L173, 1984.

55 Some recent literature on magnetic field and uniaxial stress studies of axial, isoelectronic centers in Si is reviewed by G Davies, J Phys C17, 6331, 1984.

56 H P Gislason, B Monemar, P J Dean and D C Herbert, Physica 117B,, 269, 1983.

57 R C Newman in Microscopic Identification of Electronic Defects in Semiconductors

(N M Johnson, G D Watkins and S G Bishop editors), 1985.

58 M Gal, B C Cavenett and P J Dean, J Phys C14, 1507, 1981.

59 L Canham, G Davies and E C Lightowlers, Physica 117, 118B, 119, 1983.

60 K Thonke, G D Watkins and R Sauer, Solid State Commun 51, 127, 1984.

61 K Thonke, N Burger, G D Watkins and R Sauer, J Electronic Materials 14a, 823, 1985.

62 G Davies, E C Lightowlers, R Woolley, R C Newman and A S Oates, J Phys C17, L499, 1984.

63 E E Haller, Phys Rev Lett 40, 584, 1978.

64 L M Falicov and E E Haller, Solid State Commun, March 1985.

The Author

M S Skolnick received a B.A. in Physics and a D Phil for a thesis entitled Infra-red Studies of Semiconductors from Oxford University in 1972 and 1975 respectively. He then spent two years at the high magnetic field laboratory of the Max-Planck-Institut fur Festkorperforschung in Grenoble. Since then he has been at RSRE where his main research interests are in the field of the optical properties of semiconductors, with particular activities in the high resolution spectroscopy of impurities and in whole slice imaging of GaAs crystals.

LOW DIMENSIONAL STRUCTURES

D A Anderson and C R Whitehouse

Introduction

When electrons are confined to a layer of semiconductor whose thickness is of the order of atomic dimensions the band structure, the sequence of energy levels available to the electrons, is determined to a large extent by the geometry of the system rather than by the crystal structure. This results in a fundamental change in the electronic properties of the material and offers exciting new prospects for devices. Quantum wells, as these extremely thin layers are known, are currently attracting a great deal of attention world-wide, in part because of the new physics they manifest, but also because of the control they offer over the electronic properties relevent to devices. The potential for the exploitation of quantum well structures in devices is seen as enormous. Already one important device, the quantum well laser, has made use of the dependence of the optical band-gap on layer thickness to shift the normal infra-red emission of the GaAs solid state laser into the visible part of the spectrum.

In practice a quantum well is made by growing a sandwich consisting of a layer of one semiconductor, typically 1 to 10 nanometers thick, between layers of a different semiconductor. The range of materials which can be used is severely limited by the restriction that the two semiconductors must be closely lattice matched, although the degree of lattice match necessary is one of the subjects under current investigation. In this article we will describe our recent progress at RSRE in the growth of quantum wells and discuss the new techniques which have been developed to probe the electronic properties of material only a few atomic layers thick.

Crystal Growth

Two growth techniques have emerged over the last few years which have demonstrated a capability to grow quantum well structures: molecular beam epitaxy (MBE) and metalo-organic chemical vapour deposition (MOCVD). Older techniques such as LPE and VPE have been used in some laboratories to produce quantum wells of a sort but, in general, they cannot match the control of growth, the interface abruptness and the versatility of MBE and MOCVD. We will concentrate in this article on MBE although both systems are being studied (by Colin Whitehouse, Sidney Bass, Peter Wright and colleagues) as part of the programme. Figure 1 shows a schematic diagram of an MBE reactor. As the name suggests, atomic or molecular beams of the elemental constituents of the material to be grown are directed towards the substrate in an ultra-high vacuum chamber.

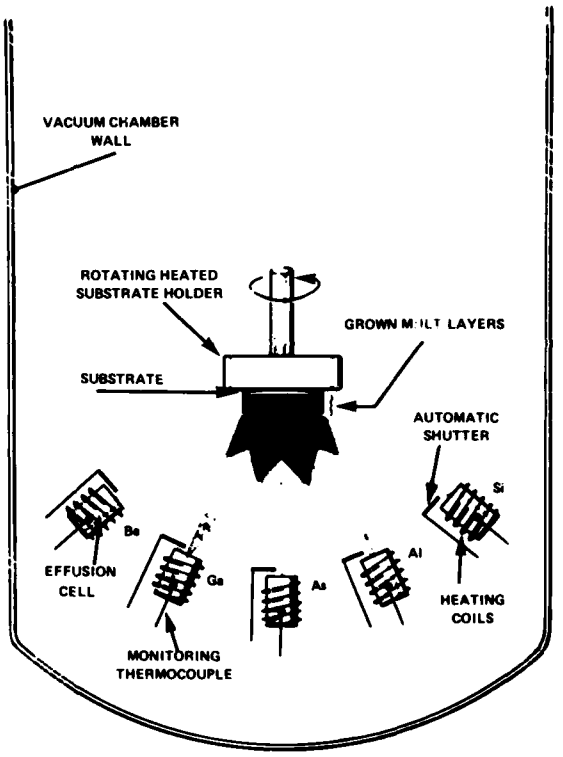

Fig 1 Schematic diagram of MBE reactor for the growth of low dimensional structures

The beams are generated in special effusion cells loaded with quantities of the purest available starting materials and heated to produce the required beam flux. Shutters positioned immediately in front of the cell oriface can be operated from outside the vacuum chamber to switch each beam on or off in a time shorter than that required to grow a monolayer of the crystal. The result is controlled planar growth of the cystal,

monolayer by monolayer, and changes in composition which are abrupt to within one monolayer.

The material system adopted almost universally for the study of quantum well phenomena is GaAs/GaAlAs. Its natural advantages include near ideal lattice match over the entire range of GaAlAs composition, an interface between the semiconductors with a low density of electrically active defects, the existence of high quality GaAs subtrates and the relative simplicity in MBE of switching from one material to another or from one composition to another. In this system the quantum well is in the GaAs, a well understood material with a proven device record. One major disadvantage is the present poor understanding of the growth and properties of the GaAlAs but, fortunately, in most of the known applications the GaAlAs plays a passive role in confining electrons in the GaAs well or, as we will see later, in supplying electrons to the well.

Although deceptively simple in concept, the growth of high quality GaAs, GaAlAs and of abrupt planar heterojuction interfaces between them requires exacting optimisation of the growth conditions and precise control over parameters such as the growth temperature and beam fluxes. Much of the previous work had used rather ad-hoc methods of measuring the growth temperature, so much so that temperatures quoted in the literature are often only approximate. At RSRE Colin Whitehouse and Martin Emeny have developed an entirely new method based on the nature of the surface electron diffraction pattern. This method has been found to be highly reproducible and, because it should be independent of the particular growth system, it will allow more meaningful comparison between laboratories. All growth temperatures are now referred to this standard. The use of this technique has resulted in our being able to grow GaAs layers with a mobility at 77K of 128,000 $cm^2V^{-1}s^{-1}$, the highest value obtained yet in the UK for MBE material, and an indication of extremely high purity.

The basic structure of multiple quantum well layers is determined at RSRE using precision transmission electron microscope cross-sectioning techniques developed by Tony Cullis and Nigel Chew. Figure 2 shows two electron micrographs of a cross-section through a multilayer sample of GaAs and GaAlAs grown by MBE at RSRE. The lighter layers are GaAlAs, highlighted by a diffraction contrast technique using the 200 reflection which is not observed in GaAs alone. Several series of layers can be seen. The widest of these corresponds to alternate layers 10 nm thick (about 30 atomic layers). Particularly striking is the regularity of the layer thickness and the planarity and abruptness of the interfaces. In successive series of layers the thickness was reduced by a factor of two. At the lower magnification (Fig

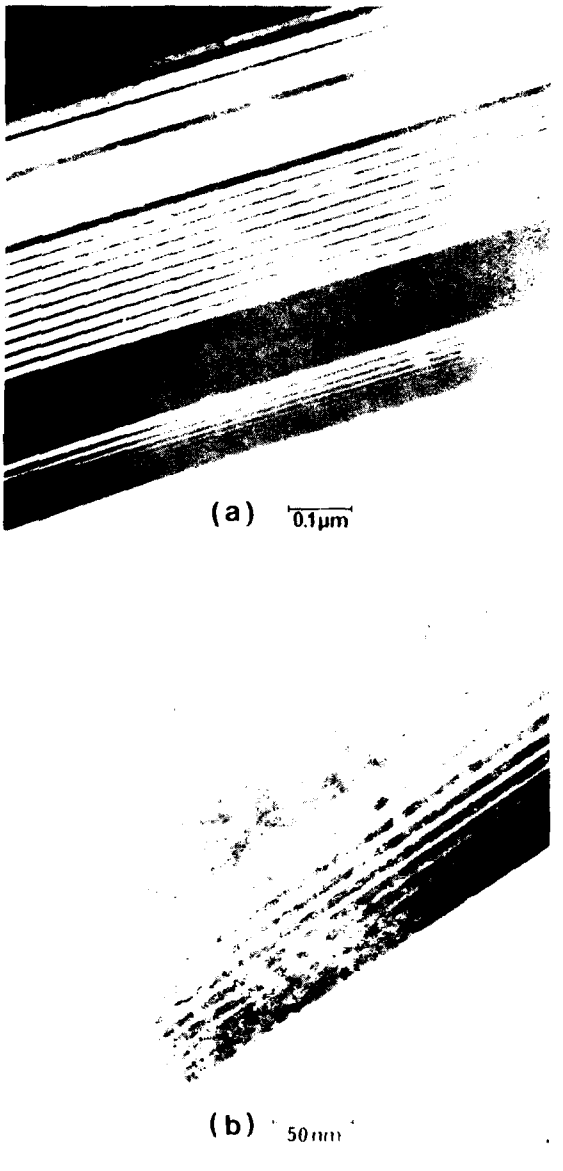

Fig 2 Cross-sectional TEM pictures of an MBE GaAs/GaAlAs multilayer sample

2(a)), the individual bands are still clearly visible down to thicknesses of only 1.2nm (4 atomic layers!) and the planarity is preserved. At higher magnification (Fig 2(b)), continuous uniform bands corresponding to a single atomic layer are still clearly observed, confirming the claim made earlier that compositional changes can be made abrupt to one monolayer.

Electronic and Optical Properties

The use of cross-sectional transmission electron microscopy to produce direct images of multilayer samples as shown in figure 2 is obviously an essential first step in characterising the grown material. It can be used to look at the way in which the epitaxial layer nucleates and at the regularity of the growth process. Invaluable data on the origins of crystallographic defects and non-planar morphology can be obtained. However, if we are to consider the device potential of these systems, much more information is required on their electronic behaviour. As we will show, the measurement techniques set up to do this can also be used in the characterisation of the layers and of the interfaces between them.

Two new techniques capable of probing the properties of semiconductor layers only a few atomic layers thick have been demonstrated at RSRE. Before we describe the way in which they can be used, however, we must first discuss some of the physics of quantum well systems. The inset in figure 3 shows the conduction and valence bands through a GaAs quantum well with GaAlAs layers on each side. The optical band-gap of GaAlAs with typically 30% Al is about 0.45 eV larger than that of GaAs. This gives rise to an abrupt step in both bands which, for this partcular system, leads to the situation shown in the diagram. The precise way in which the total band-gap difference is distributed between conduction and valence bands is a matter of some controversy at present, largely because there is no satisfactory means of measuring it. Within the GaAs, an electron in the conduction band is confined by the steps at the interfaces to a degree that the Heisenberg Uncertainty Principle becomes important. The result is that electrons can occupy only a small number of discrete quantised energies represented by the horizontal lines on the diagram. A similar situation occurs in the valence band if we recall that holes in equilibrium occupy states at the highest available energy. The allowed energies are given approximately by

$$E_n = \frac{\hbar^2}{2m^*}\left(\frac{n\pi}{L}\right)^2 \qquad n = 1,2,3 \text{ etc}$$

where L is the width of the well and m* is the appropriate effective mass for the carrier in the band. In GaAs, the situation is made more complicated by the fact that there are two types of hole in the valence band with different effective masses. These are commonly known as the light and heavy holes respectively and give rise to a double set of energy levels in the valence band. The expression given above for the quantised energies is exact in the case of infinite potential steps bounding the well. In practice a small modification is required to take account of the finite potential steps. The main part of figure 3 shows direct experimental observation of transitions between the quantised levels in a 10 nm well. The top trace was obtained using electroreflectance (ER), a technique once extensively used in the determination of crystal band structures, and now adapted at RSRE, by Philip Klipstein, Paul Tapster and Norman Apsley, to reveal the details of the band structure in quantum wells. The experiment involves measuring the changes in reflectivity of the sample as an electric field is applied normal to the surface.

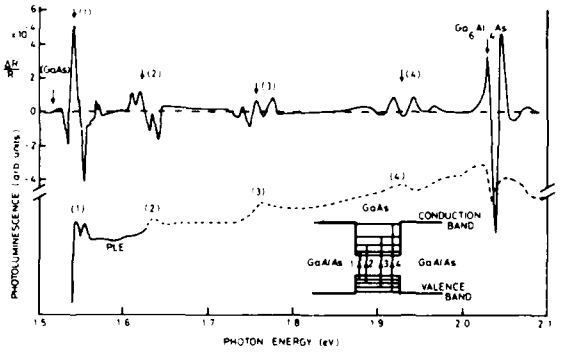

Fig 3 ER(a) and PLE(b) spectra for a 10 nm QW grown at Phillips, Redhill

This is done by evaporating a semitransparent Schottky barrier on the top surface and applying an ac bias. The reflectivity is measured with a lock-in detector at the frequency of the ac

modulation, producing the spectrum shown in the figure, as the wavelength of the light illuminating the sample is swept through the region of the GaAs band gap. Four strong features can be clearly seen in the spectrum corresponding to the transitions seen in the band diagram. A selection rule allows only transitions with equal quantum number n and only transitions to heavy hole states are observed. Nevertheless, this is a powerful demonstration that these quantised levels do indeed exist. A full analysis of the electroreflectance lineshape is now being carried out in order that the precise energy of each transition can be determined. With this, it will be possible to fit electroreflectance data to obtain precise values for the band edge steps. The addition of the shift in the energy levels with applied dc bias should even allow an analysis of the shape of the potential well. There is currently no other technique capable of doing this.

The lower trace in figure 3 shows a photoluminescence excitation (PLE) spectrum obtained by Maurice Skolnick for the same sample. This spectrum is produced by detecting the total luminescence emitted from the quantum well as it is illuminated by either a dye laser or a conventional source and monochromator. The PLE spectrum is thus a form of absorption spectrum and shows weak features at the same energies at which the electroreflectance features were seen. In this case the PLE resolves the n=1 light and heavy hole transitions which were lost in the more complex electroreflectance spectrum.

In the layer geometry we have described, the electrons are confined in the direction normal to the layer but are still free to move in the plane of the layer. The motion of the cariers is quasi 2-dimensional. Electron transport parallel to the layer is possible but the scattering is modified slightly by the reduced dimensionality. A much larger change in the scattering can be achieved if the GaAs quantum well is grown undoped and the surrounding GaAlAs is doped heavily n-type. As a result of the potential steps at the heterojunction interfaces, electrons are transferred from the GaAlAs layers into the GaAs well producing very high carrier concentrations. This process is known as remote doping because the parent donor impurities remain in the GaAlAs layers while the electrons reside in the GaAs. The separation between the electrons and the positively charged donor ions has the effect of reducing to a negligible level the scattering due to ionised impurities which usually dominates the electron mobility in heavily doped GaAs. The end product is a 2-D mobility at room temperature two to three times higher than that in normal GaAs with the same carrier density. At low temperature the effect is even more dramatic. Mobilities as much a thousand times the bulk GaAs mobility have been observed. The effect is the basis of the high electron mobility transistor or HEMT which is expected to have a major impact on the viability of GaAs based digital electronics. For all the device potential, the factors controlling the mobility in 2-dimensions are not properly understood nor is there any reliable information on the effect of higher electric fields more likely to be encountered in devices.

At RSRE we have set up a technique based on the Shubnikov de Haas effect which, together with more conventional Hall effect measurements, can help us understand the mysteries of 2-D electron transport. Shubnikov de Haas makes use of the fact that remote doping can readily supply sufficient electrons to the GaAs well to fill up the conduction band by several tens of meV. At low temperatures the Fermi level lies above the bottom of the band and the material is degenerate; it behaves like a metal and is usually referred to as a 2-dimensional degenerate electron gas or 2DEG. When the resistance of such a system is measured as a function of magnetic field at liquid helium temperatures, a series of oscillations is seen which is in fact periodic in 1/B, growing in amplitude with increasing magnetic field as shown in figure 4. The origin of the oscillations lies in the further quantising of the system due to confinement of the electrons in the plane by the magnetic field. The period of the oscillations gives a direct measurement of the density of carriers in the 2DEG. Furthermore, since the oscillatory behaviour is observed only when the field is normal to the layer, rotating the sample with respect to the magnetic field provides a simple demonstration that a 2DEG is present. Many measurements have been made on GaAs/GaAlAs structures but the figure shows data for a

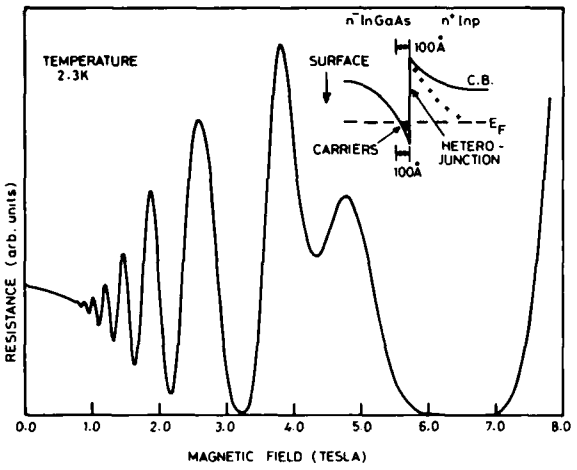

Fig 4 Shubnikov de Haas oscillations from a InGaAs/InP heterojunction

single heterojunction between InP and InGaAs grown in-house by Sidney Bass, using an MOCVD reactor. In this system the InP is the wider gap material and can be doped as before to supply electrons remotely to the InGaAs. The band bending associated with this charge transfer is such that the electrons in the InGaAs are confined within about 10 nm of the heterojunction interface and so produce a small quantum well with a 2DEG. The data from this sample can be favourably compared with any results on this material system world-wide, demonstrating that the MOCVD growth technique is also capable of producing abrupt, high quality interfaces. A full analysis of the amplitude of the oscillations as a function of temperature and electric field yields a detailed picture of the transport in the 2-D system and of the character of the interface itself.

The mechanisms controlling the transport can be conveniently studied by varying the carrier density in the 2DEG. This can be done in two ways. The simplest is to incorporate a Schottky gate in the sample being measured and then control the carrier density with gate bias, in much the same way as is done in an FET. Alternatively, we can also make use of a persistent photoconductivity effect observed in all these systems at low temperature. Illumination of the sample with a red LED can increase the carrier density by a factor of two and, below about 50 K, the carrier density remains high almost indefinitely after the light is removed. Figure 5 is a plot of mobility versus carrier density showing the effect of illumination on both GaAs/GaAlAs and InP/InGaAs heterojunctions. Note that the increase in carrier density produces an increase in mobility. This can be interpreted immediately as an indication that scattering by ionised impurities is controlling the transport, but only by measuring the slope of the mobility/carrier density curve can we distiguish between impurities in the heterojunction and in the GaAlAs (or InP) supply layer. By combining the persistent photoconductivity effect with a Schottky gate, it is possible to first increase the carrier density by illumination, then reduce it again with gate bias. Preliminary results of this experiment are also shown in the figure.

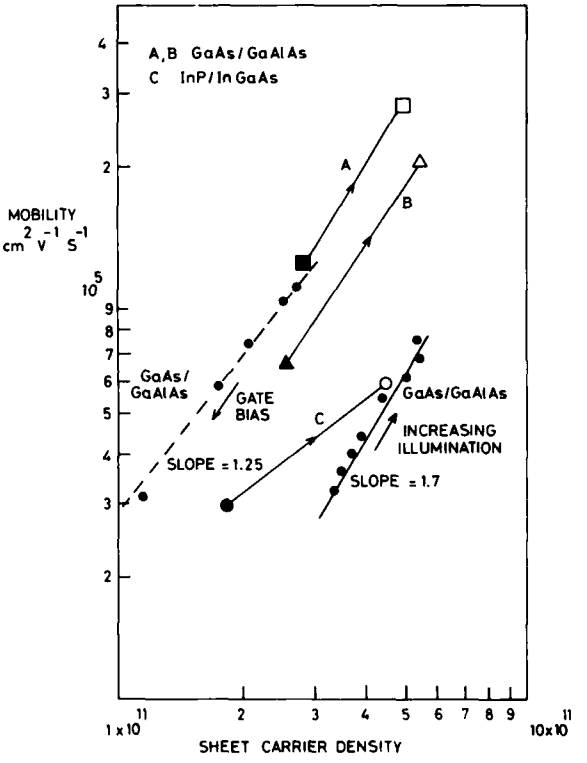

Fig 5 Mobility vs carrier density in GaAs/GaAlAs and InP/InGaAs heterojunctions

The data show considerable scatter but give a slope of 1.25, very close to the value of 1.4 predicted for scattering by remote impurities in the GaAlAs.

We can deduce that for most of the samples we have studied so far, although the mobilities fall short of the best reported values by an order of magnitude, the limiting factor is not associated with the

interface itself. We can now go on to design our heterojunction structures to minimise still further the effect of the remote dopant in the GaAlAs by better optimisation of doping levels and layer thicknesses and by incorporating an undoped GaAlAs spacer layer between the 2DEG and the doped GaAlAs. This work is now under way.

Device Prospects

There are now many examples of solid state devices taking advantage of the flexibility afforded to the designer of incorporating one or several heterojunctions in the device structure. This trend will certainly continue as demands for improved device performance intensify and as the control of the growth process steadily improves. Devices which specifically exploit the unique properties of quantum wells or other 2-dimensional structures are just beginning to appear but there are huge gaps in our present understanding of so many aspects of this new class of semiconductor that what we see now is only the tip of a very large iceberg. Almost any application for solid state devices will benefit from this new technology and we have every reason to expect a whole range of completely new device applications. Macroscopic crystals can be built up consisting of hundreds of quantum wells with essentially the behaviour of a 2-dimensional system. Beyond that, the wells can be made to interact to produce a superlattice, virtually a man-made semiconductor created monolayer by monolayer, with properties precisely tailored to fulfill a specific device requirement. At RSRE the groundwork necessary to embark on such an ambitious programme has been laid. The future possibilities are limited only by our imagination.

Acknowledgements

In addition to those mentioned explicitly in the text, I would like also to recognise the important contributions made to this programme by Michael Kane, Lesley Taylor and Trevor Martin. Thanks are due to Tony Cullis and Paul Tapster for many helpful comments on the manuscript.

The Authors

David Anderson graduated in Physics with 1st class Honours from the university of Dundee in 1972 and obtained his PhD there in 1976. Between 1976 and 1980, he held a post doctoral research fellowship at Harvard University. Since joining RSRE in 1980, David has carried out materials and device research on InP mm-wave Gunn diodes. His present research concerns the physics of low dimensional structures.

Colin Whitehouse graduated in Physics at the University of London and gained an MSc in Solid-State Physics from the University of Birmingham and obtained a PhD degree in 1978. He worked at GEC Hirst Research Centre until 1977. He held a post-doctoral research fellowship at the University of Newcastle Upon Tyne before joining RSRE in May 1980. Colin is now responsible for MBE programmes relating to the growth of III-V and II-VI low dimensional structures.

PYROELECTRIC ACTIVITY IN NON-CENTROSYMMETRIC LANGMUIR-BLODGETT FILMS

M F Daniel and G W Smith

Introduction

The recent upsurge in interest in the Langmuir-Blodgett (LB) technique[1] is primarily due to the recognition of its potential for a variety of thin-film device applications. This article concentrates on pyroelectric activity in non-centrosymmetric LB films. After outlining the basic principles of the LB technique, a novel mechanism designed and constructed at RSRE to allow the convenient deposition of non-centrosymmetric LB films is described. Finally, some early results obtained at RSRE demonstrating pyroelectricity in LB films are presented.

Other objectives of the RSRE LB programme (not discussed here) include the fabrication of highly-ordered films of aromatic molecules such as phthalocyanine derivatives (potential applications include gas sensors, dielectric layers for MIM and MIS devices, etc), and an improved understanding of the LB technique[2] which should lead to better film quality and improved device performance.

LB Technique – Basic Principles

In brief, the LB technique permits the fabrication of ultra-thin films of surface-active organics in a highly-controlled fashion. First, an insoluble layer one molecule thick (typically 1.5nm to 3.0nm) is produced at the water-air interface, usually by spreading from solution. In favourable cases this layer can be compressed until the constituent molecules are close-packed and then transferred to a solid substrate (metallised glass slide, inorganic semiconductor, etc) by passing the substrate through the interfacial region, as shown schematically in Figure 1, whilst maintaining a constant surface pressure. Further excursions of the substrate result in the build-up of a multilayer LB film. Carefully prepared LB films are remarkably uniform, with low defect densities and accurately controlled thickness. Other important advantages include the scope for modifying the molecular structure in order to vary film characteristics, and the

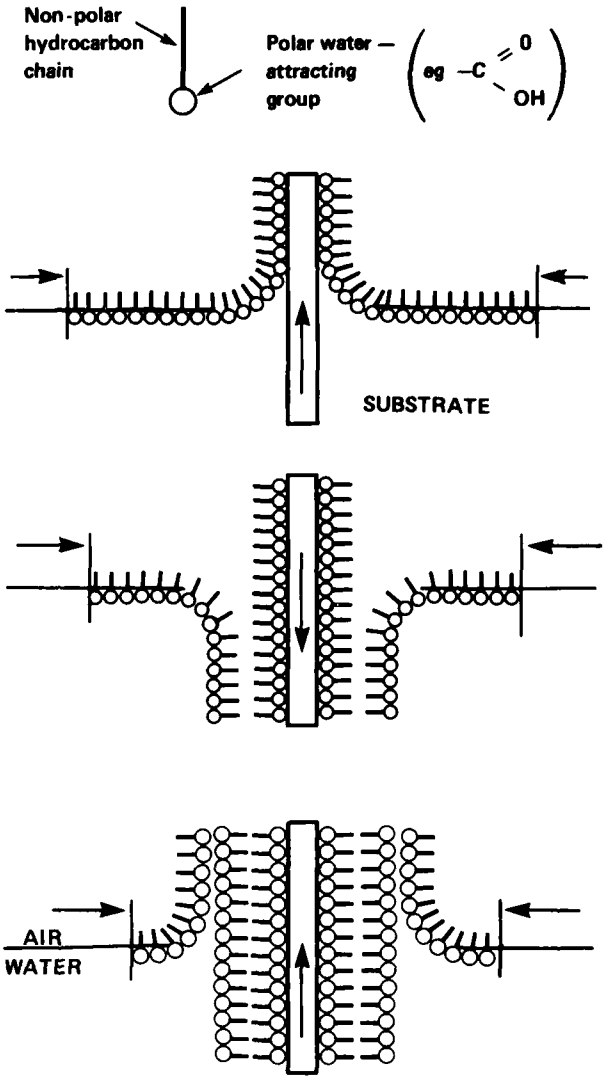

Fig 1 Transfer of monomolecular layer to hydrophilic solid substrate. Inset shows the typical structure of a surface-active molecule

ability to incorporate more than one molecular type into the film structure in order to achieve some specific behaviour.

Novel Fabrication of Non-Centrosymmetric LB Films

Films prepared in the above manner are centrosymmetric. However, if two monomolecular layers A and B are employed, their stacking order may be varied to give non-centrosymmetric structures (eg ABAB ....)

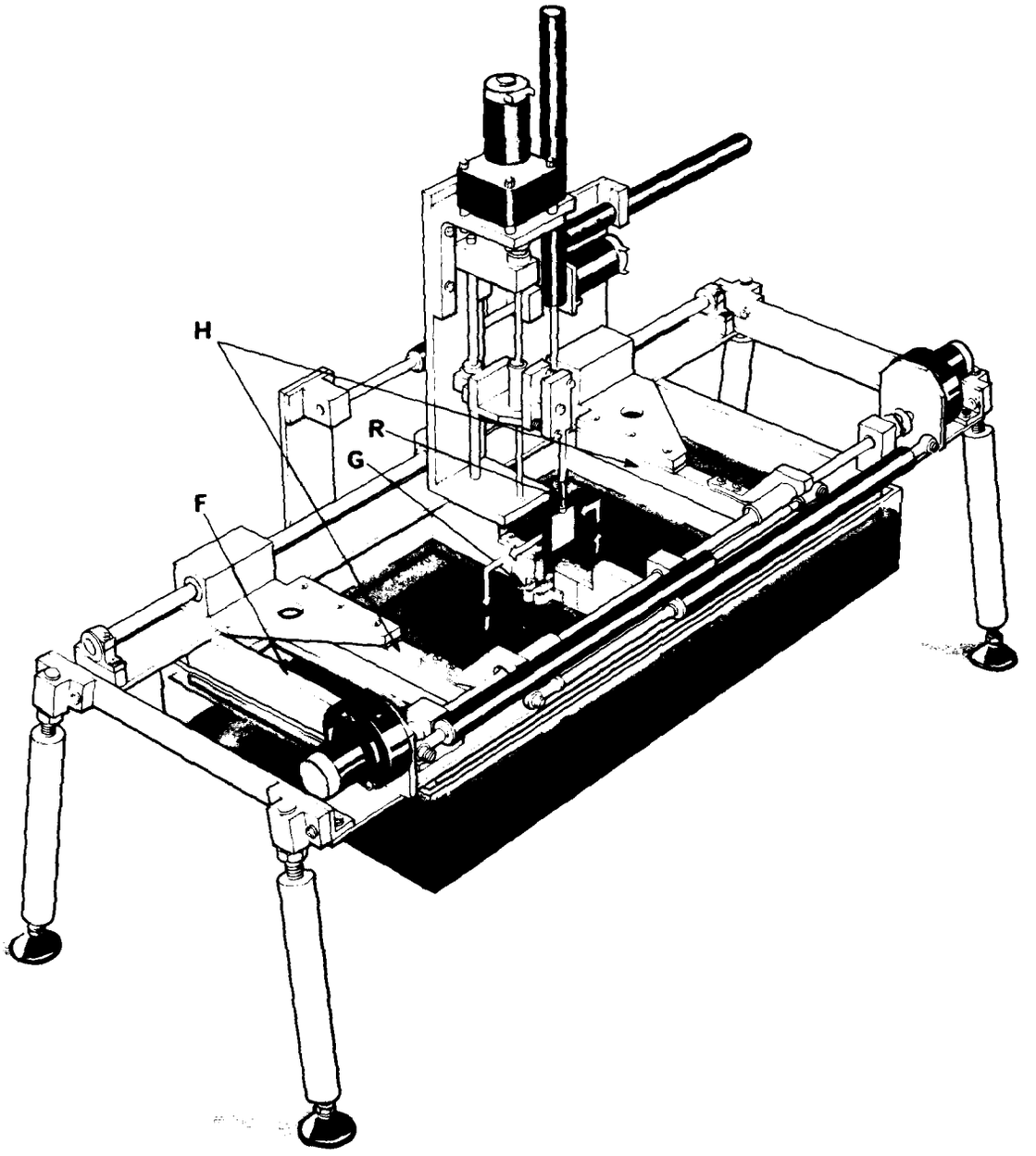

Fig 2 Novel two-compartment trough for the fabrication of non-centrosymmetric LB films

possessing a polar axis perpendicular to the substrate plane due to the additive nature of molecular dipole moments. Such films are expected to demonstrate device useful pyroelectric, piezoelectric and second-order non-linear optical effects, and the uniqueness of the LB technique in enabling their fabrication is rapidly gaining worldwide attention.

Figure 2 shows a schematic view of a new computer-controlled two-compartment LB trough[3], designed and constructed at RSRE, which incorporates a novel substrate transfer mechanism (patent application) to allow the convenient fabrication of non-centrosymmetric films. A polytetrafluorethylene (PTFE) frame (F) intersects the water-air interface and compression of the two monolayers is effected independently by two PTFE barriers (H) possessing spring-loaded end seals. The substrate path indicated is for the deposition of an ABAB sequence. In order that the substrate support rod (R) might pass through the central dividing barrier, a simple "gate" mechanism has been invented, comprising two

abutting PTFE leaf springs which intersect the water surface (G) and prevent A and B mixing. However, the thinned section of the support rod easily passes between the two springs which seal ahead of and behind it as indicated in Figure 3, thus minimising the risk of unwanted cross-contamination. Other important features of this mechanism are that it maintains conventional vertical motion of the substrate through the spread monolayers, and it allows the rapid build up of multilayer films, the rate in general being limited by the slower of the two monolayer deposition speeds. Early observations of pyroelectric behaviour in ABAB structures are described briefly below.

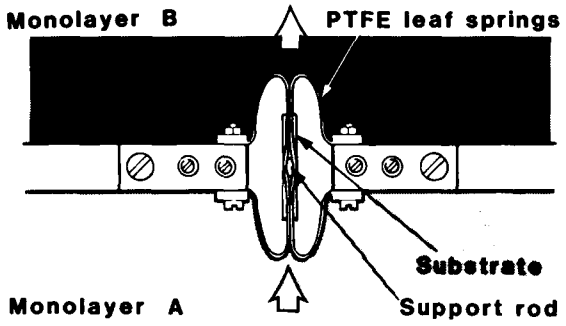

Fig 3 Plan view showing passage of substrate support rod through PTFE gate

Pyroelectric LB Films

Non-centrosymmetric films will in general possess a spontaneous electrical polarisation, P_s, perpendicular to the film plane (polar axis). Pyroelectric activity derives from the rate of change of the spontaneous polarisation with temperature. Potential advantages of LB films for pyroelectric detectors include low thermal capacity, allowing short response times, and large area capability.

An ABAB film of ω-tricosenoic acid [CH_2 = CH $(CH_2)_{20}$ COOH] and stearylamine [CH_3 $(CH_2)_{17}$ NH_2] of total thickness 150 layers, sandwiched between aluminium and thin nichrome (IR absorbing black) electrodes, produced an alternating voltage signal when exposed to a chopped IR source. This was confirmed as a pyroelectric signal and quantified by performing a charge integration experiment (Figure 4) on a sample between two aluminium electrodes over the temperature range 250K to 300K. The pyroelectric coefficient, p (= dP_s/dt), is

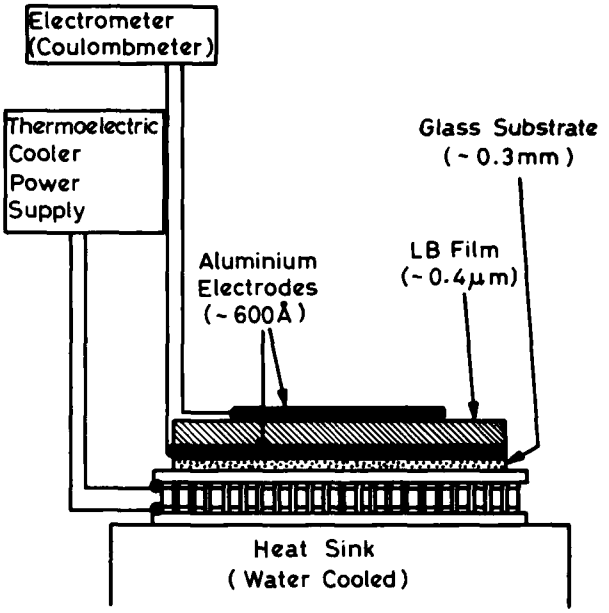

Fig 4 Schematic of charge integration experiment showing LB film sample configuration

given by

$$p = Q/\Delta T$$

where Q is the integrated charge
ΔT is a small change in temperature

For the ω-tricosenic acid/stearylamine film $p \sim 10^{-10}$ C cm^{-2} K^{-1} (cf triglycine sulphate (TGS), $p \sim 3.\ 10^{-8}$ C cm^{-2} K^{-1}; TGS is a high performance single crystal pyroelectric).

Infrared absorption measurements on the LB film have shown that the polar headgroups have exchanged a proton giving this structure (R_1COO^- $^+H_3NR_2$). Written another way ($^+H_3NR_2$ R_1COO^-) the repeat unit is somewhat similar to the chemical structure of the glycine zwitterion (^+H_3N CH_2 COO^-) which is found in TGS. The much smaller value of p exhibited by the LB film is probably due primarily to the diluting effect of the long non-polar hydrocarbon chains (R_1 and R_2) which play no part in producing the pyroelectric effect. Current work is being directed at increasing the dipole moment per unit volume by, for example, incorporating highly-polar groups into the LB film structure.

Summary

The LB technique combined with the new RSRE trough design offers the ability to produce

non-centrosymmetric organic films with useful properties such as pyroelectric and optically non-linear behaviour. Pyroelectric activity has been observed and quantified ($p \sim 10^{-10}$ C cm^{-2} K^{-1}) in an acid/amine alternating layer LB film. As new materials with custom-designed properties become available, these synthetic low-dimensional solids may be expected to produce a variety of interesting and useful effects with device potential.

Acknowledgements

The authors would like to thank collaborators at the Universities of Bristol, Durham and East Anglia for their valued support, and colleagues at RSRE for assistance and many useful discussions.

References

1. Proceedings of the First International Conference on Langmuir-Blodgett Films, Durham, UK, Sept 20-22, 1982. Thin Solid Films 99 (1983).

2. M F Daniel and J T T Hart, J Molecular Electronics, in press.

3. M F Daniel, J C Dolphin, A J Grant, K E N Kerr and G W Smith, Thin Solid Films, in press.

The Authors

Mervyn Daniel graduated in Chemistry (BSc Hons) at the University of Bristol in 1974. He joined the teaching staff at the University of Exeter as physical chemistry demonstrator and obtained his PhD entitled "Scattering Studies of Disordered Solids". He joined RSRE in 1980 and has concentrated on research into the LB technique for device applications.

Gilbert Smith graduated in Physics/Chemistry (BSc Hons) at Lancaster University in 1979 and obtained a PhD with a thesis entitled "Electrical and Electrostatic Properties of Thin Films of Organic Materials" also at Lancaster. He joined RSRE in 1982 and began work on LB films with special reference to electrical and dielectric properties.

FUNDAMENTAL STUDIES OF ION-SURFACE INTERACTIONS IN DRY ETCHING

T I Cox and V G I Deshmukh

The basic success of silicon technology lies in the fabrication of transistors, diodes and passive circuit elements of very small dimensions and the integration of these components into an entire circuit on a single 'chip' of silicon. The scale of integration is such that chips of about 1 centimetre square may be fabricated that contain about 50,000 transistors and associated circuit elements; a degree of complexity that is termed Very Large Scale Integration (VLSI). The implication is that the characteristic geometries of the individual devices, e.g. the active area beneath the gate of a Metal-Oxide-Semiconductor Transistor, are of the order of 1 μm.

The creation of the desired geometrical shapes in silicon or related materials is termed pattern transfer and is clearly a crucial operation. The transference is achieved by using photolithographic techniques and subsequent feature definition by etching. This is illustrated in Figure 1 where (a) shows a thin film covered by a layer of photoresist, which is an organic polymer. A photomask, ie a glass plate having the desired pattern of transparent and opaque areas, is brought into close proximity with the photoresist-coated sample. Exposure is effected by flooding the whole assembly with ultraviolet light. For our example of a negative-working photoresist, the exposed areas are hardened due to a photochemically induced increase in cross linking and are therefore left in place during subsequent development and rinsing of the sample as shown in Figure 1(b). This remaining photoresist can then act as a mask against chemical etching of the underlying film, Figure 1(c). The left-hand feature has been etched in a wet chemical, which being isotropic in its etching action, has undercut the photoresist mask. The right-hand feature demonstrates perfect fidelity with the photoresist mask.

For feature sizes <2μm, wet etching cannot be used and the process engineer is forced to use plasma methods. It is this reason that has led to such intense effort worldwide to produce dry etching processes and equipment.

In silicon technology, etching is required for metals and alloys, silicon compounds, polycrystalline silicon, n-type and p-type single crystal silicon of various doping concentrations, amorphous insulators such as silicon dioxide and polymeric materials. Moreoever, this range of materials is often present simultaneously in an etch cycle.

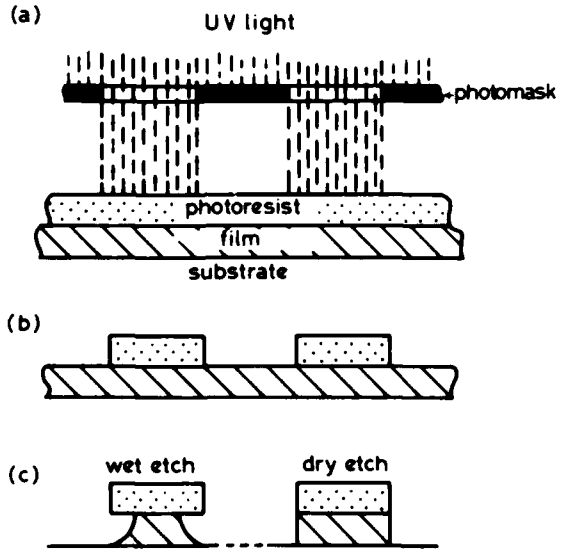

Fig 1 The photolithographic and etching process

Fig 2 Lines etched in Aℓ:Si:Cu using reactive ion etching equipment at RSRE

Empirical development has allowed dry etching processes to be achieved and an example is given in figure 2 of lines etched in Al:Si:Cu, which is a common alloy used to interconnect devices on a chip.

Although there are several types of dry etchers used in silicon technology, in all cases an electric discharge produces the chemically reactive species by fragmentation of the appropriate stable gas molecules in a vacuum chamber with pressures in the range 1 mtorr - 2 torr. Commonly, the discharge is excited by a radio-frequency source operating in the frequency range 100KHz to 20MHz. The substrate to be etched is immersed in the plasma and a sheath field develops at the substrate-glow interface. This field may be as large a 1 kilovolt over a sheath width of a few millimetres as in the case of Reactive Ion Etching (RIE).

The substrate is thus bathed in a sea of unfragmented gas molecules and uncharged fragments and also bombarded with a variety of positively charged ions, electrons, and high energy photons (up to about 10eV). The charged species possess a range of kinetic energies and for the case of RIE these may reach about 1 keV. Dry etching of the substrate proceeds by production of volatile chemical compounds via a reaction between the substrate and absorbed reactive molecular fragments generated from the plasma. Some reactions require an activation energy which may be provided by energetic ion bombardment. If etching proceeds via such an ion assisted mechanism, then the directionality of the incident ions at the surface determines the wall profiles. If the ions hit the surface at normal incidence then etched features will exhibit vertical sidewalls. The products of the reaction are desorbed and subsequently pumped away.

It is thus important that a knowledge of the interactions of energetic ions (100 to 2000 eV) with surfaces of interest is established. Even for simple systems, however, the precise mechanism of the interaction is not well understood. Seminal research by Winters and co-workers [1] has shown that energetic ion bombardment causes both physical sputtering of the substrate and can provide the activation energy necessary for particular chemical reactions to occur at the surface. Many of these experiments and those at other laboratories have been carried out under UHV conditions. The obvious reason for this UHV approach is that in seeking to elucidate the etch mechanism, it is desirable and necessary to have well-defined substrate properties and ambient surroundings. On the other hand, many practical etch processes are performed in rather poor vacua, eg base pressures $\sim 10^{-6}$ torr and operating pressures in the range of 1 to 200 mtorr.

Figure 3 shows holes etched in silicon dioxide using a reactive ion beam etching (RIBE) technique at RSRE. In this method, ions are generated in a plasma contained within an ion source which is remote from the sample. An ion beam is extracted from the source and accelerated electrostatically onto the material to be etched. As evident from figure 3, RIBE can offer very high anisotropy of etching and is thus of interest for the fabrication of ultra-small features. Additionally, as noted above, the full understanding of a standard plasma etching process is a formidable problem.

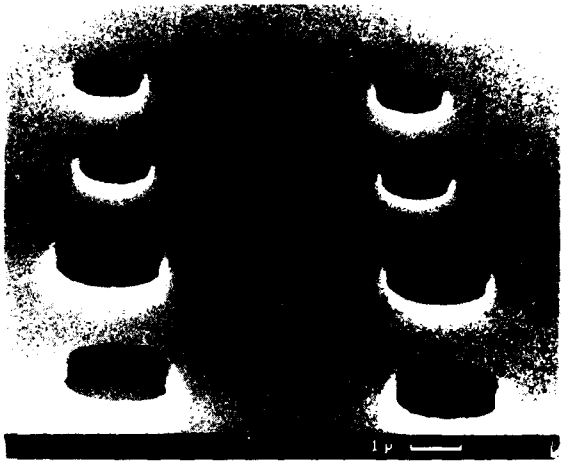

Fig 3 Holes etched in silicon dioxide using reactive ion beam etching equipment at RSRE

RIBE however is more conducive to basic studies and forms a valuable first step in the elucidation of etch mechanisms as well as offering a "bridge" between UHV experiments and true production environments. Accordingly, we have studied the RIBE of silicon using a series of fluorocarbon gases with different ratios of fluorine to carbon in the parent molecule. We have used ion bombardment-induced light emission [2,3] as a probe to yield

information on surface composition. In addition, mass spectrometry has been used to analyse the etching products arising from ion-surface interactions. All experiments were carried out in a reactive ion beam etcher of conventional design. The ion source was of Kaufman type with an accelerating voltage which could be varied between 0 and 2 kV. Electronic-grade, fluorocarbon gases (CF_4, C_2F_6, C_3F_8) were used as the source input. Gases could also be fed, via a mass flow controller directly into the sample chamber. This afforded the opportunity of studying the effect of the partial pressure of oxygen on the etching of our specimens. This is important because the presence of oxygen and water vapour in practical etchers is known to have a significant effect on etch performance, eg in etch rate, uniformity and reproducibility.

The bombardment-induced light emission was collected from a region just above the wafer surface and spectra were recorded over the range 2470-2530 angstoms; a typical spectrum is shown in figure 4. A quadrupole mass spectrometer was coupled directly to the work chamber and provided a direct line of sight to the wafer surface. Ions orginating from the surface were analysed by operating the mass spectrometer with its ionisation filament extinguished. The quadrupole mass spectrometer could also be positioned directly in the ion beam to determine the ionic composition of the source output for all of the fluorocarbon gases used in this work. For a given source condition, the beam composition from CF_4 is predominantly CF_3^+ (60%) whilst C_2F_6 and C_3F_8 contain increasing amounts of CF_2^+ and CF^+. The relative amounts of the ionic species are a sensitive function of the gas pressure and source conditions. Thus we may study ion surface interactions pertinent to dry etching for a wide range of beam compositions and ion energies.

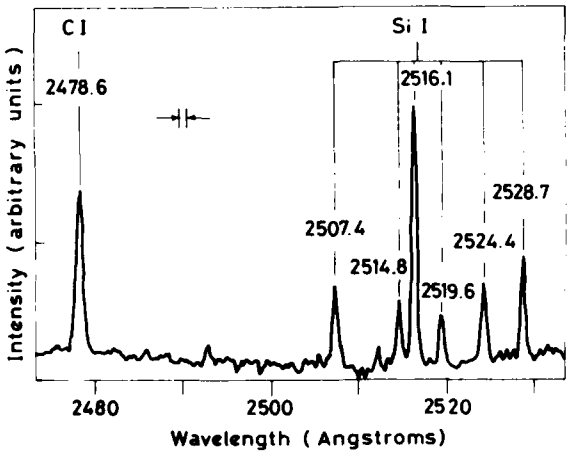

Fig 4 Light emission generated by the impact of an ion beam (1700 eV) from C_2F_6 incident on silicon

At low bombardment energies, neither a bombardment-induced silicon optical emission signal nor a signal at m/e = 28 (Si^+) in the ion spectrum was observed. It was found that there was a threshold energy V_{th} for the appearance of these signals and these are recorded together with the corresponding composition of the ion beam in Table I. We note that

$$V_{th}\ (CF_4) < V_{th}\ (C_2F_6) < V_{th}\ (C_3F_8).$$

An accepted model [4] descriptive of the behaviour when energetic CF_x^+ ions are incident on silicon is that the ion fragments according to

$$CF_x^+ \longrightarrow xF + C \qquad x = 1,2,3$$

and the energy is shared between the atomic fragments such that energy and momentum are conserved. Our mass spectrometric results confirm that the incident fluorocarbon beam is highly fragmented on impact with a silicon surface. Carbon so generated has a high probability of sticking to silicon and can thereby act as a surface passivant but may be removed by physical sputtering or by chemical combination with fluorine to form CF_4 (gas). As ion energy is increased both the physical and chemical removal rates of carbon per incident fluorine atom increase [5], and therefore the fraction of the surface covered by carbon will decrease. At full carbon coverage, silicon is not sputtered from the surface and we thus expect to see no optical signal from silicon. If the removal of carbon is the factor determining this threshold voltage, then it may be anticipated that V_{th} will increase as the ratio of carbon to fluorine atoms in the beam increases as is seen by reference to Table I.

TABLE I

Gas	CF_4	C_2F_6	C_3F_8
V_{th} (eV)	1170	1580	1800
CF^+	0.14	0.20	0.31
CF_2^+	0.17	0.21	0.27
CF_3^+	0.56	0.44	0.29

Threshold energies (V_{th}) for beams generated from different fluorocarbon gases, together with the corresponding major beam constituents.

TABLE II

p (O_2) 10^{-5} (torr)	CF_4	C_2F_6	C_3F_8
0	1170	1580	1800
2	690	1250	1520
4		1060	1320
6		840	1030
8		680	880

Values of threshold energy (V_{th}) for ion beams generated from different fluorocarbon gases as a function of oxygen partial pressure.

As stated above, many dry etch processes are performed in poor vacua and it thus of interest to determine the effects of oxygen admitted to our work chamber on our data. In Table II are recorded values of V_{th} for various partial pressures of oxygen admitted to the work chamber. The decrease in V_{th} with increasing oxygen partial pressure is explained by the fact that oxygen offers an additional route for the removal of the passivating carbon layer principally as CO, CO_2 and COF_2. Etch rate measurements have also been performed and correlate well with the model described above and our diagnostic techniques. Moreover, literature data on the variation of etch rate on vacuum quality for fluorocarbon RIBE of silicon is explicable by our results on the dependence of V_{th} on the partial pressure of oxygen in the etching chamber.

We may thus conclude that the results described here of the investigation of ion surface interactions may be used to explain artefacts observed in practical dry etching machines and thereby assist in the development of improved processes.

References

1. J W Coburn, H F Winters, and T J Chuang, J Appl Phys 48, 3532 (1977).

2. G E Thomas, Surf Sci 90, 381 (1979).

3. T I Cox and V G I Deshmukh, App Phys Lett (to be published), August 1985.

4. Ch Steinbruchel, J Vac Sci Technol 82, 38 (1984).

5. S Tachi, K Miyake, and T Toyukama, Jpn J Appl Phys Suppl 21-1, 21-141 (1982).

The Authors

Timothy I Cox joined RSRE in 1980 after obtaining a PhD in the Department of Theoretical Chemistry at Cambridge for work on light scattering studies of the structure and dynamics of molecular liquids. His main research interest at RSRE is the fundamental physics and chemistry of dry etching.

Vasant G I Deshmukh gained his PhD at St Andrew's University for NMR studies of the metal-nonmetal transition in arsenic-doped germanium. He then spent two years as a Postdoctoral Fellow at Warwick University working on the NMR of metal-molten salt solutions before joining RSRE in 1978. In addition to his research interests in dry etching and particle beam lithography, Dr Deshmukh is the 'Topic Co-ordinator' in dry etching for the Alvey Programme.

A LIQUID CRYSTAL RADAR DISPLAY

J L Glasper and C J T Smith

A liquid crystal display has been developed intramurally for the MISER radar, a RSRE experimental radar for the evaluation of millimetric surveillance techniques. The completed display, shown in figure 1 consists of two large area matrix addressed displays and twelve direct drive numeric displays for axes designation and target parameters. The circular display plots data using polar co-ordinates to produce a PPI type presentation with the square display plotting data using rectangular co-ordinates to show a magnified area of the PPI display. The axes designators define the position and extent of the enlarged region and the target parameter displays will track a selected target. The display unit is a combination of LCD modes; the large area displays are dyed phase change (DPC) driven by waveform identity addressing (WIA) whereas the numeric displays are direct drive twisted nematic. This was done as a matter of convenience; the numeric displays could also have been DPC devices. The overall dimensions of the unit are 480 x 300 x 55 mm; the main displays are 100 mm diameter and 75 x 75 mm and the numeric character height is 6 mm. The status indicators on the left hand edge are LEDs.

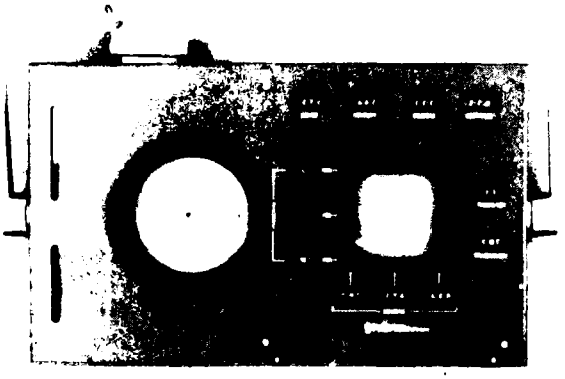

Fig 1 The MISER liquid crystal display unit

The twisted nematic (TN) electro-optic effect utilises the molecular ordering of the liquid crystal for the guiding of light between polarisers and it is this use of birefringence and polarisers which produces good contrast but gives rise to the limitations of both viewing angle and brightness experienced with these displays. The TN mode has a sharp transmission versus voltage characteristic and can be readily multiplexed but the problems become more severe as the number of lines is increased. For simplicity, the TN numeric displays used are direct drive, ie they have an individual connection to each pixel and they are driven by commercial 4 digit LCD drivers. The DPC mode exploits the changes in absorption of a dye dissolved in the liquid crystal to produce an image without the use of polarisers. This mode offers the advantages of wide viewing angle, brightness and colour and requires only a simple diffuse reflector which may be incorporated within the display cell to eliminate parallax. The DPC transmission versus voltage characteristic, however, is not very sharp and does not lend itself to conventional multiplexing but can be driven by WIA, a technique which is applicable when information is sparsely distributed on the display.

In conventional multiplexing of LCDs, unselected elements experience a finite V_{OFF} and for selected elements the ratio $V_{ON}:V_{OFF}$ approaches unity as the number of lines being multiplexed increases. To utilise these voltages, V_{ON} and V_{OFF} must bracket the threshold voltage of the LC and this imposes a requirement on the sharpness of

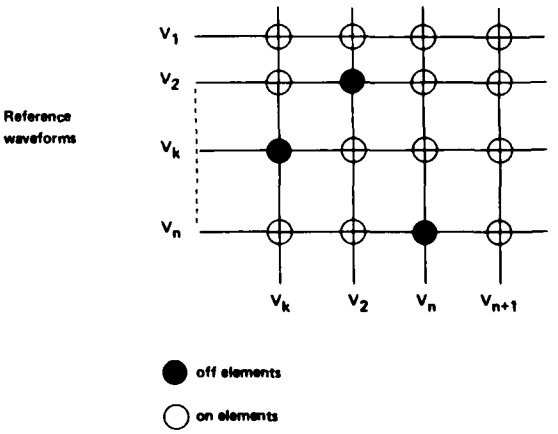

Fig 2 WIA applied to a rectangular matrix

the threshold. WIA, however, has a zero V_{OFF} and hence infinite V_{ON}:V_{OFF} subject to a limited information capability. WIA is based on the correlation properties of a set of waveforms $V_1(t)$ to $V_n(t)$ which have the property that the difference voltage between any two is an a.c. waveform and has a constant rms value. These waveforms can be used to produce a display which is mostly 'on' with selected elements 'off' as shown by figure 2. It should be noted that the PPI display is topologically equivalent to a rectangular matrix.

The set of waveforms, the reference waveforms, are applied simultaneously to the rows. The waveforms applied to the columns are chosen from the reference waveforms and are dependent upon the pixel to be selected. For the first column, the pixel on row k is to be selected so waveform V_k is applied to the column. The desired pixel experiences a zero voltage ($V_k - V_k = 0$) and is 'off' but all other pixels on that column experience a difference voltage ($(V_i - V_k)_{RMS} = V_{ON\ RMS}$) and are 'on'. If an extra reference waveform is available and is applied to a column, then all of the pixels on that column are 'on'. The fundamental information limit in this configuration is that, at most, only one pixel per column can be selected and is a consequence of the column waveform being able to cancel with only one reference waveform but the advantage of an infinite V_{ON}:V_{OFF} is important, particularly if DPC is to be used.

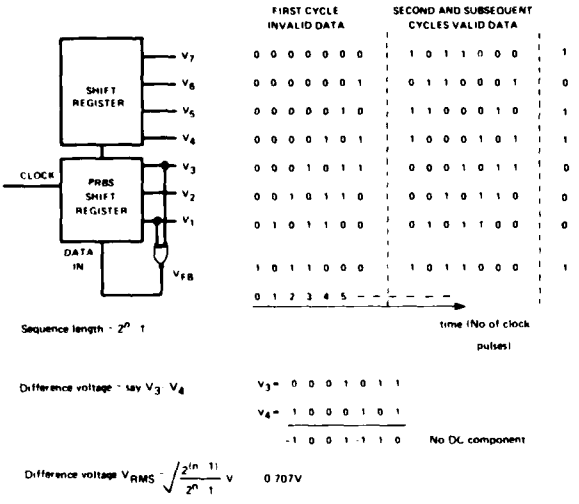

Fig 3 Seven bit PRBS generator illustrating development of the waveforms

One set of waveforms which possess the desired properties is pseudo random binary sequences (PRBS). Alternative sets are Walsh and Paley functions, but PRBS can be generated very simply using a shift register and an exclusive OR or NOR gate to provide a feedback signal as shown in figure 3.

The shift register length (n) determines the sequence length 2^n-1. Since each waveform is one bit phase shifted from the previous one, the full set of waveforms can be generated using an additional shift register. In addition to the required difference voltage, PRBS also possess a $V_{ON\ RMS}$:V_{PEAK} of 0.707 permitting the 6V to 10V RMS voltages necessary for DPC to be achieved using standard CMOS circuitry. The difference waveforms do not have the potentially troublesome lower frequency components produced by Paley functions which, under certain combinations of sequence length and clock rate can show false images.

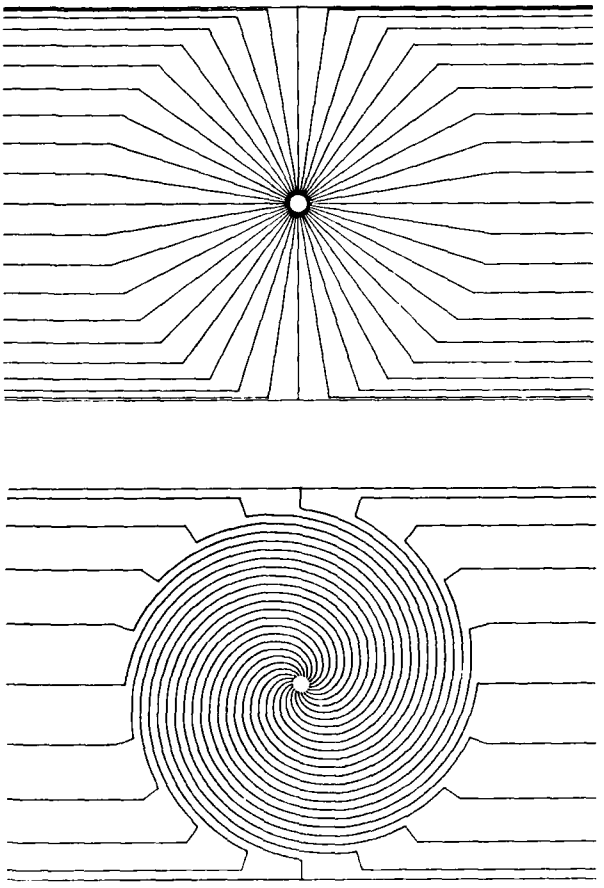

Fig 4 PPI electrode patterns. Only 20 spirals and 40 radials are shown

The circular display uses a novel electrode pattern to produce a PPI format. The simplest such matrix is defined by the intersection of a set of radial elements and a set of concentric circles. This electrode structure is feasible for a sector display but the difficulties of connecting to the innermost circles makes it unsuitable for a 360° display. The solution adopted was to replace the concentric circles with a set of spirals; each spiral starts at the innermost point of a radial and crosses each radial once only and is accessible at the edge of the display. Simplified electrodes are shown in figure 4.

The data (bearing, range) has now to be converted to an equivalent spiral number which will be a function of bearing. There are 60 linear spirals (numbered 0 to 59) and 120 radials (0 to 119) with each spiral n corresponding to two radials 2n, 2n + 1 at the centre. This intersection forms the innermost range gate for those bearings and successive range gates are accessed by moving to consecutive spirals. Thus, for a point (bearing B, range R) the equivalent spiral number S = B/2 + R (modulo 60). For the PPI display the reference waveforms are applied to the spirals giving a limit of one target per radial. The severity of this limit is reduced on the MISER display by magnifying a selectable area onto the X/Y display where several columns are assigned to each magnified bearing allowing multiple targets to be shown in any range cell. The data for both displays is processed by MISER and presented as two independent sets of co-ordinates.

The square X/Y display is defined in a conventional manner by the intersection of a set of sixty horizontal and sixty vertical lines. The numeric displays are simple seven segment electrode patterns, with decimal point and +/- where necessary, over a continuous backplane. The numeric displays are not matrix addressed but are direct drive, ie they have an individual connection to each pixel.

The main displays both have internal reflectors and differ only in their electrode patterns and plate size. The front plate comprises one set of electrodes, either spirals or vertical lines patterned in transparent indium tin oxide (ITO) by photolithography and etching. For ease of etching, the complex electrode patterns are realised using partially oxidised ITO etched by dilute hydrochloric acid, followed by annealing to obtain the high electrical conducitivity and optical transmittance required. The rear plate has either radial or horizontal electrodes patterned in a matt metallic layer to form the electrodes and to provide an internal reflector. This diffuse reflector is produced by lapping a glass plate to roughen the surface followed by a hydroflouric acid etch to reduce the angularity. Aluminium is then evaporated onto the prepared surface to produce a uniform matt layer which is also patterned by photolithography and etching. The metallic electrodes are overcoated with 300A of silicon monoxide to provide a d.c. blocking layer and surface passivation. The prepared plates are assembled using chrome complex homeotropic alignment and a thermo-setting plastic seal with glass fibre spacers to maintain a cell spacing of 9μm. The completed cells are vacuum filled with a commercial black dyed liquid crystal D85 in E63 + 3.5% CB15 (BDH Chemicals). The numeric displays, for which a lower conductivity and hence thinner ITO is adequate, have the electrodes etched in fully oxidised ITO using hydriodic acid. The plates are assembled using rubbed polyimide homogeneous alignment and sealed as previously described. The cells are vacuum filled with E43 + 0.1% CB15 (BDH Chemicals) and are completed with a front polariser and rear polarised reflector in a crossed configuration.

The electronics to drive the PPI display are shown in block form in figure 5. Information to be displayed on the PPI display is presented as a six bit range word and an accompanying external clock pulse and sync pulse from which the bearing is derived by counter 1. This range and bearing data is converted to an equivalent spiral number according to the algorithm by adder 1 and PROM 1 (modulo 60 conversion) and is written into the RAM such that the memory address represents bearing and its contents the equivalent spiral number. The 63 bit PRBS is generated by the 6 bit shift register, clocked into the spiral shift registers and loaded onto the output latches at a frequency C/128 derived from the clock frequency C. The counter 3 maintains a record of the progression of the sequence. The radial waveforms are also output through

shift registers in synchronism with the spiral waveforms but the relationship between consecutive waveforms is no longer a simple phase shift. This is accomplished by clocking the data necessary to construct the waveforms into the shift register at a frequency C and latching the outputs at C/128. The read counter addresses the RAM to present the required spiral number for that bearing to adder 2 where it is summed with counter 3 and addresses PROM 2 (in which is stored the PRBS) to determine the required data bit for that point in time. This data bit is clocked into the radial shift register and the read counter is incremented to the next bearing until all of the radial data bits have been entered. The shift registers are then latched and the RAM interrogation sequence repeated from the first bearing. The electronics to drive the X/Y display are identical to that of the PPI except that the data is stored directly as bearing and range without processing by the algorithm and the count sequences are shortened as there are only 60 bearings. The numeric displays are addressed by commercial direct-drive 4-digit drivers for which the data is also presented serially as a 4 bit word, an accompanying clock pulse and a sync pulse. The 4 bit data is paralled to all of the digit inputs and the appropriate data for any digit is latched under the control of a digit select pulse generated by scanning a logic 1 along a series of shift registers.

A completed display has been successfully built as described. The large area cells have demonstrated an extension in the size and complexity of displays which can be produced intramurally. The viewing angle for the DPC displays is very good being limited only by surface reflections from the glass and the use of an internal reflector produces displays free of image shadow effects associated with other LCD modes. The numeric displays were produced by batch processing and, being directly driven, have good contrast and viewing angle. A second unit is being constructed in which the displays will have both front and rear electrodes of transparent ITO with external

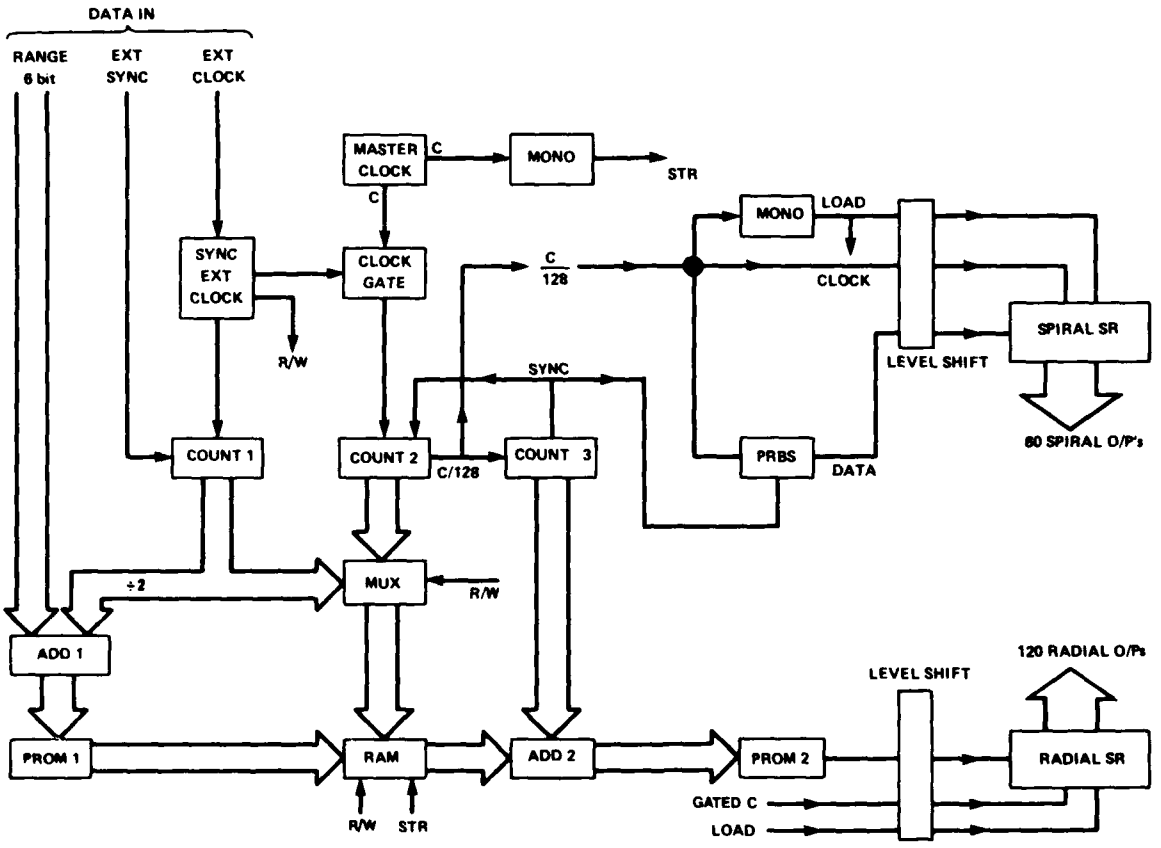

Fig 5 Electronic block diagram for the PPI display

rear trans-flectors to permit backlighting using a.c. EL panels. Future development includes internal reflectors with forward gain to enhance the brightness of the DPC displays and alternative driving schemes which exploit the intrinsic hysteresis of DPC to show multiple targets on a bearing and produce a persistence effect to aid tracking of targets.

The authors gratefully acknowledge the assistance of colleagues at RSRE, particularly the cell fabrication facility. The case and printed circuit boards were produced to a high standard by the mechanical and electronic services of RSRE.

The Authors

John Glasper was born in 1947. He worked with Burroughs for 2 years before joining RSRE in 1968. He obtained an HNC, with endorsements, in electronic engineering in 1971. He has worked on several projects including high power electronics, solid state microwave devices and circuits and CRT phosphors. He joined the displays activity in 1981 and has concentrated on waveform identity addressing of dyed phase change displays.

Charles Smith was born in 1932 and, following service in the Royal Air Force as a Radar Technician, he joined RSRE in 1954. He holds TEC and C & G Certificates in Electronics, and has extensive electronics design experience. In recent years he has specialised in the design and fabrication of research prototypes of novel liquid crystal displays. He had filed several patents and co-authored publications in the displays field.

ULTRA HIGH SPEED MICRO-OPTICAL MODULATORS IN GaAs: THE TEAM AND THE LEAM

D R Wight, P C Allen, J W A Trussler, D P Cooper, D J Esdale and P E Oliver

Abstract

The design and performance of two types of optical modulators utilising the bulk electro-absorption effect are described. Both types are of micron active dimensions and have produced modulation depths of up to 50% without being optimised. The simpler transverse structure has been tested to high frequency operation and is shown to have a flat response from DC to at least 14 GHz. The small size and high frequency performance of these new devices may offer a significant new capability in fast signal transmission and processing electronics.

We report some results from an extensive and continuing research programme on electro-absorption modulators in GaAs. Two types of modulator have been developed (1) the Transverse Electro-Absorption Modulator (TEAM) and (2) the Longitudinal Electro-Absorption Modulator (LEAM). MOCVD epitaxy, selective etching and photolithographic procedures were used to produce devices in which thin single crystal multiple layers of GaAs and GaAlAs are mounted on quartz substrates giving significant transmission of light even for wavelengths shorter than the band edge of GaAs (871 nm). The types of device structures studied are shown in Figure 1. In the TEAM structure an electric field is applied between surface electrodes transverse to the optical path, which

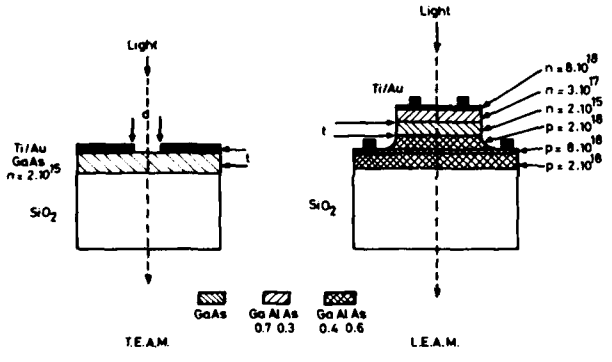

Fig 1 The Transverse (TEAM) and Longitudinal (LEAM) modulators.

produces a broadening of the absorption edge via the electro-absorption effect[1]. This broadening of the edge is due to the reduction of the periodic potential symmetry of the lattice and produces an enhancement of the absorption coefficient (α) at longer wavelengths (Franz-Keldysh Effect) and a reduction in α at wavelengths near that of the Energy Gap. The effect of applying the field is therefore to enhance or decrease the optical transmission of the structure depending on the wavelength of illumination, thus producing optical intensity modulation when AC fields are applied. Since the effect is strongly dependent on field strength, small (5-20μ) electrode spacing structures were used so that relatively low voltages were needed to produce high fields up to the limit set by avalanche breakdown in GaAs ($\sim 3 \times 10^5$ V cm^{-1}). The TEAM devices used to generate figures 2 and 4 had the following critical dimensions:- a) d = 8 μm, t = 2.0 μm. These small electrode gaps inhibit the optical aperture of the TEAM device, so the second structure (LEAM, Figure 1) where the field is applied longitudinally to the optical path, was studied. In the LEAM structure an undoped GaAs active layer is sandwiched between p and n type GaAlAs layers which form optically transparent contact layers and the field is applied by reverse biasing the resulting p-i-n diode. Very thin, highly doped GaAs layers were also employed to allow evaporated metal ohmic contacts to be applied without the need for a high temperature alloying process. The optical aperture in these devices was defined by mesa etching and circular mesas with diameters in the range (60 μm - 250 μm) were produced.

The DC and low frequency performance of the modulators was tested by measuring transmission spectra and applying various levels of DC or AC voltage to one electrode with the other at ground potential. A few microwatts of monochromatic light from a tungsten lamp/grating spectrometer assembly was focussed through the sample and detected with a photomultiplier tube (S1 cathode, 300K). A lock-in amplifier and square wave drive at 1 KHz was typically used to record the transmission changes under applied AC bias, and voltages up to about 30 V could be

sustained without significant leakage currents ($\lesssim$ 3 uA) being observed.

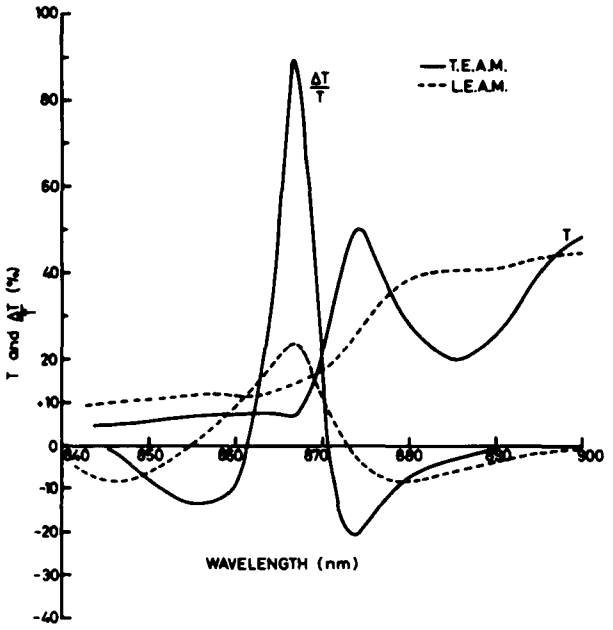

Fig 2 Transmission spectra for the TEAM and LEAM devices at 300K.

Transmission data on the two types of modulator are shown in Figure 2. For the TEAM data 30 V was applied (Field = 3,8 x 10^4 Vcm^{-1}) and for the LEAM 5 V was applied (Field = 3.7 x 10^4 Vcm^{-1}). The zero bias transmission (T) curves for the TEAM modulator show a sharp absorption edge and the minimum at 885 nm is due to an interference fringe. The LEAM device shown had an active width t = 1.3 m (fig 1) and being thinner thus passes more light at short wavelengths but the edge is less sharp due either to the built in field of the p-i-n junction or (more probably) the built in elastic strain due to the presence of the GaAlAs cladding layers. At 867 nm the output modulation depth of the TEAM $(\frac{\Delta T}{T + \Delta T})$ is as high as 50% whereas a value of about 25% is seen for the LEAM structure at an approximately equivalent electric field strength. This difference is due to the thinner active dimension, as well as the degradation of the absorption edge in the LEAM structure. When referred to the "available" input intensity (neglecting reflection losses) a modulation depth of about 20% is deduced from the TEAM results at 875 nm and it is clear that significant low loss modulators can be obtained using bulk electro-absorption structures contrary to other published opinions[2]. It should also be pointed out that the modulators in Figure 1 have not been optimised with respect to modulation efficiency and further improvements can be readily predicted.

Since the electro-absorption mechanism is expected to be extremely fast and, to a first approximation, will not depend on minority carrier lifetime, the high frequency performance of such modulators is of considerable interest. The direct modulation of laser diodes is currently limited to frequencies below about 10 GHz and small external modulators which can perform at these and higher frequencies would thus open up a new capability in ultra high speed signal transmission systems.

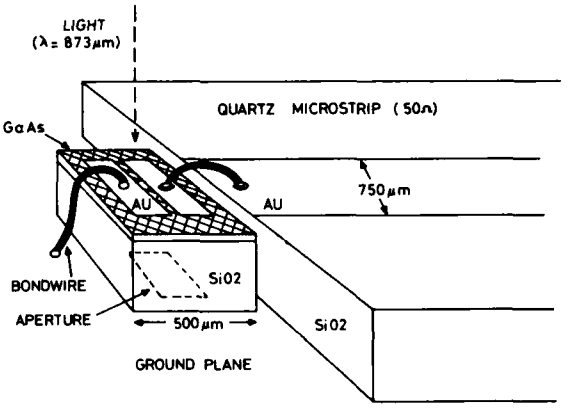

Fig 3 The RF Team device and its microstrip mount.

TEAM devices specially designed to test high frequency performance were made and mounted on a quartz microstrip launcher as shown in Figure 3. At frequencies up to 100 MHz a 50 V (50 Ω) pulse generator was used to apply a square voltage waveform and a few milliwatts of light from a solid state laser was focussed through the modulator and onto a fast (1.5 nS) rise time GaAs photomultiplier tube. The waveform of the modulated optical signal was studied using a sampling oscilloscope (200 pS rise time). The laser wavelength was tuned to the 874 nm response peak (Figure 2) by controlling the temperature of the laser mount. For higher frequency tests the pulse generator was replaced by a RF sweeper and RF amplifier combination where output power into a 50 ohm load was monitored with a 10 dB coupler and RF power meter. The microstrip launcher and modulator was connected in parallel with the 50 ohm load via a short length of high

quality 50 ohm coaxial cable. The detection system was replaced by a high speed p-i-n[3] or Shottky barrier GaAs photodetector fabricated in these laboratories and an RF spectrum analyser was used to measure the received RF electrical power. The detector was biased at -5 Volts using a suitable bias tee and the whole detection system had been previously calibrated and shown to have a flat (± 2 dB), and linear response from DC to 14 GHz. The high frequency limit of this calibration was set by the roll off of the bias tee used.

These RF tests were made without DC bias on the TEAM so that (contrary to the earlier measurements) positive and negative going voltage waveforms were applied to the modulator. Since the TEAM device is symmetrical, the response is the same for positive and negative voltages and a frequency doubling of the modulation was observed which assisted in the suppression of RF pick up in the detector circuit. However, as the test frequency was raised above 1 GHz this problem of RF pick up became serious such that the optically transmitted signal was difficult to measure. The problem was overcome by inserting second harmonic suppression filters in the drive circuit.

The response of the TEAM was approximately linear with applied field for voltages between 5 and 30 V so the modulated waveform could be predicted as a negative going full wave rectified sine wave. It is straightforward to show by Fourier analysis that the second harmonic amplitude is 0.43 times the peak value (P) of this full wave rectified waveform, so the peak modulation depth could be deduced from the AC (RMS) and DC signals received in the detector. A check of the validity of this calculation was made by recognising that mean DC level of the signal reduces by 0.39 P when the RF is applied and measuring this depression. The measurements were made with 1 Watt RF drive, ie a 20 V peak amplitude in the notional full wave rectified electrical waveform (the peak voltage on an open circuit line is twice the travelling wave peak amplitude). Responses for 20 V applied were recorded for all the lower frequency and DC data, so the modulation depth of the optical intensity for this applied voltage could then be obtained over the whole range of frequencies measured, and is shown in Figure 4. It can be seen that the response is flat from DC to 14 GHz where the drop in signal is due to the bias tee roll off. (Note that the frequency scale is changed from linear to logarithmic at 1GHz, and that the drive frequency was half of that shown due to the frequency doubling action of the device).

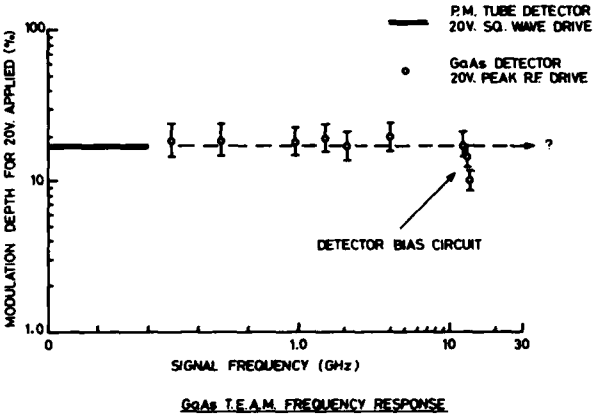

Fig 4 The frequency response characteristics of the TEAM in figure 3.

During the course of this work other workers reported similar studies on multiquantum (MQW) electro-absorption structures which gave similar modulation performance, and response speed was measured using impulse rather than CW testing[4]. The impulse response of the TEAM modulator is difficult to estimate because no sign of a roll off can be detected in Figure 4. However if we assume an RC roll off characteristic with a 3 dB corner frequency of 15 GHz, an upper limit to the full-height-half maximum impulse response of 7 pS is deduced which is considerably shorter than the currently published data on the MQW structures.

In conclusion we can state that TEAM and LEAM devices offer significant performance as micro-optical modulators with speeds in the case of the TEAM that are (at worst) similar to the fastest optical modulators ever reported[5]. Since these new devices will also act as ultra high speed optical detectors and are eminently suitable for insertion into fibre systems or on-chip integration in waveguides, they may be instrumental in opening up a new transmission and signal processing capability in ultra-high-speed electronic systems. Work is in hand to fully optimise these structures and test both device types to higher frequencies so that this new

capability can be further explored.

References

1 ASPNES D E: 'Third derivative modulation spectroscopy with low field electro-relectance', Surface Science, 37, 418-442. (1973).

2 MILLER D A B, CHEMLA D S, DAMEN T C, WOOD T H, BURRUS C A, GOSSARD A C, and WIEGMANN W: 'Novel optical level shifter and self linearised optical modulator using a quantum well self electro-optic effect device', Optics Letters, Vol 9, No 12, 567-569. (1984).

3 ESDALE D J, WIGHT D R, BALL G and OLIVER P E: 'The fabrication and assessment of high speed MOCVD GaAlAs PIN detectors', J Cryst Growth, 68, 461-465. (1984).

4 WOOD T H, BURRUS C A, MILLER D A B, CHELMA D S, DAMEN T C, GOSSARD A C, and WIEGMANN W: 'High speed optical modulation with GaAs/GaAlAs quantum wells in a p-i-n diode structure', App Phys Lett, 44, (1), 16-18. (1984).

5 GEE C M, THURMOND G D, and YEN H W: '17 GHz Bandwidth electro-optic modulator', App Phys Lett, 43, (11), 1, 998-1000. (1983).

The Authors

Don Cooper, Peter Oliver, John Trussler and David Wight each have twenty years or more experience of work in the Scientific Civil Service with the bulk of their careers being spent at the Services Electronics Research Laboratories, Baldock before its transfer to Malvern about four years ago.

Don Cooper and John Trussler have now retired and have most recently been responsible for photolithography and materials/device processing technologies respectively. Peter Oliver has experience in materials growth technologies and has played a pioneering role in the Metal Organic epitaxy process over the past ten years. Phil Allen has spent a few years both at SERL and RSRE and took time off to acquire a BSc at the University of East Anglia, Norwich, he left RSRE in 1984 to work at BP Research Labs. Dan Esdale is a microwave engineer with an interest in optical devices and joined RSRE in 1982 having studied for a PhD and BSc at Leeds University. David Wight obtained a BSc and PhD (1968) in solid state physics at King's College, London and has worked on materials and device physics in GaP (Light Emitting Diodes) GaAs (Photocathodes) and II-VI compound semiconductors.

PHOTOLUMINESCENCE STUDIES OF SILICON GROWN BY MBE

D J Robbins, D B Gasson, R W Hardeman and A D Pitt

Introduction

Molecular beam epitaxy (MBE) is attracting increasing interest as a means of depositing epitaxial Si at temperatures significantly lower than can be achieved by chemical vapour deposition (CVD) from silane and its derivatives[1]. The latter process, which is the basis for all commercial Si epitaxy, involves a pyrolytic reaction and is conventionally carried out at temperatures greater than 1000°C, whereas high quality Si epitaxy can be achieved below 800°C by MBE if the substrate surface is well cleaned prior to deposition. The process of MBE is effectively UHV evaporation of Si, providing independent control of deposition rate and substrate temperature. The practical lower limit to the epitaxial temperature in MBE is then set by defects which are introduced during substrate cleaning and layer deposition, which control the electrical properties of the deposited layer and therefore determine its acceptability for any particular application. In practice reduction in processing temperature is likely to prove very important in future Si technology, reducing thermal stresses as wafer size increases and minimising solid state diffusion to allow fabrication of devices and circuits at submicron feature size. An understanding of defects in Si grown at reduced temperature is therefore essential.

We have undertaken a systematic photoluminescence (PL) study of defects in Si MBE layers, the first time such a study has been reported. Here we outline briefly the use of PL to study three kinds of defects introduced during wafer cleaning and subsequent growth: (i) dislocations in epi-layers nucleated by residual substrate surface oxide, (ii) residual crystallographic damage introduced by sputter-cleaning of the substrate, (iii) carbon incorporated during growth.

Experimental

The MBE samples were grown on 2"-diamter substrates in a VG366 Si MBE equipment[2]. The samples were not intentionally doped, and were typically n-type with a background carrier concentration $\lesssim 5.10^{14}cm^{-3}$. PL spectra were measured at liquid He temperature using 488 nm radiation from an Ar^+ laser and a cooled Ge detector. The interpretation of the spectra depends heavily on correlation with other assessment techniques, particularly transmission electron microscopy (TEM).

Discussion

(i) Incomplete Removal of Substrate Surface Oxide

Good quality epitaxy depends critically on removal of the native oxide from the surface of the substrate Si wafer. If the oxide is in its normal stable form (SiO_2) then at the reduced temperartures of interest (typically <850°C) it can only be removed by a chemical[3-5] or physical[6,7] etching process. We have investigated reactive etching by an impinging Si atomic beam in UHV[3,8], according to the reaction:

$$SiO_2 + Si \longrightarrow 2SiO \uparrow$$

This process is attractive since it involves no'foreign' atoms. We have studied the kinetics of this process using transient mass spectrometry and X-ray photoelectron spectroscopy (XPS) and shown it to be thermally activated with an activation energy $E_A \sim 3.9$ eV[9]. For an impinging Si flux of $\sim 5.10^{14}$ atoms cm^{-2} s^{-1}, equivalent to a deposition rate ~ 0.1 nm s^{-1}, the etching reaction is complete within a few seconds when the substrate temperature $T_s \gtrsim 800$°C. At this temperature the oxide is efficiently removed before Si deposition begins, producing a good quality layer free of extended defects as measured by TEM. However at lower temperature the etching rate is decreased and with the same impinging flux the etching is not completed before a Si layer nucleates and grows over the residual oxide. This leads to a heavily-dislocated layer in TEM.

This difference in nucleation of the MBE layers has a marked effect on their PL spectra, as illustrated in Figure 1. The

spectra of layers grown at 850°C and 900°C, which should be free of extended defects, show only impurity bound exciton luminescence close to the Si band gap of 1.17 eV, which is attributable to excitation of the substrate wafer material; of particular interest here is the absence of significant deeper luminescence in these layers. However the spectra of layers grown at 625°C and 750°C, which would be expected to have a high density of dislocations and microtwins, are dominated by deep luminescence bands in the range 0.8-1.0 eV. The principal bands, labelled D1-D4, are analogous to bands observed in plastically-deformed bulk Si and are the characteristic PL signature of a relaxed dislocation network[10].

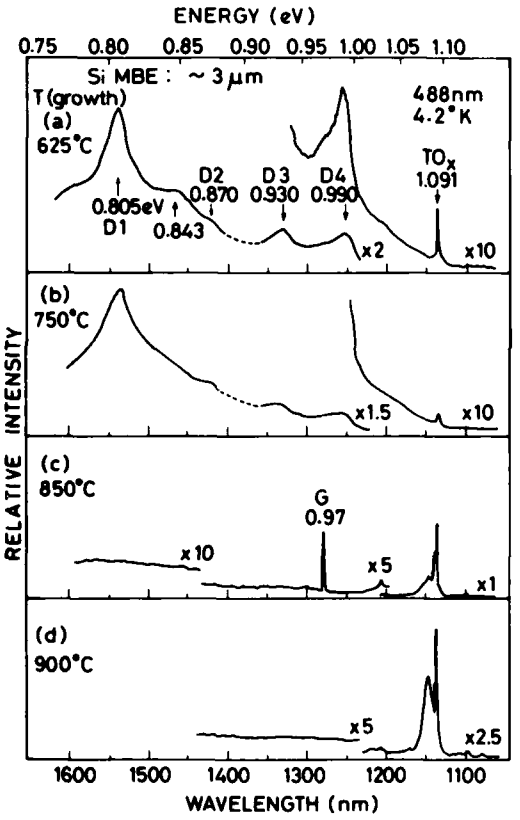

Fig 1 PL of layers grown at different temperatures on substrates with native oxide

(ii) Residual Ion-Damage From Sputter Cleaning

A second method for removal of substrate surface oxide is physical etching by bombardment with rare gas ions[6]. In order to minimise lattice damage we use Ne^+ ions[7], typically at 5-6 kV and 1 μA cm^{-2}. The oxide is removed below the detection limit for XPS by a 2.5 minute irradiation under these conditions. The surface is rendered amorphous, but is observed to reconstruct by electron diffraction (RHEED) at ~620°C, when implanted Ne atoms are evolved from the wafer surface. If subsequent annealing and deposition takes place at 750°C, TEM reveals a band of crystallographic damage (mainly small dislocation loops) extending ~30 nm below the epi-layer/substrate interface caused by the Ne^+ implantation. This damage is removed from substrates annealed at 900°C.

The PL spectra of MBE layers up to several microns thickness grown on ion-cleaned substrates at temperatures < 850°C are very distinctive in showing a pair of bands, labelled D5 and D6, with peak energies in the ranges, 0.951 ± 0.006 eV and 1.011 ± 0.006 eV respectively. These bands also have analogues in bulk Si deformed under particular conditions[10]. The peak energies and band shapes in MBE material vary slightly between samples, but the separation between the two bands remains almost constant, 59 ± 3 meV. Figure 2 shows the spectra of two layers of similar thickness

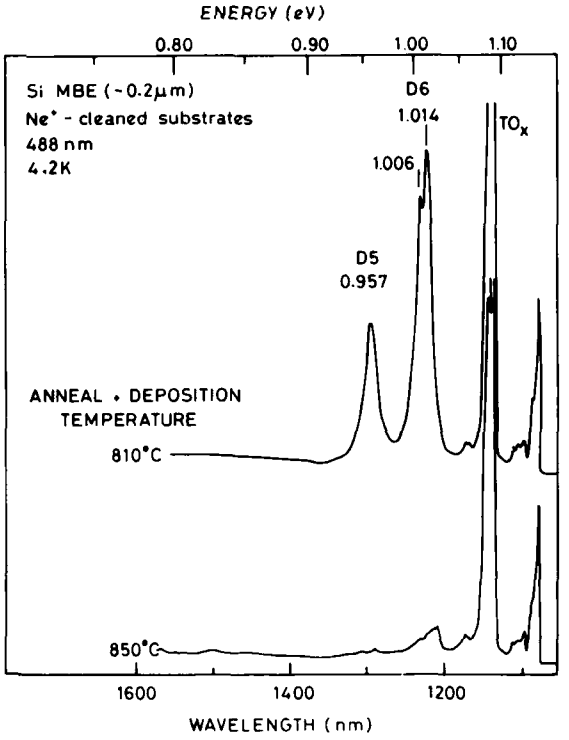

Fig 2 PL of layers grown at 810°C and 850°C on sputter-cleaned substrates

grown at different temperatures on ion-cleaned substrates, and illustrates the effect of annealing. The layer grown at 810°C shows the D5 and D6 luminescence bands, with the latter unusually resolved into two components in this case. The layer grown at 850°C does not show these bands, and they are similarly absent from layers grown at 750°C on substrates which had been annealed at 900°C, and which TEM showed to be free of the residual crystallographic damage produced by Ne^+ implantation. This correlated annealing behaviour of features in PL and TEM is strong evidence that the luminescence bands D5 and D6 originate from defects associated with the residual ion damage, and that their presence is an indication of incomplete annealing of this damage.

(iii) Carbon Contamination During Growth

Incorporation of carbon from components in the vacuum chamber or from the substrate wafer is a major source of background acceptor doping in GaAs layers grown by MBE[11]. The possibility of a similar incorporation process in Si MBE has not received much attention, presumably because in a Group IV elemental semiconductor substitutional C atoms are not electrically-active in first order. However carbon can associate with other impurities and defects and can form electrically-active complexes in subsequent processing or under the influence of irradiation. We have demonstrated incorporation of carbon from the vacuum ambient by repeated interruption of growth to allow accumulation on the layer surface; peaks in carbon concentration corresponding to the points of interruption can then be detected in subsequent profiling of the layer by secondary-ion mass spectrometry (SIMS).

However the presence of carbon is difficult to detect below ~10 ppm in epitaxial layers. The detection limit in SIMS is in general $>10^{17}$ cm^{-3}, and the thickness of the layers is usually too small to allow detection by IR absorption. We have devised a technique which appears useful for detecting the presence of low levels of carbon in epitaxial layers, at least on a semi-quantitative basis. This technique involves two stages:

1. the MBE layer is irradiated by a 20 kV electron beam to generate an optically-active carbon complex with a characteristic PL spectrum.
2. the intensity of the induced carbon-related luminescence is measured and compared with the intensity from a reference sample of bulk Si which has undergone identical irradiation and for which the carbon concentration is known from IR measurements.

The penetration depth of the 20 kV electron beam is ~ 2.5 μm, ensuring that only the near-surface region is activated. If the MBE layer thickness is greater than this only the epitaxial material should be probed.

Figure 3 shows the spectrum of an MBE layer before and after e-beam irradiation. This sample was grown at 750°C on an ion-cleaned substrate and therefore shows the bands D5 and D6 in its as-grown condition. After irradiation an additional line at 0.97 eV is evident. This is the so-called G-line, much studied in bulk Si which has been subjected to high energy ionising radiation[12]; our work represents the first observation of this spectrum by relatively low energy irradiation. The defect responsible for the luminescence is known to be a complex involving a pair of substitutional C atoms with a neighbouring interstitial Si atom[13]. There may also be slight changes in relative intensity of other spectral bands after

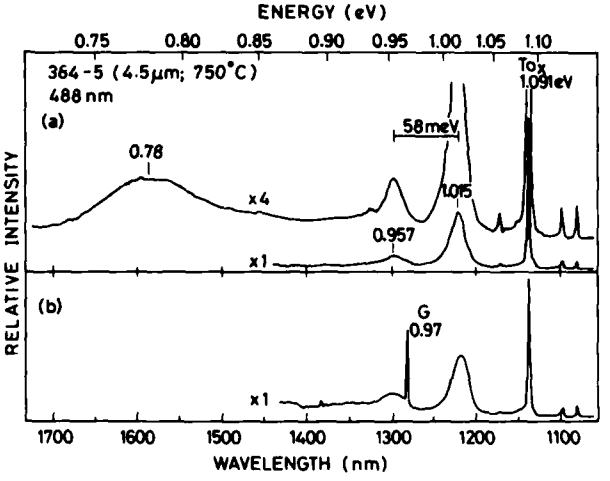

Fig 3 (a) PL of a layer on a sputter-cleaned substrate

(b) Spectrum after e-beam irradiation (20 kV, 5 min)

irradiation, but these are comparatively small as demonstrated by comparison of Figures 3(a) and 3(b).

Figure 4 is a plot of the observed G-line intensity vs. carbon concentration as determined by IR absorption for a series of bulk Si samples. Two e-beam irradiation times were used and the data normalised for the sample containing 2.10^{17} C atoms cm^{-3}. Also shown are ranges of relative intensity of G-line luminescence from MBE layers and from an epitaxial layer grown by CVD, all of which have a residual carrier concentration $<2.10^{16}$ cm^{-3}. The results indicate significantly higher intensity for the MBE material, which suggests a higher level of carbon incorporation.

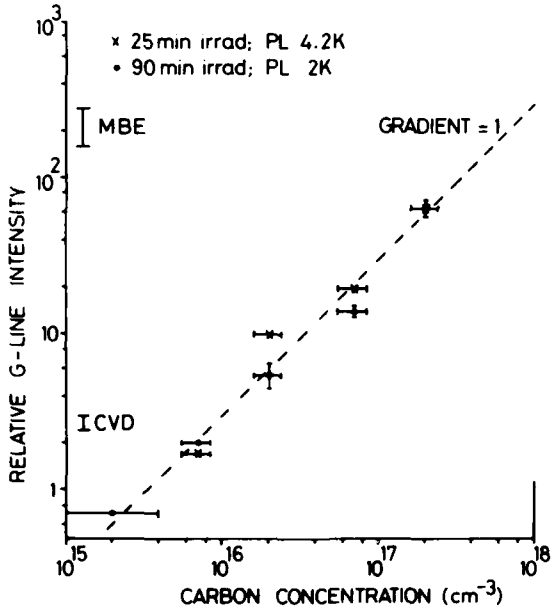

Fig 4 G-line intensity vs carbon concentration for bulk samples. Relative intensities for MBE and CVD samples are indicated

Clearly there is a good correlation between G-line intensity and measured carbon concentration for the bulk samples, suggesting that the technique is capable of giving semi-quantitative information. However a number of points must be borne in mind when applying this method. First, PL is a difficult technique to apply quantitatively, so there will always be some uncertainty even in relative intensities. Secondly, it is possible that carbon is incorporated and distributed differently in MBE and CVD layers compared with bulk Si, so the sensitivity to the e-beam irradiation may be different in the different materials. Thirdly, the technique may only be useful for layers in which the level of other impurities is relatively low. There is evidence that in heavily-doped layers ($>10^{18}$ cm^{-3} B) the active complex is not induced by the e-beam irradiation, possibly due to inhibition of the formation mechanism in the presence of an excess of other impurities. Nonetheless this PL technique is at present the only technique for sampling carbon at low levels in thin Si MBE layers.

Acknowledgements

Thanks are due to N G Chew and A G Cullis for the TEM measurements used in interpretation of the PL data, to R Series for supply of the bulk Si with measured carbon concentration, to L Reed for assistance in setting up the PL measurements, and to R A A Kubiak (City of London Polytechnic) who supplied the B-doped MBE layers. The contribution of W Bardsley in initiating the Si MBE project in this laboratory is also acknowledged.

References

1. Y Ota Thin Solid Films 106 1 (1983).

2. W Bardsley and K G Barraclough RSRE Newsletter and Research Review 6 51 (1982).

3. M Tabe Jap J Appl Phys 21 534 (1982).

4. S Wright and H Kroemer Appl Phys Lett 36 210 (1980).

5. H T Yang and W S Berry J Vac Sci Technol B 2 206 (1984).

6. J C Bean, G E Becker, P M Petroff and T E Seidel J Appl Phys 48 907 (1977).

7. I Yamada, D Marton and F W Saris Appl Phys Lett 37 563 (1980).

8. T Yonehara, S Yoshioka and S Miyazaira J Appl Phys 53 6839 (1982).

9. R W Hardeman, D J Robbins, D B Gasson and A Daw Proc 1st Int Symp on Si MBE, Electrochem Soc Spring Meeting, Toronto (May 1985).

10. R Sauer, J Weber, J Stolz, E R Weber, K-H Kusters and H Alexander Appl Phys A 36 1 (1985).

11. M Heiblum, E E Mendez and L Osterling J Appl Phys 54 6982 (1983).

12. G Davies, E C Lightowlers, M C do Carmo, J G Wilkes and G R Wolstenholme Solid State Commun. 50 1057 (1984).

13. K P O'Donnell, K M Lee and G D Watkins Physica 116B 258 (1983).

The Authors

D J Robbins graduated from Cambridge University in 1968 and obtained his PhD degree from the University of East Anglia in 1971. He held an SRC Personal Fellowship at Oxford before joining RSRE in 1973. He worked on luminescence of phosphor and semiconductor materials until 1981, when he took sabbatical leave at IBM Research Laboratories, Yorktown Heights, New York. Since 1983 he has been leader of the section studying techniques for deposition of silicon at reduced temperatures.

D B Gasson has been with RSRE for 20 years, working on growth of oxide crystals for lasers and more recently on Si materials. Previously he worked at AEI Laboratories at Aldermaston on bulk Si growth and on MBE.

R W Hardeman graduated in 1976 from University of Cambridge in Metallurgy and Materials Science and worked for two years with British Steel Corporation as a Graduate Metallurgist. After PhD research again at Cambridge he joined RSRE in 1981 and has worked on silicon molecular-beam epitaxy with particular interests in surface analysis.

A D Pitt joined RSRE in 1978, and since 1982, has been working on Semi-conductor Luminescence. He is also presently studying for HTEC in Applied Physics at Gloucester College of Art and Technology.

HISTORICAL REVIEW

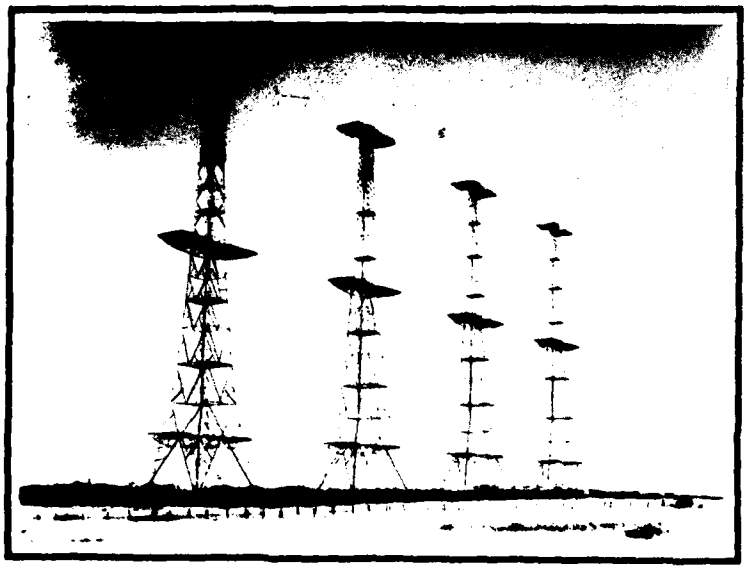

HISTORY OF THE RSRE

E H Putley

This article shows how RSRE was formed from the amalgamation of research establishments involved in the development of radar for the second world war, and how its expertise in electronics, optics and computing has led to a key role in developing British military technology and increasingly giving a lead to industry.

The Royal Signals and Radar Establishment is the main centre for research and development of electronic devices and techniques within the Ministry of Defence. The advanced technology pioneered by RSRE is utilised by British industry to provide equipment for the armed forces but the essential research foundation is sufficiently broad to provide a useful base for much civil development with considerable benefit to the national economy.

RSRE was formed in 1976 by the amalgamation of three earlier MOD establishments: the Royal Radar Establishment (RRE) at Malvern, the Signals Research and Development Establishment (SRDE) at Christchurch and the Services Electronics Research Laboratory (SERL) at Baldock. By the end of 1980 the establishment had been concentrated at Malvern, although the former airfields at Defford and Pershore are still in use for work requiring more space or isolation than can be provided at Malvern.

The establishments amalgamated in 1976 to form RSRE had themselves evolved from earlier military research stations some of which could trace their history to the first world war or even earlier. This is illustrated by a simplified chronology (figure 1).

The events which ultimately shaped the present establishment and indeed led to the growth of modern electronics occurred in the middle 1930s. At that time, with the threat of the second world war rapidly growing, many people - military experts and politicians as well as scientists and ordinary citizens - were preoccupied with the fear of air attack. Most could see little hope of defence against the bomber, but Britain was fortunate that a group of scientists and senior RAF officers at the Air Ministry was not prepared to accept such a pallid view. Nevertheless, they did not themselves at first see an answer to the problem. After Mr A P Rowe (who at that time was assistant to the Air Ministry Director of Scientific Research, Dr H E Wimperis) had made a personal study of all the relevant files on air defence, he suggested to his Director that the only hope was to search for a new approach and proposed that they should seek the advice of an independent group of eminent scientists. Wimperis gained the support of the Air Minister for this suggestion and as a result a small committee chaired by Tizard was set up. The original members were H T Tizard, A V Hill and P M S Blackett, all scientists with military experience, and with Wimperis and Rowe (secretary) representing the Air Ministry.

The Tizard committee decided to start work by ridding themselves of a problem which at that time was continually plaguing military scientists. This was the 'death ray menace'. The menace was not that any death rays existed but that swarms of inventors (some honest, many not) were claiming the discovery of new wonder rays. A lot of time was being wasted in investigating these claims. The Tizard committee therefore approached Watson-Watt who then was in charge of the DSIR's Radio Research Laboratory at Slough (an outstation of NPL, see Pyatt 1984) to advise them whether or not electromagnetic energy could be transmitted with sufficient intensity to cause injury or damage at great distance. Watson-Watt asked one of his colleagues, A F Wilkins, to make a simple calculation which showed that this idea was completely impracticable. Wilkins, however, reminded Watson-Watt that the Post Office Research Laboratory at Dollis Hill and the Bell Telephone Laboratories had recently noted that the passage of aircraft through the beams of short-wave communication transmitters could be detected. Watson-Watt therefore replied to the Tizard committee that whilst they could discount the possibility of a radiation weapon there was a good prospect of developing an aircraft detection system.

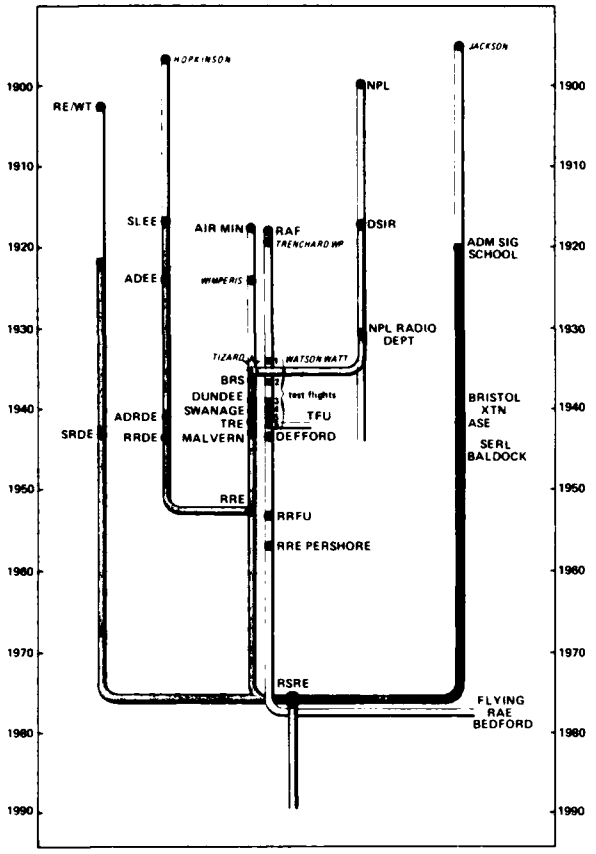

Fig 1 Origins of RSRE

The story began with the formation of the Air Ministry and the RAF in 1918. In 1919 Trenchard, then Chief of the Air Staff, wrote a White Paper laying down the lines of development for the RAF in which he emphasised the importance of scientific research. In 1924 Dr H E Wimperis was appointed Director of Research with a broad speculative brief. This did not make him or his assistant, Mr A P Rowe, popular with the orthodox but it led to Sir Henry Tizard's committee in 1935. This brought together many of the older strands. In 1895 Captain H B Jackson had begun the Navy's interest in

* * *

At this time the only method for obtaining early warning of aircraft was by detecting the sound of the engines. Despite the valiant attempts of the army scientists to exploit this technique to the full, the rapidly increasing speed of aircraft was making their task impossible. Watson-Watt was asked therefore to demonstrate radio detection and, with the aid of Wilkins, he did so early in 1935 detecting a Heyford bomber by the signal reflected by it from the BBC transmitter at Daventry.

The response of the Air Ministry to Watson-Watt's demonstration was immediate and generous support for a secret research programme to develop a system of radio location of aircraft that would provide the RAF with sufficient early warning of an approaching attack. Initially Watson-Watt,

Abbreviations

ADEE - Air Defence Experimental Establishment; ADRDE - Air Defence Research and Development Establishment; ASE - Admiralty Signals Establishment; BRS - Bawdsey Research Station; DSIR - Department of Scientific and Industrial Research; NPL - National Physical Laboratory; RAE - Royal Aircraft Establishment; RAF - Royal Air Force; RE - Royal Engineers; RRDE - Radar Research and Development Establishment; RRE - Radar Research Establishment (after 1957 Royal Radar Establishment); RRFU - Radar Research Flying Unit (RAF); RSRE - Royal Signals and Radar Establishment; SEE - Signals Experimental Establishment; SERL - Services Electronics Research Laboratory; SLEE - Search Light Experimental Establishment; SRDE - Signals Research and Development Establishment; TFU - Telecommunications Flying Unit (RAF); TRE - Telecommunications Research Establishment. Exptl flights: Experimental flying units provided by the RAF for radar research: 1, First radio detection of Heyford from Farnborough; 2, First ground-controlled interception using radar, 32 Squadron Biggin Hill; 3, RAF Martlesham Heath; 4, RAF Scone and St Athan; 5 RAF Christchurch; 6, RAF Hurn.

☼ ☼ ☼ ☼ ☼

radio that led directly to SERL but in 1919 (by then Admiral of the Fleet Sir Henry) he had advised DSIR to undertake the fundamental studies of radio propagation which formed the prelude to Watson-Watt's radar work. The army's interests can be traced back to the Royal Engineers' experiments with radio and with searchlights and other electrical devices initiated by Professor J Hopkinson. The army was responsible for some aspects of air defence that at times brought them in conflict with the RAF but with the emergence of radar the different parties drew closer together, ultimately forming RRE.

* * *

Wilkins and several other members of the Slough Laboratory were seconded to an Air Ministry site at Orford Ness. Later as they recruited further staff they were transferred to the Air Ministry and larger premises were obtained at Bawdsey, near Felixstowe. In 1938 Watson-Watt moved to the Air Ministry and A P Rowe took over Bawdsey, remaining in charge until the end of the war. This was the origin of what later became TRE and arrived at Malvern in 1942 to form the nucleus which eventually developed into RSRE.

The birth of TRE has been described at some length not only because it formed the central nub around which RSRE has evolved but more importantly it was at the heart of the development of a new branch of science - modern electronics. The part played by

The First British Radar

The first operational British radar, the Air Ministry Experimental Station Type 1 (AMESS Type 1) more commonly known as the Chain Home or CH, was derived from the apparatus used by Watson-Watt and his colleagues to measure the height of the ionosphere. In its final form it operated on a wavelength around 10-20m, somewhat shorter than originally used for ionospheric research. The wavelength finally chosen represented a compromise between the need for a short wavelength to give sufficient angular discrimination with a finite-sized aerial for the accurate determination of the bearing and elevation of the target and the need for a sufficiently powerful transmitter to enable single aircraft to be detected at ranges out to 200 miles (320 km). Watson-Watt fully appreciated the desirability of using much shorter wavelengths but did not believe the necessary valves and components could be developed in time.

The first CH stations were in use in 1938 before the Munich crisis. The transmitting aerial consisted of a stack of six to eight horizontal full-wave dipoles backed by a corresponding stack of reflectors. This arrangement floodlit an area out to sea in front of the station, the amount of radiation transmitted inland being minimised by careful adjustment of the reflectors. The transmitting aerial array was slung between 360 ft (110m) steel towers which for many years were such a prominent feature in coastal districts. The receiving aerials were made up of several groups of dipoles and reflectors mounted on 240 ft (73m) wooden towers. The transmitted beam was fixed and bearings were determined by comparing the signals from different pairs of receiving dipoles. By using a pair of crossed dipoles the azimuth could be determined whilst by using pairs mounted at different heights up the tower the elevation could be found.

The main weakness of this system was that its performance at low altitudes (less than 1000 ft, 305m) was poor. By 1940 it had been backed up by the CHL (Chain Home Low) operating on 1.5m wavelength and later in the war (about 1943) even lower coverage was provided by 10 cm wavelength installations. The vital part the CH played in the Battle of Britain is well known, but what is usually overlooked is that despite the introduction of newer radar systems during the course of the war the CH remained the main component of the British early warning system throughout.

In 1944, as the war neared its end, the CH found two remarkable new applications. The first was its use to detect the flight of the V2 rockets. The interception of these missiles was of course out of the question but by measuring the range of launch from several stations (the flight time was too short for bearing determination) the launch sites could be located for subsequent attack. The second application of the CH at the end of the war was made by the enemy. By 1944 their own early warning radar covering the North Sea had been put out of action, by jamming or by aerial attack. However they found that from the coast of north Europe they could detect not only the direct signals from the CH transmitters but also signals reflected from aircraft over the North Sea or south-east England. The time delay between the direct and reflected signals defines an ellipse on which the reflector must be located. By also taking a bearing on the reflected signal the precise position of the target is then determined. A German installation using this method (known as Kleine Heidelberg) was first installed at Boulogne but was later moved to north Holland where it remained in use until the capitulation of the German forces in Holland. Another installation was also built in Denmark.

It was the success of the CH which inspired and impelled the later developments in radar but of these original installations little now remains apart from a few museum relics.

New Valves for Radar

It was clear from the start that the potentialities of radar could only be exploited by using much shorter wavelengths than that of the CH. Rangefinders for naval guns and locators for anti-aircraft guns were obvious requirements. A more novel one was the fitting of radar sets in aircraft. The initial need for this arose because the CH could only locate a target to within about a mile (roughly 1½ km). This was quite good enough for daytime air attacks from large formations which our fighters could easily see at that distance but useless for locating individual aircraft at night or in cloudy weather. Hence the need was foreseen for airborne equipment. Since the size of aerial array that an aircraft could carry was severely limited, it was evident that a wavelength of only a few centimetres was ideally required.

In 1936, when this work started, research on centimetre-length waves was being carried out in America, Europe and in Japan but none of it looked sufficiently promising to be of military value. Attempts were also being made to evolve types of triode that could operate down to a few tens of centimetres, although these did not look very encouraging either. At this point the collaboration between Bawdsey and the Admiralty Signals School Valve Laboratory began.

The first task undertaken by the Admiralty for radar was the development of improved transmitter valves for the CH. A programme for shorter-wave valves was then planned. Attempting to forecast the effort required for a worthwhile reduction in wavelength against the shortening timescale of international crisis, it was decided to aim for 50 cm valves, even though ideally a shorter wavelength would be preferred, especially for the airborne requirements. By this time the Admiralty valve laboratory was fully committed to the silica valves designed for the CH. The Admiralty began a collaborative programme with industry, initially with the GEC Research Laboratory at Wembley. GEC had already begun research on centimetre-wavelength magnetrons and was developing new types of valve design to aid in the production of the CH valves. In a short time GEC in collaboration with the Admiralty produced the first of the micropup series of decimetre triodes. This valve enabled the Admiralty radar group to design the first British naval rangefinders that were later to play a vital part in engagements between surface ships. It was found that the micropup was very useful at 1.5m and that versions of it could be made to operate down to about 25 cm (figure 2).

The 1.5m valve was used in the first successful British airborne radars, the first ASV (air-to-surface-vessel) systems used in the Battle of the Atlantic and the first AI (air interception) used by our night fighters in the blitz. It was also used in Oboe, the precision bombing aid, and in a number of mobile ground radar systems mainly used overseas. This valve was included in the 'black box' taken to America by the Tizard mission in 1940.

With the outbreak of war in 1939 the effort on valve research was greatly expanded with the help of university groups, working under the overall co-ordination of the Admiralty research group. The most outstanding success of these groups was the invention by Randall and Boot at Birmingham of the resonant cavity magnetron. This provided the missing link that made the exploitation of the 10-1 cm waveband a practical proposition. The invention of this valve has been described in detail many times already. It was probably the most significant advance in electronics resulting from the radar programme. One aspect of its story may not have been stressed sufficiently in earlier accounts - the speed with which the original laboratory model was turned into an engineered product. GEC was mainly responsible for this but one reason was that its earlier independent research programme coupled with the collaborative (CVD) Admiralty programme on the decimetre valves had provided the company with the techniques and expertise to produce the new magnetron very quickly.

Thus we see that the Bawdsey Admiralty valve research programme, planned in conformity with Watson-Watt's principle of the third best (we never achieve the perfect. The second best takes too long. Therefore if we need it now we must be content with the third best), not only led to the timely development of the valves required for the first airborne and naval radars but also laid foundations that enabled the unexpected arrival of the first best to be exploited immediately without that delay that often follows a major invention whilst its significance becomes fully appreciated.

Watson-Watt and the early TRE in the development of radar has been misunderstood by several recent commentators who have pointed out, quite correctly, that radar development was taking place before 1939 in the secret laboratories of all the major participants in the second world war and that in many details the work elsewhere preceded or was more advanced technically than the early British work. The British secret invention was not just the radar itself, important though this was, but the employment for the first time of a scientific attack on a specific military problem, that of designing a system for the most effective deployment of fighter aircraft for defence against bomber attack. After the successful demonstration of this system in 1940 General Adolf Galland (1955), who was both a skilful flyer and a penetrating analyst of aerial warfare, commented that it had taken the Germans completely by surprise even though they themselves had been using radar from the outbreak of the war.

The War Years

Before 1939 the progress of TRE (or the Bawdsey Research Station as it was called then) began to react upon other British military laboratories. In the first place the programme on the development of sound locators was brought to a halt. Then others became interested in the possibility of applying the new radio technique to their own problems. A most fruitful collaboration began with the Royal Naval Scientific

Fig 2 Micropup triodes

The valve on the left is a VT90. Designed for 1.5 m wavelength it went into production in 1939. It was used in AI Mk II and all the remaining 1.5 m AIS and in all the 1.5m ASVS, in Oboe and in mobile ground radars. The valve on the right is an NT99 which was the main 50 cm transmitter valve. It was used in the naval radars and it was also used in the fighter control radars used by the RAF for the D-Day operations in 1944. A pair of these valves in push-pull gave up to 100 kW (peak) output. The overall length of the valves (excluding leads) is approximately 10cm.

Service. An outstanding naval problem was rangefinding for the heavy guns of the capital ships. The standard equipment in 1939 was the optical rangefinder, but this suffered from two serious defects. Firstly, the percentage error increased with range and secondly it could only be used in daylight with clear visibility. With gun ranges approaching 20 miles (32 km) they were thus unreliable when they were most needed. The radar technique offered a solution. Simple optical considerations show that to obtain the precision of location of a target necessary for an artillery rangefinder the aerial system would need to be many wavelengths in dimensions. Therefore if it were to be sufficiently small to be accommodated on a ship or an aircraft or to be mobile in the field a much shorter wavelength would have to be used than was immediately practicable in 1936.

The naval laboratories were already involved in the development of high-power transmitting valves for communications systems. They therefore undertook the development of improved valves firstly for Watson-Watt's original radar system and secondly for much shorter wavelengths. Realising that for this task to succeed the collaboration of the valve manufacturers would be essential, the naval research department began a programme of collaboration with first GEC and later other manufacturers. This was the origin of CVD*, a collaborative enterprise between the MOD and industrial electronics companies which today plays a major part in British electronics research.

**The initials CVD now stand for Components, Valves and Devices. For a long time they meant Coordination of Valve Development but their original meaning in 1938 (apparently like Radio Direction Finding, RDF, to confuse the enemy) was USW Communication: Valve Development.*

The extended Admiralty programme on new valves led to an expansion of the valve laboratory which on the outbreak of war was further expanded and broadened to include university groups, particularly at Bristol, Birmingham and Oxford. At the end of the war this activity was concentrated at SERL, Baldock, where it remained until its incorporation into RSRE. The immediate result of the collaboration was the development of a series of new valves for radar, including the cavity magnetron. These made possible not only the radar which contributed to the destruction of the Bismarck and the Scharnhorst but also gave Britain a world lead in the development of airborne radar, starting with the first radar for night fighters (AI) in 1939 and going on the the anti-submarine radars and the ground-mapping radars (H2S) used at the end of the war.

The army also had an interest in artillery control radars particularly for anti-aircraft guns, but also for coast defence artillery. Scientists from the War Office laboratories were brought into radar development at the end of 1936. They later formed the Air Defence Research and Development Establishment (ADRDE), afterwards renamed Radar Research and Development Establishment Establishment (RRDE), which came to Malvern with TRE in 1942 and which in 1953 was merged with TRE to form RRE (the Radar Research Establishment, later the Royal Radar Establishment), one of the components of RSRE. The third component of RSRE was originally concerned with the

Solid State Physics

Electronics in the 1940s was almost entirely dependent upon the thermionic vacuum tube, or in normal English parlance, valve. The re-emergence of the silicon 'cat's whisker' detector for centimetre waves was a then unsuspected precursor of modern technology but it was not this which caused the growth of solid state physics after 1945. Ever since Lindemann (later Lord Cherwell) had proposed it in 1914, there had been an interest in infrared as a means of detecting ships, aircraft and general military activity. There had been a small amount of British work on this for many years, and like radar, this topic had also been pursued in secrecy by all the main military powers. Unfortunately, progress had been restricted because the only effective detectors of thermal radiation (roughly the band 3-15 μm) were thermopiles which were too slow and too delicate for practical use. About 1944 the Allies discovered that the Germans had succeeded in making photoconductive infrared detectors using both natural galena and chemically deposited layers of lead sulphide. This resulted in a resurgence of interest in infrared.

Although the lead sulphide cell attracted wide interest it left a lot to be desired. Its spectral response extended only to about 3.5 μm so that it only just reached the band of interest. Manufacture was an art rather than a science. What was needed was a research programme to establish fundamental principles and to lead to photoconductors sensitive to longer wavelengths, to 10 μm or beyond. The significance of 10 μm is that the black body radiation from a source at normal ambient temperature peaks around there and also it is at the centre of an atmospheric transmission band.

To R A Smith and G G MacFarlane the study of the PbS detector seemed a most appropriate subject for the new TRE physics department. By 1945 study of the German manufacturing process had enabled us to produce PbS cells but MacFarlane (1948) in a short unpublished memo proposed that systematic research should be based on the growth of single crystals and the study of their electrical and optical properties. By about 1950 W D Lawson had grown single crystals of the related compounds lead selenide and telluride (Lawson 1951). At that time most other semiconductor research groups were still using polycrystalline material. The use of single-crystal materials is now taken for granted. RSRE still continues to pioneer techniques for preparing new and better quality electronic materials. After the lead salts considerable study was made of III-V compounds of which gallium arsenide is probably now the best known example.

To return to the infrared, Lawson's research eventually led to the discovery of a 10 μm photoconductor, the mixed compound cadmium mercury telluride. This is now the most commonly used detector material for the 10 μm band. After the initial discovery, the impetus of research on this material shifted to the USA for some years but more recently RSRE has made major contributions to infrared technology both in the basic design of thermal imagers and in novel cadmium mercury telluride detector configurations (Putley 1984).

Technology Transfer

At least since the days of Wedgewood-Benn's Ministry of Technology the transfer of technology from research centres to gainful employment by industry has been recognised as one of the major problems the British economy has to solve. Although a lot is said about fallout from defence research the objective measurement of the contribution made by laboratories such as RSRE is difficult. One indicator that at least points to areas where significant contributions have been made is the scheme of Awards to Industry for Technological Achievement sponsored by HM the Queen. To qualify, work must not only represent a technological advance but it must also be of demonstrable economic value. At first these awards were confined to manufacturers but to recognise the importance of technology transfer from research to manufacture the research laboratories who have collaborated with industry are now also eligible. In the last few years RSRE has received five awards.

One of the first products of this collaboration was the Malvern Correlator in which fundamental research on photon scattering statistics was exploited. It provides a method of measuring motion, from that of ships to that of molecules, by studying the scattered light from the target. Its applications range from mechanical and aeronautical engineering to molecular biology and medicine (Pike 1979). The industrial development was carried out by Malvern Instruments. In 1977 the company received the Queen's Award for Technological Achievement and, jointly with RSRE, the MacRobert Award.

In 1979 RSRE received Queen's Awards for the development of liquid crystal technology and for crystal growing techniques. In 1982 another Queen's Award was received for application of the pyroelectric effect to infrared detection and in 1983 two more awards were received, one for the invention and exploitation of the SPRITE (Signal Processing in the Element), a novel form of cadmium mercury telluride infrared detector used in thermal imagers, and the other for the development of a new x-ray phosphor material (zinc tungstate) which was required for fast high-resolution x-ray imaging systems that provide better quality images with a reduced x-ray dosage (figures 3 and 4). These examples were all dependent on research of the most basic nature at RSRE but they also depended upon a high level of mutual trust and collaboration between RSRE and the manufacturers. Whilst in some areas RSRE may have been responsible for unique and outstanding research it is in the construction of the matching interfaces between the researchers and the appliers of new knowledge that RSRE can claim to point the way to future advances in technology.

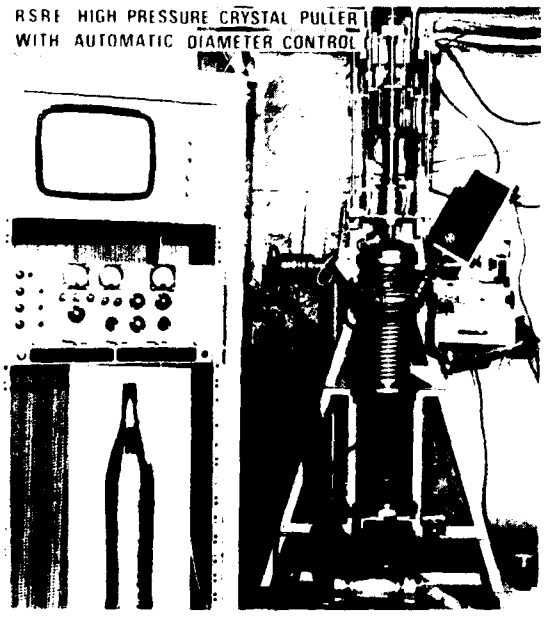

Fig 3 Crystal puller

RSRE has pioneered techniques for growing single crystals of materials required for modern electronics. The availability of these materials is one reason why RSRE is a world leader in electronics. Crystal pullers to RSRE designs have been produced commercially and their success earned RSRE a Queen's Award for Technological Innovation in 1979. Of the other four Queen's Awards that RSRE has received, three depended on single crystals developed by RSRE. The photograph shows a puller suitable for materials such as indium phosphide (see inset) that must be grown at high pressure. Note the TV camera for remote viewing of the melt.

development of army signalling and communications. During the second world war it was reorganised as the Signals Research and Development Establishment and was concentrated at Christchurch in 1943. Its interests began to broaden from purely

signals applications to such early examples of military electronics as mine detectors and it worked in close collaboration with ADRDE on the application of the new microwave techniques to communications. This resulted in the first microwave telephone link, the No 10 Set which Montgomery found so valuable during his advance into Germany in 1945.

Post War Reconstruction

During the war years TRE expanded explosively, from about 150 civilian staff when Mr Rowe took charge of Bawdsey to over 4000 in 1945. This total does not include a comparable number of service personnel on longer or shorter term attachment. The other components of RSRE had grown in a similar way. Many of the wartime staff had been seconded from universities or industry and not all were physicists or engineers. In fact at TRE there was a strong contingent of distinguished biologists who appeared to have a peculiar expertise for dealing with the human-electronics interface - many years before the wholesale appearance of television and the VDU. Naturally, many people wished to return to their original work at the end of the war but there was a desire in government circles to maintain a larger and better organised scientific establishment than had existed pre-war. This led to the construction of a Scientific Civil Service covering all aspects of government science which in particular for RSRE resulted in the setting up of new research laboratories additional to the project laboratories directly descended from the wartime work. The TRE physics department and SERL at Baldock were the two main examples within the fold of RSRE. A smaller research group was set up at SRDE which concentrated mainly on night vision aids. RRDE at this time concentrated on basic electronics techniques until the merger with TRE when a unified research programme evolved.

Of these research groups the physics department at TRE, initially led by Dr R A Smith, Dr (now Sir George) MacFarlane, Dr F

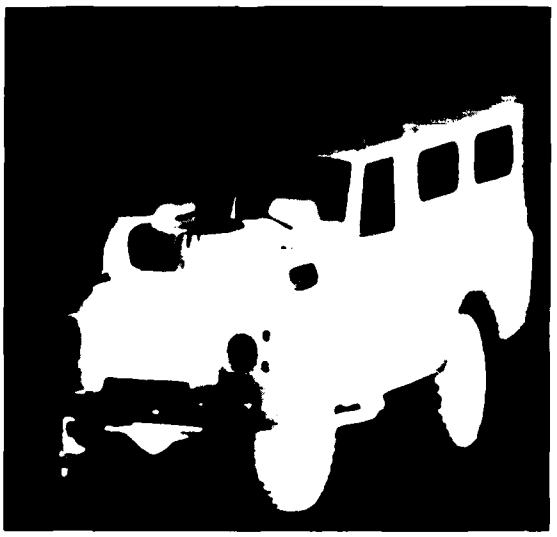

Fig 4 Thermal imaging

A modern thermal imager using a multi-element cadmium mercury telluride detector cooled with liquid air produced by a miniature Joule-Thomson liquefier from the compressed air in the cylinder attached to the tripod leg. Land Rover viewed with the imager and in normal daylight.

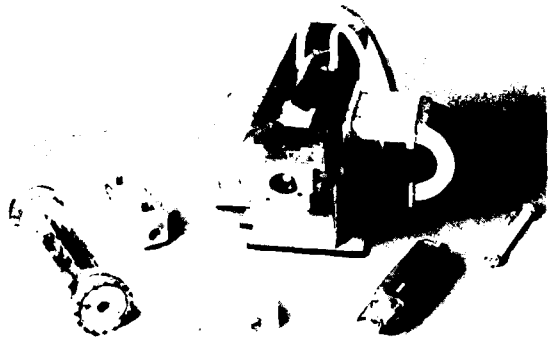

Fig 5 Laser development

RSRE discovered the molecular gas laser in 1963 and invented the first far-infrared laser. A number of CO_2 lasers developed by RSRE and available by 1979 are shown. They have a high efficiency and operate in the 9-11 m region where atmospheric transmission is good. The first CO_2 lasers were too bulky for use outside the laboratory but RSRE has made a series of inventions leading to today's compact and reliable lasers. Lasers based on RSRE development are now manufactured by Ferranti and Marconi Avionics.

E Jones and Dr A M Uttley, can now be seen to have made a lasting contribution to the development of electronics. One topic it chose to concentrate on was the study of semiconductors. In the war important semiconductor devices, such as the silicon mixer crystal for microwave receivers and the lead sulphide infrared cell, had emerged. It was believed that they would grow in importance but to make this happen research was needed of quality up to the best university standards but on a scale no university could then have supported. The wartime success of radar won the necessary resources for an ambitious programme which, in turn, has made major contributions to the development of today's British electronics industry.

Centre of Excellence

The research laboratories of the Ministry of Defence are now organised into seven 'centres of excellence' of which RSRE is the one responsible for electronics, electro-optics, sensors, lasers (figure 5), electronic warfare and computing. It is interesting to note in passing that three of the directors of these seven establishments were members of the TRE physics department. In the present organisation the Ministry of Defence is implementing the Strathcona plan to give private industry a greater share of development projects whilst freeing the Research Establishment for more fundamental studies. At the same time, by the evolution of the 'Malvern links' concept a more positive effort is being made to obtain a more direct involvement of RSRE with civil ventures. Thus another attempt is being made to use the resources of defence research to economic ends, as had previously been attempted by the old Ministry of Technology and before that in the immediate post-war years by the DSIR.

Certainly the list of successful civil projects emerging from the research at RSRE without the benefit of any very positive mandate is an impressive one. The earlier attempts to regularise this activity were nullified by a combination of military imperatives and Treasury shortsightedness. The present attempts will involve a greater degree of industrial participation at the higher management levels. We must remember that research involves risks but committees tend to be overcautious. Few committees can be expected to have the independence and stature of the Tizard committee which began this story. Let us hope the present organisation will be able to match the challenge of the past; only then are they likely to overcome the challenges of the future.

References

Galland, A. 1955 The First and the Last (London: Methuen) p 69.

Lawson, W.D., 1951 'A method of growing single crystals of lead telluride and selenide' J. Appl. Phys.22 1444-7.

MacFarlane, G.G., 1948 'The scientific approach to the study of photoconductive infrared detectors'. TRE Maths Group Memo 61/GGM.

Pike, E.R., 1979 'The Malvern correlator - case study in development' Phys. Technol. 10 104-9.

Putley, E.H., 1984 Recent Advances in

Medical Thermology eds E.F.J. Ring and B. Phillips, (New York, London: Plenum) pp 151-66.

Pyatt, E., 1984 'The National Physical Laboratory - a history' Phys. Technol. 15 157-63.

Acknowledgement Reprinted by kind permission of the Editor, Physics in Technology.

The Author

Dr Ernest Putley worked on radar during the war, later going on to research into solid state physics and infrared devices and applications. Since he retired from RSRE in 1982 has been studying the history of these subjects, concentrating particularly on infrared physics and on RSRE. His "History of IR detectors" can be found in Infrared Physics (1982 22 125-31, 189-91).

Publications by RSRE Authors 1983-85

Albrow, F.R. The background to Ada. IEE Colloquium, An Introduction to Ada - A Real Time Language for Engineers, pp.1/1-2, (1983).

Almond, T. Considerations pertinent to propagation prediction methods applied to airborne microwave equipments. AGARD Conf. Proc. 346, pp.28/1-11, (1984).

Almond, T.; Clarke, J. Consideration of the usefulness of microwave propagation prediction methods on air-to-ground paths. IEE Proc. F, 130, pp.649-656, (1983).

Anderson, D.A.; Apsley, N. Electronics: semiconductor superlattices. Nature, 305, pp.668, (1983).

Appleby, R. A technique for the investigation of the coherent coupling of observers to electro-optic sensors viewed via optical magnifiers. RSRE Memo 3570

Appleby, R. An interference refractomter to measure the pressure and temperature dependence of the refractive index of liquids. Spectrochim. Acta, 40A, pp.785-788, (1984).

Appleby, R.; Cox, A.F.J. Performance modelling of image intensified night vision goggles. SPIE, 467, pp.33-41, (1984).

Ashen, D.J.; Anderson, D.A.; Apsley, N.; Emeny, M.T. The role of vapour etching in the growth of epitaxial InP. J. Cryst. Growth, 60, pp.225-34, (Dec 1982).

Ashley, T.; Elliott, C.T. Accumulation effects at contacts to n-type cadmium-mercury-telluride photo- conductors. Infrared Physics, 22, pp.367-76, (1982).

Ashley, T.; Elliott, C.T.; White, A.M.; Wotherspoon, J.(*); Johns, M.(*) Optimisation of spatial resolution in Sprite detectors. Infrared Physics, 24, pp.25-33, (1984). (* - Mullard.)

Ashley, T.; Elliott, C.T.; White, A.M.; Wotherspoon, J.T.M.(*); Johns, M.D.(*) Optimisation of spatial resolution in Sprite detectors. 2nd Int. Conf. Advanced Infrared Detectors and Systems, pp.67-72, (1983). (* - Mullard Ltd.)

Astles, M.G.; Blackmore, G.W.; Gordon, N.; Wight, D.R. Use of alternative solvents for the low temperature LPE growth of CdTe films. RSRE Memo 3733.

Astles, M.G.; Gordon, N.; Bradley, D.; Wight, D.R.; Dean, P.J.; Blackmore, G.W. Doping of LPE layers of CdTe grown from Te solutions. J. Electron. Mat., 13, pp.167-89, (1984).

Astles, M.G.; Hill, H.; Steward, V.W. An experimental investigation of edge-growth effects in the LPE growth of GaAs and (GaAl)As. J. Cryst. Growth, 62, pp.61-66, (1983).

Bagshaw, D.; Brown, M.R.; Mansfield, F.; Roberts, J.D. Heavy duty precision pan and tilt head. RSRE Memo 3691

Ballingall, R.A.; Blenkinsop, I.D.; Lees, D.J.; Baker, I(*); Jenner, M.D.(*); Lockett, R.A.(*) Two dimensional random access infrared arrays. 2nd Int. Conf. Advanced Infrared Detectors and Systems, pp.6-11, (1983). (* - Mullard, So'ton)

Bardsley, W. Capabilities of molecular beam epitaxy and materials prospects. Vacuum, 34, pp.391-4, (1984).

Barnes, D.H. The provision of security for user data on packet-switched networks. IEEE Symp., Security and Privacy, pp.121-126, (1984).

Barraclough, K.G. Control of foreign point defects during Czochralski silicon crystal growth. Proc. Electrochem. Soc., 83-84, pp.176-188, (1983).

Barraclough, K.G.; Ward, P.J(*). Iron contamination in silicon processing. Proc. Electrochem. Soc., 83-89, pp.388-395, (1983). (* - Ples y)

Barraclough, K.G.; Pollard, C.J.(*); Speight, J.D.(*). Scanning electron beam annealing of oxygen donors in Czochralski silicon. Mats. Res. Soc. Symp. Proc., 13, pp.413-418, (1983). (* - British Telecom Research Lab.)

Bass, S.J.; Pickering, C.; Young, M.L. Metal-organic vapour phase epitaxy of indium phosphide. J. Cryst. Growth, 64, pp.68-75, (1983).

Bass, S.J.; Young, M.L. High quality epitaxial InP and indium alloys grown using trimethylindium and phosphine in an atmospheric pressure reactor. J. Cryst. Growth, 68, pp.311-318, (1984).

Beale, M.I.J.; Chew, N.G.; Uren, M.J.; Cullis, A.G.; Benjamin, J.D. Microstructure and formation mechanism of porous silicon. Appl. Phys. Letts., 46, pp.86-88, (1984).

Bennett, J.W. Sensor data combination. IEE Colloquium, Scene Matching in Multi-site Sensors, pp.2/1, (1984).

Berry, T.R. Picture formatting and hardware considerations. AGARD Lecture Series 119, pp.5/1-21, (1982).

Bertero, M.(*); Boccacci, P.(*); Pike, E.R. On the recovery and resolution of exponential relaxation rates from experimental data. II - The optimum choice of experimental sampling points for Laplace etc. Proc. Roy. Soc., A393, pp.51-65, (1984). (* - University of Genoa)

Bond, S.G. Flex - a computer architecture for advanced software development. IEE Colloquium, Computer-Aided Software Development, pp.3/1-2, (1984).

Bond, S.G.; Woodward, P.M. Guide to Algol 68 for users of RS systems. (Publisher: Edward Arnold)

Braddock, P.W.; Smith, R.F.; Skilton, P.J.; Slingsby, C.G.; Perkins, S.J.; et al. Satellite communications to a vehicle on the move. IEE 3rd Int. Conf. Satellite Systems for Mobile Comms. & Navigation, pp.135-139, (1983).

Bradshaw, M.J. Physical properties of nematic liquid crystals. PhD Thesis, Exeter Univ., (1984).

Bradshaw, M.J. Liquid crystal devices. Phys. Educ., 18, pp.20-26, (1983).

Bradshaw, M.J.; Constant, J.; McDonnell, D.G.; Raynes, E.P. The physical properties of cyanophenylcyclohexyl ethanes (PECH). Mol. Cryst. Liq. Cryst., 97, pp.177-194, (1983).

Bradshaw, M.J.; Hilsum, C.; Raynes, E.P. A new form of liquid crystal touch switch. Electron. Letts., 18, pp.1106-1108, (1982).

Bradshaw, M.J.; Raynes, E.P. The elastic constants and electric permitivities of mixtures containing terminally cyano substituted nematogens. Mol. Cryst. Liq. Cryst., 91, pp.145-155, (1983).

Bradshaw, M.J.; Raynes, E.P. The bend and splay elastic constants on approaching an injected smectic phase. Mol. Cryst. Liq. Cryst., 99, pp.107-116, (1983).

Bradshaw, M.J.; Raynes, E.P.; Fedak, I.(*); Leadbetter, A.J.(*) A correlation between short range smectic-like ordering and the elastic constants of nematic liquid crystals. J. Physique, 45, pp.157-162, (1984).

Bradstreet, D.W.G.; Hill, L.D. Instrumentation for and results of measurements with 6-ports at RSRE. IEE Colloquium, Advances in S-parameter Measurements at Microwavelengths, pp.3/1, (1983).

Braim, S.P. A background criterion for use in thermal imager range modelling. SPIE, 467, pp.18-23, (1984).

Braim, S.P.; Campbell, A.P. TED(Sprite) detector MTF. 2nd Int. Conf. Advanced Infrared Detectors and Systems, pp.63-66, (1983).

Brammer, D.J.; Williams, D. Antennas mounted on vehicles.

'Applications of computational techniques in electromagnetics', chapter 11.

Broughton, C.; Mifsud, V.J. Exposure modelling of particle beam lithography. RSRE Memo 3690.

Brown, G.T.; Cockayne, B.; Elliott, C.R.(*); Regnault, J.C.(*); Stirland, D.J.(**); Augustus, P.D.(**) A detailed microscopic examination of dislocation cluster in LEC InP. J. Cryst. Growth, 67, pp.495-506, (1984). (* - British Telecom Research Lab.; ** - Plessey)

Brown, G.T.; Cockayne, B.; MacEwan, W.R. The nature of prismatic dislocation loops in undoped InP. J. Electron. Mat., 12, pp.93-106, (1983).

Brown, G.T.; Cockayne, B.; MacEwan, W.R. A HVEM study of dislocation clusters in LEC InP. 7th Int. Conf. on HVEM, pp.411-416, (1983).

Brown, G.T.; Whitehouse, C.R.; Woodward, J. The effect of annealing on structure defects in bulk InP. J. Cryst. Growth, 64, pp.129-136, (1983).

Brown, G.T.; Young, I.M.; Warwick, C.(*); Booker, G.R.(*) An examination of dislocations in Si-doped LEC GaAs by double crystal X-ray topography, SEM cathodoluminescence and chemical etching. 3rd Oxford Conf. Microsc. Semicond. Mater., pp.371-376, (1983). (* - Oxford Univ)

Brown, R.G.W. An exploration of new optical techniques for turbulence measurement using photon correlation laser anemometry. PhD Thesis, Surrey Univ., (1984).

Brown, R.G.W. Combined transform Doppler anemometry. (Chapter from book on Laser Doppler Anemometry. Publisher: Gulbenkian Foundation.)

Brown, R.G.W., Inman, P.N.(*). Direct comparisons of laser Doppler, transit, hot-wire and pulsed wire anemometer measurements. ICIASF '83, pp.158-164, (1983). (* - Surrey Univ.)

Brown, R.G.W.; Gill, M.E.(*). A comparison of photon correlation laser Doppler anemomtery data processing techniques. SPIE, 369, pp.220-228, (1983). (* - Cranfield Inst. of Technology.)

Brown, R.G.W.; Jones, R. Burst-correlation laser Doppler velocimetry results. ICIASF '83, pp.214-219, (1983).

Brown, R.G.W.; Jones, R. Burst-correlation laser Doppler velocimetry. Optics Letts., 8, pp.449-451, (1983).

Brown, R.G.W.; Pike, E.R.; Stokes, J.M.(*). Laser Doppler velocimeter experiments in an AMTE water tunnel. RSRE Report 82002. (* - AMTE.)

Brown, R.G.W.; Richards, P.H.(*). Measurements of shear layers in transonic flows with a laser transit anemometer. J. Phys. D, 15, pp.1891-1905, (1982). (* - CEGB, Marchwood Engineering Lab.)

Brown, R.G.W.; Richards, P.H.(*). Oscillatory correlograms measured with a laser transit anemometer. Optica Acta, 29, pp.1299-1302, (1982). (* - CEGB, Marchwood Engineering Lab.)

Browning, K.A. Air motion and precipitation growth in a major snowstorm. Quarterly J. Roy. Met. Soc., 109, pp.225-242, (1983).

Browning, K.A. Mesoscale forecasting in the Meteorological Office: the way ahead? Meteorol. Mag., 113, pp.302-313, (1984).

Browning, K.A. The role of radar in weather forcasting. Phys. Technol., 14, pp.140-145, (1983).

Browning, K.A.; Carpenter, K.M. Frontiers - five years on. Meteorol. Mag., 113, pp.282-288, (1984).

Browning, K.A.; Hill, F.F. Structure and evolution of a mesoscale convective system near the British Isles. Quarterly J. Roy. Met. Soc., 110, pp.897-913, (1984).

Browning, K.A.; Monk, G.A. A simple model for the synoptic analysis of cold fronts. Quarterly J. Roy. Met. Soc., 108, pp.435-452, (1982).

Browning, T.I. High speed saw spectrum analyser data handling. RSRE Memo 3450

Burgess, D.E. Pyroelectric infra-red sensors. Recent Advances in Medical Thermology; ed. E. Francis, J. Ring & B. Phillips, pp.241-250, (1984).

Burgess, D.E.; Putley, E.H. Rumford and the teapots: a demonstration of thermal imaging. Phys. Educ., 19, pp.20-23, (1984).

Cameron, D.C.; Irving, L.D.; Whitehouse, C.R.; Woodward, J.; Lee, D. Planar self-aligned ion implanted MISFETS for fast logic applications. 10th Int. Symp. GaAs and Related Compounds, pp.461-468, (1983).

Cameron, D.C.; Irving, L.D.; Whitehouse, C.R.; Woodward, J.; Brown, G; Cockayne B. Factors influencing the performance of InP MISFETs. Thin Solid Films, 103, pp.61-70(1983).

Carmichael, I.C. The influence of the temperature coefficient of refractive index to a thermal imager. RSRE Memo 3398

Carmichael, I.C.; Dean, A.B.; Wilson, D.J. Optical immersion of a cryogenically cooled 77oK photoconductive CdHgTe detector. 2nd Int. Conf. Advanced Infrared Detectors & Systems, pp.45-48, (1983).

Carmichael, I.C.; Roberts, J.D. Servo-system for the athermalisation of a germanium lens. RSRE Memo 3527

Cattell, A.F.; Cockayne, B.; Dexter, K.; Kirton, J.; Wright, P.J. Electroluminescence from films of ZnS: Mn prepared by organometallic chemical vapour deposition. IEEE trans. Electron Devices, ED-30, ,pp.471-475, (1983).

Cattell, A.F.; Cullis, A.G. The variation in luminescent and structural properties of sputter-deposited ZnS: Mn thin films with post deposition annealing. Thin Solid Films, 92, pp.211-217, (1982).

Chew, N.G.; Cullis, A.G.; White, J.C.; Cox, T.I. Transition electron microscope studies of MOS silicon device structures. Microscopy of Semiconducting Materials, pp.473-478, (1983).

Chew, N.G.; Cullis, A.G. Iodine ion milling of indium-containing compound semiconductors. Appl. Phys. Letts., 44, pp.142-144, (1984).

Chew, N.G.; Cullis, A.G.; Williams, G.M. Identification of tellurium precipitates in cadmium telluride layers grown by MBE. Appl. Phys. Letts., 45, pp.1090-1092, (1984).

Chew, N.G.; White, J.C.; Cullis, A.G.; Day, D.J.; Janes, T.W.; Wilkinson, C.D.(*) Comparative study of small geometry MOS device structures using transmission electron microscopy. Microcircuit Engng. '83 Conf., pp.457-464, (1983). (* - Glasgow University.)

Chew, N.G.; Williams, G.M.; Cullis, A.G. Transmission electron microscope studies of heteroepitaxial CdTe on (001) InSb substrates. Inst. Phys. Conf. Series, 68, pp.437-440, (1984).

Clark, M.G. Energy-efficient display technology. Electronics and Power, 30, pp.43-46, (Jan 1984).

Clark, M.G. Materials for flat panel displays. IX Int. Vacuum Congress & V Int. Conf. Solid Surfaces, pp.499-509, (1983).

Clark, M.G.; McDonnell, D.G.; Bone, M.F.(*); Price, A.H.(*). Dielectric studies of monoester and diester nematogens. Liquid Crystals and Ordered Fluids, 4, pp.799-830, (Plenum, 1984). (* - Univ. College of Wales, Aberystwyth.)

Clark, M.G.; Saunders, F.C. Asymmetric orientational distribution of an anthraquionone dye in nematic liquid crystal hosts. Mol. Cryst. Liq. Cryst. Lett. ,82, pp.267-276, (1982).

Clarke, J. The principles and practice of modern airborne early warning radar. Int. Radar Conf., India, pp.613-624, (1983).

Clarke, J. Microwave airborne early warning radar. Military

Microwaves '84 Conf., pp.129-136, (1984).

Clarke, J. The Chinese remainder theorem and multi-PRF radars. RSRE Memo 3650

Clarke, J. A review of United Kingdom airborne radar. IEEE NAECON, pp.1391-1398, (1983).

Clarke, J. Advanced electronic warfare technology. (Publishers - MEPL)

Clarke, J. Experimental study of orthomode couples for use in power combining and distribution. IEE Proc. H, 130, pp.125-130, (1983).

Clarke, J.; Leacy A.C, Mission avionics for Nimrod AEW. IEEE NAECON, pp.1399-1403, (1983).

Clarke, J.; Davies, D.E.N(*); Radford, M.F(**); Slater, K.F.(***). Review of UK radar. IEEE trans. Aerospace & Electron. Syst., AES-20, pp.506-520, (1984). (* - Univ. College, London; ** - Marconi; *** - ARE, Portsdown).

Clarke, J.; King, J. A British AEW radar system. Radar'82, pp.41-45, (1982).

Cloude, S.R. Polarimetry: characterisation of polarisation effects. Thesis, Birmingham Univ., (1984).

Cloude, S.R. Polarimetric techniques in radar signal processing. Microwave Journal, 26, pp.119-127, (1983).

Clough, L.D.; Lloyd, D.E.; Parker, J.C.; Richmond, W. Integration produces small Ku-band altimeter. Microwaves and RF, 22, pp.79-80, (1983).

Cockayne, B., ed. Materials aspects of indium phosphide: proc. of 2nd NATO Workshop. (Published in J. Cryst. Growth, 64(1), (1983)).

Cockayne, B.; Brown, G.T.; MacEwan, W.R. Control of dislocation structures in LEC single crystal InP. J. Cryst. Growth, 64, pp.48-54, (1983).

Cockayne, B.; Brown, G.T.; MacEwan, W.R.; Ashen, D.J. Mechanical strength of LEC Ge-doped single crystal InP. J. Mat. Sci. Letts., 2, pp.667-669, (1983).

Cockayne, B.; Brown, G.T.; MacEwan, W.R.; Blackmore, G.W. SIMS profile analysis for Ge-, Co- and Fe-doped InP substrates used in epitaxial growth. J. Mat. Sci. Letts., 2, pp.309-313, (1983).

Cockayne, B.; MacEwan, W.R.; Harris, I.R.; Brown, G.T. Precipitate identification in Ge-doped LEC grown InP single crystals. J. Mater. Sci. Letters, 3, pp.990-992(1984).

Cockayne, B.; Wright, P.J. Metal-organic chemical vapour deposition of wideband GaP II-VI compounds. J. Cryst. Growth, 68, pp.223-230, (1984).

Cockayne, B.; Wright, P.J.; Blackmore, G.W.; Williams, J.O.; Ng, T.L.(*). A structural and compositional analysis of interfaces in ZnSe 0.94 S 0.06 layers grown on to GaAs by OMCVD. J. Mat. Sci., 19, pp.3726-3731, (1984). (* - Univ. of Wales, Aberystwyth.)

Collier, C.G. Remote sensing for hydrological forecasting. Facets of Hydrology, vol. 2, (John Wiley).

Collier, C.G.; Larke, P.R.; May, B.R. A weather radar correction procedure for real-time estimation of surface rainfall. Quarterly J. Roy. Met. Soc., 109, pp.589-608, (1983).

Conder, P.C.; Jenkins, R.M.; Redding, J.R.; Spencer, T.W. Long life sealed-off CO2 waveguide lasers. Laser '82, pp.640-644, (1983).

Conder, P.C.; Jenkins, R.M.; Roper, V.G.; Parcell, E.W.; Redding, J.R.; Spencer, T.W. A compact rugged carbon dioxide waveguide laser. Nat. Quantum Electronics Conf., pp.79-82, (1983).

Connelly, T.G.; Griffiths, M.P. Research using a Discus-based network emulator. RSRE Memo 3539

Connelly, T.G.; Griffiths, M.P. Intermediate access switch - a multiprocessor application. RSRE Report 83004

Cook, J.O. Calibration and display of stack departure times for aircraft inbound to Heathrow Airport. RSRE Memo 3750

Cowley, E.B.; Clarke, J.; Scroop, I.W.; Clifton, K.; King, J. Instrumentation and analysis of airborne pulse-Doppler radar trials. Radar'82, pp.134-137, (1982).

Cox, T.I.; Deshmukh, V.; Hill, J.R.; Cullis, A.G.; Chew, N.G.; Webber, H.C. Electrical and structural properties of pulse laser annealed polycrystalline silicon films. IEEE trans. Electron Devices, ED-30, pp.737-744, (July 1983).

Craig, D.; Miller, A.; Matthew, J.G.H.(*). Optical switching in a CdHgTe etalon at room temperature. Appl. Phys. Letts., 46, pp.128-130, (1985). (* - Heriot-Watt Univ.)

Crocker, A.; Jenkins, R.M.; Johnson, M. A frequency agile sealed-off CO2 TEA laser. J. Phys. E., 18, pp.133-135, (1985).

Cullis, A.G. Ultra-high speed solidification and crystal growth in transiently molten semiconductor layers. Laser-Solid Interactions and Transient Thermal Processing of Materials, pp.75-82, (1983).

Cullis, A.G. TEM studies of ultra-rapid solidification phenomena in semiconductors. Electron Microscope Soc. Am., 41st Mtg., Proc., pp.134-137, (1983).

Cullis, A.G. Microstructure and topography laser annealing of semiconductors. Laser Annealing of Semiconductors, pp.147-201, (1982).

Cullis, A.G. Defect structure transitions in silicon induced by Q-switched laser annealing. Physica, 116B&C, pp.527-536, (1983).

Cullis, A.G. Modulated structures and metastable dopant concentrations in silicon annealed with Q-switched laser pulses. J. Vac. Sci. Technol. B, 1, pp.272-277, (1983).

Cullis, A.G.; Chew, N.G.; Webber, H.C., Smith, D.J.(*). Orientation dependance of high speed silicon crystal growth from the melt. J. Cryst. Growth, 68, pp.624-638, (1984). (* - Cambridge Univ.)

Cullis, A.G.; Webber, H.C.; Chew, N.G. Amorphous silicon laser quenched from the melt-preparation and characterisation. Proc. Mat. Res. Soc. Mtg., Laser and Electron Beam Interactions with Solids, pp.131-140, (1982).

Cullis, A.G.; Webber, H.C.; Chew, N.G. Amorphization of germanium, gallium phosphide and gallium arsenide by laser quenching from the melt. Appl. Phys. Letts., 42, pp.875-877, (1983).

Cullis, A.G.; Webber, H.C.; Chew, N.G. Ultra-rapid solidification of transiently molten laser-annealed silicon. Microscopy of Semiconducting Materials, pp.167-172, (1983).

Cullis, A.G.; Webber, H.C.; Chew, N.G. Ultrafast melting and solidification behaviour of amphorous and crystalline silicon. Mats. Res. Soc. Proc., 23, pp.105-110, (1984).

Cullis, A.G.; Webber, H.C.; Chew, N.G.; Poate, J.M.(*); Baeri, P.(**). Transistors to defective crystal and the amphorous state induced in elemental Si by laser quenching. Phys. Rev. Letts., 49, pp.219-222, (1982). (* - Bell Labs; ** - Univ. of Catania, Italy.)

Cullis,A.G. Q-switched laser annealing of semiconductor silicon. Nat. Quantum Electronics Conf., pp.89-96, (1983).

Currie, I.F. In praise of procedures. RSRE Memo 3499

Currie, I.F.; Foster, J.M. Curt: the command interpreter language for Flex. RSRE Memo 3522

Currie, I.F.; Foster, J.M.; Edwards, P.W. Kernel and system procedures in Flex. RSRE Memo 3626

Currie, I.F.; Peeling, N.E. Modular compilation systems for high level programming languages. RSRE Memo 3460

Daniel, M.F.; Lettington, O.C.; Small, S.M. Investigations into Langmuir-Blodgett film-forming ability of amphiphiles with cyano head groups. Thin Solid Films, 99, pp.61-69, (1983).

Daniel, M.F.; Lettington, O.C.; Small, S.M. Langmuir-Blodgett films of amphiphiles with cyano headgroups. Mol. Cryst. Liq. Cryst., 96, pp.373-385, (1983).

Daniel, M.F.; Smith, G.W. Preparation of non-centrosymmetric Langmuir-Blodgett films with alternating merocyanine and sterylamine layers. Mol. Cryst. Liq. Cryst. Letts., 102, pp.193-198, (1984).

Daniel, M.F.; Smith, G.W. Langmuir-Blodgett films. Phys. Educ., 18, pp.266-269, (1983).

Davies, B.H.; Bates, A.S. Internetworking in the military environment. RSRE Memo 3391

Day, D.J.; Middleton, G.W.R. Passivation and maskless processing with anisotropic etches in silicon. J. Electrochem. Soc., 131, pp.407-410, (1984).

Deacon, J.; Moore, R.K.; Platt, R.L.; Russell, M.J.; Tomlinson, M.J. RSRE speech data base recording (1983): Part 1. Specification of vocabulary and recording procedure. RSRE Report 83010

Dean, A.B.; Elliott, C.T.; White, A.M. Photoconductive detectors employing an optically induced non-linearity. SPIE, 510, pp.149-153, (1984).

Dean, P.J. Oxygen in gallium phosphide - a canonical deep donor. Physica, 117/118B&C, pp.140-145, (1983).

Dean, P.J. Comparison of MOCVD-grown with conventional II-VI materials parameters for EL thin films. Phys. Stat. Solidi A, 81, pp.625-646, (1984).

Dean, P.J. Deep levels in semiconductors. Europhysics News, 14(3), pp.9-10, (1983).

Dean, P.J.; Cockayne, B.; Roberts, S.H.(*); Grande, M.(**); Batstone, J.L.(**); Steeds, J.W.(**); Wright, P.J. Spatial distribution of donors in MOCVD ZnSe. Inst. Phys. Conf. Series, 67, pp.337- , (1983). (* - Oxford Instruments; ** - Bristol University.)

Dean, P.J.; Fitzpatrick, B.J.; Bhargava, R.N. Optical properties of ZnSe doped with Ag and Au. Phys. Rev. B, 26, pp.2016-2035, (1982).

Dean, P.J.; Herbert, D.C.; Gislason, H.P.(*); Monemar, B.(*) Crystal field splitting of excitons bound to neutral complexes in GaP. Physica , 117/118B, pp.269-271, (1983). (* - Univ. of Lund, Sweden)

Dean, P.J.; Magnea, M.(*); Pautrat, J.L.(*); Le Si Dang(*); Romestain, R.(*). Defects in Zn-fired ZnTe: detection of a double acceptor (SiTe?). Solid State Comms., 47(9), pp.703-707, (1983). (* - Centre d'Etudes Nucleaires de Grenoble.)

Dean, P.J.; Pitt, A.D.; Wright, P.J.; Young, M.L.; Cockayne, B. The optoelectronic properties of donors in organo-metallic grown ZnSe. Physica, 116B&C, pp.508-513, (1983).

Dean, P.J.; Simmonds, P.E.(*); Venghaus, H.(*); Sooryakumar, R.(*). Electron and hole g-values from magnetoluminescence in ZnTe and CdTe. Solid State Comms., 43(5), pp.311-314, (1982). (* - Max Planck Inst., Stuttgart)

Dean, P.J.; Skolnick, M.S. Donor identification and bound exciton spectra in InP. J. Appl. Phys., 54(14), pp.346-359, (1983).

Dean, P.J.; Skolnick, M.S.; Cockayne, B.; MacEwan, W.R.; Iseler, G.W(*) Residual donors in LEC InP. J. Cryst. Growth, 67, pp.486-494, (1984). (* - Lincoln Labs,MIT.)

Dean, P.J.; Skolnick, M.S.; Herbert, D.C.; Uihlein, Ch.(*) New aspects of oxygen donor in gallium phosphide. J. Phys. C, 16, pp.2017-2051, (1983). (* - Max Planck Institut)

Dean, P.J.; Skolnick, M.S.; Taylor, L.L. Identification of donors in vapour grown InP. J. Appl. Phys., 55(4), pp.957-963, (1984).

Dean, P.J.; Stutius, W.(*); Bhargava, R.N.(**); Fitzpatrick, B.J.(**) Ionization energy of the shallow nitrogen acceptor in zinc selenide. Phys. Rev. B, 27, pp.2419-2428, (1983). (* - Xerox, California; ** - Philips)

Dean, P.J.; Thomas, D.G.(*); Frosch, C.J.(**) New iso-electronic trap luminescence in gallium phosphide. J. Phys. C, 17, pp.747-762, (1984). (* - Bell Labs, Holmdel; ** - Bell Labs, Murray Hill)

Dean, P.J.; Williams, G.M.; Blackmore, G. Novel type of optical transition observed in MBE CdTe. J. Phys. D, 17, pp.2291-2299, (1984).

Dean, P.J.; Wright, P.J.; Cockayne, B. Exciton recombination processes in zinc selenide. J. Phys. C, 16, pp.3493-3500, (1983).

Dennis, P.N.J. Photodetectors. (Publisher - Plenum Press).

Dennis, P.N.J. Comparison between millimetre waves and infra-red for short-range surveillance. IEE Colloquium, Millimetre Waves, pp.10/1-6, (1983).

Deshmukh, V.G.I. MOS damage in plasma etching. IEE Colloquium, Dry Etching Related to Silicon, pp.4/1-2, (1982).

Dore, M.J.; Anstey, G.J. An atmospheric refractive index fluctuation meter. RSRE Memo 3433.

Edwards, G.W. The objective measurement of MRTD for thermal images. SPIE, 467, pp.47-54, (1984).

Elliott, C.T. An infrared detector with integrated signal processing. IEEE Int. Electron Devices Mtg. Technical Digest, pp.132-135, (1982).

Elliott, C.T.; Cappocci, F.A.(*); Forder, S.(*); Hubbert, D.A.(*); Charlton, D.E.(*); Lockett, R.A.(*) Advances in cadmium mercury telluride detectors for CO2 laser detectors. 2nd Int. Conf. Advanced Infrared Detectors and Systems, pp.36-39, (1983). (* - Mullard Ltd.)

Esdale, D.J.; Wight, D.R.; Ball, G.; Oliver, P. The fabrication and assessment of high speed MOCVD GaAlAs PIN detectors. J. Cryst. Growth, 68, pp.461-465, (1984).

Evans, R.A.; McCanny, J.V.; McWhirter, J.G.; Wood, D.; McCabe(*); Wood, K.(**) A CMOS implementation of a systolic multi-bit convolver chip. VLSI '83 Int. Conf., pp.227-236, (1983). (* - GEC Hirst Research Centre; ** - Prestwick Circuits)

Fane, N.C.W.; Cusdin, A.R.(*) The performance of an inferometer-angle measuring receiver against non line-of-sight transmitters. IEE Proc. F, 130, pp.695-700,(1983). (* - Philips Research Labs)

Farrow, R.F.C.; Sullivan, P.W.; Williams, G.M. The performance of a double oven as an arsenic dimmer source for MBE. Molecular Beam Epitaxy and Clean Surface Techniques, pp.169-172, (1982).

Fickenscher, G. The user of Mascot philosophy for the construction of Ada programs. RSRE Report 83009

Fickensche., G. Automatic distribution of programs in Mascot and Ada environments - a feasibility study. RSRE Memo 3696.

Field-Richards, H.S. Discus : a distributed control micro-processor system. Thesis, Imperial College, (1982).

Foord, R.; Jones, R.; Vaughan, J.M.; Willetts, D.V. Precise comparison of experimental and theoretical signal to noise ratios in CO2 laser heterodyne systems. Appl. Optics, 22, pp.3787-3795, (1983).

Ford, R.L. On the use of height rules in off-route airspace. J. Navigation, 36(2), pp.269-287, (1982).

Foreman, B.J.; Cameron, D.C.(*) The correlation of channel mobility with interface state measurements on InP MOSFET structures. Solid State Electronics, 27, pp.305-309, (1984). (* - NIHE, Dublin)

Foster, J.M. Checkline microcode algebraically. RSRE Memo 3748.

Foster, J.M.; Currie, I.F.; Edwards, F.W. Flex: a working computer with an architecture based on procedure values. RSRE Memo 3500

Gallagher, J.G.; Brammer, D.J. Reactive surface scattering

characteristics. IEE Colloquium Digest 76, pp.5/1-4, (1983).

Gallagher, J.G.; Brammer, D.J. Electromagnetic scattering by an infinite array of periodic broken wires buried in a dielectric sheet. 13th European Microwave Conf, pp.778-782, (1983).

Gallagher, J.G.; Brammer, D.J. A plane wave expansion solution for the scattering from a frequency-selective surface in the presence of a dielectric. RSRE Memo 3618

Gardner, K.; Pike, E.R.; Miles, M.J.(*); Keller, A.(*); Tanaka, K.(*). Photon-correlation velocimetry of polystyrene solutions in extensional flow fields. Polymer, 23, pp.1435-1442, (1982). (* - H.H.Wills Physics Lab.)

Gardner, K.; Vaughan, J.M. Resonant modes in a dispersive cavity. SPIE, 369, pp.253-256, (1983).

Giess, S.C. Edge detection in SAR imaging using gradient operators. RSRE Memo 3743

Gill, S.S. Synthesis of silicon dioxide layers by high dose ion implantation. Appl. Phys. Letts., 85, pp.67-74, (1984).

Gill, S.S.; Anjumm M.(*), Shahid,M.A.(*), Sealy,B.J.(**), Marsh,J.H.(**). Ion implantation in GaInAs. Mats. Res. Soc. Symp., 27, pp.317-322, (1984). (* - Surrey Univ.; ** - Sheffield Univ.)

Gill, S.S.; Dawsey, J.R.; Cullis, A.G. Contact resistivity of IR lamp alloyed Au-Ge metallisation on GaAs. Electron. Letts., 20, pp.944-945, (1984).

Gill, S.S.; Sealy, B.J.(*) Annealing of selenium implanted InP using a graphite strip heater. J. Appl. Phys, 56, pp.1189-1194, (1984). (* - Surrey Univ.)

Gill, S.S.; Sealy, B.J.(*) Rapid thermal annealing of selenium implanted InP. J. Phys. Colloquium, 44, pp.C5/253-259, (1983). (* -Surrey Univ.)

Gill, S.S.; Sealy, B.J.(*) Transient annealing of ion implanted indium phosphide. J. Cryst. Growth, 64, pp.174-180, (1983) (* - Surrey Univ.)

Gill, S.S.; Wilson, I.H(*). Formation of oxide layers by high dose implantation into Si. Mats. Res. Soc. Symp, 27, pp.275-280, (1984). (* - Surrey Univ.)

Goillau, P.J. Predictive display design for a two-axis control task. RSRE Memo 3532

Goillau, P.J.; Carr, K.J.(*); Megan, E.D.(*) Eye movements and visual search: a bibliography. RSRE Memo 3543 (* - Birmingham Univ.)

Gorton, E.K. Continuously coupled unstable resonators: problem of large output beam divergence. Optics & Laser Technol., 15, pp.274-275, (1983).

Gorton, E.K.; Gorton, P.J.; Parcell, E.W. LIMP in continuously coupled unstable resonators. J. Phys. D, 16, pp.517-524, (1983).

Gorton, E.K.; Parcell, E.W. A preliminary study of a retro-reflective mirror resonator. Optics Comms., 46(2), pp.112-114, (1983).

Gorton, E.K.; Parcell, E.W. Thermal defocusing(LIMP) in stable CO2 resonators. J. Phys. D, 16, pp.1827-1835, (1983).

Gorton, E.K.; Parcell, E.W.; Gorton, P.J. Laser induced medium perturbation (LIMP) effects in long pulse CO2 lasers. Inst. Phys. Conf. Series, 72, pp.313-318, (Aug 1984).

Grant, A.J. A review of millimetre wave devices. RSRE Memo 3372

Gray, K.W.; Darby, B.J. Future requirements for VLSI in the military field. IEE Systems on Silicon Seminar, pp.85-88, (1984).

Greenaway, A.H.; Huiser, A.M.J.(*). Phaseless object reconstruction. Optica Acta, 31, pp.767-774, (1984). (* - Lausanne Polytechnic, Switzerland.)

Griffin, E.J. The multistate reflector. RSRE Memo 3625

Griffin, E.J.; Hodgetts, T.E. Theoretical comparison of sixport reflectometer junction designs. IEEE MTT-S Int. Microwave Symp. Digest, pp.575-577, (1984).

Griffin, E.J.; Hodgetts, T.E. Comparing different theoretical designs of six-port reflectometer junctions. RSRE Memo 3684

Griffin, E.J.; Hodgetts, T.E.; Slack, G.J. A broadband 6-port circuit using 4 directional couplers and its calibration at VHF. IEE Colloquium , Advances in S-parameter Measurements at Micro-wavelengths, p.2/1, (1983).

Griffin, E.J.; Slack, G.J.; Hill, L.D. Broadband six-port reflectometer junction. Electron. Letts., 19, pp.921-922, (1983).

Griffiths, D. The impact of thermal imaging in systems. Military Microwaves '82, pp.13-18, (1982).

Griffiths, M.P. A portable input/output package for Coral based 8080 systems. RSRE Memo 3589

Griffiths, R.J.M.; Chew, N.G.; Cullis, A.G.; Joyce, G.C. Structure of GaAs-GaI-xAlxAs superlattices grown by metal-organic chemical vapour deposition. Electron. Letts., 19, pp.988-990, (1983). (Also presented at Rank Prize Fund Mtg, Malvern, 26-28 July 1983.)

Gunton, D.J. Dielectric loss measurement at millimetre wave frequencies using an untuned cavity. RSRE Memo 3597

Hanes, S. Data privacy in an electronic office system. Int. Conf. Networks and Electronic Office Systems, pp.225-230, (1983).

Harp, J.G. Image processing for target detection and tracking. M.Phil/PhD thesis

Harris, M.R.; Willetts, D.V. Acoustic phenomena associated with a TEA laser discharge. J. Phys. D: 16, pp.125-133, (1983).

Harris, N. A chemical milling method of producing thin-walled waveguide thermal isolating sections. RSRE Memo 3438.

Harris, R.L.; Braddock, P.W.; Smith, R.F. Satellite communication to a vehicle on the move. IEE Conference Pub. 222, pp.135-142, (1983).

Harrison, K.J. Guest-host liquid crystal displays. Seminex '82, pp.269-289, (1982).

Harvey, D.; Johnson, R.H. Hydraulic waveguide flange clamp for precision measurements. Electron. Letts., 19, pp.730-731, (1983).

Hazell, M.S.; Davies, B.H. A fully distributed approach to the design of a 16kbit/sec VHF packet radio network. IEEE MILCOM '83, pp.645-649, (1983).

Hazell, M.S.; Davies, B.H. A fully distributed approach to the design of a 16k bit/sec VHF packet radio network. RSRE Report 84003

Herbert, D.C. A new hot electron kinetic equation analytical results. J. Phys. C., 17, pp.6749-6767, (1984).

Herbert, D.C. An extension of Hayne's rule for bound excitons. J. Phys. C., 17, pp.901-903, (1984).

Herbert, D.C.; Till, S.J. Field dependent scattering and hot electron kinetics. Physica, 117/118B&C, pp.217-219, (1983).

Herbert, D.C.; Till, S.J. The intra-collisional field effect in semiconductor. J. Phys. C, 15, pp.5411-5423, (1982).

Hill, F.F. Use of average annual rainfall to derive estimates of orographic enhancement of frontal rain over England and Wales for different wind directions. J. Climatol., 3, pp.113-129, (1983).

Hill, F.F. The development of hailstorms along the south coast of England - 5th June, 1983. Meteorol. Mag., 113, pp.345-363, (1984).

Hill, J.R.; Parry, G.; Miller, A. Auger reconstruction and nonlinear refraction index changes in cadmium mercury telluride at 10.6um. Physica, 117/118B&C, pp.410-412, (1983).

Hill, L.D. A new method for producing and mounting barretter elements for power measurement in waveguides. Electron. Letts., 19, pp.352-354, (1983).

Hill, L.D. Implementing waveguide bandwidth six-port reflectometer circuits at millimetre wavelength. RSRE Memo 3678

Hilton, K.P.; Woodward, J. Reactive ion etching of via holes for GaAs MMIC's. IEE Colloquium Digest 107, pp.7/1-4, (1984).

Hodge, A.M.; Lewis, M.F. Detailed investigations into SAW convolvers. IEEE Ultrasonics Symp., pp.113-118, (1982).

Hodgetts, T.E.; Griffin, E.J. A unified treatment of the theory of six-port reflectometer calibration using the minimum of standards. RSRE Report 83008

Holland, R.; Blackmore, G.W. SIMS analysis of epilayers. J. Cryst. Growth, 68, pp.271-281, (1984).

Hollins, R.C.; Jordan, D.L. Pressure shift in an atmospheric pressure CO2-N2-He gas mixture. J. Phys. B, 15, L491-L493, (1982).

Hollins, R.C.; Jordan, D.L. Quantum limitations to sensitivity of rectifying optical heterodyne receivers. Infrared Physics, 24, pp.463-468, (1984).

Hollins, R.C.; Jordan, D.L. Measurements of 10.6 um radiation scattered by a psuedo-random surface of rectangular grooves. Optica Acta, 30, pp.1725-1734, (1983).

Hollins, R.C.; Jordan, D.L. Electro-optic frequency shifts in a Q-switched CO2 laser. J. Phys. D, 17, pp.1327-1334, (1984).

Hollins, R.C.; Jordan. D.L.; Cross, P.H. Passive frequency stability of pulsed CO2 lasers. J. Phys. E: 15, pp.1300-1301, (1982).

Home, R. The processes of visual perception and the implications of optimisation of displays. RSRE Report 83001

Hope, D.A.O.; Cockayne, B. New etch features in germanium- and silicon-doped GaAs. J. Cryst. Growth, 67, pp.153-167, (1984).

Hughes, A.J. Other types of display. AGARD Lecture Series 126, pp.11/1-12, (1983).

Hughes, A.J. Liquid crystal displays. AGARD Lecture Series 126, pp 7/1-17, (1983).

Hughes, A.J. Status of large oven LCD's. IEE Colloquium, Problems of High Information Density LCD's, pp. 2/1-5, (1983).

Hulme, K.F.; Collins, B.S. A CW CO2 laser rangefinder/ velocimeter using heterodyne detection. Military Microwaves '82, pp.59-65, (1982).

Hulme, K.F.; Pinson, J.T. Improved acousto-optic modulators for CO2 heterodyne laser systems. SPIE, 415, pp.127-134, (1983).

Hulme, K.F.; Pinson, J.T. Improved acousto-optic modulators for CO2 heterodyne laser systems. Electron. Letts., 19, pp.254-256, (1983).

Humphrey, P.T. The evolution of methods of air traffic control. RSRE Memo 3724.

Humphreys, R.G. Radiative lifetime in semiconductors for infrared detection. Infrared Physics, 23, pp.171-175, (1983).

Humphreys, R.G.; Brand, S.(*); Jaros, M.(*). Electronic structure of the divacancy in silicon. J. Phys. C., 16, pp.L337-L343, (1983). (* - Newcastle University.)

Humphreys, R.G.; Herbert, D.C.; Holeman, B.R.; Tapster, P.; Bickley, W.P.(*). Optically pumped photoconductivity and its use for assessing traps in Si:Pt. J. Phys. C, 16, pp.1469-1485, (1983). (* - Plessey.)

Humphreys, R.G.; Webber, R.F.; Holeman, B.R. A nitrogen cooled extrinsic silicon multiplex addressed staring array. 2nd Int. Conf., Advanced Infrared Detectors and Systems, pp.26-29, (1983).

Hurle, D.T.J. Melt temperature fluctuations: causes and responses of the solidification front. Adv. Space Res., 3, pp.43-50, (1983).

Hurle, D.T.J. Analytical representation of the shape of the meniscus in Czochralski growth. J. Cryst. Growth, 63, pp.13-17, (1983).

Hurle, D.T.J. Convective transport in melt growth systems. J. Cryst. Growth, 65, pp.124-132, (1983).

Hurle, D.T.J. The effect of soret diffusion on the morphological stability of a binary alloy crystal. J. Cryst. Growth, 61, pp.463-472, (1983).

Hurle, D.T.J.; Jakeman, E.; Wheeler, A.A. Hydrodynamic stability of the melt during solidification of a binary alloy. Phys. Fluids, 26, pp.624-626, (1983). (* - Univ. of East Anglia)

Ide, J.P. A broadband waveguide transfer standard for the disseimination of UK national microwave power standards. RSRE Memo 3390

Irvine, S.J.C.; Mullin, J.B.; Royle, A. Epitaxial growth of mercury telluride (HgTe) by a MOVPE process. J. Cryst. Growth, 57, pp.15-20, (1982).

Irvine, S.J.C.; Mullin, J.B.; Tunnicliffe, J. Photo-sensitisation : a stimulant for the low temperature growth of epitaxial HgTe. J. Cryst. Growth, 68, pp.188-193, (1984).

Irvine, S.J.C.; Mullin, J.B.; Robbins, D.J.; Glasper, J.L. UV absorption spectra and photoanalysis of some group II and VI alkyls. Proc. Mat. Res. Soc. Symp., Laser Chemical Processing of Semiconductors, pp.253-258, (1984).

Irvine, S.J.C.; Tunnicliffe, J.; Mullin, J.B. A study of transport and pyrolysis in the growth of CdxHg1-xTe by MOVPE. J. Cryst. Growth, 65, pp.479-484, (1983).

Irvine, S.J.C.; Tunnicliffe, J.; Mullin, J.B. The growth of highly uniform CMT by a new MOVPE technique. Materials Letts., 2, pp.305-307, (1984).

Jackson, A. Some problems in the specification of rolling ball operating characteristics. Int. Conf. Man Machine Systems, pp.103-106, (1982).

Jackson, A. Performance of rolling ball and isometric joystick on a 2-D target alignment task. RSRE Memo 3695.

Jakeman, E. Light scattering and non-Gaussian fields. Coherence and Quantum Optics V; ed. L. Mandel and E. Wolf, Plenum Pub., pp.1039- 1049, (1984).

Jakeman, E. Fraunhofer scattering by a sub-fractal diffuser. Optica Acta, 30, pp.1207-1212, (1983).

Jakeman, E. Speckle statistics with a small number of scatters. Optical Engineering, 23, pp.453-461, (1984).

Jakeman, E. Statistics of scattered waves. IEE Colloquium, Inverse Scattering by Electro-Magnetic and Allied Methods, pp.9/1-3, (1982).

Jakeman, E. Fresnel scattering by a corrugated random surface with fractal slope. J. Opt. Soc. Am., 72, pp.1034-1041, (1982).

Jakeman, E. Scattering by fractals. Nature, 307, pp.110, (12 Jan 1984).

Jakeman, E.; Hoenders, B.J.(*). Scattering by a random surface of rectangular grooves. Optica Acta, 31, pp.853-865, (1982). (* - Univ. of Groningen, Netherlands.)

Jakeman, E.; Jefferson, J.H. Scintillation in the Freshnel region behind a sub-fractal diffuser. Optica Acta, 31, pp.853-865, (1984).

Jakeman, E.; Klewe, R.C.; Richards, P.H.; Walker, J.G. Application of non-Gaussian scattering of laser light to measurements in a propane flame. J. Phys. D, 17, pp.1941-1950, (1984).

AD-A163 899 RSRE (ROYAL SIGNALS AND RADAR ESTABLISHMENT) 1985 3/3
RESEARCH REVIEW(U) ROYAL SIGNALS AND RADAR
ESTABLISHMENT MALVERN (ENGLAND) A J GRANT ET AL. 1985
UNCLASSIFIED DRIC-BR-90221 F/G 17/9 NL

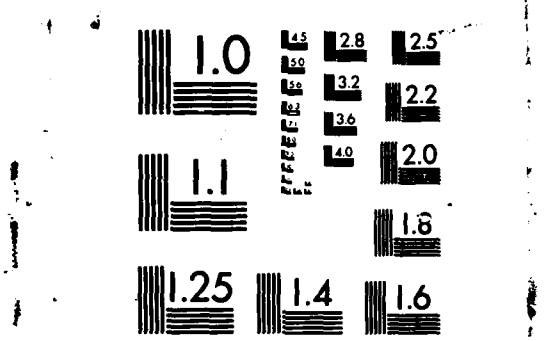

MICROCOPY RESOLUTION TEST CHART
NATIONAL BUREAU OF STANDARDS-1963-A

Jakeman, E.; Sarker, S.; Elgin, J.N.(*); Drazin, P.(**); Hawkins, S.C.(**) Photon statistics of the chaotic regime of the Maxwell-Bloch equations. Coherence and Quantum Optics V, pp.1233-1237, (1984). (* - Imperial College, ** - Bristol Univ.)

Jakeman, E.; Shepherd, T.J. Population statistics and the counting process. J. Phys. A, 17, pp.L745-L750, (1984).

James, G.E. Moon bounce communications to small terminals. RSRE Memo 3765

James, P.K. The WPL profiler: a new source of mesoscale observations. Meteorol. Mag., 112, pp.229-236, (1983).

Jefford, P.A.; Howes, M.J. Modulation schemes in low-cost microwave field sensors. IEEE trans. Microwave Theory and Techniques, MTT-31(8), pp.613-624, (1983).

Jefford, P.A.; Royds, R.J.; Tearle, C.A. Experimental 35 and 79GHz radars. IEE Colloquium, Millimetre Waves, pp.14/1-5, (1983).

Jenkins, R.M.; Devereux,R.W.; Blockley,A.F. Pulsed operations of compact longitudinally excited small bore carbon dioxide lasers. Nat. Quantum Electronics Conf., pp.67-70, (1983).

Johnson, M. A device-independent 2-D plotting package written in Fortran. RSRE Memo 3776.

Johnson, R.H.; Cummings, P. Capabilities and limitations of attenuation measurement by time interval ratio. IEE Colloquium, Advances in S-parameter Measurement at Micro-Wavelengths, pp. 16/1-9, (1983).

Jones, G.R. P4 Division - Electronic Materials Division, *RSRE, MOD. Queens Award Magazine, (1983).*

Jordan, D.L.; Hollins, R.C. A compact frequency stable pulsed CO2 laser. RSRE Memo 3670

Jordan, D.L.; Hollins, R.C. Measurements of Gaussian speckle statistics using both direct and heterodyne detection of CO2 laser radiation. Optica Acta, 30, pp.417-423, (1983).

Jordan, D.L; Hollins, R.C.; Jakeman, E. Infrared scattering by a fractal diffuser. Optics Comms., 49(1), pp.1-5, (1984).

Jordan, D.L.; Hollins, R.C.; Jakeman, E. Scattering from multi-scale surfaces. RSRE Memo 3656.

Jordan, D.L.; Hollins, R.C.; Jakeman, E. Speckle phenomena at 10 micron wavelength. 8th Int. Conf. Infrared and Millimeter Waves, p.TH 6.6, (1984).

Jordan, D.L.; Hollins, R.C.; Jakeman, E. Experimental measurements of non-Gaussian scattering by a fractal diffuser. Appl. Phys. B, 31, pp.179-186, (1983).

Kane, M.J.; Dean, P.J.; Skolnick, M.S.; Hayes, W.(*). Contrasts in triplet bound excitons in copper-doped gallium phosphide. J. Phys. C, 17, pp.6127-6138, (1984). (* - Oxford Univ.)

Keen, J.M.; White, J.C. The magic of the chip. New Scientist, no.1422, pp.37-42, (20 Sept 1984).

Kershaw, J. Gemini multiprogrammer's handbook. RSRE Report 82015.

Kidd, S.J. Implementation of the sign-location arithmetic F.F.T. RSRE Memo 3644

King, J. Implementation of an information retrieval service for component data. Radio and Electronic Engineer, 53, pp.190-194, (1983).

King, T.E.G. Application of queueing theory to communications networks - a review. RSRE Memo 3666.

King, T.E.G. System dynamics and network control. RSRE Memo 3755

Lamberton, H.M.; Sherlock, J.F. Zooming and smoothing using convolution procedures. RSRE Memo 3623

Lettington, A.H. IR optical scanning technique. Military Microwaves '82, pp.124-127, (1982).

Lettington, A.H.; Butler, A.L.(*); Ipson, S.S.(**) An energy band model for transition metals and compounds with applications to copper, tungsten and cuprous oxide. J. Phys. C., 16, pp.6335-6344 (1983). (* - Plessey; ** - Bradford Univ)

Lewis, K.L.; Arthur, G.S.(*) Surface and free carrier adsorption processes in C.V.D. zinc selenide. NBS Special Publication, 669, pp.86-101, (1984). (* - AWRE)

Lewis, K.L.; Arthur, G.S.(*); Edwards, P.H.(*). The incorporation of iron impurities in cubic ZnS. J. Cryst. Growth, 59, pp.201-209, (1982). (* - AWRE.)

Lewis, K.L.; Arthur, G.S.(*); Banyard, S.A.(*) Hydrogen-related defects in vapour-deposited zinc sulphide. J. Cryst. Growth, 66, pp.125-136, (1984). (* - AWRE)

Lewis, K.L.; Pitt, A.M.; Savage, J.A. The mechanical properties of CVD grown ZnS and their dependence on the conditions of youth. Proc. 9th Int. Conf. Chemical Vapor Deposition, pp.530-535, (1984).

Lewis, K.L.; Savage, J.A.; Marsh, K.J.; Jones, A.P.C. Recent developments in the fabrication of rare-earth chalcogenide materials for infra-red optical applications. SPIE, 400, pp.21-28, (1983).

Lewis, M.F. Low-loss SAW devices employing single stage fabrication. IEEE Ultrasonics Symp., 1, pp.104-108, (1983).

Lewis, M.F. Group-type unidirectional SAW devices employing intratransducer reflector banks. Electron. Letts., 19, pp.1085-1087, (1983).

Lewis, M.F. SAW filters employing interdigitated interdigital transducers(IIDT). IEE Colloquium, SAW Devices, pp.6/1-3, (1983).

Lewis, M.F. SAW components for radar front ends. IEE Colloquium, Advances in Microwave Integrated Front Ends, pp.7/1-6, (1984).

Lewis, M.F. A different approach to the wave-scattering properties of interdigital transducers. IEEE trans. Sonics/Ultrasonics, SU-30, pp.55-57, (1983).

Lewis, M.F.; Lowe, P.J(*); Picken, W.G.(*) MSK SAW filter to complement today's SAW convolver. IEEE Ultrasonics Symp., pp.256-261, (1982). (* - Cossor)

Lewis, M.F.; Lowe, P.J.(*); Picken, W.G.(*) MSK SAW filter to complement today's SAW convolver. IEE Colloquium, SAW Devices, pp.16/1-2, (1983). (* - Cossor)

Lewis, M.F.; West, C.L. The design and performance of SAW convolvers with extended integration times. IEEE Ultrasonics Symp., vol.1, pp.189-194, (1983).

Lewis, M.F.; West, C.L.; Deacon, J.(*); Humphryes, R.(*). Recent developments in SAW devices. IEE Proc. A, 131, pp.186-214, (1984). (* - Signal Technology.)

Loudon, R.; Shepherd, T.J. Properties of the optical quantum amplifier. Optica Acta, 31, pp.1243-1269, (1984).

Ludlow, J.H. Assessment of complete thermal imagers. Course at SIRA Ltd, Chislehurst, 16 Feb 1983.

Madden, P.; Kwelson, D. A consistent molecular treatment of dielectric phenomena. Adv. Chem. Phys., 56, pp.467-566, (1984).

Madden, P.A. Interaction-induced phenomena. NATO ASI Series C, 135, pp.431-474, (1984).

Madden, P.A.; Fowler, P.W.(*) In-crystal polarizabilities of alkali and halide ions. Phys. Rev. B, 29, pp.1035-1042, (15 Jan 1984). (* - University Chemical Lab, Cambridge)

Madden, P.A.; Fowler, P.W.(*) In-crystal hyperpolarizabilities of F- and Cl-. Phys. Rev. B, 30, pp.6131-6135, (1984). (* - University of Durham)

Magill, S.A.N.; Ord, G. Air traffic management concepts for the UK in the 1990s - a review of recent work at RSRE. RSRE Memo 3714

McCanny, J.V.; Evans, R.A. Bit-level systolic arrays. IEE Colloquium, Systolic Arrays, pp.2/1-5, (1984).

McCanny, J.V.; McWhirter, J.G. Yield enhancement of bit-level systolic arrays chips using fault tolerant techniques. Electron. Letts., 19, pp.525-527, (1983).

McCanny, J.V.; McWhirter, J.G. Bit-level systolic array circuit for matrix and vector multiplication. IEE Proc. G, 130, pp.125-130, (1983).

McCanny, J.V.; McWhirter, J.G.; Oliver, C.J.; Wood, K.W.(*). The relationship between word and bit-level systolic arrays as applied to matrix x matrix multiplication. SPIE, 431, pp.114-120, (1983). (* - Westglen)

McCanny, J.V.; McWhirter, J.G.; Wood, K.(*). Optimised bit-level systolic array for convolution. IEE Proc. F, 131, pp.632-637, (1984). (* - Prestwick Circuits.)

McDermid, J.A. Ada on multiple processors. RSRE Memo 3464.

McWhirter, J.G. Recursive least-squares minimization using a systolic array. SPIE, 431, pp.105-112, (1983).

McWhirter, J.G. A systolic array for recursive least-squares minimization. Electron. Letts., 19(18), pp.729-730, (1983).

McWhirter, J.G.; Evans, R.A.; McCanny, J.V.; Wood, McCabe(*); Wood, K.(**). Multibit convulution using a bit level systolic array. IEEE trans. Circuit & Systems, CAS-32, pp.95-99, (1985). (* - GEC; (** - Prestwick Circuits.)

McWhirter, J.G.; Shepherd, T.J. The least-squares lattice algorithm for adaptive channel equalisation - a simple derivation. IEE Proc. F, 130, pp.532-542, (1983).

McWhirter, J.G.; Shepherd, T.J. Adaptive alogarithms in the space and time domains. IEE Proc. H, 130, pp.17-21, (1983).

McWhirter, J.G.; Shepherd, T.J. A comparison between the least-squares lattice and fast Kalman algorithms for adaptive channel equalisation. RSRE Memo 3567

Mears, A.L. Very high performance integrated circuits. Military Microwaves '82, pp.592-597, (1982).

Merrifield, B.C. Data variation programs for the RSRE Ebeam data format. RSRE Memo 3550

Merrifield, B.C. Ebeam: an operating system for particle beam lithography. RSRE Memo 3512

Mifsud, V.J.; Broughton, C. A Fortran plotting package for graphic VDU's. RSRE Memo 3739.

Miller, A.; Fox, M.; Manning, R.J.; Marsh, J(*). Picosecond absorption saturation in GaInAsP at 1.05um. Electron. Letts., 20, pp.601-603, (July 1984). (* - Sheffield University.)

Miller, A.; Manning, R.J.; Fox, A.M.; Marsh, J.H.(*). High excitation electron dynamics in GaInAsP. Springer Ser. Chem. Phys., 38, pp.199-201, (1984). (* - Sheffield University.)

Miller, A.; Parry, G. Optical bistability in semiconductors with density dependent carrier lifetimes. Optical & Quantum Electronics, 16, pp.339-348, (1984).

Miller, A.; Parry, G.; Daley, R. Low power nonlinear Fabry-Perot reflection in CdHgTe at 10 um. IEEE J. Quantum Electronics, QE-20, pp.710-715, (1984).

Milner, J.G. Radar mortar locator development in the UK: the first thirty years. IEE Proc. F, 131, pp.233-239, (1984).

Moore, R.K. Techniques for automatic speech recognition. AGARD Lecture Series 129, pp. 4/1-12, (1983).

Moore, R.K. Assessment of speech systems. AGARD Lecture Series 129, pp. 6/1, (1983).

Moore, R.K.; Russell, M.J.; Tomlinson, M.J. Locally constrained dynamic programming in automatic speech recognition. IEEE Int. Conf. ASSP , pp.1270-1273, (1982).

Moore, R.K.; Russell, M.J.; Tomlinson, M.J. The discrimative network: a mechanism for focusing recognition in whole-world pattern matching. IEEE Int. Conf. ASSP, pp.1041-1044, (1983).

Morison, J.D.; Peeling, N.; Thorp, T.L. Ella: a hardware description language. IEEE Int. Conf. Circuits and Computers, pp.604-607, (1982).

Morison, J.D.; Peeling, N.E.; Thorp, T.L. Hardware specification - a use for hardware description languages. IEE Systems on Silicon Seminar, pp.37-42, (1984).

Moule, G.L. SAW compressive receivers for radar intercept. IEE Proc. F, 129, pp.180-186, (1982).

Mullin, J.B.; Irvine, S.J.C.; Royle, A.; Tunnicliffe, J.; Blackmore, G.W. A study on the purity and SIMS profiling of MOVPE-cadmium mercury telluride. J. Vac. Sci. Technol. A, 1, pp.1612-14, (1983).

Mullin, J.B.; Irvine, S.J.C.; Tunnicliffe, J. MOVPE of narrow gap II-VI's. J. Cryst. Growth, 68, pp.214-222, (1984).

Mullin, J.B.; Jones, C.A.; Straughn, B.W.; Royle, A. Crystal growth and characterisation of CdTe: a modified solvent evaporation technique. J. Cryst. Growth, 59, pp.135-142, (1982).

Mullin, J.B.; Royle, A. Surface oxidation and anomalous electrical behaviour of cadmium mercury telluride. J. Phys. D, 17, pp.L69-L72, (1984).

Mullin,J.B.; Irvine, S.J.C. The growth of cadmium merury telluride (CdxHgi-xTe) using organometallics. J. Vac. Sci. Technol., 21, pp.178-181, (1982).

Myers, J.G. Quantum transport effects in semiconductors. RSRE Memo 3580

Napper, E. Review of climatic protection techniques for electronic equipments. RSRE Memo 3530

Newton, C.O.; Young, P.A.(*) Optimisation of global rating for the UK 5000 gate array by iteration. IEEE 20th Design Automation Conf., pp.651-657, (1983). (* - GEC Hirst Research Centre)

Oldfield, L.C.; Ide, J.P. Measurement of a complex reflection coefficients in W-band using a 4-port reflectometer and precision waveguide spacers. IEE Colloquium, Advances in S-parameter Measurement at Micro-wavelengths, pp.8/1-6, (1983).

Oliver, C.J. Fundamental properties of high-resolution sideways looking radar. IEE Proc. F, 129, pp.385-402, (1982).

Oliver, C.J. A model for non-Rayleigh scattering statistics. Optica Acta, 31, pp.701-722, (1984).

Oliver, C.J. An analysis of template matching in image regiatration. Optica Acta, 31, pp.233-248, (1984).

Oliver, C.J. The dependence of the statistics of the detected intensity on the scattering. 13th European Microwave Conf., pp.552-557, (1983).

Parfitt, H.T.; Robertson, D.S.; Wilson, A.R(*). The preparation of indium phosphide layers by chloride-hydride reactions. J. Mat. Sci., 19, pp.2211-2218, (1984). (* - B.D.H. Chemicals)

Parker, P.; Pike, E.R.; Bertero, M.(*); Brianzi; P(*). Resolution in diffraction limited imaging , a singular value analysis. III: The effect of sampling and truncation of the data. Optica Acta, 31(2), pp.181-201, (1984). (* - Genoa University.)

Parkes, D.M. Measurement techniques for non-linear devices. IEE Colloquium, Protective Devices for EMP, pp.3/1-4, (1982).

Parry, G.; Hill, J.R.; Miller, A. Low intensity non-linear refraction in cadmium mercury telluride at 10.6um. SPIE, 369, pp.266-268, (1983).

Parry, G.; Schatzel, K.(*). Real-time Moire measurement of phase gradient. Optica Acta, 29, pp.1441-1445, (1982). (* - Kiel Univ.)

Peeling, N.E.; Morison, J.D.; Whiting, E.V. Adam: an abstract database machine. RSRE Report 84007.

Peeling, S.M. Noise reduction and segmentation of IR images

using co-median filters. RSRE Memo 3582

Pell, C. Some aspects of multistatic radar for long range air defence. Military Microwaves '84, pp.85-90, (1984).

Pell, C. ; Wallington, J.R.(*). Analogue processing for radar array antennas. IEE Colloquium, Signal Processing Arrays, pp.9/1-7, (1984). (* - Marconi.)

Pell, C.; Griffiths, H.D.(*); Forrest, J.R.(*); Williams, A.D.(*) Digital beamforming for bistatic radar receivers. 3rd Int. Conf. Antennas and Propagation (ICAP83), part 1, pp.80-84, (1983). (* - University College, London)

Pell, C.; Schoenenberger, J.G.(*); Forrest, J.R.(*). Systems and techniques studies of bistatic/multistatic radar independent receivers. Radar '82 Conf., pp.174-178, (1982). (* - University College, London)

Pickering, C. Non-destructive characterisation of n-type InP epitaxial layers by infrared reflecting measurements. J. Phys. D, 16, pp.213-223, (1983).

Pickering, C. Far-infrared reflectivity for semiconductor assessment. Physics Bull., 34, pp.97-98, (1983).

Pickering, C.; Beale, M.I.J.; Robbins, D.J.; Pearson, P.J.(*). Greef, R.(*). Optical studies of the structure of porous silicon films formed in p-type degenerate and non-degenerate silicon. J. Phys. C, 17, pp.6535-6552, (1984). (* - Southampton Univ.)

Pickering, C.; Tapster, P.R.; Dean, P.J.; Taylor, L.; Giles, P.L.(*); Davies, P.(*) Optical characterisation of acceptors in doped and undoped VPE InP. J. Cryst. Growth, 64, pp.142-148, (1983). (* - Plessey, Caswell)

Pickering, C.; Tapster, P.R.; Dean, P.J.; Ashen, D.J. Determination of impurity concentration in n-type InP by a photoluminescence technique. 10th Int. Symp. GaAs and Related Compounds, pp.469-476, (1983).

Pike, E.R.; Bertero, M.(*) Resolution in diffraction-limited imaging, a singular value analysis. The case of coherent illumination. Optica Acta, 29, pp.727-746, (1982). (* - Genoa University)

Pike, E.R.; Bertero, M.(*) Particle size distributions from Fraunhofer diffraction. I: An analytic eigenfunction approach. Optica Acta, 30(8), pp.1043-1049, (1983). (* - Genoa University.)

Pike, E.R.; Bertero, M.(*); Boccacci, P.(*) Resolution in diffraction-limited imaging, a singular value analysis. II. The case of incoherent illumination. Optica Acta, 29, pp.1599-1611, (1982). (* - Genoa University)

Pike, E.R.; Bertero, M.(*); Boccacci, P.(*) On the recovery and resolution of experimental relaxation rates from experimental data. A singular value analysis of the Laplace transform conversion in the presence *of noise. Proc. R. Soc.* A, 383, pp.15-29, (1982). (* - Genoa University).

Pike, E.R.; Bertero, M.(*); Brianzi, P.(*); Parker, P. Resolution in diffraction-limited imaging, a singular value analysis. III. The effect of sampling and truncation of data. Optica Acta, 31, pp.181-201, (1983). (* - Genoa University)

Pike, E.R.; Brown, R.G.W. The light in motion indicates the movement. Rev. Polytech. (Switzerland), no.12, pp.1473-1477, (1983). [In French]

Pike, E.R.; Danielsson, L.(*) Long range laser *anemometry* - a comparative review. J. Phys. E, 16, pp.107-118, (1983). (* - Aeronaut. Res. Inst. of Sweden, Broma, Sweden)

Pike, E.R.; McWhirter, J.G.; Bertero, M.(*); de Mol, C.(**). Generalised information theory for inverse problems in signal processing. IEE Proc. F, 131, pp.660-667, (1984). (* - Genoa University; ** - Brussells University)

Pike, E.R.; Walker, J.G.; Bertero, M.(*); de Mol, C.(**). Resolution in diffraction-limited imaging,a singular value analysis. IV: The case of uncertain localisation or non-uniform illumination of the object. Optica Acta, 31(8), pp.923-946, (1984). (* - Genoa University; ** - Brussells University)

Pike, E.R.; Watson, D.(*); McNeil-Watson, F.(*). The analysis of polydisperse scattering data. II. Meas. Suspended Part Quasi-Elastic Light Scattering Conf., pp.107-128, (1983). (* - Malvern Instruments Ltd.)

Pike, E.R.; de Villiers, G.; Bertero, M.(*); Brianzi, P.(*); Lan, K.H.(**); Ostrowsky, N.(**). Light scattering polydispersity analysis of molecular diffusion by Laplace transform inversion in weighted spaces. J. Chem. Phys., 82(3), pp.1551-1554, (1985). (* - Genoa University; ** - Nice University)

Rorison, J.; Herbert, D.C.; Dean P.J.; Skolnick, M.S. A model for the neutral donor bound exciton system in InP at high magnetic field. J. Phys. C, 17, pp.6435-6453, (1984).

Rorison, J.; O'Brien, M.C.M.(*). A prescription for Gamma x Epsilon Jahn Teller matrix elements. J. Phys. C, 17, pp.3449-3461, (1984). (* - Oxford University.)

Rorison, J.M.; O'Brien, M.C.M.(*) A 2 mode treatment of the 4T2 Gamma x Epsilon Jahn Teller system V2+ : MgO. J. Phys. C, 17, pp.6723-6733, (1984). (* - Oxford University)

Russell, M.J.; Moore, R.K.; Tomlinson, M.J.; Deacon, J.C.A. RSRE speech database recordings 1983: Part II. Recordings made for automatic speech recognition assessment and research. *RSRE Report 84008.*

Russell, M.J.; Moore, R.K.; Tomlinson, M.J. Some techniques for incorporating local timescale variability information into a dynamic time-warping algorithm for automatic speech recognition. IEEE Int. Conf. ASSP, pp.1037-1040, (1983).

Sarkar, S. The hydrodynamics of disclinations in nematics. Mol. Cryst. Liq. Cryst., 97, pp.111-117, (1983).

Sarkar, S. A simple attractor in the Driven Dicke system. Phys. Letts., 103A, pp.6513-6521, (1982).

Sarkar, S. Hydrodynamics of nematic liquid crystals in the presence of a continuous density of disclinations. J. Phys. C, 15, pp.6513-6521, (1982).

Sarkar, S.; Broomhead, D.S.; Jakeman, E.; Elgin, J.N.(*); Hawkins, S.C.(**); Drazin, P.(**). Statistical properties in the chaotic regime of the Maxwell-Bloch equations. Optics Comms., 50(1), pp.56-62, (1984). (* - Imperial College; ** - Bristol University.)

Sarkar, S.; Elgin, J.N(*). Quantum fluctuations and the Lorenz strange attractor. Phys. Rev. Letts., 52, pp.1215-1217, (1984). (* - Imperial College.)

Sarkar, S.; Elgin, J.N.(*) Quantum fluctuations and chaotic states in two-level atomic systems. Coherence and Quantum Optics V, pp.695-700, (1984). (* - Imperial College.)

Sarkar, S.; Elgin, J.N.(*) A simple attractor in the Driven Dicke system. Phys. Letts., 103A, pp.1-2, (1984). (* - Imperial College.)

Sarkar, S.; Elgin, J.N.(*). Exact results for photon statistics for a model of optical bistability. Coherence and Quantum Optics V , ed. L.Mandel and E.Wolf, pp.51-53 (Plenum, 1984). (* - Imperial College.)

Sarkar, S.; Tough, R.J.A. The effect of nearest neighbour *correlations on the elastic constants of a nematic liquid* crystal. J. Physique, 43, pp.1543-1555, (1982).

Saunders, F.C. Some studies in the physics of liquid crystals and their use in electro-optic devices. PhD thesis, Nottingham Univ.

Saunders, F.C.; Harrison, K.J.; Raynes, E.P.; Thompson, D.J.(*). New, photostable anthroquinone dyes with high order parameters. IEEE trans. Electron Devices, ED-30, pp.499-503, (1983). (* - ICI, Organics Divn., Manchester)

Saunders, F.C.; Wright, L.; Clark, M.G. Intermolecular guest-host interactions and the optical order parameter of pleochroic dyes. Liquid Crystals and Ordered Fluids, 4, pp.831-852, (Plenum, 1984).

Savage, J.A. Infrared optical materials and their anti-reflection coatings. Bristol, Adam Hilger, 1985, (isbn 0-85274-790-X).

Savage, J.A.; Lewis, K.L.; Pitt, A.M.; Whitehouse, R.H.L.

The role of a CVD research reactor in studies of the growth and physical properties of ZnS IR optical material. SPIE, 505, pp.47-51, (1984).

Scott, A.M. Phase conjugation by Brillouin enhanced and Rayleigh wing induced 4-wave mixing. SPIE, 365, pp.153-159, (1983).

Scott, A.M. Enhanced phase conjugation by Brillouin enhanced four wave mixing. Optics Comms., 45(2), pp.127-132, (1983).

Scott, A.M. Phase matching and frequency detuning efforts in Brillouin enhanced 4 wave mixing. SPIE, 369, pp.276-283, (1983).

Scott, A.M. Efficient phase conjugation by Brillouin enhanced nearly degenerate 4 wave mixing. Optics Comms., 45, pp.127-132, (1983).

Scott, A.M. Four-wave mixing due to the optical Kerr effect and Rayleigh wing scattering. Optics Comms., 45, pp.207-211, (1983).

Self, A.G. Expendable communications jammers - some problems and solutions. Microwaves and R.F. Journal, 23, pp.143-149, (1984).

Self, A.G. Intercept time and its prediction. IEE Colloquium, ESM Systems, pp.3/1-7, (1983).

Series, R.W. Determination of oxygen and carbon in silicon wafers. RSRE Memo 3479

Series, R.W.; Barraclough, K.G. Carbon contamination during growth of Czochralski silicon. J. Cryst. Growth, 60, pp.212-218, (1982).

Series, R.W.; Barraclough, K.G. Control of carbon in Czochralski silicon crystals. J. Cryst. Growth, 63, pp.219-221, (1983).

Shand, W.A. Performance requirements for an infrared staring sensor. SPIE, 467, pp.133, (1984).

Shand, W.A. Atmospheric limitations on imaging systems. SPIE, 467, pp.157-161, (1984).

Shanks, I.A. Liquid crystal displays: an *established example* of molecular electronics. IEE Proc. I, 130, pp.198-208, (1983).

Simcock, A.L. The Axis test box hardware report. RSRE Memo 3584

Simcock, A.L. An introduction to the Axis test box. RSRE Memo 3583

Simcock, A.L. The Axis test box software report. RSRE Memo 3585

Simcock, A.L. The Axis test box: operating guide. RSRE Memo 3517

Simpson, P.; Roberts, J.B.G. Real time speech recognition on a distributed digital processing array. RSRE Memo 3643

Simpson, P.; Roberts, J.B.C. Speech recognition on a distributed array processor. Electron. Letts., 19(24), pp.1018-1020, (1983).

Skilton, P.J. Recent developments in small mobile military Satcom terminals. IEE Conf. Pub. 209, pp.249-253, (1982).

Skilton, P.J.; Westall, I.L.(*) 'Manpack' SHF satellite ground terminal. Military Microwaves '82, pp.87-93, (1982). (* - Ferranti Electronics)

Skolnick, M.S. Transition metal diffusion in InP: photoluminescence *investigation*. J. Appl. Phys., 55, pp.2951-2961, (1984).

Skolnick, M.S.; Brozel, M.R.(*); Reed, L.J.; Grant, I.(**); Stirland, D.J.(***) Inhomogenity of the deep centre EL2 in GaAs observed by direct infrared imaging. J. Electron. Mat., 13, pp.107-125, (1984). (* - Trent Polytechnic; ** - Plessy; *** - Cambridge Instruments)

Skolnick, M.S.; Dean, P.J. Near gap energy levels of InP-luminescence and photoconductivity study. J. Phys. C, 15, pp.5863-5874, (1982).

Skolnick, M.S.; Dean, P.J. Bound and free exciton states in InP. Physica, 117/118B&C, pp.266-268, (1983).

Skolnick, M.S.; Dean, P.J.; Cockayne, B.; Kane, Hayes(*); Uihlein(**) Zeeman spectroscopy of crystal field transitions of Co-doped InP. J. Phys. C, 16, pp.5277-5291, (1983). (* - Clarendon Lab, Cambridge Univ., ** - Max Planck)

Skolnick, M.S.; Dean, P.J.; Duncan, K.R.(*); Eaves, L.(*); Randane, A.(*); Roys, W.B.(*) An investigation of the 1.36eV photoluminesence spectrum of heat-treated InP using Zeeman spectroscopy and strain effects. J. Phys. C, 17(7), pp.1233-1245, (1984). (* - Nottingham Univ.)

Skolnick, M.S.; Dean, P.J.; Groves, S.H.(*); Kuphal, E.(**) Donor identification in liquid phase epitaxial indium phosphide. Appl. Phys. Letts., 45, pp.962-964, (1984). (* - MIT Lincoln Lab; ** - FDBFZ, Darmstadt)

Skolnick, M.S.; Dean, P.J.; Kane, M.J.; Hayes, W.(*). Zeeman spectroscopy of vanadium-doped indium phosphide. J. Phys. C, 17, pp.6455-6467, (1984). (* - Oxford Univ.)

Skolnick, M.S.; Dean, P.J.; Pitt, A.D. et al. Optical properties of copper-related centres in InP. J. Phys. C, 16, pp.1967-1985, (1983).

Skolnick, M.S.; Dean, P.J.; Robbins, D.J.; Cockayne, B.; MacEwan, W.R.;Kane,M.J. (*); Hayes,W.(*); Uihlein.C.(**). Zeeman spectroscopy of luminescence from vanadium-doped indium phosphide. J. Phys. C, 16, pp.L767-L775, (1983). (* - Clarendon Labs,Cambridge Univ; ** - Max Planck, Grenoble)

Skolnick, M.S.; Dean, P.J.; Taylor, L.L.; Anderson, D.A.; Najda, S.P.(*); Armistead, C.J.(*); Stradling, R.A.(*) Identification of germanium and tin donors in InP. Appl. Phys. Letts., 44(9), pp.881-883, (1984). (* - St. Andrews Univ.)

Skolnick, M.S.; Foulkes, E.J.(*); Tuck, B.(*) Transition metal diffusion in InP - photoluminesence investigation. J. Appl. Phys., 55, pp.2951-2961, (1984). (* - Nottingham Univ.)

Skolnick, M.S.; Humphreys, R.G.; Tapster, P.R.; Cockayne, *B.; MacEwan, W.R. Electrical properties of* cobalt-doped InP. J. Phys. C, 16, pp.7003-7018, (1983).

Skolnick, M.S.; Reed, L.J.; Pitt, A.D. Photo-induced quenching of IR absorption non-uniformities of large diameter GaAs crystals. Appl. Phys. Letts., 44, pp.447-449, (1984).

Skolnick, M.S.; Uihlein, Ch.(*); Krath, H.(*). Zeeman spectroscopy of cobalt-doped InP. Physica, 117/118B&C, pp.170-172, (1983). (* - Max Planck Inst.,Grenoble)

Slack, G.J.; Graham, T.N.W. A reassessment of the measurement uncertainty of the XT-90 twin T dual admittance bridge. RSRE Memo 3632

Sleigh, A.C. Image understanding for military systems: a discussion of the way forward for PRIP research in Britain. RSRE Memo 3560

Sleigh, A.C.; Hearn, D.B. An IKBS approach to image understanding. RSRE Memo 3683

Slingsby, C.G. A de-triggerable astable circuit for microprocessor reset. RSRE Memo 3447.

Smith, A.C.; Searle, G.C.L.(*). A comparison between conventional and adaptive beamformers using underwater acoustic data. IEE Colloquium, Signal Processing Arrays, pp.2/1-5, (1984). (* - RANRL, Australia)

Smith, D.A. Thermal imaging : current technology and future trends. Military Microwaves '84, pp.206-212, (1984).

Snowball, T.; Berry, T.R.; Pardoe, A.M. An equipment for simulating airborne radar video. IEEE Radar '82 Conf., pp.250-253, (1982).

Stanley, M. Software configuration management across project boundaries and in distributed development environments. RSRE Memo 3704

Stanley, M. Software configuration management in an

integrated programming support environment. RSRE Memo 3578

Stanley, M. Software cost estimating. RSRE Memo 3472.

Stark, D.S. Catalysts for sealed gas lasers. Platinum Met. Rev., 28, pp.166-167, (1984).

Stark, D.S.; Crocker, A. A sealed, high-CO2, high-PRF, semiconductor-preionised TEA laser without a solid catalyst. Optics Comms., 48, pp.337-342, (1984).

Stark, D.S.; Crocker, A.; Lowde, N.A. A semiconductor preionised sealed TEA laser operating at high CO2 concentrations and repetition rates up to 100Hz. J. Phys. E, 16, pp.1069-1071, (1983).

Stark, D.S.; Crocker, A.; Steward, G.J. A sealed 100-Hz CO2 TEA laser using high CO2 concentrations and ambient temperature catalysts. J. Phys. E, 16, pp.158-161, (1983).

Stark, D.S.; Harris, M.R. Catalysed recombination of CO and O2 in sealed CO2 TEA laser gases at temperatures down to -27oC. J. Phys. E, 16, pp.492-496, (1983).

Staromlynska, J.; Saunders, F.C.; Harrison, K.J.; Tandy, D. Observation of the crystalline nature of LB monolayers of w-tricosenoic acid. Mol. Cryst. and Liq. Cryst. Letts., 102, pp.175-180, (1984).

Staromlynska, J.; Saunders, F.C.; Smith, G.W. A technique for the characterisation of Langmuir-Blodgett films. Mol. Cryst. Liq. Cryst., 109, pp.233-245, (1984).

Sullivan, P.W.; Farrow, R.F.C.; Jones,G.R. Insulating epitaxine films of BaF2, CaF2 and BaxCa1-xF2 grown by MBE on InP substrates. J. Cryst. Growth, 60, pp.403-413, (1982).

Summers, J.E. Measurements of the effects of mutual coupling in waveguide horn phased arrays. RSRE Memo 2668

Summers, J.E.; Groves, J.R. Measurements of the effects of mutual coupling in ridged waveguide horn and in dipole phased arrays. RSRE Memo 2753

Summers, J.E.; Wright, N.P. An investigation into the effect of sidelobe cancellation upon the general sidelobe level. RSRE Memo 3525

Tapster, P.R. A DLTS study of electron irradiated InP. J. Cryst. Growth, 64, pp.200-205, (1983).

Tapster, P.R. Emission and capture measurements on deep levels in InP. J. Phys. C, 16, pp.4173-4180, (1983).

Tarry, H.A. A scanning optical microprobe for infrared detector measurement. RSRE Memo 3745.

Tarry, H.A. The potential of Sprite CMT detectors for 3-5um infrared imaging. 2nd Int. Conf. Advanced Infrared Detectors and Systems, pp.59-62, (1983).

Taylor, G.N. ed. Adaptive arrays: a special issue. IEE Proc. F, 130(1), (Feb 1983).

Taylor, L.L.; Anderson,D.A. The growth of ultra-pure InP by vapour phase epitaxy. J. Cryst. Growth, 64, pp.55-59, (1983).

Taylor, L.L.; Apsley, N. A method for the VPE growth of n+/n-/n+ InP layers. J. Cryst. Growth, 60, pp.203-205, (1982).

Till, S.J.; Herbert, D.C. The intra-collisional field effect in semiconductors. II - Numerical results. J. Phys. C, 16, pp.5849-5866, (1983).

Tough, R.J.A. Self diffusion in a suspension of interacting Brownian particles. Molecular Physics, 46,pp.465-474, (1982).

Tough, R.J.A.; Bradshaw, M.J. The determination of the order parameters of nematic liquid crystals by mean field extrapolation. J. Physique, 44, pp.447-454, (1983).

Tough, R.J.A.; Pusey, P.N.; Ackerson,B.J.(*) Time dependence of the fourth-order correlation function in colloidal and polymer solutions. J. Chem. Phys., 81, pp.3331-3333, (1984). (* - Oklahoma State University.)

Tough, R.J.A.; Stone, A.J.(*) Spherical tensor theory of long-range intermolecular forces. Chem. Phys. Letts., 110, pp.123-129, (1984). (* - Cambridge University.)

Tough, R.J.A.; Willetts, D.V. Density perturbations induced by a discharge in a laser cavity. J. Phys. D, 15, pp.2433-2442, (1982).

Tozer, T.C. Opportunities and constraints of on-board processing. IEE Colloquium Digest no. 94, pp.1/1-4, (1984).

Troughton, N. Investigation of the effect of annealing on the dislocation and sub-grain boundary content of solvent-evaporation-grown CdTe. RSRE Memo 3680.

Tunnicliffe, J.; Blackmore, G.W.; Irvine, S.J.C.; Mullin, J.B.; Holland, R. SIMS analysis of impurities at CMT/CdTe heterostructure interfaces. Materials Letts., 2, pp.393-395, (1984).

Tunnicliffe, J.; Irvine, S.J.C.; Dosser, O.D.; Mullin, J.B. A new MOVPE technique for the growth of highly uniform CMT. J. Cryst. Growth, 68, pp.245-253, (1984).

Tyler, A.C.F. A tool for analysing the design and performance of a Mascot ACP network. Introductory Report. RSRE Memo 3475

Vaughan, J.M. Quasi-elastic light scattering from polymer systems. NATO Advanced Study Inst. Series C, 94, pp.305-347, (1982).

Vaughan, J.M. Infra-red laser velocimetry. Military Microwaves '82, pp.625-629, (1982).

Vaughan, J.M.; Woodfield, A.A(*). Wind measurement with coherent laser radar at 10 um. ESA-SP-202, pp.231-238, (1984). (* - RAE)

Vaughan, J.M.; Willetts, D.V. Temporal and interference fringe analysis of TEM01* laser modes. J. Opt. Soc. Am., 73, pp.1018-1021, (1983).

Vere, A.W.; Cole, S.; Williams, D.J. The origin of twinning in cadmium telluride. J. Electron. Mat., 12, pp.551-561, (1983).

Vere, A.W.; Straughn, B.W.; Williams, D.J.; Shaw, N.; Royle, A.; Gough.; Mullin. Growth of CdxHg1-x Te by a pressurised cast recrystallise anneal technique. J. Cryst. Growth, 59, pp.121-129, (1982).

Vere, A.W.; Williams, D.J.; Cole, S.(*). On the origins of twinning in CdTe. J. Electron. Mat., 12, pp.551-561, (1983). (* - Southampton Univ.)

Vere, A.W.; Williams, D.J.; Mullin, J.B. The phase diagram CdHgTe. RSRE Memo 3387

Walker, J.G. Optical imaging with resolution exceeding the Rayleigh criterion. Optica Acta, 30, pp.1197-1202, (1983).

Walker, J.G.; Berry, M.V.(*); Upstill, C.(*) Measurement of twinkling exponents of light focussed by randomly rippling water. Optica Acta, 30, pp.1001-1010, (1983). (* - Bristol Univ)

Walker, J.G.; Jakeman, E. Observation of sub-fractal behaviour in a light scattering system. Optica Acta, 31, pp.1185-1196, (1984).

Ward, J.S. Figures of merit for VLSI implementations of digital signal processing algorithms. IEE Proc. F, 131, pp.64-70, (1984).

Ward, J.S. Number representations for prime length DFT's. Electron. Letts., 20, pp.301-302, (1984).

Ward, K.D. Radar sea clutter model and it's application to performance assessment. IEE Radar '82 Conf., pp.203-207, (1982).

Ward, K.D. The performance of high resolution radars in sea clutter. Thesis - Birmingham Univ.

Ward, K.D.; Watts, S.(*) Radar clutter in airborne maritime reconnaissance systems. Military Microwaves '84, pp.222-228, (1984). (* - Thorn EMI.)

Warner, F.L. 'Attenuation.' (McGraw-Hill Encyclopaedia of

Science and Technology.)

Warner, F.L.; Herman, P. Very precise measurement of attenuation over a 90dB range using a voltage ratio plus gauge block technique. IEE Colloquium , Advances in S-Parameter Measurements at Micro-wavelengths, pp.17/1-7, (1983).

Warner, F.L.; Herman, P.; Cummings, P. Recent improvements to the UK national microwave attenuation standards. IEEE trans. Instr. & Meas., IM-32(1), pp.33-37, (1983).

Warner, F.L.; Herman, P.; Parkes, G.W.; Guldbrandsen, T.(*); Guldbransden, B.(*) Experimental test of a new precision model for microwave rotary vane attenuators. IEEE trans. Instr. & Meas., IM-32(1), pp.289-291, (1982). (* - Tech. Univ. of Denmark, Lyngby.)

Warner, J. Performance estimate of a reflecting light pipe for infrared detectors. RSRE Memo 3661

Warwick, C.A.; Brown, G.T.; Booker, G.R.(*); Cockayne, B. Dependent inhomogeneity in Czochralski-grown indium phosphide ingots doped with germaniun. J. Cryst. Growth, 64, pp.108-114(1983). (* - Oxford University.)

Watton, R.; Goss, A.J.(*); Nixon, R.D.(*); Wreathall, W.M.(*). Infrared television using the pyroelectric vidicon. GEC J. Res., 2, pp.198-203, (1984). (* - EEV.)

Watton, R.; Manning, P.A.; Burgess, D.E.; Gooding, J. The pyroelectric/CCD focal plane hybrid analysis and design for direct charge injection. Infrared Physics, 22, pp.259-275, (1982).

Watton, R.; Manning, P.A.; Burgess, D.E. Interface design for the pyroelectric/ccd hybrid. SPIE, 395, pp.78-85, (1983).

Watton, R.; Smith, C. Sensor head performance responsivity and NETD using pyroelectric linear arrays. RSRE Memo 3608

Watton, R.; Smith, C.; Gillham, J.P.; Manning, P.; Burgess, D. Performance and technologies for linear and two dimensional pyroelectric arrays. 2nd Int. Conf. Advanced Infrared Detectors and Systems, pp.49-53, (1983).

Webb, A.R. Estimation of target positions using planar arrays. RSRE Memo 3675.

Webber, H.C.; Cullis, A.G.; Chew, N.G. Computer simulation of high-speed melting of amphorous silicon. Appl. Phys. Letts., 43(7), pp.669-671, (1983).

West, C.; Robbins, D.J.; Dean, P.J.; Hayes, W.(*). The luminesence of copper in zinc oxide. Physica, 116B&C, pp.492-499, (1983). (* - Clarendon Labs, Oxford.)

West, C.L. Multiple passband transducers for tone selection from a frequency comb generator. RSRE Memo 3647.

West, C.L. SAW convolver employing unidirectional transducers for improved efficency and variable bandwidths. IEE Colloquium, SAW Devices, pp.11/1-4, (1983).

West, C.L.; Lewis, M.F. Efficient SAW convolver with 30us integration time. Electron. Letts., 19, pp.413-419, (1983).

White, A.M. An overview of detector techniques. Military Microwaves '84 Conf., pp.99-106, (1984).

White, A.M. Recombination in a graded n-n+ contact in a narrow gap semiconductor. J. Phys. C, 17, pp.4889-4896, (1984).

White, A.M.; Migliorato, P.(*). Common anion heterojunctions : CdTe-CdHgTe. Solid State Electron., 26, pp.65-69, (1983). (* - Rome University)

White, T.A.D. Ada/APSE: a sucessor to Coral 66 in the 80's. RSRE Memo 3540

White, T.A.D. AF-Coral: language features to integrate Mascot with Coral 66. RSRE Report 82019

Wight, D.R.; Allen, P.; Oliver, P.E.; Trussler, J.; Cooper, D. Electro-absorption modulators in GaAs/GaAlAs. IEE Colloquium Digest no. 93, pp.11/1, (1984).

Wight, D.R.; Bradley, D.; Williams, G.; Astles, M.; Irvine, S.J.C.; Jones, C. Minority carrier diffusion length in CdTe. J. Cryst. Growth, 59, pp.323-331, (1982).

Wight, D.R.; Harding, W.; Thomas, B. Improved green luminescence efficiency in a n-GaP grown by isotherm LPE. 10th Int. Symp. GaAs and Related Compounds, pp.203-208, (1983).

Wilkinson, R.M. A compounded delta modulator with low power consumption. RSRE Report 76001

Willets, D.V.; Harris, M.R. Causes of intrapulse chirping in TEA carbon dioxide lasers. Nat. Quantum Electronics Conf., pp.53-57, (1983).

Willetts, D.V. Field-induced gain in homonuclear diatomic molecules. J. Phys. B, 17, pp.473-481, (1984).

Willetts, D.V.; Harris, M.R. A plasma effect in injection-mode selection of TEA CO2 lasers. Appl. Phys. B, 33, pp.91-93, (1983).

Willetts, D.V.; Harris, M.R. A novel laser heterodyne technique for the measurement of election density in gas discharges : application to a TEA CO2 laser plasma. IEEE trans. Plasma Science, PS-11, pp.68-71, (1983).

Willetts, D.V.; Harris, M.R. Scaling laws for the intrapulse frequency stability of an injection mode selected TEA CO2 laser. IEEE J. Quantum Electronics, QE-19, pp.810-814, (1983).

Willetts, D.V.; Harris, M.R. Electro-optic refractive index compensation applied to the intrapulse frequency stabilisation of a carbon-dioxide TEA laser. J. Phys. D, 18, pp.185-189, (1985).

Willetts, D.V.; Harris, M.R. Laser-induced frequency sweeping in an electron-beam sustained CO2 laser. Optics Comms., 49(2), pp.151-154, (1984).

Willetts, D.V.; Harris, M.R. Heterodyne investigations of the acoustic effects caused by a pulsed TEA discharge. Inst. Phys. Conf. Series, 72, pp.325-330, (Aug 1984).

Williams, D.J. Eutectic microstructures in the Cd-Hg-Te system. J. Cryst. Growth, 58, pp.657-666, (1982).

Williams, G.M.; Young, I.M. Indium antimonide - strain induced by solder mounting in MBE. J. Cryst. Growth, 62, pp.219-224, (1983).

Wiseman, S.R. Two advcanced computer architectures: a study of their support for languages and operating systems. RSRE Report 82013

Wood, J.W.; Hall, T.J.(*); Fiddy, M.A.(*) A comparison study of some computational methods for locating the zeros of entire functions. Optica Acta, 30, pp.511-527, (1983). (* - Queen Elizabeth College)

Wood, M.A. An improved calibrationprocedure for hopmodyne network analysers. IEE Colloquium, Advances in S-parameter Measurement at Micro-wavelengths, pp.15/1-6, (1983).

Wood, M.A. The precise calibration of a rotary vane attenuator at 35 GHz using a homodyne network analyser. Electron. Letts., 18, pp.1025-1026, (1982).

Wray, F.E.; Capocci, F.A.(*); Harker, A.T.(*); Wilson, M.C.(*); Lacklison, D.E.(**) Thermoelectrically-cooled cadmium mercury telluride detectors of CO2 laser radiation. 2nd Int. Conf. Advanced Infrared Detectors and Systems, pp.40-44, (1983). (* - Mullard Ltd., ** - Philips Research Labs.)

Wright, P.J.; Griffiths, R.J.M.; Cockayne, B. The use of heterocyclic compounds in the organometallic chemical vapour deposition of epitaxial ZnS, ZnSe and ZnO. J. Cryst. Growth, 66, pp.26-34, (1984).

Wyndham, B.A.; Shaw, J.M. The reduction of multipath induced azimuth errors in a monopulse secondary radar. IEE Colloquium Digest no. 52, pp.8/1-4, (1983).

RSRE Main site and the Malvern Hills

The main site of RSRE lies below the town of Great Malvern at the foot of the Malvern Hills. There are two further facilities, one for Satellite Communications at Defford, and the other for Night Vision simulation at Pershore.

Malvern is served by British Rail InterCity express from London (Paddington) and is within easy reach of Motorway links to Birmingham (International Airport, NEC), Bristol and South Wales.

END

FILMED

3-86

DTIC